Joao Cruz
Mairead Atcheson *Editors*

Floating Offshore Wind Energy

The Next Generation of Wind Energy

Springer

Green Energy and Technology

More information about this series at http://www.springer.com/series/8059

Joao Cruz · Mairead Atcheson
Editors

Floating Offshore Wind Energy

The Next Generation of Wind Energy

 Springer

Editors
Joao Cruz
Cruz Atcheson Consulting Engineers
Lisbon
Portugal

Mairead Atcheson
Cruz Atcheson Consulting Engineers
Lisbon
Portugal

Printed on acid-free paper

Preface

There has been a rapid evolution of floating wind turbines in recent years, with the technology progressing from an eccentric research topic to the verge of commercialisation in a relatively short period of time. The first full-scale prototypes have been tested at sea, with these projects being largely successful and assisting in the demonstration of the technology. Plans are currently in place to install the first pre-commercial floating offshore wind farms in the next few years, which should lead to a significant expansion of the sector. Demonstrating the economic feasibility of projects will follow.

This book presents an overview of the current status and underlying design principles that apply to floating offshore wind energy technologies. Given the topics covered and the link between all of them, it can be considered one of the first textbooks in this field. It was compiled by a select group of authors, invited to contribute to the publication based on their experiences and expertise in floating offshore wind technologies or related disciplines. The publication aims to provide a solid first reference, which can be used either as a starting point for newcomers to the field, or by any interested reader with an engineering background.

We would like to gratefully acknowledge and thank all of the authors who contributed to this book, and without whom this book would not exist. Finally, it would be unfair not to acknowledge Springer, namely Dr. Christoph Baumann and Ms. Vani Gopi, for their continuous support and guidance throughout the project.

Lisbon, Portugal
Joao Cruz
Mairead Atcheson

Contents

Looking Back

Mairéad Atcheson and Andrew Garrad

Offshore wind turbines are a leading renewable energy technology with significant potential to support the drive for a low-carbon economy in Europe. Since the installation of the first offshore wind farm in Denmark in 1991, the installed capacity of offshore wind farms in Europe has grown significantly. By the end of 2015, the cumulative installed offshore wind capacity in Europe was over 11 GW, which is sufficient to cover 1.5 % of the EU's total electricity consumption (EWEA 2016). The majority of the wind farms are currently (end of 2015) located in the North Sea (69.4 %), the Irish Sea (17.6 %) and the Baltic Sea (12.9 %), at an average water depth of 27.2 m (EWEA 2016).

The offshore wind industry has the potential to continue to grow, however the installation of offshore wind turbines currently relies on fixed monopile foundations, space frame jacket or tripod structures, which are depth limited to shallow water sites (approx. <50 m). As the availability of shallow water sites declines, floating offshore wind turbine (FOWT) technologies can play a leading role in accessing deeper water sites and unlocking the full-potential of the offshore wind market.

A fundamental difference between fixed and floating wind turbine support structures is the additional compliance introduced by the motions of the floating platform. The offshore environmental forces acting on the floating platform induce motions, which need to be restrained within acceptable limits for the operation of the turbine, station keeping and safety purposes. The three dominant floating support structure classifications used in the FOWT industry, namely the semisubmersible, spar and tension leg platforms (TLP), stem from offshore technologies

M. Atcheson (✉)
Cruz Atcheson Consulting Engineers Lda, Lisbon, Portugal
e-mail: Mairead.atcheson@cruzatcheson.com

A. Garrad
DNV GL, Bristol, UK
e-mail: andrew.garrad@garradbalfour.com
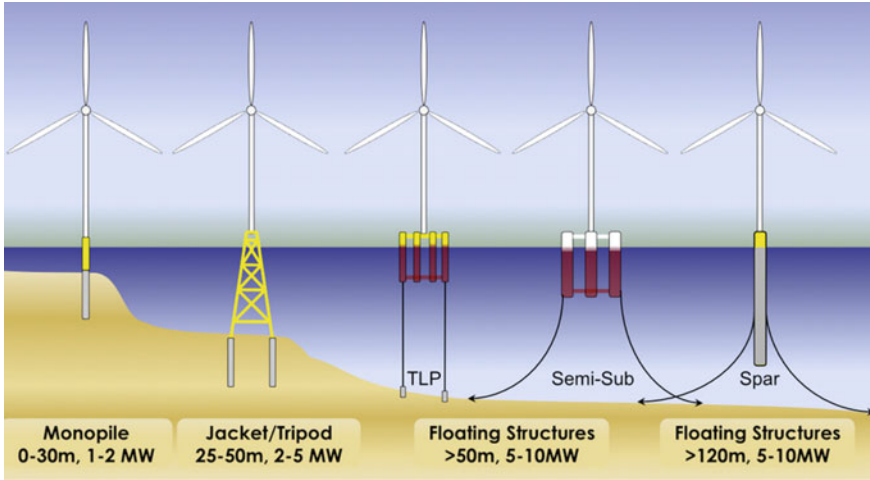
Fig. 1 Offshore wind foundations (courtesy of Principle Power)

developed primarily for the oil and gas industry. Figure 1 illustrates the different types of offshore wind foundations used by the wind industry.

In this chapter an historical overview of the floating offshore wind energy and offshore engineering industries is presented. The progression of the offshore wind industry into deeper water mirrors the trend seen in the oil and gas industry when platforms moved from fixed to floating foundations to access deeper water sites. Section 1 briefly describes the evolution of the offshore engineering industry and assesses potential parallels with the offshore wind industry. Section 2 is written by a prominent expert in the wind energy sector and provides insight into early days of the floating offshore wind turbines. A brief overview of the state of the floating wind industry is presented in Sect. 3, including an overview of research and development activities undertaken to-date. Finally, to conclude the chapter Sect. 4 provides an overview of the chapter layout for the book.

1 Evolution of the Offshore Engineering Industry

Mairéad Atcheson

Since the first offshore oil production platforms were installed in approximately 4 m of water in the Gulf of Mexico in the 1940s, offshore technologies have progressed significantly over the past 70 years and at present floating platforms are recurrently installed in depths greater than 1000 m. The successful move offshore

was at least in part driven by the development of innovative structures capable of operating and surviving in more challenging and hostile deep water environments. However, the advancement of the offshore industry was not solely attributed to a single technology breakthrough, but due to a collective effort of related innovations in technologies, the supply chain and specialist services required to support the offshore industry.

A brief overview of the evolution of offshore platforms is presented in the following section, which describes how the oil and gas industry moved from shallow water fixed platform to the variety of floating structures currently installed in deep water sites around the world.

1.1 The Early Days of the Offshore Industry

Kerr-McGee Oil Industries (now part of Anadarko Petroleum Corporation) drilled the first offshore producing well (Kermac 16) beyond the sight of land in the US Gulf of Mexico in 1947. This is commonly considered as the birth of the modern offshore oil and gas industry (Pratt et al. 1997). Prior to 1947, companies had extracted oil in the Gulf of Mexico, but these expeditions were confined to pro- tected inland waters in sight of the shoreline. The Kermac 16 rig, installed ten and a half miles off the coast of Louisiana in 4.6 m of water, stood in open waters exposed to the offshore environment. This represented a new era of innovation in offshore technologies and the beginning of the exploration and production of oil in deeper waters.

By 1948, Humble's Grand Isle Block 18 platform represented the state-of-the-art in self-contained offshore exploratory platforms, which could be subsequently transformed into an effective production facility. The dual platform, installed in approximately 14 m of water, included two significant advances in platform con- struction; the platform was manufactured from steel and constructed using tem- plates (or jackets) fabricated onshore and subsequently installed offshore. However, one of the biggest drawbacks of the platform was its cost. Explorative drilling was a gamble with no guarantee of finding oil, and the need for a mobile drilling rig for exploration was clear. Initially, submersible drill rigs and mono-hull drillships, like the CUSS I [the first drill ship, designed by Robert F. Bauer (see Burleson 1999)] were used by the industry. However, submersibles were depth limited and drillships were found to move significantly in heave, pitch and yaw in large waves. The industry needed a more stable platform capable of operating in deep water, which saw the introduction of semisubmersible platforms.

During the 1950s, through the development of many technology innovations the industry was able to produce competitively priced oil from offshore wells. By 1953, 70 steel platforms had been installed in the Gulf of Mexico, the deepest in 21 m of water. This successful move offshore was not solely attributed to a single

technology breakthrough, but due to a collective effort of related innovations. These included:

- achieving greater mobility in exploration through a breakthrough in mobile drilling rigs;
- structural design improvements in platform construction; improved methods for installing platforms at sea, and
- the establishment of new specialised suppliers and services required for offshore operations.

In the 1960s, fixed platforms for offshore environments had been proven, but there was an appetite to progress further into deeper water. Deeper water sites posed more challenging environmental conditions, along with a need for larger and heavier fixed jacket structures. Many assumptions about the environment loading on structures and the interaction between the pile and soil adopted in previous designs needed to be validated before progressing to these more challenging environments. More sophisticated design processes were required, incorporating more calculations and greater precision. Following investments into research activities in the 1950s, a new generation of engineers specialising in mathematics and design analysis techniques joined the offshore industry to support this process (Pratt et al. 1997). The first semisubmersible was developed in the 1960s, with the conversion of an existing submersible rig (Blue Water 1) into a floating drilling unit for operation in the Gulf of Mexico. In the years that followed many semisubmersible platforms were built, mainly for drilling operations, and the offshore industry made great advancements, with production operations moving into water depths of more than 100m by the 1970's.

During the 1970s, when alternatives to fixed platforms were under investigation, the conversion of a semisubmersible drilling unit into a production platform was considered as a viable option. Semisubmersible platforms are composed of a deck, multi-columns and pontoons, restrained with a compliant spread mooring or dynamic positioning system. The first application of a semisubmersible as a more permanent production platform was in 1975. The first application of a semisubmersible as a more permanent production platform was in 1975 in the North Sea Argyll oil field. Over time production semisubmersible platforms have evolved from converted mobile operating drilling units (MODUs), to high capacity purpose built designs for ultra-deep water, which can simultaneously drill and produce from wells below the vessel.

1.2 Moving into Deeper Water

Significant achievements in deep water advances were made in the 1970s and 1980s. Two important developments were key to enabling this progression. Firstly, by the early 1970s the offshore industry began to standardise practices by sharing

experience and information (the first American Petroleum Institute (API) Recommended Practice (RP) document for the design, fabrication and installation of offshore platforms was issued in October 1969); and secondly, the oil embargo of the 1973 by the Organisation of Petroleum Exporting Counties (OPEC) provided the economic incentive with a sustained period of high oil prices. In terms of offshore technologies, by the early 1970s improved jacket designs, better fabrication and installation techniques, and developed theories on the dynamic response of offshore structures, meant that the move into greater depths (beyond 122 m) was conceivable for the first time (Pratt et al. 1997).

In June 1975, the Piper Alpha oil platform was installed at a depth of 144 m in the North Sea. In the following years, the installation depth of platforms increased significantly, leading with the installation of the Cognac platform in the Gulf of Mexico during 1977 and 1978. The Cognac was a template-type structure with the jacket divided into three parts and was installed at a depth of 312 m, and at the time it was the world's heaviest platform weighing 59,000 t. In the early 1980s, the Cerveza and Cerveza Ligera platforms reformed conventional jacket designs to achieve a lighter platform design, providing a more economical design for fixed structures in deeper water. The Cerveza and Cerveza Ligera platforms weighed significantly less than the Cognac, at weights of 39,500 and 23,100 t, respectively.

Even with improvements in the design of jacket platforms, as water depths increased beyond 305 m, fixed jacket structures become more susceptible to stress amplification, with the natural frequency of the structure approaching that of the wave periods in the offshore environment. This meant that fixed jacket structures became less practical in water depths beyond 305 m and new technological innovations were required to find cost effective, structurally sound offshore platforms in deeper water.

In the late 1970s, two promising compliant designs emerged: tension leg platforms (TLPs) and compliant (guyed) towers. The compliant tower designs increased the natural frequency of the structure making it larger than the wave energy period, and subsequently mitigating the susceptibility of the structure to stress amplifications. The Lena platform was the first compliant platform installed in 305 m of water in the Gulf of Mexico in 1983. Two additional compliant towers were installed in the Gulf of Mexico in 1998, the Amerada Hess Baldpate and the Petronius, in water depths of 502 and 535 m, respectively.

The TLP was a floating platform, and its distinctive feature was the mooring system, which consists of vertical tendons driven into the seabed, which restrain the heave motion of the platform. The first commercial TLP was installed in 150 m of water in the Hutton Field in the UK section of the North Sea during 1984.

Until the mid-1990s, and aside from the Hutton platform, which was a rectangular 6-column unit, conventional TLPs were typically square 4-column units. Since the late 1990s, a variety of TLP configurations have been designed and built, including: an extended TLP (ETLP, designed by ABB Co.), a minimum offshore surface equipment structure TLP (MOSES, designed by MODEC Co.) and the SeaStar (or mono-column) TLP (SeaStar, designed by Atlantia Co.). The MOSES and SeaStar TLP platforms are more favourable for the production of smaller deep

water fields, when using a more conventional floating production platform would be uneconomical. At the time of writing, the Big Foot ETLP is the deepest TLP installed, at a water depth of 1581 m in the Gulf of Mexico.

During the 1990s spar platforms were introduced for production, drilling and work over operations of oil wells. A spar platform consists of a deep draft cylindrical floating caisson with a small water plane area moored to the seabed. The world's first offshore production spar was the Neptune spar installed in 1996 in the Gulf of Mexico in a water depth of 588 m. Prior to this, spars had been used as marker buoys and for gathering oceanographic information [the Flip spar was commissioned in 1965 primarily for ocean acoustic measurements; it was owned by the Navy and operated by Scripps Institute of Oceanography in California (Fisher and Spiess 1963)]. In the early 1960s, a spar was also installed by Nippon Telegraph off the coast of Japan to carry a microwave relay station.

Since the implementation of floating spar platforms in the offshore oil and gas industry, these have been used for drilling, production or both [as well as storage operations in the earlier days—the Brent Spar oil storage and offloading platform was installed in the North Sea in the mid-1970s (Bax and de Werk 1974)]. Some spar platforms (e.g. Genesis, Diana and Holstein) are equipped for both drilling and production, but most spars in service do not incorporate full drilling capacities. A key feature of a spar platform is its ability to support top tensioned steel risers due to very low motions of the platform, particularly in heave. This enables production controls (or as they are commonly known *Christmas trees*) to be placed at the top of the riser on the spar platform, rather than on the seabed, which allows direct access to the controls reducing maintenance tasks.

Three types of spars have been designed; the original spar design, truss spars and cell spars. The original spar design was developed in the 1990s for the Neptune platform and was a single cylindrical hull. Due to a large part of the cylindrical hull being under the water, spars are susceptible to strong currents and the creation of vortex eddies which may cause vibrations. Typically, strakes (fins that spiral down the outside of the cylindrical structure) are used to mitigate against any current-induced vibrations. The enclosed cylindrical structure of the spar also acts to protect the risers and subsea cables for a distance through the water column.

The next generation of spar designs was the truss spar. This design followed in the footsteps of the original spar and shared many similarities. The truss spar is a single cylindrical structure, but the cylinder is shorter than a conventional spar with a truss section incorporated into the structure. The first truss spars were the Boomvang and Nansen platforms installed in the Gulf of Mexico in 2002, at water depths of 1053 and 1121 m, respectively. The most recent rendition of the spar was the cell spar. The cell spar design incorporates six pressure vessels gathered around a central seventh vessel which provide the buoyancy for the platform. A structural steel framework holds the pressure vessels in place and extends deeper than the vessels, maintaining the deep-draft feature of a spar. The cell spar is a scaled down version of the much larger truss spar, this design is more suited to smaller deep water fields. Only one cell spar has been fabricated to date, the Red Hawk platform, deployed in the Gulf of Mexico in 2004 at a water depth of 1616 m.

Halkyard (2005) is recommended to the reader for a more detailed description on the design of floating offshore oil and gas platforms.

1.3   Synergies with the Offshore Wind Sector

Parallels may be drawn between the evolution of the offshore oil and gas and the offshore wind industry. At a certain depth, the application of floating structures becomes more attractive than fixed platforms. Floating structures with various degrees of compliance have been developed by the offshore oil and gas industry to develop deep water sites. Similarly, floating offshore wind support structures currently under development fall within three classifications of floating structures: semisubmersible, spar and TLP. Whilst the oil and gas industry continues to explore greater water depths, moving into the realm of ultra-deep water (defined as water depths exceeding 1524 m) the challenges faced by the floating offshore wind industry varies. In the context of offshore wind, deep water is typically used to describe water depths greater than 50 m, and unlike large bespoke oil and gas platforms, the commercialisation of floating offshore wind turbines requires large arrays of (relatively) smaller devices.

The floating offshore wind industry may seek guidance from the more mature offshore oil and gas industry, both in terms of engineering design and experiences gained during the evolution of the industry. One important outcome to note is that the industry's success was not based on technology innovations alone, but due to a collective effort of innovations across related sectors. This stresses the requirement for the parallel growth of floating offshore wind technologies and the necessary specialist support services required to design, manufacture and install technologies offshore.

FOWT support structures involve relatively new applications for the offshore platform concepts. Although the floating platform classifications (spars, semisubmersibles and TLPs) are similar to those used in the offshore industry, floating wind turbines have very different requirements to the large oil and gas production platforms. The differences between the offshore applications will be significant to achieve the necessary cost reduction required for floating wind turbine applications. Some of the fundamental differences include:

- FOWTs are typically un-manned, unlike oil and gas platforms that provide permanent residence for personnel. This means that floating wind platforms have a lower risk to human life and the additional safety mechanisms required for crewed offshore platforms are not applicable.
- The potential risks posed to the environment due to the failure of a floating wind turbine is significantly lower than that of an offshore oil and gas production facility.

- Offshore oil and gas platforms are installed in very deep water (typically greater than 300 m), whereas floating wind turbine deployments are planned for water depth in the range of 50 to 200 m.
- At a commercial scale, wind platforms will be mass produced, providing opportunities for cost savings based on economies of scale.

2 The Early Days of Floating Offshore Wind Turbines

Andrew Garrad

The recent rapid evolution of floating wind turbines has taken us all by surprise. I write this section on an auspicious day, March 31 2016, which sees both the simultaneous closure, for environmental reasons, of four coal power stations in the UK with a total capacity of 7.4 GW and the inauguration of Europe's largest floating photovoltaic farm—so there should be very little in this new era of renewable power and low carbon thinking that should surprise us!

The earliest work on floating turbines of which I am aware was that of Heronemus (1972), a man who was the inspiration and tutor of many of the generation of wind engineers who have now, themselves, reached retirement. Even today his multi-rotor floating concept looks ambitious (see Heronemus 1972). How much more so would it have seemed in 1972. It could be that the present modern approaches are still far too cautious to fully capture the potential of the wind. In Heronemus's day the power of the individual turbines in his array was measured in kW. If we now replace those kW machines with, say, 6 MW turbines then the single floating body that he proposed would be rated at 120 MW or thereabouts.

Onshore wind turbines have now become commodities. They will continue to improve and the electricity which they produce will continue to be become cheaper and cheaper, and more and more reliable, but a major quantum leap is not envisaged. However, offshore we are far from that position even for the ground-mounted turbines. Offshore we are free from the constraint of being good neighbours, rotors can rotate faster, be down-wind and have two blades. The turbines can be as big as the vessels and cranes allow. The theoretical limit for the diameter of a rotor (the diameter at which a blade might buckle under its own weight) is measured in kilometres not in metres. If you further remove the constraint of conventional foundations by making them float, then the only limit is the engineers' imagination. In another few decades Heronemus may look cautious rather than ambitious.

Now consider the designs which can trace their heritage directly to the present day. The earliest serious considerations started in a university in Japan. For some considerable years the researcher was a lone voice exploring what, then, was seen as an eccentric idea with little technical or financial merit. Two key parameters which have a strong effect on offshore wind farm cost are distance from shore and

water depth. In Japan the water becomes very deep very quickly and hence it is no surprise that the early investigations were undertaken in that country. It is worth remembering that, in those days, wind energy in itself was seen as somewhat naïve and eccentric, offshore wind turbines even more so and hence floating offshore activity was on the verge of madness. Engineers engaged in the development of onshore wind were still being patronised by conventional generators and being told and *when they grew up* they would realise that the only way to make electricity in serious quantities was by burning fossil fuels or through nuclear or hydro. How things have changed in a few decades!

At the same time, of course, the exploration of oil fields using floating rigs was well established. It is interesting to investigate how these two areas of activity have collaborated or, indeed, ignored one another. In the early days of ground-mounted offshore turbines they were very much in two camps. The wind energy industry considered that it was competent at building wind farms and, to do the same thing offshore was simply an extension of the onshore expertise. The offshore oil fraternity took the view they could build anything anywhere. Was an offshore wind farm just a wind farm which happened to be offshore, or was an offshore wind farm an offshore structure that happened to be a wind farm? In fact, it took quite a long and painful process to recognise that offshore wind farming was indeed a discipline in its own right. The oil industry was used to building single, huge structures whose revenue stream was so commensurately huge that the capital cost of the structure itself was of secondary importance. Offshore wind farms, however, are very cost sensitive and consist of multiple—hundreds or even thousands—of similar structures. The coalescence of these two technologies has only happened in the last few years. The most recent offshore wind farms to be built have by and large been delivered on time and on budget. That was not the case for the earlier projects.

There was early governmental interest in offshore wind in the UK going back to the 1970s, sometime before serious interest was shown by other European countries or indeed further afield. In the UK, the Department of Energy was a generous funder of technological research in the early 1980s. One result of this research was the demonstration of the high cost of the offshore substructures and the strong dependence of cost on water depth. As a result, a specific project called FLOAT was initiated to investigate floating offshore wind. It was conducted by a small consortium of Tecnomare (UK) Ltd (Tecnomare), BMT Offshore Ltd (BMT) and Garrad Hassan and Partners Ltd (GH). Tecnomare is a UK subsidiary of an Italian offshore consultant working primarily in the oil industry; BMT is a well-established research laboratory dealing with offshore technology and specifically hydrodynamics; GH was a specialist wind energy consultant, now part of DNV GL, with specific expertise in turbine design. The work of this consortium was the first serious, quantitative investigation of floating offshore turbines and associated wind farms. It represents the first attempt at a marriage between the wind industry and the oil and gas technology of the time. It made an effort to consider the whole spectrum of challenges represented by this new technology including not only engineering but also legal, environmental, manufacturing and logistics. A summary report of this project is provided by Tong (1994).

It is interesting to note that, even as long as 20–25 years ago, the main motivation for offshore wind was the perceived lack of space in Europe which presented an obstacle to the full exploitation the wind potential. At the time of the initiation of the FLOAT project, some early and tentative steps had been taken in conventional offshore wind in both Denmark and Sweden. These projects were, of course, fixed structures in relatively shallow water. It was recognised that the limitation to the shallow water sites was an important one.

The FLOAT project was divided into three phases. Phase 1 was a preliminary design stage to define the configuration as a whole. A range of floater concepts were considered, both conventional and unconventional. The unconventional systems included a semi-submersible, a doughnut shape and a catamaran. The turbine configuration was also examined and some additional freedom was allowed which would not have been available for onshore projects in particular the use of high speed rotors on slender blades. It was however recognised that this project should not concentrate on the turbine but rather on the support structure and moorings.

For the more detailed work, in Phase 2, a conventional design in the form of a Spar buoy was selected. It was recognised that, although the best currently available analyses were used for the design, the complexity of the structure and its dynamic interaction with both the wind and the waves was difficult to model. Dynamic analysis tools aimed at the proper prediction of aeroelastic and hydrodynamic behaviour of floating wind turbines are now well developed. Then there were tools for quite accurate aeroelastic analysis of onshore wind turbines and hydrodynamic analysis or offshore floating structures, but the two had not been combined. Their combination was beyond the scope of the FLOAT project. For that reason, and because BMT was an experienced test centre, a testing phase, Phase 3 involved quite comprehensive testing in a towing tank. The proper consideration of the model and the various inputs proved to be a demanding and difficult problem.

The rudimentary dynamic analysis that was undertaken concluded that the influence of wave loading on the floater and on the fatigue of the rotor and drive train was minimal. More modern analysis confirms this conclusion. The tower structure was considered to be more sensitive to the wave loading. That analysis also concluded that, as a result of the very low solidity of the rotor, the extreme loads were likely to occur during the operation.

This project was European based and hence two European sites were chosen for consideration: one in the Northern Irish Sea and one in the central Aegean Sea. BMT undertook a quite detailed investigation of the site conditions of these two sites and derived a comprehensive set of design parameters: joint probability of wave height and wind speed and significant wave height. The 50-year design wave was determined using the Department of Energy guidance notes (Department of Energy 1990). The extreme and fatigue loads were analysed using a spectral approach and the conventional JONSWAP wave spectrum. Since deep water of the order of 50–300 m was being considered breaking waves were thought unlikely to be design drivers and were ignored.

The design selected for further analysis is shown in Fig. 2. The turbine was a three-bladed design rated and 1.4 MW with a diameter of 60 m. The hub height was 45 m above the still water level (SWL). The steel tripod tower was bolted onto the deck of the cylindrical concrete buoy. By modern standards this turbine was rather small for offshore duty and its hub height rather low. At the time the diameter was considered quite large and the hub height was deliberately chosen to be small in order to minimise the overturning moment on the Spar buoy. Dynamic stability turned out to be a major consideration in the design. Some considerable effort was therefore made to reduce both the nacelle mass and the hub height. Quite extensive dynamic analysis was undertaken but, given the tools available at that time, the approach proved inadequate to capture the dominant dynamic behaviour.

The only innovative elements of the turbine design were a free yawing concept and a fast rotating downwind rotor. This choice of yaw system was made because there was concern that the floater and the associated moorings would not be able to provide sufficient reactive torque. It is interesting to reflect that, although rotor
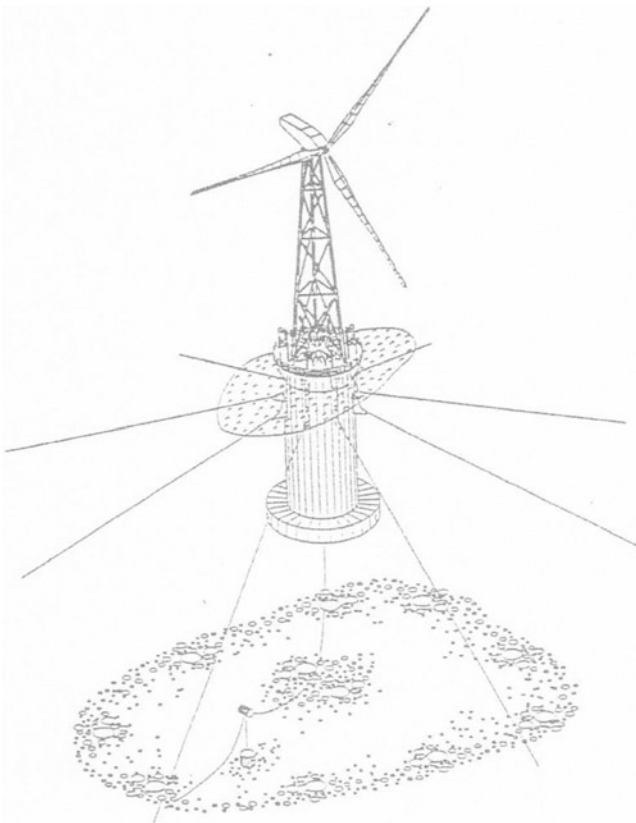

Fig. 2 FLOAT design—perspective view (Tong 1994)

speeds have become faster offshore, to date no modern turbines have adopted either the downwind configurations or the free yaw concept—perhaps they are being too conservative. The combination of free yaw and downwind is, of course, a linked approach and free yaw is probably not possible with an upwind rotor. Subsequent analysis after the design was complete indicated that sufficient yaw reaction would, in fact, have been available for the use of active yaw. The maximum tip speed of 120 m/s is still quite high even by modern standards. The nacelle mass was 51 t. The final buoy design had 3570 t displacement and consisted of a circular cylinder 12 m in diameter and 28.5 m in height and 780 t of ballast was required. The ballast consisted of concrete at the bottom and foam at the top.

This design was intended for water depths between 75 and 500 m. The mooring system was of course a critical part of the design. The mooring lines were catenary chains or taut wire synthetic fibre rope—the choice depended on water depth. Mooring lines were connected to pile anchor points on the seabed thus allowing turbines to share mooring points. Considerable thought was given to the detailed design of the tensioning systems.

The turbine design was placed in a small wind farm consisting of three arrays of three machines. Most turbines in the array shared either two or four mooring lines. There was a lot of discussion about the level of redundancy needed in the mooring lines in order to meet the Department of Energy Guidelines. This level of redundancy created significant extra cost compared to what might be thought practical. It is interesting to note that this matter is still one of heated debate. The question remains, not just for floating wind turbines, but for wind turbines in general—what is the correct safety factor to use for wind turbines offshore or onshore, floating or fixed? What are they? Do they risk human life? Do they represent environmental risks? They are not ships and they are not oil rigs. In terms of future cost reduction and full scale exploitation, this question needs to be carefully explored and a favourable conclusion reached.

The system was proposed to generate at 3.3 kV and connect to a subsea transformer. Transmission to shore was at 33 kV. A mixture of static and dynamic cables was used. A configuration of submerged buoys and anchor points was adopted. No consensus has yet appeared about the location of the local transformers. It will be interesting to see if the approach adopted by FLOAT becomes standard practice.

Detailed consideration was given to the fabrication and installation using equipment which was available at that time. Two concepts for floatation and delivery were considered: one in which the floater was essentially towed to the site and the other a dry approach with the floaters placed on the barge. The smaller size of this design, as compared to those of the present day, gave more freedom in this respect. Initial placement at the buoy in the mooring was followed by gradual tensioning of the lines in opposing pairs.

A brief environmental impact assessment of the project was undertaken. It was concluded that the main physical environmental effects would occur during the installation phase, small areas of the seabed would be damaged due to the piling of

the anchors and trenching of the cables. It was a far cry from the level of environmental investigation which now is considered standard.

An unusual feature of this project was the inclusion of model tests at a 1:48 scale. The model was subject to the joint impact of wind and waves. The test took place in BMT's towing tank and its purpose was to investigate the dynamic behaviour of the system as a whole. The three-dimensional motion of the floater and turbine assembly were all measured.

These tests were difficult to perform because of the mechanical complexity of the model and the need to excite it simultaneously by both wind and wave. In some conditions the model was found to execute very large motions. Given the relatively crude tools available at that time to model the whole system mathematically the tests were also difficult to interpret. These tests, although very interesting, posed more questions than they answered. Observation of the turbine in the tank certainly led to the conclusion that very careful dynamic analysis would be needed before building a prototype!

It was recognised that the mooring system was likely to be an expensive solution compared with the designs in shallow water using foundations attached to the seabed. The cost estimates were therefore considered carefully.

The site selected was in the North Irish Sea, 10 km from shore in 100 m water. The nominal wind farm output was 12.6 MW. The overall capital cost of the farm was approximately £30 million or £2.4 million/MW in 1994 currency. After adjusting for inflation the estimated cost would be £4.3 million/MW today. The different elements of cost, in percentage terms, for the FLOAT wind farm of 12.6 MW was: moorings 28 %; buoy fabrication 19 %; turbines 18 % and power cables 15 %.

The FLOAT project may reasonably claim to mark the beginning of serious consideration of floating offshore wind. The design options evaluated, the resulting solutions and, indeed, the cost estimates are not far removed from today's projects. Some of the more innovative ideas have not yet been adopted. The biggest change between undertaking a design then and now is the greatly improved prediction capability. It will be key to the proper design of these complicated dynamic structures.

It took the tragic events of Fukushima to provide one important stimulus to start the development of floating offshore wind turbines in earnest. At the same time activity was starting in the Nordic countries for quite different reasons. The early days of floating wind, as briefly described here, are not very long ago aside, perhaps, from the work of Heronemus. The technology has moved from naïve eccentricity to the verge of industrial deployment in just twenty years. By 2036 when, we shall have to be well on our way to zero carbon electricity generation by every means available, floating wind may be a standard way to produce electricity. The staggering characteristics of renewable energy are not just that it is clean and relies on free, inexhaustible fuel but also that its speed of development is extraordinary. The next couple of decades should be very interesting—perhaps during that period we can realise Heronemus's 1970 aspirations.

3   State of the Floating Offshore Wind Industry

Mairéad Atcheson

The floating offshore wind industry is in its infancy, with the majority of work in the sector completed to-date in the research and development phase. In more recent years, as the industry begins to progress and mature, prototype devices have been deployed. An overview of some of the prototype FOWT devices that have been deployed is presented in Chapter "State-of-the-Art". This section provides a summary of some early research activities in the floating wind sector and an overview of some the more recent large publicly funded research projects helping to move the industry forward.

3.1   Early Research Activities

The concept of floating offshore wind turbines has existed since the 1970s, when Professor William E. Heronemus first proposed the idea of an array of wind turbines supported on floating buoys (see Sect. 2). However, it was not until the early 1990s, that the industry started to research the idea in more detail. Section 2 already describes one of the first research projects undertaken to investigate the feasibility of floating wind turbine systems, the FLOAT project. Another study carried out in the UK by a group at University College London (UCL) in collaboration with W.S. Atkins and ECN (Energy Research Centre of the Netherlands) was the Multiple Unit Floating Offshore Windfarm (MUFOW) project, which investigated the possibilities of installing several turbines on a single structure (Henderson et al. 2000). Results from the MUFOW project present the main advantages and disadvantages of the multiple turbine arrangement compared to a single unit (Barltrop 1993). Figure 3 presents an illustration of one of the MUFOW multi-turbine arrangements considered during the project.

Around the same period of time, a group in Milan developed and investigated the ELOMAR concept, which placed a single turbine on to a toroidal-shaped float, with tensioned moorings (Bertacchi et al. 1994). The complex platform shape was originally chosen to minimise the wave motion response of the structure, but had the drawback of being difficult and expensive to build.

A detailed feasibility study, *Drijfwind* or *FloatWind* was performed in The Netherlands by a consortium led by TNO and including ECN, MARIN, Lagerwey the WindMaster and TUD MSC (Bulder et al. 2002). The project presented a comprehensive study of the technical and economic feasibility of floating offshore wind energy systems, reporting on ancillary issues such as grid connection and operation and maintenance (O&M). An in-depth analysis into various floating wind concepts identified the semi-submersible triple floater (shown in Fig. 4) as the most

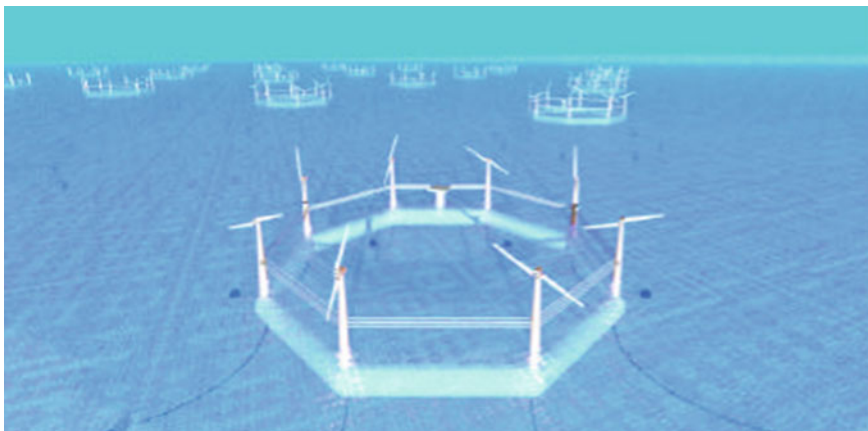**Fig. 3** Artist impression of a non-weathervaning MUFOWs (courtesy of Andrew Henderson)

Fig. 4 Tri-floater concept
from the Drijfwind project
(Bulder et al. 2002)

suitable for the conditions considered. Conclusions from the study indicated that the
technology may not be ready for commercial application at the time, but that the
margin to the economic viability of the technology was getting closer (Henderson
et al. 2004).

A number of TLP floating wind technologies were also undergoing development during the 2000s, including a three-leg star TLP at Marseille Engineering University (Molin et al. 2004) and a similar TLP concept investigated by the Massachusetts Institute of Technology (MIT) and the National Renewable Energy Laboratory (NREL) in the United States (Sclavounos 2004). In Germany, the engineering consultancy Arcadis were also developing a floating concept suitable for relative shallow waters, such as those in the Baltic Sea, with a tension-leg design and concrete gravity anchoring considered. Blue H technologies, a European multi-national technology developer, were the first to install a large-scale TLP floating wind turbine off the Italian coast in 2008.

Semi-submersible floating offshore wind technologies were also under investigation during the same period. A French consortium of Nass & Wind, Saipem and DCNS, together with a number of consultants, developed a semi-submersible floating foundation, the Winflo device. Whilst a Norwegian consortium investigated a multi-turbine concept, WindSea based on a tri-floater design but with a turbine on each column inclined outwards and the third turbine in a downwind position. A review of the floating offshore wind projects is presented in the Main(e) International Consulting LLC (2012) report, including further information on the Winflo and WindSea projects mentioned previously.

3.2 Collaborative Research and Development Projects

In recent years, a number of projects with large consortiums have been conducted, researching various aspects of floating offshore wind technologies. A brief overview of some of the large publicly funded research and development (R&D) projects and initiatives carried out by the industry is provided.

UpWind was a European funded project that investigated the possibility of up scaling wind turbines (up to 20 MW) both onshore and offshore (Fichaux et al. 2011). The project was composed of a consortium of 40 partners, led by the Risø National Laboratory (DTU) and ran between 2006 and 2011. Task 2 of work package 4 (WP4.2) focused on support structure concepts for deep-water sites, which included floating and bottom mounted compliant structures. The final report produced under WP4.2 reviews and compares several floating support structure concepts including a semi-submersible, TLP and spar buoy (De Vries et al. 2011). The concepts are compared based on statistics, extreme events analysis, instabilities and fatigue life evaluations. Results from the study found that: the simple barge (semi-submersible) floater may prove cost effective in benign sea conditions; the spar buoy is better suited for harsh conditions, but the structure is relatively more expensive; in terms of ultimate strength and fatigue consideration, the TLP performed the best, but the installation procedure and the large mass make it an expensive structure (De Vries et al. 2011).

DeepCwind is a consortium established in the United States in 2010 and led by the University of Maine. It is composed of over 30 members from a broad range of

sectors, including universities, utilities, manufacturing firms, with a common aim of developing deep water offshore wind technology. The DeepCwind research objectives span from environmental impact assessment studies to the fabrication and deployment of FOWTs. The project is organised into successive phases; the design and testing of a 1:3 scale floating turbine prototype at the Monhegan test site, followed by the design and deployment of a full-scale turbine prototype and culmination with the construction of a number of commercial floating wind farms. As a part of the initial phase, tank tests were carried out in the MARIN basin in The Netherlands on 1/50th scale models of a semi-submersible, TLP and spar. A case study providing details on the DeepCwind testing at MARIN is presented in Chapter "Modelling of Floating Offshore Wind Technologies", Sect. 6.

The HiPRWind (High Power, High Reliability Offshore Wind Technology) project was a 5-year European funded project focused on the development of future deep water technologies based on floating systems (Quesnel et al. 2011). The project consortium was composed of 19 European partners, led by Germany's Fraunhofer Institute for Wind Energy and Energy Systems (IWES). One of the main objectives of the project was to install a 1:10 scale model of a future 10 MW commercial scale floating wind turbine. In June 2015, the HiPRWind project was terminate. It had been planned to install and use the 1.5 MW-scale HiPRWind floating test platform at an offshore site near Trondheim (Norway). This aspect of the project was due to be completed in collaboration with a national research infrastructure project FlexWT (Floating Experimental Wind Turbine), which would take over the facility following the end of the HiPRWind project. However, the FlexWT project was not completed, and without this collaboration it was no longer possible to continue the HiPRWind work.

Finally, the DeepWind project was a European funded project led by the Technical University of Denmark (DTU), which ran from 2010 to 2014. The objective of the project was to explore technologies needed to develop a simple floating offshore concept with a vertical axis rotor and a floating and rotating foundations. The project consortium includes partners from across Europe and the USA from various organisation types including: universities, companies and research centres. Further information on DeepWind project is presented in Chapter "Overview of Floating Offshore Wind Technologies", Sect. 2.

4 Chapter Layout

The introductory chapter (this chapter) presents the main objectives of the book and provides an historical overview of the offshore engineering and floating wind energy industries. Section 1 presents an overview of the evolution of the offshore engineering industry, highlighting the lessons learnt from the offshore oil and gas sector and the potential synergies with the development of the FOWT industry. Written by a prominent expert in the wind energy sector, Sect. 2 provides an insight into the early days of floating offshore wind turbine developments. Finally, in

Sect. 3 an overview of the state of the floating wind industry is presented, including a brief summary of some of the research and development activities undertaken to-date.

Chapter "The Offshore Environment" describes the offshore resource, including meteorological and oceanographic conditions, to establish the environmental design basis for an offshore structure at a proposed installation location. Other phenomena which may be important in specific cases include (but are not limited to) ice conditions and seismic activity are also considered. Details are provided on the key environmental variables used to describe the environmental site conditions. This information is critical to the design of a FOWT, as it is required to estimate the environmental loads acting on device and assess the behaviour of a structure subject to these loads.

A review of the key technology components that can be directly related to a floating wind turbine, namely the floating platform, wind turbine oprtions and mooring systems are presented in Chapter "Overview of Floating Offshore Wind Technologies". The fundamental characteristics of different floater concept designs are assessed and compared in Chapter "Overview of Floating Offshore Wind Technologies", Sect. 1. Chapter "Overview of Floating Offshore Wind Technologies", Sect. 2 presents a high level comparison of the wind turbine options available, namely horizontal axis wind turbines (HAWTs) which are most commonly used by the wind industry, and vertical axis wind turbines (VAWTs). Chapter "Overview of Floating Offshore Wind Technologies", Sect. 3 describes the various mooring systems which can be used to maintain the position and orientation of a FOWT.

Chapter "Modelling of Floating Offshore Wind Technologies" describes the modelling options for FOWTs, presenting an overview of numerical and experimental approaches applied. Loads on a FOWT are a function of several processes (waves, wind, structural motion, mooring tension, etc.) occurring simultaneously and interacting with one another, which result in fluid forces on the structure. A primary objective of a FOWT model is to determine the net forces on the structure, to inform the design loads required for structural analysis and detailed design of a device. The different modelling components required for a FOWT include: aerodynamics; hydrodynamics; mooring dynamics; structural analysis; and the input environmental conditions. A description of the different modelling theories used in design codes to model the dynamic response of FOWTs are presented in Chapter "Modelling of Floating Offshore Wind Technologies", Sects. 1–4, respectively. Several simulation codes capable of modelling FOWTs are currently under development, Chapter "Modelling of Floating Offshore Wind Technologies", Sect. 5 presents an overview of some of the codes available. Finally, Chapter "Modelling of Floating Offshore Wind Technologies", Sect. 6 provides information on the experimental modelling of a FOWT and presents a case study on the DeepCwind testing at MARIN.

Chapter "Key Design Considerations" provides an overview of the design considerations of a FOWT and explains the link between environmental conditions and design loads, which when combined with industry standard or guideline

requirements, can be used to create site specific design load cases (DLCs) to cover a range of design situations (Chapter "Key Design Considerations", Sect. 1). A key design consideration that a FOWT system must achieve is an acceptable level of structural reliability, based on the environmental conditions that it will be exposed to. Certification is a means of providing evidence that certain standards for a FOWT have been met with respect to structural safety. An overview of the certification process and dedicated standards for FOWT technologies are presented in Chapter "Key Design Considerations", Sect. 2.

Chapter "State-of-the-Art" presents the state-of-the-art in the FOWT industry. As a relatively new sector, only a few prototype devices have been deployed in recent years. A description of some of the FOWT technologies that have reached the prototype stage are provided by the associated technology developers. The technologies presented include: Principle Power's semisubmersible WindFloat device (Chapter "State-of-the-Art", Sect. 1); the Hywind spar under development by Statoil (Chapter "State-of-the-Art", Sect. 2); the Goto Island project in Japan (Chapter "State-of-the-Art", Sect. 3) and the Sway system (Chapter "State-of-the-Art", Sect. 4). The information presented for each technology includes a description of the device, the concept development process and prototype testing campaigns, and in conclusion a summary of the commercialisation route planned for the technology is presented.

Finally, Chapter "Looking Forward" examines the future prospects for the FOWT industry, providing an overview of current global market activities and potential commercial applications envisaged for FOWT technologies. In recent years, significant progress has been made to prove FOWT technologies through prototype deployments (as presented in Chapter "State-of-the-Art"). This ongoing work acts to increase confidence in FOWT technologies and attract more industry player to the sector. However, to achieve the necessary investment to drive the technology forward technical, political and economic barriers need to be address. Chapter "Looking Forward" concludes with a brief overview of some of the potential barriers faced by the industry and an overview of the future outlook.

References

Barltrop N (1993) Multiple floating offshore wind farm (MUFOW). Wind Eng 70(4):183–188

Bax JD, de Werk KJC (1974) A floating storage unit designed specifically for the severest environmental conditions. Society of Petroleum Engineers (SPE), Paper 4853

Bertacchi P, Di Monaco A, de Gerloni M, Ferranti G (1994) Eolomar—a moored platform for wind turbines. Wind Eng 18(4):189

Bulder B, van Hees M, Henderson AR et al (2002) Studie naar haalbaarheid van en randvoorwaarden voor drijvende offshore windturbines. Drijfwind Report—ECN, MARIN, Lagerwey the Windmaster, TNO, TUD MSC, December 2002

Burleson CW (1999) Deep challenge! The true epic story of our quest for energy beneath the sea. Gulf Publishing Company, Houston

De Vries WE, Vemula NK, Passon P et al (2011) Final report WP 4.2: support structure concepts for deep water sites: deliverable D4.2.8 (WP4: offshore foundations and support structures). UpWind project, March 2011

Department of Energy (UK) (1990) Offshore installations: guidance on design, construction and certification. Consolidated Edition 1990, HMSO, Norwich

European Wind Energy Association (EWEA) (2016) The European offshore wind industry—key trends and statistics 2015. A report by the European Wind Energy Association, Feb 2016

Fichaux N, Frandsen S, Sorensen JD (2011) UpWind design limits and solution for very large wind turbines, a 20 MW turbine is feasible. UpWind final report, Mar 2011

Fisher FH, Spiess FN (1963) FLIP-floating instrument platform. J Acoust Soc Am 35:1663–1644

Halkyard J (2005) Floating offshore platform design. In: Chakrabarti SK (ed) Handbook of offshore engineering, vol 1. Elsevier, Amsterdam

Henderson AR, Watson GM, Patel MH, Halliday JA (2000) Floating offshore wind farms—an option? In: Proceedings of the offshore wind energy in mediterranean and other European seas, Siracusa, Sicilia, Italy, Apr 2000

Henderson AR, Zaaijer MB, Bulder B (2004) Floating windfarms for shallow offshore sites. In: Proceedings of the international society of offshore and polar engineers conference (ISOPE), Toulon, France, 23–28 May 2004

Heronemus WE (1972) Pollution-free energy from offshore wind. In: Proceedings of the 8th annual conference and exposition marine technology society, Washington DC, USA, 11–13 Sept 1972

Main(e) International Consulting LLC (2012) Floating offshore wind foundations: industry consortia and projects in the United States, Europe and Japan—an overview. Main(e) International Consulting LLC, Sept 2012

Molin B, Remy F, Facon G (2004) Etude expérimentale du comportement hydro-aéro-elastique d'une eolienne offshore sur ancrages tendus, Ocean Energy Conference, Brest France, 20–21 Oct 2004

Pratt JA, Priest T, Castaneda CJ (1997) Offshore pioneers: Brown & Root and the history of offshore oil and gas. Gulf Publishing Company, Houston

Quesnel L, Bard J, Hanssen JE (2011) Introducing HiPRWind, high power, high reliability offshore wind technology. In: Proceedings of the European wind energy association conference (EWEA), Brussels, Belgium, 14–17 Mar 2011

Sclavounos PD (2004) Deep water floater concepts for offshore wind turbines: design, modeling and testing. Presented at the deepwater wind energy research & planning workshop, Washington D.C., USA, 26–27 Oct 2004

Tong KC (1994) Technical and economic aspects of a floating offshore wind farm. J Wind Eng Ind Aerodyn. In: Proceedings of the OWEMES seminar. Rome, Italy, 24–25 Feb 1994

The Offshore Environment

Lucy Cradden, Pauline Laporte Weywada and Mairéad Atcheson

An accurate assessment of the offshore environment, including the meteorological, oceanographic and other relevant environmental conditions, is fundamental to the design of FOWTs. Using this information, the environmental loads acting on a device may be estimated, and the behaviour of a structure subject to these loads for both operational and extreme events can be predicted.

The characterisation of the offshore environmental and the creation of a metocean design basis for projects involving FOWTs will necessarily cover the site's offshore wind resource, the local wave climate and other key parameters such currents. All of these aspects are reviewed in detailed in Sects. 1–3 (respectively), where a brief description of the physics associated with each type of environmental input is presented alongside details on how to measure and map the resources.

L. Cradden
School of Earth Sciences, Energy Institute, University College Dublin, Dublin, Ireland
e-mail: lucy.cradden@ucd.ie

P.L. Weywada · M. Atcheson (✉)
Cruz Atcheson Consulting Engineers Lda, Lisbon, Portugal
e-mail: Mairead.atcheson@cruzatcheson.com

P.L. Weywada
e-mail: pauline.laporte-weywada@cruzatcheson.com

1   Offshore Wind Resource

Lucy Cradden

1.1   Origins of the Resource

The Origins of Wind

Wind energy is an indirect form of solar energy caused by the heating of the earth's surface by the sun. As the air above the surface absorbs the heat, it expands and the pressure falls. This lower density parcel of warm air then tends to rise. Cool air has a higher pressure due to its higher density, and it therefore tends to sink. The process of heating is uneven over the surface of globe—the equator receives more heat than the poles due to the relative positions of the earth and the sun. Landmasses also tend to heat up and cool down more quickly than bodies of water. This uneven heat distribution means different air masses will have different temperatures and pressures on both a large and small scale. In order to try and restore equilibrium, air will then tend to move from areas of high pressure to those of low pressure, thereby creating wind.

Further movement is induced by the spinning of the planet. As the earth rotates on its own axis, the path along which the air is moving appears to deflect relative to the surface. This is known as the Coriolis effect and leads to winds appearing to veer to the right of their direction in the northern hemisphere, and to the left of their direction in the southern hemisphere. The effect is largest at the poles and minimal at the equator.

Global Wind Patterns

In general, air will tend to move from the high pressure, cold poles to the low pressure, warm equator. This movement away from the poles generates polar winds that turn due to the Coriolis effect, and thus tend to an easterly direction (blowing from the east). As the warm air at the equator is heated, it rises and spreads. As it spreads pole-wards, it cools, and begins to sink again at around a latitude of 30°, and the pressure increases. Some of it is then drawn back towards the equator, forming the 'trade winds'. Because of the Coriolis effect, the trade winds will tend to turn from a northerly (in the northern hemisphere) or southerly (in the southern hemisphere) direction (i.e. coming from the north or from the south) to blow parallel to the equator in an easterly direction (from the east). The air that continues to move towards the poles from 30° to 60° latitude forms what are known as the 'westerlies', as the Coriolis effect causes them to tend to curve and blow in a westerly direction. A schematic of the overall trend in global winds is shown in Fig. 1.

Winds High in the Atmosphere

The movement of any fluid over a surface will be affected by friction. At a point far above the surface of the earth, typically between 500 and 1000 m, the influence of friction on the air flow is diminished. At this point, when the Coriolis effect and the
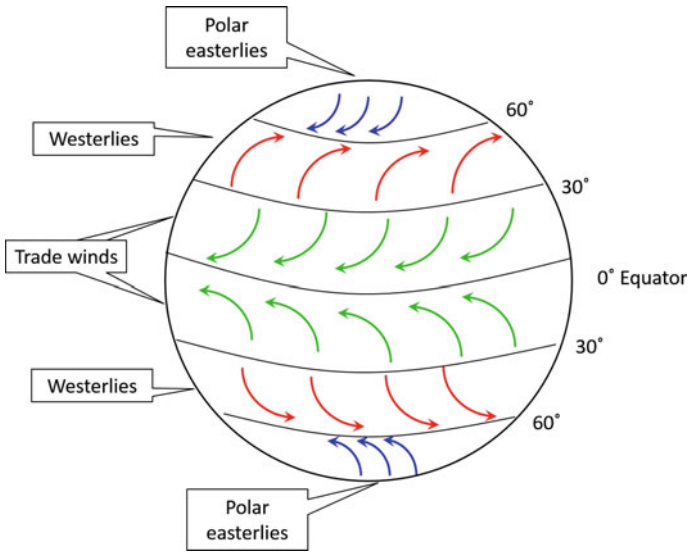
Fig. 1 Schematic diagram of global wind patterns (after Strahler and Strahler 1992)

pressure gradient are balanced, the wind will tend to blow in a direction perpendicular to the pressure gradient (i.e. following the isobars—lines of constant pressure), with the low pressure to its left in the northern hemisphere, and to its right in the southern hemisphere, as shown in Fig. 2 (Barry and Chorley 1998). The wind described solely by the balance between the influence of the pressure gradient and the Coriolis effect is known as the 'geostrophic wind'.
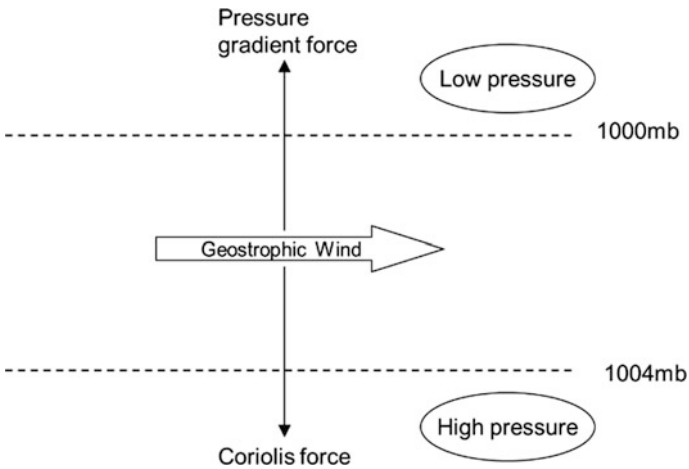

Fig. 2 Geostrophic balance in the northern hemisphere

The magnitude of the geostrophic wind, G, is given by:

$$G = \frac{1}{f\rho} \cdot \frac{dp}{dn} \tag{1}$$

where f is the Coriolis parameter which varies with latitude, ρ is air density and $\frac{dp}{dn}$ is the mean sea level pressure gradient. If the mean sea level pressure pattern for a region is known, it is possible to calculate the geostrophic wind velocity, which is representative of a hypothetical wind with no interaction with the surface. In actual fact, isobars are very often not parallel but circular, forming around a low or high pressure centre, and this leads to an additional centripetal acceleration. Balanced flow will be achieved in this situation with winds rotating anticlockwise around a low pressure centre in the northern hemisphere and clockwise around a high pressure centre (Barry and Chorley 1998). These winds are known as the gradient winds.

Localised Features of the Wind Resource

Geostrophic flow is only representative of wind conditions far above the earth's surface. In order to understand the wind velocity—and thus the available wind energy resource—at the height of a wind turbine, surface effects must be accounted for. The presence of obstacles, height changes and the wider characteristics of the terrain over which it is flowing can all influence the wind up to hundreds of metres from the surface.

Considering firstly the topography of the area in which the wind is blowing, account must be taken of the presence of hills, valleys, cliffs, ridges and other height changes in the surface. Coastal breezes are caused by the different heating and cooling patterns of the land and the sea. As the land heats up more rapidly than the sea during the day, the warm air onshore tends to rise and there is a drop in pressure. This draws in cooler, denser air from over the sea causing an onshore breeze. At night, the process reverses—with the land cooling down more quickly, the air above it sinks and moves towards the lower pressure areas over the sea, causing an offshore breeze (Strahler and Strahler 1992). Similar effects can occur around mountains and valleys—the air within a valley will heat up during daytime and tend to rise up the slope of the mountains, and as it cools over the mountain at night, will tend to sink back down into the valley.

The local wind flow will be directly disrupted by both smooth and abrupt changes in surface height causing, for instance, flow separation behind a steep drop, or speed-up over a hill (Troen et al. 1989). The nature of the effects on the flow will depend on atmospheric conditions and the wind speed itself (Stull 1988). Far offshore, obstacles or height changes are unlikely, but in coastal regions the physical presence of beaches and cliffs can exert a strong influence on the wind speed and direction. Additionally, individual obstacles near to a particular point of interest may have an effect on the wind experienced at that point. In an offshore setting, such obstacles could be the platform on which the measurement is being taken or perhaps the presence of local islands or a nearby coast.

Table 1 Standard roughness lengths assumed for different types of terrain (World Meteorological Organisation 2008)

Terrain description	z_0 (m)
Open sea, fetch at least 5 km	0.0002
Mud flats, snow; no vegetation, no obstacles	0.005
Open flat terrain; grass, few isolated obstacles	0.03
Low crops; occasional large obstacles, x/H > 20	0.10
High crops; scattered obstacles, 15 < x/H < 20	0.25
Parkland, bushes; numerous obstacles, x/H ≈ 10	0.5
Regular large obstacle coverage (suburb, forest)	1.0
City centre with high- and low-rise buildings	≥ 2

Another feature that affects the wind resource is the surface itself. When the air moves against the surface of the earth, its velocity is reduced due to friction with the ground. The magnitude of the frictional force is dependent on the characteristics of the particular surface in a location. These characteristics are summarised by the term *roughness length*, which is the theoretical height above a surface at which the effect of friction reduces the wind to zero velocity (American Meteorological Society 2015). Areas with a larger value of surface roughness will cause a greater reduction in the wind velocity and it will theoretically reach zero at a height further from the ground. Water typically has a lower characteristic surface roughness length than might be found onshore and is often given a constant value of 0.0002 m (see Table 1).

In reality, the roughness length at sea varies according to the impact of changes in wind speed on wave conditions, and is therefore not truly constant. The Charnock formula is often used to describe sea surface roughness, z_0, in the following form (Fairall et al. 1996; Lange et al. 2004),

$$z_0 = \alpha \frac{u_*^2}{g} \qquad (2)$$

where α is a constant found from empirical measurements, u_* is the friction velocity (a measure of wind stress on the ocean) and g is acceleration due to gravity. The constant, α, is given a range of values in the literature, for example 0.0185 (Lange et al. 2004) and 0.012 (Peña et al. 2009).

The Charnock formula is generally applicable in fully-developed seas where the wind is blowing at reasonable strength over a large fetch but has been shown to break down in low wind conditions (Fairall et al. 1996). A number of extensions to the formula have been developed to account for the effects of different conditions on sea-surface roughness (Lange et al. 2004).

Vertical Profiles

The frictional and physical influences on the wind caused by the surface diminish with height above the surface, and the wind will generally increase in velocity with height. At some point far enough above the surface, normally between 500 and 1000 km, the wind will approach geostrophic conditions.

The effect of thermodynamics on the vertical air flow requires some additional consideration. As the ground is warmed by the sun during the daytime, the air above it is heated, and as it loses density the parcel of air will begin to rise upwards. Under what are known as *stable* conditions, as it rises, the air reaches a lower temperature than the surrounding air and will tend to fall back down again. A larger increase in wind speed with height is usually seen with a stable atmosphere. Under *unstable* conditions, the rising parcel of air cools but stays at a slightly higher temperature than the surrounding air and will continue to rise higher in the atmosphere. The change in wind speed with height will be lower than for stable conditions. The third condition is known as *neutral*, and in this case, the rising air maintains the same temperature as the surrounding air (Burton et al. 2001).

The change in wind speed with height above the surface is referred to as wind shear. Analysing the wind shear is an important part of a typical site assessment for wind for two main reasons—firstly, when taking measurements at a height that is not the hub height of the wind turbine, so that the measurements can be transposed to the correct height, and secondly when considering turbine design in order to consider loading across the turbine blades. Neutral conditions are perhaps most relevant, as they most often occur with strong winds and indicate a high degree of turbulent mixing (Burton et al. 2001). However, particularly at coastal locations, it is also important to understand the stable and unstable conditions.

In the absence of multiple measurements at a range of heights, theoretical wind profiles can be derived from measurements at one reference height. The wind speed, U, at a height above ground level, z, can be calculated for neutral stability using the following equation:

$$U = \frac{u_*}{\kappa} \left[ln \frac{z}{z_0} \right] \tag{3}$$

where u_* is the quantity known as *friction velocity* and represents the stress applied by the wind on the surface over which it is blowing, κ is the Von Karman constant and z_0 is the local surface roughness length. The derivation of this equation, known as the *log law*, is described in full in Manwell et al. (2009) and it requires a priori knowledge of the surface conditions at the measurement point. Using this equation and assuming that there are no obstacles or complex topography in the vicinity which will cause additional flow disruptions, wind speed U_{ref} measured at height z_{ref}, can be related to an unknown wind speed U at height z, using the following ratio:

$$\frac{U}{U_{ref}} = \frac{ln \frac{z}{z_0}}{ln \frac{z_{ref}}{z_0}} \tag{4}$$

where z_0 is the surface roughness length. For example, wind measurements taken at 10 m above the surface can be transposed to turbine hub-height. Accounting for

atmospheric stability requires the inclusion of an additional term in the equation derived from a principle called Monin-Obukhov theory, such that:

$$U = \frac{u_*}{\kappa}\left[ln\frac{z}{z_0} - \Psi_m\frac{z}{L}\right] \tag{5}$$

where $\Psi_m\frac{z}{L}$ is known as the *integrated stability function* and can be derived using various formulations (Lange et al. 2004). In stable conditions, the term z/L is positive and for unstable conditions it is negative. This modifies the ratio between the reference wind speed and the speed at the desired height as follows:

$$\frac{U}{U_{ref}} = \frac{ln\frac{z}{z_0} - \Psi_m\frac{z}{L}}{ln\frac{z_{ref}}{z_0} - \Psi_m\frac{z_{ref}}{L}} \tag{6}$$

The difference in the wind profile for neutral (log law only), stable and unstable (using Monin-Obukov correction) is shown in Fig. 3 using a roughness length of 0.0002 m, and where the 80 m wind speed is ~ 10 m/s, following the calculation of Ψ_m as set out in Lange et al. (2004).

Another method frequently used to describe the vertical wind speed profile is the *power law*:

$$\frac{U}{U_{ref}} = \left(\frac{z}{z_{ref}}\right)^\alpha \tag{7}$$

Fig. 3 Vertical profiles based on different stability conditions (after Petersen et al. 1998; Lange et al. 2004)
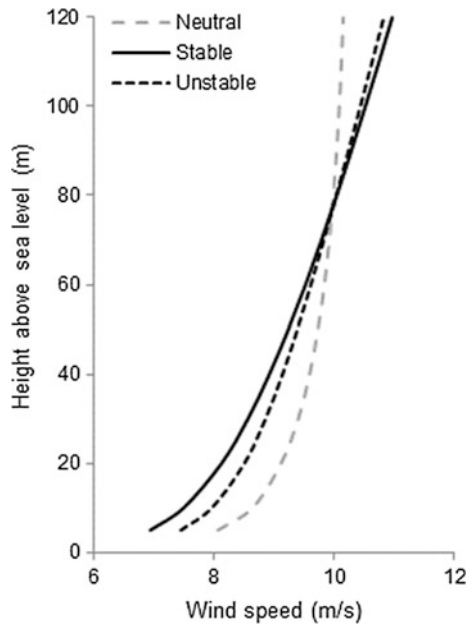
where α is referred to as the exponent, and is frequently assumed to have a value of 0.14 (Manwell et al. 2009; Petersen et al. 1998) or 0.2 (IEC 61400-1 2005). As both studies describe, the exponent can vary widely in reality, but the law is often used as a simple solution when data is not available.

Both the log law (with stability correction) and the power law have been found to incorporate error when applied offshore. Van Wijk et al. (1990) found that applying the Monin-Obukhov stability correction to the logarithmic profile assumption for locations in the North Sea improved the estimations of mean wind speed but with a degree of error remaining. Lange et al. (2004) found that for a site offshore to the south of Denmark, the Monin-Obukhov theory underestimated the increase in wind speed with height. Lange et al. (2004) suggests that the influence of the transition from land to sea in terms of the thermal effects can have an impact on wind conditions up to 100 km from the coastline, and application of a further correction to the Monin-Obukhov element can reduce the error. The author also indicates that the recommended standard assumption of 0.2 for the power law can lead to an underestimate in the wind shear. The difference in vertical profile for different exponents can be seen from Fig. 4.

Turbulence

Turbulence occurs on a number of scales within wind flow, induced by frictional and thermal effects. It can be seen as high frequency variations superimposed on a plot of measured mean hourly or half-hourly wind speeds, or as high frequency peaks in the analysis of wind power spectra. Generally, turbulent variations refer to scales of seconds and minutes, as opposed to variations that occur over hours and

Fig. 4 Vertical profiles based on the power law with different exponents (after Lange et al. 2004)
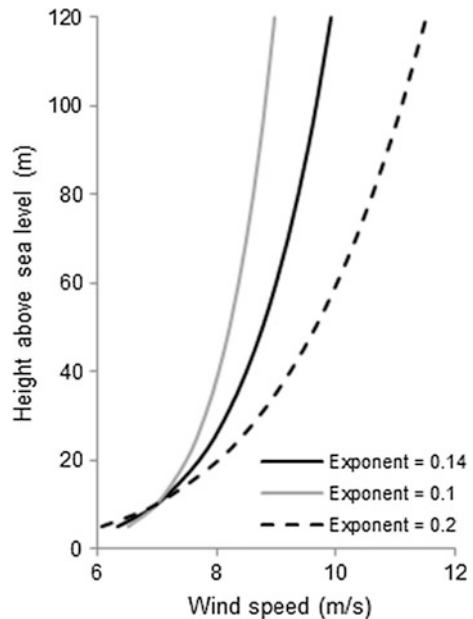
days. The characterisation of turbulence at a site is a significant part of the International Electrotechnical Commission (IEC) design requirements (IEC 61400-3 2009). Turbulence is usually quantified at wind energy sites by the turbulence intensity, *TI*:

$$TI = \frac{\sigma}{U} \tag{8}$$

where σ is the standard deviation of the 10-min mean wind speed U. Measurements should be conducted at a high sampling rate (~ 1 min) for a sufficient period of time to capture a range of potential conditions.

For the case of offshore sites obtaining suitable measurements is potentially more difficult. Petersen et al. (1998) discuss the relationship between stability, surface roughness and turbulence, and give the *TI* for neutral conditions over the sea as being around 8 %, somewhat lower than for open grassland at 13 %. Hasager (2014) also discusses the relatively low ambient turbulence in the boundary layer above the sea compared to onshore locations. The IEC state that since the sea-surface roughness increases with wind speed, the turbulence will therefore also increase (IEC 61400-3 2009). In order to calculate *TI* for design purposes, the surface roughness length, z_0 found from an adaptation of the Charnock formula (by solving Eq. 3 for u_* and replacing in Eq. 2) can be used to calculate σ:

$$\sigma = \frac{U}{ln\frac{z}{z_0}} + 1.28 \times 1.44 \times I_{15} \tag{9}$$

where I_{15} is the expected value of turbulence at a wind speed of 15 m/s, with some reference values for particular turbine designs given in IEC 61400-1 2005. However, the IEC design criteria for offshore wind turbines (IEC 61400-3 2009) states that larger values of σ than those given as reference values, have been found offshore and this assumption is therefore somewhat uncertain.

Diurnal, Seasonal and Long-Term Trends

At a given point, the average wind conditions experienced will vary throughout the day, the season and from year-to-year. The diurnal variation pattern over land for mid-latitude regions such as Northern Europe is well-documented, and generally shows that the mean speed peaks around mid-day, and is minimum at night. This is due to thermal effects caused by the heating of the land by the sun, and thus the effect peaks in summer, but is minimal in winter (Manwell et al. 2009). In complex terrain, influences such as mountain and valley breezes can change this pattern. Offshore, less diurnal variation may be expected (Plate 1982) but studies suggest it is inconsistent: some work has identified little or no diurnal variation (e.g. Coelingh et al. 1996), whilst others (e.g. Barthelmie et al. 1996) have found considerable variability in the diurnal pattern, possibly depending on proximity to land.

Seasonally, wind conditions in northern Europe display a well-known pattern of higher mean wind speeds in autumn and winter, with lower speeds in spring and summer. Some differences in this pattern are apparent in the conditions across the
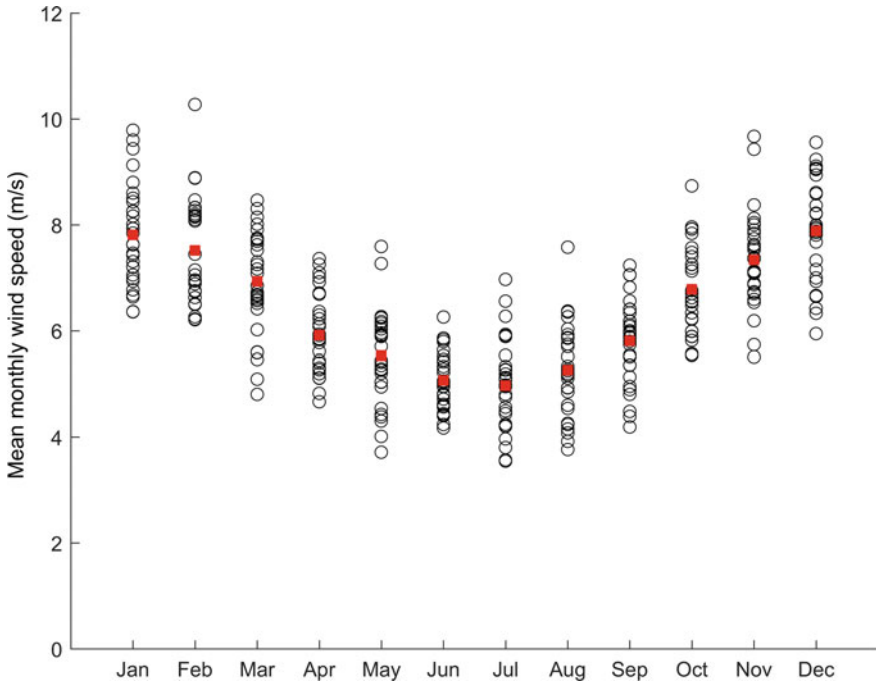
Fig. 5 Mean monthly wind speeds at a location off the coast of Cornwall from ERA-40 Reanalysis 1961–90

United States, as discussed in Manwell et al. (2009). Considerable variability can also be seen from year-to-year, and can also be significant inter-decadally. For the purposes of identifying long-term trends such as climate change influences (e.g. Pryor et al. 2005; Cradden et al. 2012), 30 years is considered to be the minimum period of study in order to capture normal inter-annual fluctuations. Figure 5 shows the monthly mean wind speeds for a 30-year period at a site off the south-west coast of England, using data taken from the ERA-40 Reanalysis (Uppala et al. 2005). The mean monthly pattern over the 30 years is shown by the filled dots, whilst each individual monthly mean is indicated by an open dot. There is a distinct, and expected, seasonal pattern but also considerable variability within the months from year to year.

Extremes

In the context of wind energy, it is critical to consider the design implications of the strongest wind conditions experienced at a site. Extreme winds are generally associated with storms, and are often defined by their *return period*, i.e. the period over which a certain level of wind speed could be expected to recur (Manwell et al. 2009). The IEC design criteria for offshore wind turbines (IEC 61400-3 2009) stipulate the requirement for the calculation of a 50-year extreme wind, which would be considered a reasonable design limit based on their expected 20–30-year

lifespan. It would be anticipated that due to the tendency for offshore winds to be higher, that offshore extreme wind speeds will also be relatively high compared to onshore. This has particular implications for turbine design and maintenance requirements.

Expected values for different return period wind speeds, where sufficient data are available, are generally found by statistical extrapolation of measurements. Using, say, 10 years of data to derive 50-year return period wind speeds can, however, incorporate uncertainty. The most widely applied method involves selecting a set of the highest occurring wind speeds in a time series (for example, the annual maxima) and fitting an appropriate distribution to these. Using the cumulative distribution function, $F(U_{annual\,maximum})$, the wind speed with a 50-year return period is that with an occurrence once every 50 years, or where $1 - F(U_{annual\,maximum}) = 1/50$ (Manwell et al. 2009). For a full explanation of methods used to select an appropriate set of extreme values and suitable distributions to fit to these, see Palutikof et al. (1999).

The IEC standard IEC 61400-1 (2005) recommends the assumption of values for the one year $V_{e,1}$ and 50-year $V_{e,50}$ return period wind speeds based on the following:

$$V_{e,50}(z) = 1.4V_{ref}\left(\frac{z}{z_{hub}}\right)^{0.11} \tag{10}$$

$$V_{e,1}(z) = 0.8V_{e,50}(z) \tag{11}$$

where z is the height at which the extreme value is being estimated, z_{hub} is the hub height of the turbine and V_{ref} is the reference wind speed provided by the turbine manufacturer and relates to the *class* of wind turbine into which the particular design fits (see IEC 61400-1 2005). Comparison of the statistical predictions and these values will help to inform the suitability of a turbine design for a particular location.

Considering specifically offshore wind turbines, combinations of extreme winds and extreme waves require additional analysis to understand maximum loads on the structure. The IEC indicates in IEC 61400-3 (2009) that it is unlikely that extreme winds and extreme waves will occur together, and for the purposes of design loads, extreme waves can be combined with a reduced version of the extreme winds.

1.2 Measuring the Resource

Typically, measurement of the wind resource involves recording the variation in time of the wind speed and direction at a single point, or several points spread throughout an area. It has traditionally been undertaken by national meteorological offices as part of their analysis of many weather parameters, but more recently, the

wind energy industry themselves have begun to establish new and bespoke mea-
suring techniques for application to wind energy developments.

A number of different resource-related factors are important for determining
whether a potential wind farm site is suitable for development and for analysing the
more detailed requirements in terms of turbine design. Different factors may be
investigated at different stages of a development, perhaps starting with a relatively
low-resolution map of a region and moving on to more comprehensive measure-
ments taken at a high temporal resolution at several locations around the site in
question. When a promising site has been identified, further detail in terms of
spatial and temporal variation is required, for instance to achieve the optimum farm
layout—known as *micrositing*.

The electricity generation potential is, obviously, a critical factor in the wind
resource assessment, as it underpins the financial viability of a development. The
available wind power density, P, for a given cross-sectional area of flow, A, is a
cubic function of wind speed, U:

$$\frac{P}{A} = 0.5 \times \rho \times U^3 \tag{12}$$

where ρ is the air density. A turbine can only extract a small amount of the available
power, with the typical extraction characteristics being described by a *power curve*,
such as that shown in Fig. 6. It can be seen that the turbine has a *cut-in* speed of
around 3–4 m/s and reaches its maximum output at around 15 m/s, and additional
speed above this value does not result in further power output. The turbine will cut
out entirely to protect itself from damage at high speeds of around 25 m/s. For the
purposes of power calculations, the relevant IEC standards (IEC 61400-1 2005; IEC
61400-3 2009) indicate a requirement for wind energy site assessments to be of the
10-min average wind speed, and this is usually sampled at hourly or half-hourly
time steps. If possible, several years of measurements would be available in order to
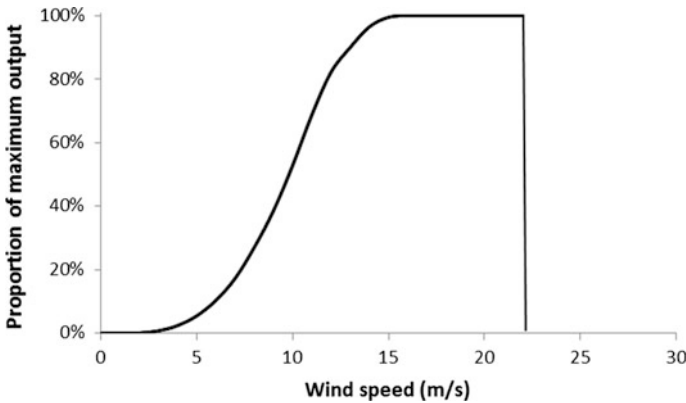capture seasonal and inter-annual variations, but depending on the stage of project

Fig. 6 Typical wind turbine power curve

development, shorter periods can be sufficient to estimate the site's potential, or additional modelling can be used to extrapolate the time series.

Traditional Anemometry

The technology used for measuring wind speeds at weather stations on land is usually based on a simple design using cup-shaped blades rotating around a central vertical axis, known as *cup anemometers*. The rotational speed of the cups around the central axis is proportional to the wind speed. A wind vane is generally used to record direction. Before the proliferation of wireless communication, measurements from anemometers were recorded manually on a form which was returned to a meteorological office, but newest stations record and transmit automatically.

Sonic anemometers work based on the time taken for a sound wave to travel between two points. A pair of transducers/receivers are set up opposite each other and each sends a sonic pulse towards the other. Based on the distance between them, the time taken for each pulse to be received at the other end can be used to derive the wind speed along that direction. Using several pairs of transducers at different orientations, the three components of wind velocity can be derived. Due to their ability to provide high frequency measurements over small distances (10^1 cm) these devices are particularly useful for characterising turbulence. The instruments are, however, sensitive to their positioning, which is particularly critical in non-horizontal terrain. In all cases, sonic anemometers will require careful calibration and post-processing (Wilczak et al. 2001).

Onshore, there are often large networks of weather stations including cup anemometers covering wide areas. For example, in the UK, the UK Met Office operates around 200 automatic weather stations each recording parameters including wind speeds at hourly time intervals and returning the information back to a central processing department (Met Office 2011). These records are held in a database for many years. Offshore, long-term measurements of weather parameters are often more sporadic due to the higher costs of installation and maintenance of measurement equipment at sea (Hasager 2014). Coastal and offshore wind speeds are traditionally recorded by lighthouses/lightships but in the past these may frequently have been estimated by observers rather than by using an instrument so the longer-term historical record may not be entirely robust. Networks of VOS (volunteer observing ships) exist that also record weather conditions and return the data to meteorological organisations, for example the Voluntary Observing Ships program in the United States (National Data Buoy Center 2014). The measurements, however, do not have a wide coverage. Meteorological buoys (met buoys) with anemometers on board are also deployed in specific locations in offshore waters providing, among other parameters, wind speed (and usually wind direction) measurements (see National Data Buoy Center 2015a for a map of buoys around the world). They return data in a similar way as onshore weather stations, via wireless communication networks to onshore data processing stations.

Measuring wind speeds at different heights is crucial to gain an understanding of vertical profiles (i.e. how the wind speed changes with distance from the surface), turbulence, and ultimately the potential for wind power generation and turbine design

requirements at a site. Met masts installed for the purposes of wind energy site evaluation can consist of several anemometers at different heights to capture the nature of the vertical profile under different conditions, and nowadays these often use sonic or ultrasonic anemometers alongside standard mechanical devices. Offshore, met masts of this type either require to be installed on a foundation which is fixed to the seabed, or on some kind of moored floating platform. It can be expensive to install such a foundation or platform and maintain the instrument in an offshore location.

In all cases, for accurate measurement of wind conditions, it is important that the anemometer is placed sufficiently high above surface level such that immediately local obstacles do not influence the wind speed being measured. Usually, in onshore cases, the masts are placed as far away as possible from trees, buildings etc. and are typically 10 m above ground level. The surrounding features need to be taken into account when interpreting the data. Offshore, achieving a constant height above surface level can be difficult as tidal fluctuations and waves can cause variations in the height of the water surface. Additionally, it depends on whether the platform on which the instrument is located is fixed or floating—for example it could be on a ship which is constantly in motion, or fixed to a seabed mounted pile which will not itself move. Taylor et al. (1999) discuss the issue of placement of anemometers on ships and the potential for interference from the vessel motion and structure on the measurements. Floating meteorological buoys that measure wind often do so at a height of around 2–3 m above sea level, which along with the motion of the buoy potentially introduces uncertainty to measurements, particularly in stormy conditions.

Some representative data has been obtained from the UK Met Office for wind speeds measured at the Sevenstones lightship moored off the south-west coast of England (Met Office 2006a). The anemometer is at 14 m above sea level (National Data Buoy Center 2015b) and the time period presented is 2014. The hourly sampled 10-min average time series of wind speed for the month of January 2014 is
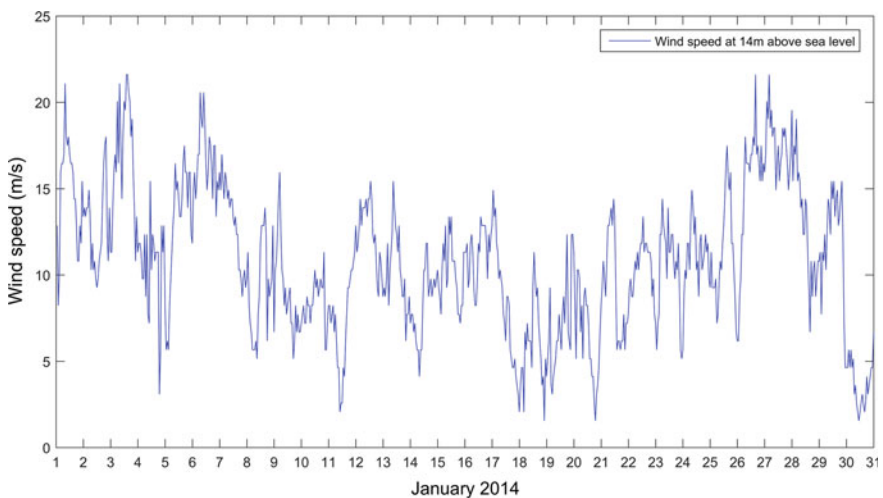

Fig. 7 Time series of wind speed at Sevenstones lightship (Jan 2014) (Met Office 2006a)
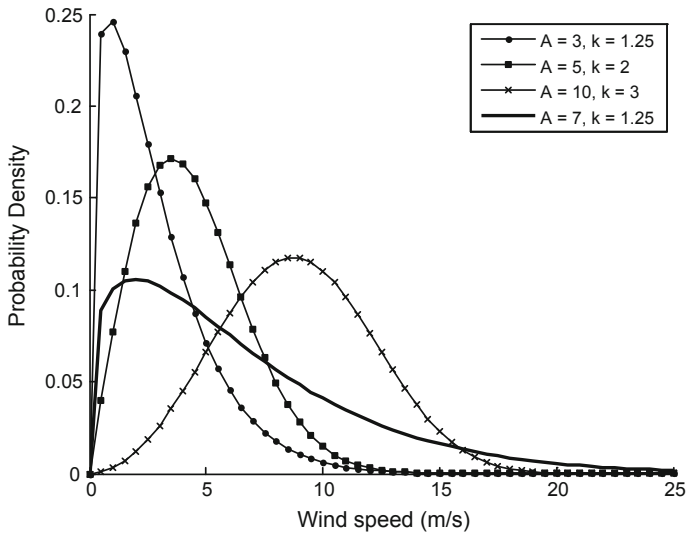
Fig. 8 Some shape and scale parameters for Weibull distributions

shown in Fig. 7. There is a large degree of hour-to-hour variation, which is generally present in these types of observation record.

Frequency Distribution

When carrying out a wind energy site assessment, the half-hourly or hourly measurements over a specific time period are usually summarised in the form of their frequency distribution. Wind speeds typically fit the pattern of a two-parameter Weibull distribution, as shown in Fig. 8, which can be described by two parameters, the *shape* and the *scale*. The scale parameter is related to the mean wind speed, whilst the shape parameter describes the variability of the wind speeds at the site—a lower shape parameter will have greater variability, with more frequent occurrences of high or low speeds, whilst a higher shape parameter indicates less variability. In the case of a site where a long period of hourly measurements is not available, the mean wind speed can be used to derive a Rayleigh distribution, which is a special case of the Weibull distribution, with a shape parameter fixed at a value of 2.

Combining the frequency distribution of wind speeds with the power curve will inform the developer of the expected energy output of a turbine at the site over the period measured, and thus the financial viability can be analysed. The distribution for Sevenstones is shown in Fig. 9, along with the fitted Weibull distribution with shape parameter 2.21 and scale parameter 9.99.

Direction

Analysis of the wind direction is a key feature of wind energy site assessments. Meteorological convention dictates that direction is expressed in terms of where the wind is blowing from (i.e. the opposite of the vector direction), and measuring in degrees clockwise from 0° at North. IEC 61400-3 (2009) specifies that directions
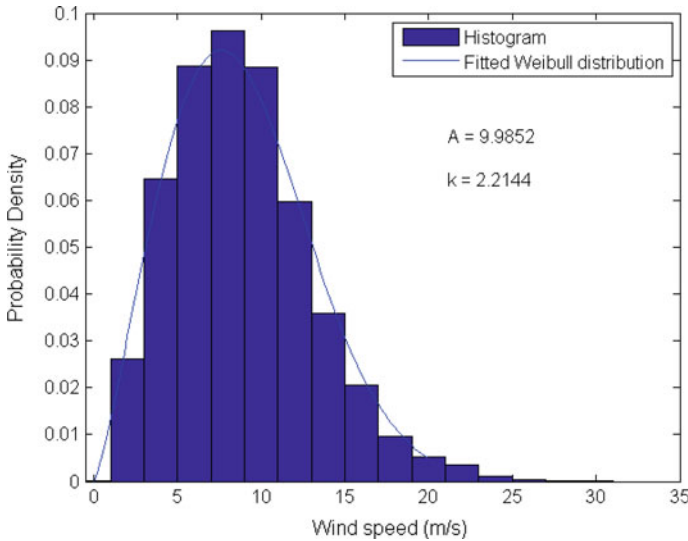
Fig. 9 Distribution of wind speeds at Sevenstones

are classified into sector bins with a maximum size of 30° for the purposes of creating a *wind rose*. Directional information may be required both for *micro-siting* considerations, including how to lay out the turbines within the wind farm and for turbine design and loading analysis.

Figure 10 shows the wind rose measured over a year at Sevenstones with sector bins of 10°. As would be expected, for this location a large proportion of the winds come from the west and south-west. At low speeds (dark blue), the directions are actually less heavily weighted to the west, but for wind speeds in peak range for generation (10–20 m/s), the majority of these occur in the western quadrants.

Remote Sensing

There is an increasing demand, somewhat driven by the wind energy industry, for alternatives to mechanical measurement systems, featuring the use of sound-waves, and more recently, laser beams to measure wind speeds. These can often be located some distance away from the site of interest, hence the term *remote* sensing. In the case of offshore wind developments, developers are interested in using these techniques at existing wind farms, locating devices temporarily on current infrastructure in order to better capture information about turbine wakes and wind profiles (Hasager et al. 2008).

Sodar (SOnic Detection And Ranging) systems work by sending out sonic pulses. As these beams meet turbulent structures in the atmosphere (eddies) they reflect a certain amount of the beam (backscatter). Due to the Doppler effect, if there is a change in frequency of the reflected wave, this indicates movement towards or away from the receiver along the axis of the beam. This way, the speed of the air movement can be determined. Lidar (LIght Detection And Ranging) wind measurement devices send out a laser beam, rather than a sound wave. When the beam
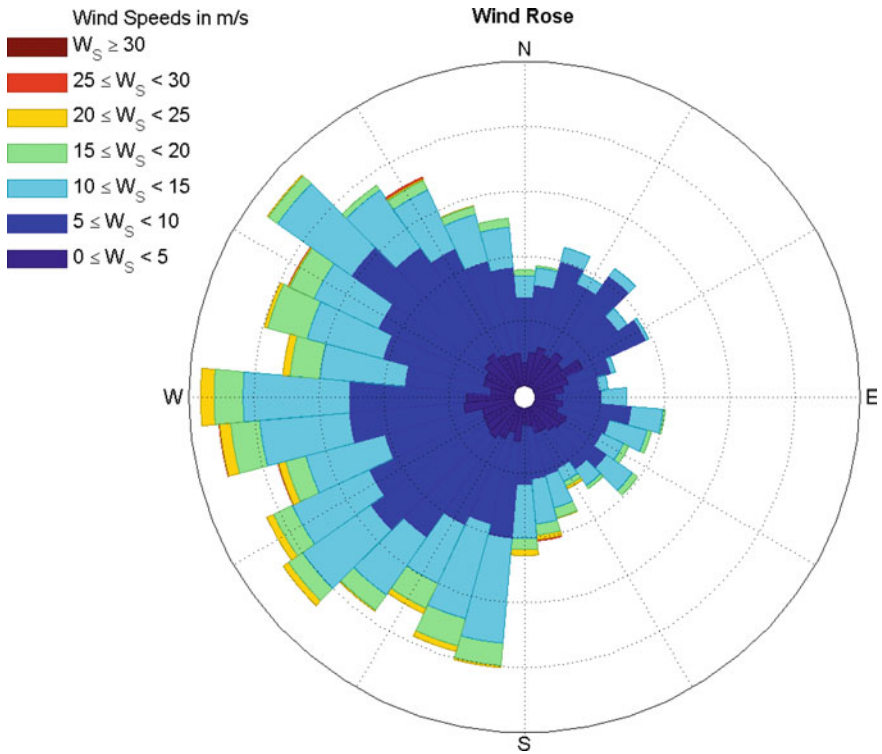
Fig. 10 Wind rose for Sevenstones

encounters particles in the air (pollen, dust etc.) the beam is scattered and some of the scattered light is reflected back towards the device (Smith et al. 2006). Again, due to the Doppler effect, the change in frequency of the reflected light can be used to determine the velocity of the particle along the beam axis. The device needs to scan in multiple directions to capture the full information on the wind velocity, and a post-processing algorithm is required to transform the information from the laser beam into wind velocity data.

Lidar is frequently used to analyse specific aspects of the wind field—for example, variations in speed across a turbine rotor, or in its wake, to map wind fields over a region in 2-dimensions, and to look in detail at vertical profiles (Peña et al. 2009). The technology can be expensive, but there are a number of proprietary devices developed by wind energy consultancies around the world that developers can rent or purchase (see Hasager et al. 2008). A significant proportion of their accuracy is dependent on the post-processing of the Doppler shift information into accurate wind velocity data, as well as the specifics of the laser technology involved. Cloud, mist and rain can all potentially introduce error into the wind speed measurements from Lidar (Smith et al. 2006). Det Norske Veritas (DNV) provide a recommended practice DNV-RP-J101 (2011) to operating and using data from remote sensing equipment, which states that the output should be verified against the

measurements from an in situ met mast, and that consideration of the positioning of the device is crucial to avoid interference from nearby obstacles, for example trees and buildings. The presence of particularly complex flow situations can also influence output and should be accounted for when analysing the results.

Satellites

In the case where a wider-scale picture of the offshore wind field is required rather than at a single point, there is an option to use data measured remotely from devices attached to satellites. The first instruments, deployed by NASA in the 1980s passively measured the microwave radiation associated with the roughness of the sea surface, and correlated this to the magnitude of the local wind speed (Hasager 2014). More recently, active devices called scatterometers are being used that emit and measure the backscatter of microwave radiation. The degree of backscatter in the microwaves along different axes caused by very small waves on the ocean surface (wavelengths on the order of centimetres) can be detected by the instrument. An algorithm is applied which relates the magnitude of the backscatter along the different axes to the local wind speed and direction as it blows over the ocean surface. The algorithms are developed and calibrated based on empirical relationships identified between the backscatter and either in situ measurements, model data or both (Sempreviva et al. 2008).

Satellites follow pre-determined tracks around the globe with the ability to take measurements covering areas around 2000 km wide as they pass, so each orbit gives good daily coverage of the whole earth. Several world-wide organisations are now responsible for operating satellite scatterometers, including NASA (RapidScat; NASA 2015), and EUMETSAT (Jason-2; EUMETSAT 2015). The frequency of travel of the satellite over a particular part of the ocean determines the time resolution of measurements, which can be between 2 and 6 times daily, with a spatial resolution typically in tens of kilometres. Where higher spatial resolution is required, an instrument called a SAR (synthetic aperture radar) can be used instead of a scatterometer. This emits a single microwave beam directly perpendicular to the sea surface and from the backscatter, the localised wind speed can be determined. SAR measurements are typically available at lower frequency than scatterometers (perhaps a few times per month) but at a much higher resolution of 10^1 m (Hasager et al. 2006; Sempreviva et al. 2008).

For all types of satellite technology, the accuracy of the algorithm used to interpret the backscatter signal and relate it to the local wind conditions is key to the accuracy of the data. Further processing is required to map the measurements taken from each pass of a satellite over an area of ocean onto a regular grid covering the region of interest. In coastal regions, there is often a lot of interference from the land, so measurements using scatterometers here tend to be unsuccessful, whilst for some types of scatterometer, the presence of raindrops will also adversely affect the accuracy of measurements (Weissman et al. 2002). Hasager et al. (2006) indicates that SAR is generally considered to be more useful for coastal measurements and also demonstrates that SAR measurements are sufficiently detailed to capture the wake effects from an offshore wind farm.

1.3   Resource Mapping

Obtaining information about spatial variations in wind conditions over a specific area requires some degree of modelling to *fill in the gaps* where measurements are not available. For instance, a wind farm developer may wish to find the site with the best resource in a particular area, but measurements are only available from one point within the area, or policy-makers may wish to map the resources for their whole region, but again, only measurements from specific points within the region are available. As previously mentioned, in the case of offshore wind existing measurements are particularly rare, and thus modelling offers a reasonable alternative. Different modelling techniques are appropriate for modelling at different scales, and for different applications depending on the accuracy and resolution requirements.

Statistical Models

With growing interest in the wind industry in the 1990s, but at a point where computing power was still very limited compared with what we are familiar with today, the use of statistical models to relate wind speeds measured at one location to those experienced at another location of interest was prevalent. A technique known as Measure-Correlate-Predict (MCP) was (and often still is) widely used to develop a relationship between winds measured over a short period at a specific site of interest for wind energy development and longer-term measurements—perhaps 3–10 years—from a nearby location. This allows the characteristics of the longer time period to be taken into account when considering the energy potential or design requirements at the proposed site. A number of different software packages exist that apply MCP techniques.

Given a location, *A*, with a long record of wind speeds and a second location, *B*, with a shorter period of records (which overlaps with some of the period of the *A* record), the fundamental process involves firstly *binning* each set of wind speed measurements by directional sector. For the short period in which the measurements overlap, a relationship is found between the two sets of wind speeds in each directional sector. The relationship is commonly derived using simple linear regression, but it can also involve relating the parameters of the fitted Weibull distributions, or other more complex methods such as neural networks (Carta et al. 2013). This relationship is then applied to the wind speeds from site *A* to derive corresponding *measurements* for site *B* and extrapolate its short record to cover the longer period of the *A* record. Where the terrain is smooth between the two sites, with no complex features such as mountains to drastically alter the flow, this technique is usually successful. In the case of more complex topography, however, the relationships can carry a larger degree of variability, and thus the associated uncertainty can be higher.

Going from an onshore site *A* to an offshore site *B* is an example of where such uncertainty might be found, as the coastal processes and the change in flow as the wind goes from on—to offshore or vice versa will introduce complexity that may not be fully represented by a statistical relationship. By way of demonstration, two
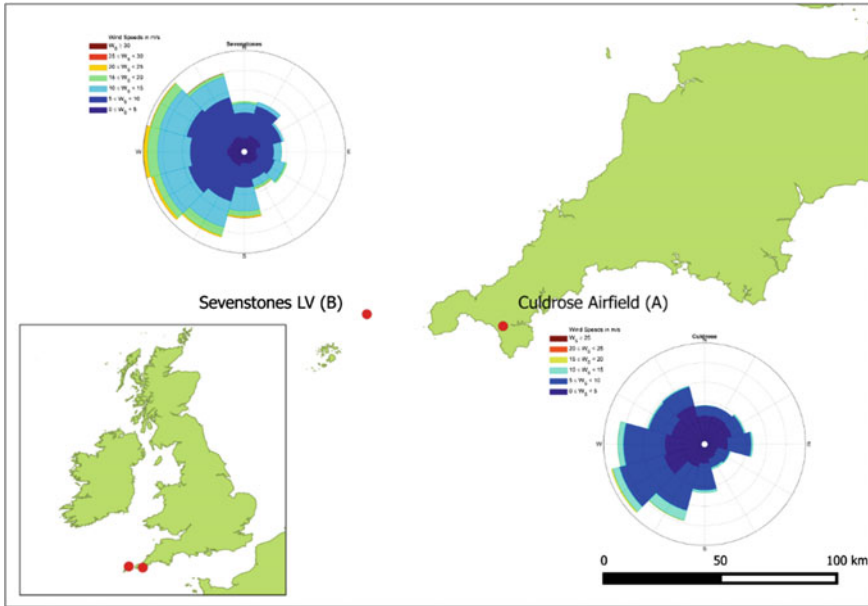
Fig. 11 Site locations and wind roses used in the MCP example

sets of recorded wind speeds have been obtained, one from an onshore weather station (Met Office 2006b) and one from a light ship moored approximately 60 km away (Met Office 2006a). The record covers the year 2014, so has been initially divided in two, so that the first 6 months can be used to develop a simple linear relationship between wind speeds at each site, and the second 6 months of offshore wind will then be predicted using the second 6 months of onshore records. The predictions can then be compared to what actually occurred to assess the degree of error in the method. A map of the two sites and the associated wind roses from the two met masts is shown in Fig. 11.

At each time step, the data from both sites was binned according to the direction occurring at site A, Culdrose, and for each directional bin, a regression was carried out with the two sets of wind speeds to fit a simple linear relationship between the occurrences at each site. The R-squared correlation coefficients for the overall six-month period was 0.68, and Pramod Jain (2011) suggests that a correlation coefficient of >0.65 for two sets of 10-min average wind data is sufficient to proceed with a MCP analysis. Individual R-squared coefficients for each bin were quite varied, with those in bins from the south-southeast to west showing R-squared values of 0.7–0.9, whilst for winds coming from the north and east, the R-squared values were only around 0.4–0.6. Considering the locations on the map, this would correlate to the fact that both sites are similarly exposed to the south and south-west, whilst for winds from the north and east, the terrain and topography are quite significantly different at the two sites. Other authors, as discussed in Carta et al.

(2013), indicate a requirement for a greater correlation between the two sites and in this case, it would be considered that the uncertainty may be quite high. The fact that seasonal variation may not be adequately captured within the 6-months of concurrent data may also be a contributing factor.

The regression coefficients have been used to derive the second 6-month period of wind data for the offshore location from the onshore record. Comparing the predicted and actual offshore values for the 6 months predicted, the overall R-squared value is around 0.6, indicating a not insignificant difference. Using the original and predicted data to calculate the wind power output using a standard power curve shows that the MCP method under-predicts the production for those 6 months by around 4 %. This may indicate that the wind speed distribution is reasonably well captured but the time-sequence is not so successful. Therefore, care must be taken when using statistical methods to ensure that they are robustly applied and that the error is sufficiently understood.

Micro-Scale Modelling

Micro-scale models are, as the name might suggest, used when dealing with relatively small spatial scales. A solution which builds upon the premise of relating wind measured at one site to another nearby site was developed in the 1990s and is known as the Wind Atlas Methodology. This is a physical model, rather than a statistically-based solution, and forms the basis for a well-known piece of wind analysis software, Wind Atlas Analysis and Application Program (WAsP). The method and its application to mapping the wind climate of Europe is described in great detail in Troen et al. (1989). The model attempts to capture the effects of three main influences on wind speed: local obstacles such as buildings, the general surface conditions (see Table 1) and the topography, which refers to height changes in the terrain such as hills or cliffs. The premise behind the Wind Atlas Methodology is that given a measurement at a point within a region and a description of the surrounding location, the known influence of all three categories can be removed from the initial record, leaving a representation of a more general regional wind climate. For a point of interest within the region at which no measurements are available, the influence of particular local features at this new point can be added back into the regional climatology to provide a representative record here.

A key advantage of the Wind Atlas Methodology is that it requires relatively low computational effort, but it does neglect non-linear influences on local wind conditions. This makes it less successful in very complex terrain, such as mountainous areas. In an example situation of a resource assessment for a coastal location on an island above quite steep cliffs and nearby to a mountainous area, the WAsP model was identified as being invalid due to an established inability to capture these local effects (Palma et al. 2008). WAsP assumes a constant surface roughness of 0.0002 m over water, rather than the more complex assumption whereby z_0 varies with wind speed. It also makes some simplified assumptions about heat flux, which inform the stability conditions in the model (Lange and Højstrup 2001). The use of WAsP offshore was studied in Lange and Højstrup (2001), which indicated that

whilst mostly successful, a combination of the assumptions in the model do cause some errors in wind power estimates compared to reference measurements. Longer fetches appear to show under-prediction and shorter fetches over-prediction of the resource.

As computing power and confidence in the modelling techniques increase, non-linear models show much greater accuracy in complex situations than simpler statistical and wind atlas type methods. Computational Fluid Dynamics (CFD) typically use Reynolds-averaged Navier-Stokes (RANS) equations to model the fluid (i.e. air) motion in a locality as it interacts with obstacles and terrain features. Non-linear effects are included in these models but the computational effort required is substantially more than that for a linear flow model. Some bespoke software has been developed specifically for wind energy purposes, but more generally applicable CFD models can be set up for a wide range of fluids and environments and can thus also be used to carry out wind modelling. The use of these kinds of models require extensive verification and validation, for example using wind tunnels (Ayotte 2008), to ensure that they are truly representative of the situation they are modelling and to understand their sensitivities and uncertainties. In Palma et al. (2008), the use of CFD alongside a number of anemometers showed good comparisons with the measurements and also allowed features such as flow separation and turbulence intensities at the proposed development sites to be mapped to a high resolution.

Mesoscale Models

Mesoscale model is a term widely used to describe numerical weather prediction models that have the ability to resolve weather features that are on a scale of 10^1– 10^2 of kilometres. Solving equations representing atmospheric physics and dynamics, the models can calculate parameters including air temperature, pressure, density and velocity. They are used in both forecasting and hindcasting mode, to predict incoming weather or reanalyse historical weather. Their operation is similar in either case, but for hindcasting, instead of propagating a known situation forwards, they are propagated backwards in time, and constrained by known boundary conditions measured throughout the time period of the hindcast to reproduce a representative historical climate. For wind power applications, these models are typically used when information is needed on wind speeds over wide areas, such as a state or country. Their scale and computational demand is such that they are typically set to produce wind conditions averaged over grid cells between 3 and 50 km length.

Generally, the models produce time series of wind vectors (or wind speed and direction)—for example, hourly—in gridded format. Whilst the output is expected to be representative of the climate throughout the grid cell in question, it may not be an exact match for the wind speeds at any given specific point within the cell, particularly if the terrain varies widely within the cell. Their main benefit is in providing a way to look cumulatively at the wind climate for an area, how it varies within the wider area, and perhaps to model aggregate wind power output over this area (see for example Harrison et al. 2015).

As discussed in Watson and Hughes (2014), the models do not always capture the finer details of the offshore resource as might be relevant in a more localised energy potential assessment, for example the directional changes and stability conditions at a site. The authors found greater accuracy compared with met mast data further offshore than close to the coast, indicating that as with most other types of model, capturing the land-sea interactions is problematic. Their output can, however, be used as input to finer-scale models, such as those using CFD, which can apply the influence of more localised conditions. Mesoscale models can also be used as input conditions to wave forecast/hindcast models and can potentially be used in this way to look at concurrent wind and wave loading conditions for offshore wind developments.

Examining some output from a 10-year simulation at 3 km spatial resolution around the UK and Ireland of the WRF (Weather Research and Forecasting—Skamarock et al. 2008) mesoscale model (Hawkins 2012), firstly it can be noted that the areas with highest wind speeds in this region can be seen to the west and north west and to a lesser extent in the northern North Sea area (Fig. 12). Secondly, clearly the spatial variability of the offshore wind conditions is much less than
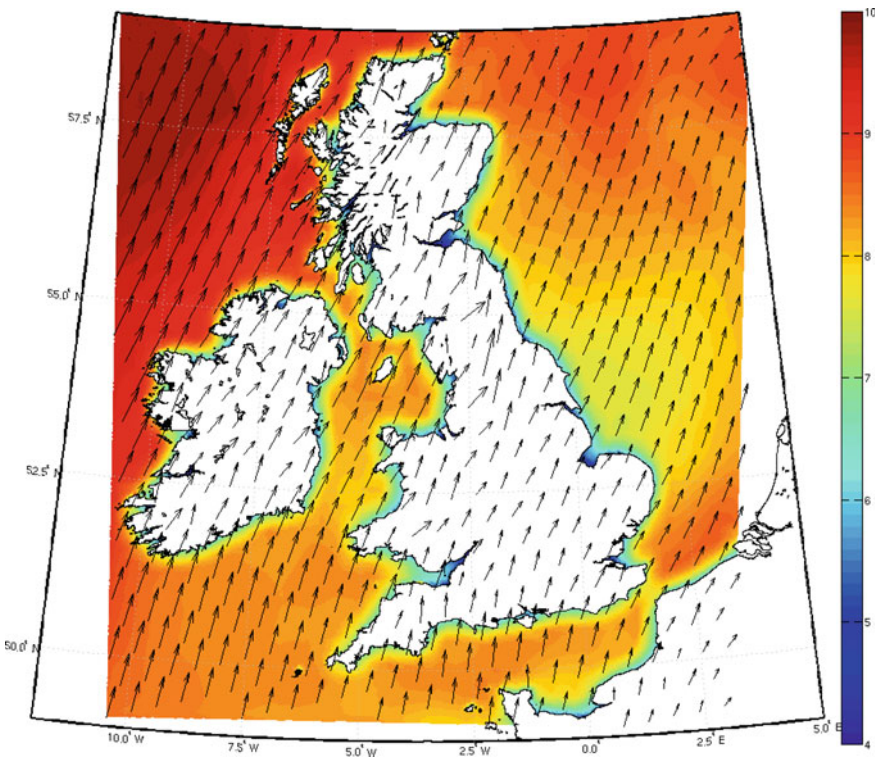

Fig. 12 Mean 10 m wind speed from WRF mesoscale model at 3 km resolution from 2001 to 2010
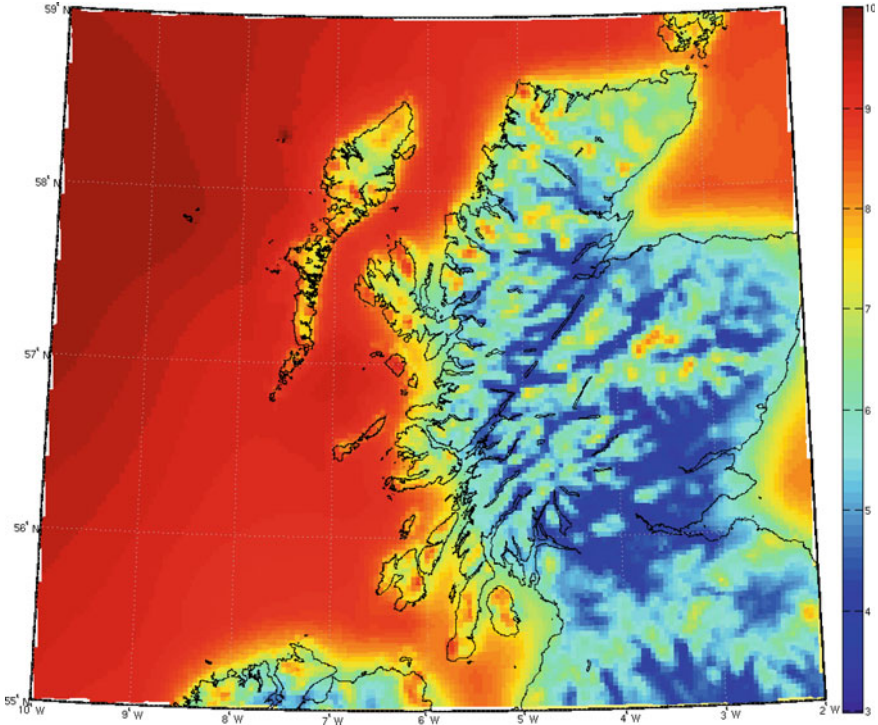
Fig. 13 Close-up of Scotland showing differences in the spatial variability of wind speeds for onshore and offshore

would be found onshore, as the surface conditions are much more consistent. This gives rise to smooth contours of mean wind speed across swathes of ocean and reasonably consistent directional patterns over wide areas of ocean, since there are no large obstacles or terrain height variations, the larger-scale climate features are the predominant influence. This is highlighted in Fig. 13, showing the difference in spatial variations on- and offshore, and is explored further in Cradden et al. (2014), where it is also demonstrated that, for a given location, hourly wind speeds from the hindcast are less variable offshore than at locations with complex terrain onshore. Coastal wind velocities are usually 10–20 % lower than the areas further offshore which is borne out by the model output shown here (Barry and Chorley 1998).

The theoretical capacity factor of a generic 3 MW wind turbine has been calculated using the 80 m wind speeds extracted from the WRF model output for 2010 and is shown in Fig. 14. Generally following the pattern of the 10 m wind speeds, the highest capacity factors are found in the west and north west of the map. The water depth in this region, however, increases very steeply moving out from the coast and the resource is only likely to be exploitable using floating turbine platforms rather than fixed foundations. For the region to the west of the English Channel where the resource is also promising, the water depth is much more
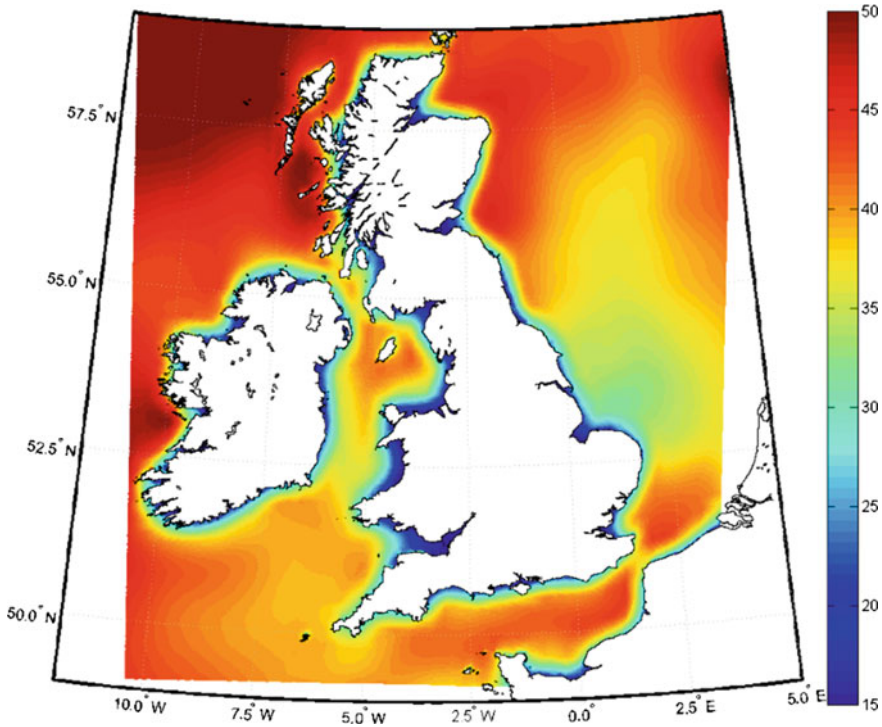
Fig. 14 Hypothetical capacity factor for a generic wind turbine using 80 m wind speeds extracted from WRF for the year 2010

shallow and fixed foundations are suitable. In the areas of the North Sea to the east of Scotland, the water depth is quite variable but can reach the limit of the newer fixed foundations, making floating platforms a viable option here also.

Global Wind Resource Maps

Maps of wind speeds around the world give an overall picture of where the most significant resources are located. A typical source of input data for such maps is either satellite records (Hasager et al. 2006; Risien and Chelton 2006; Hasager 2014) or alternatively using the reanalysis datasets. Reanalysis data have been created by several meteorological organisations around the world by running numerical weather prediction models in hindcast mode for several decades, with recorded observations included in the simulation to constrain the model with real data. Examples of reanalysis projects include ERA-40 (Uppala et al. 2005), its successor ERA-Interim (Dee et al. 2011) and NCEP-CFSR (Saha et al. 2010). The maps in this section have been generated using the MERRA reanalysis which uses satellite information recorded since 1979 assimilated into a global circulation model (Rienecker et al. 2011). The data covers almost all of the offshore areas of the world
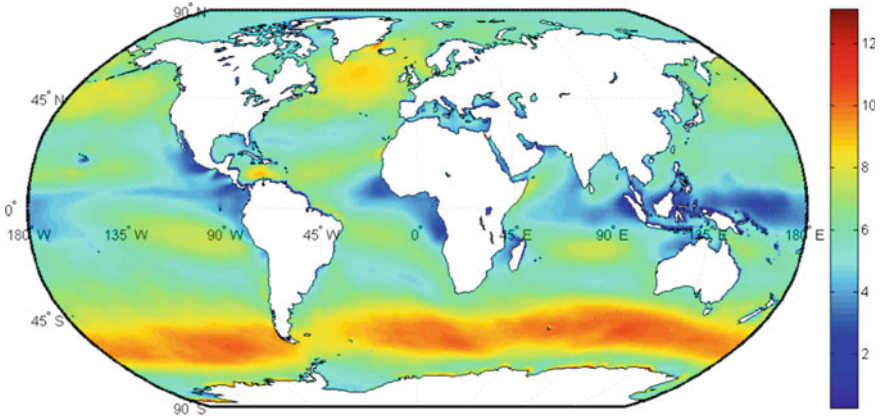
Fig. 15 MERRA mean annual surface level wind speed (2014)

at a resolution 0.5° latitude by 0.667° longitude. It is freely available for download from (Goddard Earth Sciences Data and Information Services Center 2013).

The average wind speed at 10 m above sea level (a.s.l) for the year 2014 is shown in Fig. 15 and the mean annual wind power density is shown in Fig. 16. The area known as the *doldrums* is quite evident around the equator, with the trade winds in each hemisphere appearing as the green-yellow zones above and below this area. The peaks around the areas of 45° north and south of the equator are the westerlies. These tend to be somewhat weaker in the northern hemisphere due to the larger land mass. The seasonal variation in wind speeds during 2014 can be seen to some extent in Fig. 17, which shows mean 10 m a.s.l wind speeds for December and July. It is clear that the northern Atlantic and Pacific Ocean regions see a large difference between the summer and winter wind speeds, whilst the regions around the Indian Ocean and the Arabian sea, for instance, show the opposite trend.
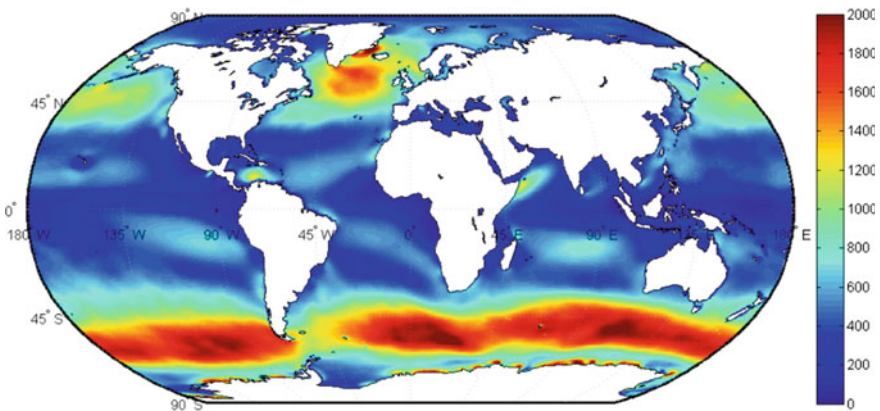

Fig. 16 MERRA Mean annual wind power density (W/m^2) for 2014 at 80 m (extrapolated from 10 m using power law and exponent = 0.14)
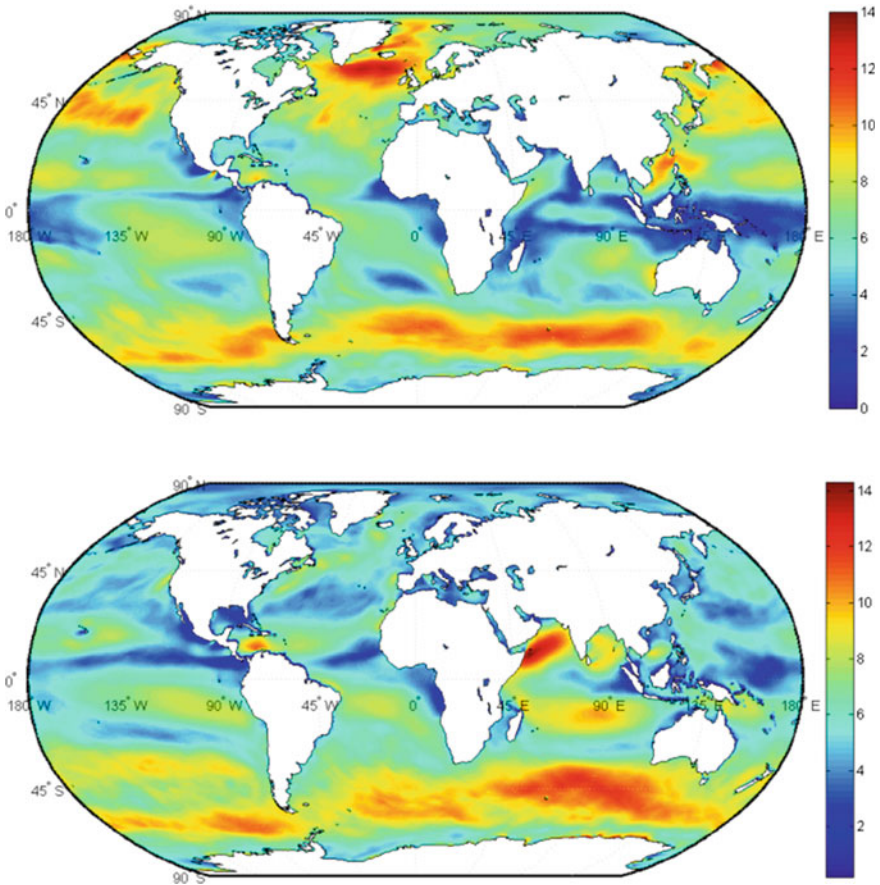
Fig. 17 MERRA Mean December (*top*) and July (*bottom*) surface level wind speed (2014)

The Atlantic coast of Europe has a very strong wind resource, and generally, the wind speeds are higher along the northern areas of this coast, compared to those in the south. The winter climate is also strongly influenced by the North Atlantic Oscillation, a phenomenon which refers to the presence of a low pressure centre over Iceland, and a high pressure located around the Azores, to the west of Portugal. Since winds in the northern hemisphere will always blow with the pressure centre to the left of the wind vector, this leads to a strong tendency for dominant west-south-westerly winds to blow in from the Atlantic. A weather classification system known as *Grosswetterlagen* categorises the circulation patterns over Europe into 29 distinct patterns (Hess and Brezowsky 1952) with the most frequently occurring types being *anti-cyclonic westerly*, *cyclonic westerly* and *maritime westerly* (James 2007), all three of which are dominated by the Icelandic low/Azores high.
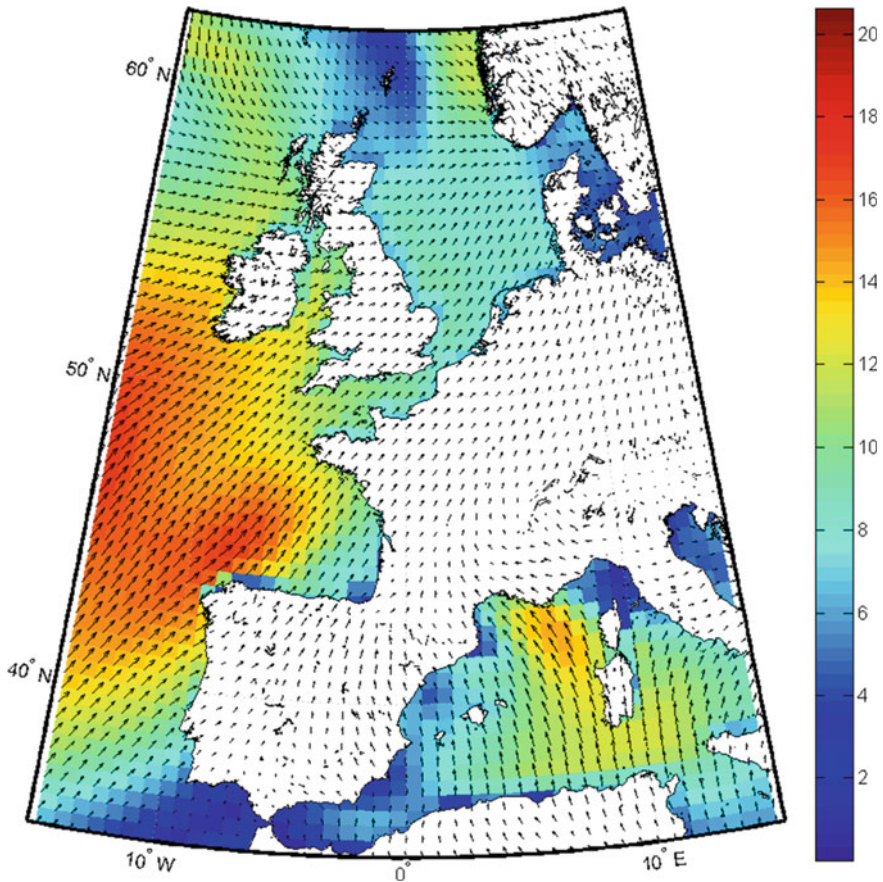
Fig. 18 Daily 10 m wind speed and vectors for January 5th 2014 over Europe

A plot of daily mean wind speed and vectors for a stormy day in January 2014 (Fig. 18) reflects the pressure pattern shown in Kendon and McCarthy (2015), with low pressure centres over the north west of Europe and also around the Mediterranean Sea area. The winds were very strong, with the daily mean reaching 15 m/s along the south-west coast of Ireland and the north-west of Spain. There are also very high winds shown in the northern Mediterranean Sea, to the south of France. It can be seen that the North Sea is somewhat more sheltered, whilst still experiencing relatively strong winds.

As an indicator of the pattern of extreme winds over the whole of 2014, the map of the 95 % percentile daily mean wind speed in 2014 from MERRA is shown in Fig. 19. This shows, as might be expected, the most severe conditions occurring along the north-western Atlantic coasts of the British Isles and Norway. Values of above 10 m/s are seen along all western shores north of Portugal and also throughout the North Sea, and in part of the Mediterranean Sea.
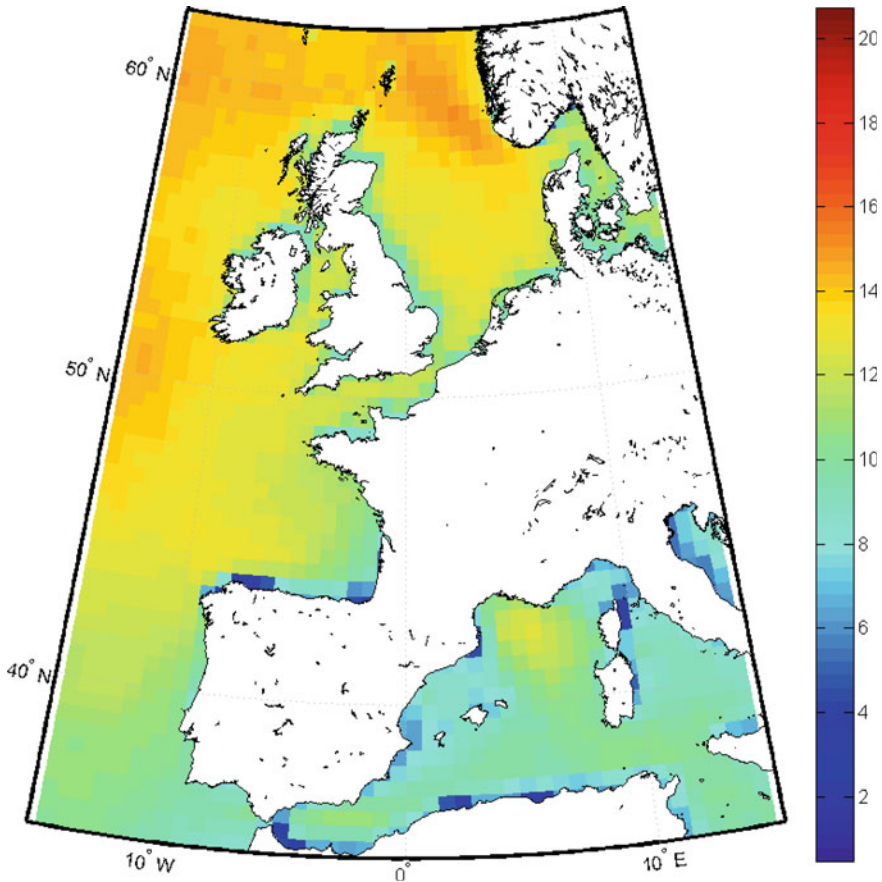
Fig. 19 95th percentile of daily average 10 m wind speed from MERRA in 2014

Both Figs. 18 and 19 demonstrate that there is an issue with the resolution of the coastline in the MERRA model, which is particularly evident along the north coast of Spain. The low values given by the model here are perhaps not as would be reflected by measurements in this area but due to the model resolution, it cannot always capture the true conditions. This should be taken into account when analysing coastal wind speeds from any model.

1.4 Discussion

Over the last 20–30 years, since the onshore wind energy industry became established, it has seen an enormous amount of rapid development. The experience that has been obtained has led to significant improvements in efficiency, reliability and

design. It is now important to be able to use this knowledge to accelerate the development of offshore wind. When considering the offshore wind energy resource, it is important to bear in mind the differences compared to the conditions experienced onshore, and how this will impact on a site in terms of power production and reliable design. The mean wind speeds experienced far offshore are typically higher than those found onshore, and are in general found to show less variability in time and space. This would indicate that in terms of power production, offshore sites are more favourable. It is important to consider, however, that some of the assumptions used—for example, to calculate vertical wind shear—are perhaps not automatically transferrable from on-to offshore. In particular, throughout this section, reference has been made to the fact that conditions in coastal regions often show significant deviation from expected patterns, and are particularly difficult to model. In this case, measurement campaigns are critical to understanding the resource, exploiting it optimally and dealing with the difficulties. Additionally, as computing power becomes cheaper and more accessible, the ability to incorporate new knowledge and model these zones effectively becomes easier, providing a more complete picture of the conditions.

2   Wave Climate

Pauline Laporte Weywada

The knowledge of waves has been a topic of research for many decades, as it defines in a large measure the design and operational safety of offshore structures such as oil platforms. Estimating the environmental loads acting on a FOWT and its support structure therefore requires the quantification of the local wave climate. The accurate characterisation of the wave resource will establish and inform the relevant environmental conditions for the design of the support structure at the proposed location.

2.1   Origins of the Resource

Classification and Origin of Ocean Waves
Ocean wave is a generic term that gathers very different types of waves. Various studies have aimed at providing a classification of ocean waves, one of the first being proposed by Munk (1950). The classification is based on the energy source that creates the wave, and their period or wave length. Table 2 summarises the ocean waves categories defined by Munk.

The category of ocean waves proposed by Munk with the largest period is the *trans-tidal* waves. These are generated by low frequency fluctuations in the Earth's

Table 2 Tentative classification of ocean waves according to wave period (based on Munk 1950)

Classification	Period	Source
Trans-tidal waves	24 h and up	Storms, sun and moon
Ordinary tides	12–24 h	Sun and moon
Long-period waves	From 5 min to 12 h	Storm and earthquakes
Infra-gravity waves	From 30 s to 5 min	Wind
Ordinary gravity waves	From 1 to 30 s	
Ultra-gravity waves	From 0.1 to 1 s	
Capillary waves	Less than 0.1 s	

crust and atmosphere. The gravitational pull of the sun and moon on the earth also causes waves, with a period of between 12 and 24 h. These waves are *tides*. The next type of waves in the ocean wave classification are *long-period waves* generated by severe storms, with low atmospheric pressure and the high wind speed. Other hazardous waves can also be caused by underwater disturbances that displace large amounts of water quickly such as earthquakes, landslides, or volcanic eruptions. These very long waves are called *tsunamis*. The shortest period waves are called *capillary waves*, generated by wind but dominated by surface tension.

However, the most common association with the term *ocean waves*, and the focus of this section, are surface waves with periods between 0.1 and 30 s. These are dominated by gravity and caused by wind blowing along the air-water interface, creating a disturbance that steadily builds as wind continues to blow and the wave crest rises. These wind-driven waves can be separated in two sub-categories: the irregular and short crested *wind sea*, when they are generated by local wind; and the more regular and long-crested *swell*, when the wave system leaves its generation area.

Sea State and Wave Spectrum

The wind-driven generation of waves is a highly chaotic phenomenon that cannot be described by a single time record of the sea surface. Instead, for resource characterisation the use of a frequency domain representation of the sea surface is largely adopted, in which the wave system is represented as the sum of a large number of elementary component wave trains with different frequencies and directions and random phases. This directional wave spectrum describes the complex phenomenon of wind-generated ocean waves in terms of contributions from waves propagating in different directions with different wavelengths. Its purpose is to describe the sea surface as a stochastic process, i.e. to characterise all possible time records that could have been made under the conditions of the actual observation.

The directional wave spectrum is a fundamental parameter of wave modelling that quantifies the relationship between energy content and directional distribution. The forces acting on offshore structures and their response to waves depend on the characterisation of the directional spectrum.

The basic concept of the wave spectrum flows from the decomposition of any record of surface elevation, $\eta(x, y, t)$, as the sum of a large number of harmonic wave components, i.e. as a Fourier series:

$$\eta(x, y, t) = \sum_{p=1}^{P} a_p \cos\left(2\pi t f_p - k_p x \cos \theta_p - k_p y \sin \theta_p + \alpha_p\right) \tag{13}$$

where the amplitude a_p, wave number k_p, wave direction θ_p and direction of wave propagation α_p describe the wave components. Two basic approaches, following stochastic and deterministic principles, are possible to describe the wave field as presented in Benoit et al. (1997).

Stochastic methods are based on the random phase assumption, and the wave field can then be described in a continuous way as:

$$\eta(x, y, t) = \iint \sqrt{2S(f, \theta)dfd\theta} \cos(2\pi t f - kx \cos \theta - ky \sin \theta + \alpha) \tag{14}$$

where the variance density spectrum $S(f, \theta)$ and the wave amplitude a are linked following linear assumptions:

$$S(f, \theta) = \lim_{\Delta f \to 0} \lim_{\Delta \theta \to 0} \frac{1}{\Delta \theta \Delta f} E\left(\frac{1}{2} a^2\right) \tag{15}$$

As the phase function is randomly distributed, the wave components are independent from each other and these methods are typically unsuited for situations where phase-locking may occur (e.g. close to a reflective structure). In such occasions, the deterministic approach is preferred.

The following conventional decomposition of the directional spectrum is often used:

$$S(f, \theta) = E(f)D(\theta, f) \tag{16}$$

The one-dimensional frequency spectrum $E(f)$, which does not contain any directional information, can be obtained from this frequency-direction spectrum by integration over all directions:

$$E(f) = \int_0^{2\pi} S(f, \theta)d\theta \tag{17}$$

The direction distribution, or directional spreading function $D(\theta, f)$ is defined such that:

Table 3 Definition of the key spectral parameters

Spectral nomenclature	Definition	Description
H_{m0}	$4\sqrt{m_0}$	Significant wave height (H_s)
T_{m-10}	m_{-1}/m_0	Energy period (T_e)
T_{m01}	m_0/m_1	Mean period (T_m)
T_{m02}	$\sqrt{m_0/m_2}$	Zero-upcrossing period (T_z)

$$\int_0^{2\pi} D(\theta,f)d\theta = 1 \, D(\theta,f) \geq 0, \quad [0, 2\pi] \tag{18}$$

The latter expresses that the directional spreading function is a non-negative function, whilst the former is a direct consequence of the definition of the frequency variance spectrum.

The main statistical characteristics of wind waves that can be extracted from the frequency spectrum $E(f)$ are described in Table 3, expressed in terms of the *nth*-order moments of that spectrum:

$$m_n = \int_0^{\infty} f^n E(f)df \quad \text{for } n \in \mathbb{Z} \tag{19}$$

Typically, a sea state is characterised by the significant wave height, a spectral period such as the zero-upcrossing period, main direction and the shape of the spectrum. Following Goda (2000), the zero-upcrossing period relates to the mean period between consecutive crests, where the surface profile crosses the zero line upwards in a time-series surface elevation plot (relative to the mean water level). Depending on its nature, the shape of the spectrum can vary significantly, and several models exist to fit the conditions, as described at the end of this sub-section.

The one- or two-dimensional spectrum is acquired using in situ or remote-sensing measurements of the sea-surface, or using numerical wave models based on wind, tide and seabed topography information. These techniques are detailed further in Sects. 2.2 and 2.3.

Wave Propagation and Transformation of the Wave Resource

In the near-shore region, several factors are involved in the wave physics and interact to various extents with the waves changing their characteristics, in terms of the total wave energy as well as directional spectrum distribution of that energy. These are complex physical processes that need to be taken into account when considering wave propagation in shallow water. They can be categorised as wave interaction processes with the atmosphere, the seabed, the current or with other

waves, as presented below. A general description of each of these wave transformation process is given by Sarpkaya and Isaacson (1981).

As well as being a driving phenomenon in the wave generation, the wave-atmosphere interaction also takes part in energy dissipation processes such as white capping or wave propagation against the wind. The former is also known as wave breaking, and is due to an excessive wave steepness during wave generation and propagation. Breaking waves play a major role in the engineering design of offshore structure because the effect can be considerable (Young 1999): the accelerations that are involved in those situations are often large and potentially damaging if they impact a structure. The average wave steepness for an irregular sea state is defined as:

$$S_x = \frac{2\pi}{g} \frac{H_s}{T_x^2} \tag{20}$$

where S_x is the wave steepness relating to the period parameter T_x (typically, zero-crossing period T_z, peak period T_p or mean wave period T_m). Unless site-specific information is available, the limiting steepness S_z can be taken as 1/10 for $T_z < 6s$, 1/15 for $T_z > 12s$ and interpolated linearly between the two (DNV-RP-C205 2010).

Energy dissipation processes also occur with wave-bottom interaction such as bottom friction, essentially a transfer of energy and momentum from the orbital motion of the water particles just above the seabed in the turbulent boundary layer. Bottom friction causes wave height reduction as the water depth becomes more and more shallow and is of special importance over large areas with shallow water. Wave breaking can also occur with wave-bottom interaction, when the wave height becomes greater than a certain fraction of the water depth. Other wave-bottom interaction effects are depth-induced refraction which, at small depths, modifies the directions of the wave and then implies an energy transfer over the propagation directions, and shoaling where the wave height variation process as the water depth decreases, due to the reduced wavelength and variation of energy propagation velocity. Diffraction by a coastal structure (breakwater, pier, etc.) result in an energy transfer towards the shadow areas beyond the obstacles blocking the wave propagation.

Wave-current interaction can dissipate energy through wave blocking due to strong opposing currents, or affect the wave propagation process through current-induced refraction, which causes a deviation of the wave and an energy transfer over the propagation directions, or interactions with unsteady currents, inducing frequency transfers (e.g. as regards tidal seas).

Finally, non-linear wave-to-wave interaction can occur at great depths (mostly resonant quadruplet interactions) and small depths (mostly triad interactions), these interactions are further described in Hasselmann (1962, 1963).

Wave generation, interactions and dissipation processes need to be accounted for when considering the propagation of waves to a specific prediction point in numerical wave models. The first generation model did not consider nonlinear wave interactions. Second generation models, available by the early 1980s, parameterised these

interactions. Third generation models, further presented in Sect. 2.3, explicitly represent all the physics relevant for the development of the sea state in two dimensions.

Short Term Wave Conditions

A typical sea state may consist of several spectral components: one generated locally by local winds (wind-driven component), plus one or more swell components. These various components, to a good approximation, behave in a simple additive fashion, as regards both water movements and energy flows.

During the last decades, several wave spectrum models have been proposed to characterise short term stationary irregular sea states. Today the Pierson and Moskowitz (1964) model is the most generally accepted to describe fully-developed wind-driven wave systems. These situations occur when stable conditions have prevailed for a long period, in a long enough fetch. In younger seas or for shorter fetches, the JONSWAP experiment showed that the wave system may not have the time to fully develop (Hasselmann et al. 1973). This typically leads to a higher peak at a higher peak frequency. As the sea state develops, the nonlinear wave-to-wave interactions move the peak toward lower frequencies and flatten it, converging to the Pierson-Moskowitz model. The model used since to describe developing sea states is generally known as the JONSWAP spectrum.

After the wind ceases to provide input to the waves, they propagate freely as swell, travelling away from the storm area. Long waves travel faster than the short ones, and the swell system progressively loses its high frequency components, becoming more peaked and less broad banded.

When the peak frequencies are well separated, the spectrum has a double (or more) peak. Several double-peak spectra models have been proposed to describe such mix sea states. Strekalov et al. (1972) suggested the combination of one high frequency spectrum describing the wind-driven wave system and a Gaussian shaped model describing the swell. Ochi and Hubble (1976) combined a JONSWAP and a Pierson Moskowitz spectra. Guedes Soares (1984) and then Torsethaugen (1993) adopted two JONSWAP spectra using respectively four and seven parameters.

When considering individual waves, the short term distribution of individual wave heights can be modelled using a 2-parameter Weibull distribution, based on Forristal (1978).

$$F_H(h) = 1 - \exp\left(-2.263\left(\frac{h}{h_s}\right)^{2.126}\right) \tag{21}$$

where h is the wave height and h_s the significant wave height.

Intermediate Time Scales

Seasonal Variability

Aside from a large spatial variation in wave resource, a significant seasonal variability can also be evidenced by comparing the wave climate in winter and summer. Challenor et al. (1990) used satellite wave height measurements during the period between November 1986 to November 1987 to map the seasonal variations in the

global wave climate. The largest significant wave heights occurred during winter in the Southern Ocean (June–September) with only a slight reduction during the southern summer (December–March). In the North Atlantic and North Pacific the significant wave heights were lower and there was a larger variation between summer and winter.

Young (1999) presented significant wave height, peak and mean wave period and wave direction in terms of mean monthly statistics. The data set presented by Young (1999) was obtained from a combination of satellite remote sensing and model predictions covering a 10-year period. The results highlight the zonal variation in wave height, with more extreme conditions occurring at high latitudes. The important role played by the intense wave generation systems of the Southern Ocean was also evidenced, where swell generated from storms in the Southern Ocean penetrates throughout the Indian, South Pacific and South Atlantic Oceans. During the Southern Hemisphere winter, this swell propagates into the North Pacific.

At a local scale, seasonality effects are also typically studied as part of a site assessment. An example can be found in the resource assessment for the WaveHub site, Cornwall, as part of the Marine Energy in Far Peripheral and Island Communities (MERIFIC) project, presented in Smith and Maisondieu (2014). The seasonal power variation, with the mean power calculated for spring (March–May), summer (June–August), autumn (September–November) and winter (December–February) months are presented in Fig. 20. The monthly variation in T_{m-10} is
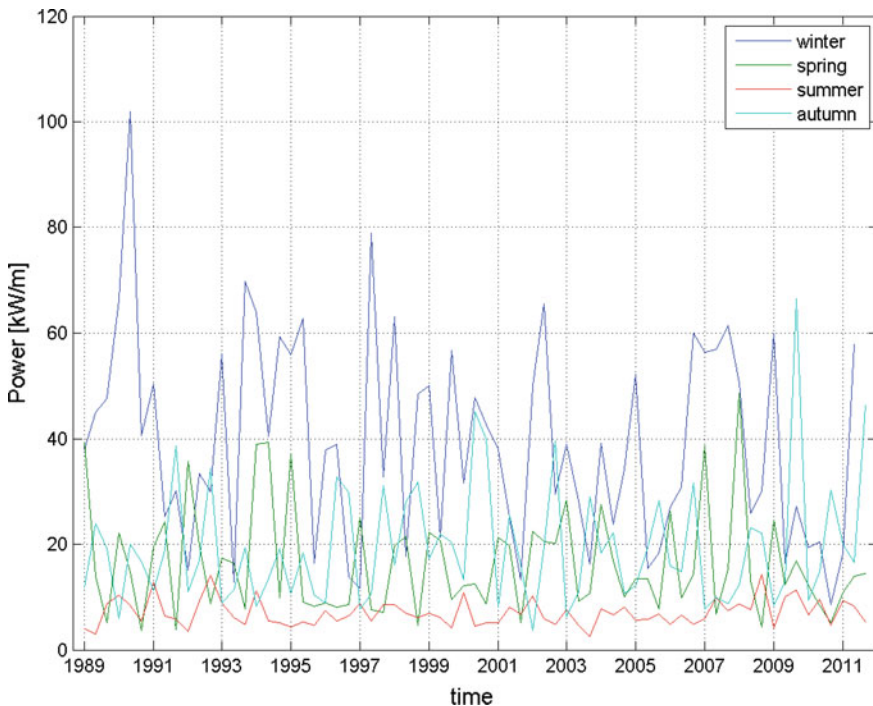

Fig. 20 Seasonal variation of power at Wave Hub (Smith and Maisondieu 2014)
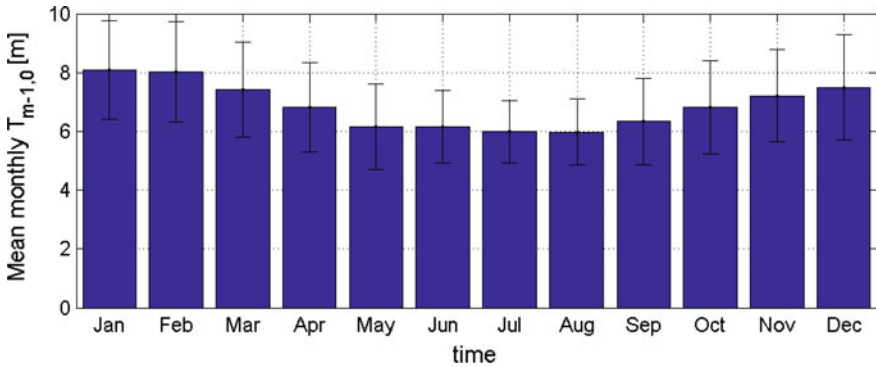
Fig. 21 Monthly variation of T_{m-10} at Wave Hub, with bars showing the standard deviation in the data (Smith and Maisondieu 2014)

shown in Fig. 21. The variation in power levels over each year is substantial. Averaged over the entire dataset, it can be seen that the winter months are the most energetic.

Marine Operations

For certain design situations involving marine operations in the order of days or of weeks, an important aspect of the wave climate that must be considered involves the expected occurrence of weather windows that allow for operations such as transport, deployment, recovery and maintenance. The objective is to avoid delays in critical marine operations due to significant wave heights exceeding prescribed operational levels (limits), leading to a possible increase in the duration of the operations and/or increased damage to the FOWTs. In such cases, the probability of occurrence of sea states in which H_s, is at, or below, a specified threshold value, for at least a specified number of hours, combined with the wait time for a number of weather windows specified by a H_s threshold and minimum window length is of interest to the project developer. An example of characteristic durations of operation limited by a given significant wave height for a given number of hours, along with the expected *mean* duration, and 10, 50 and 90 percentiles (*P10*, *P50* and *P90* respectively) is given in Fig. 22, taken from a Statoil study presenting a metocean design basis for a proposed FOWT installation site in Scotland (Mathiesen et al. 2014).

Long Term Wave Conditions—Extremes

The assessment of extreme wave conditions is essential to the design of floating support structures. For design considerations, interest is often on the most likely maxima or on the extreme values that occur within a very long period of time.

The long-term variation of the wave climate can be described in terms of generic distributions or in terms of scatter diagrams for governing sea state parameters such as H_s, T_z or θ. A scatter diagram provides the frequency of occurrence of a given parameter pair (e.g. H_s, T_{m02} as shown in Fig. 23). Both marginal distributions and

Hs < 2m for 12 hours

Mean — P10
P50 ----- P90

Duration (days)

Jan Feb Mar Apr May June July Aug Sept Oct Nov Dec

Month
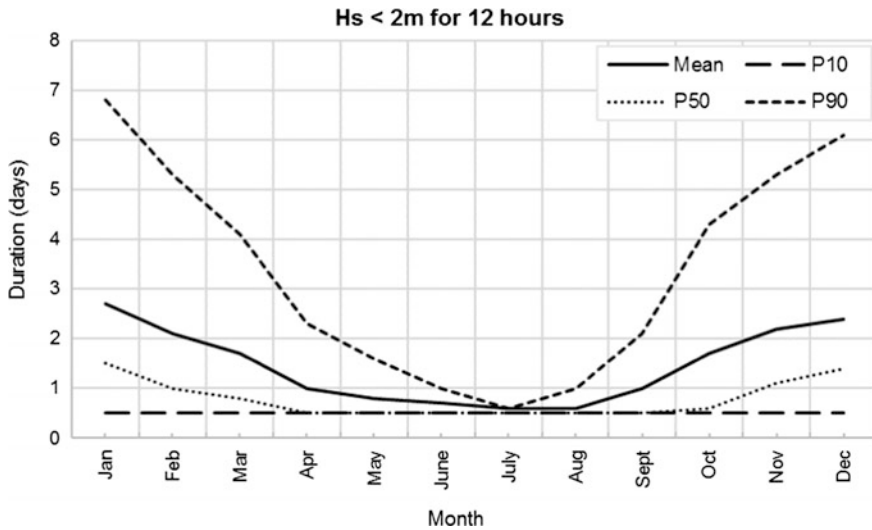
Fig. 22 Characteristic durations, including waiting time, in order to perform operations limited by a significant wave height of 2 m for 12 h (figure based on data presented in Mathiesen et al. 2014)

From 4295 data

H_{m0} [m]

T_{m02} [s]

occurrence [%]
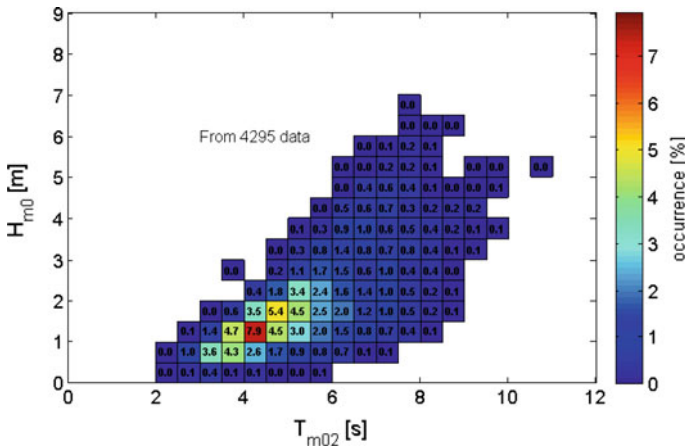
Fig. 23 Annual $H_{m0} - T_{m02}$ scatter plot for the Wave Hub region using data from November 2009 to October 2010 from a combination of ADP and wave buoy records (Smith and Maisondieu 2014)

joint environmental models can be applied to describe the wave climate. The generic models are generally established by fitting distributions to measured wave data from the site of interest.

In cases where the weather is relatively calm most of the time, and there are few very intense events, an event based approach is used for the analysis of the wave

data, where observations over some threshold level are used (e.g. Peak Over Threshold, POT, method). In an event based model like POT, the results may be sensitive to the adopted threshold level. A lower threshold decreases statistical uncertainty (by allowing more peaks over the threshold) but may reduce the accuracy by including data points that do not belong in the tail of the distribution. A suitable threshold will be associated with stable estimates beyond its value, and exponential distribution or a two-parameter Weibull distribution can then be fit with more confidence to the remaining data points.

The annual extremes of an environmental variable, for example the significant wave height or maximum individual wave height, can be assumed to follow a Gumbel distribution;

$$F(H_s) = \exp\left(-\exp\left(-\frac{H_s - U}{A}\right)\right) \tag{22}$$

where A and U are distribution parameters related to the standard deviation and the mean of the Gumbel distribution.

The significant wave height with return period T_R in units of years is then given by:

$$H_{s,T_R} = F^{-1}\left(1 - \frac{1}{nT_R}\right) \tag{23}$$

where $\left(1 - \frac{1}{nT_R}\right)$, is the quantile of the distribution of significant wave heights, with n the number of sea states per year. To accompany the H_{s,T_R} significant wave height and complete the definition of the T_R year design sea state, the T_p or T_z values are typically varied within a period band about the mean or median period.

For reliability analysis, joint environmental models can be used. A common approach for establishing a joint environmental model is the Conditional Modelling Approach (CMA) (e.g. Bitner-Gregersen and Haver 1991), where a joint density function is defined in terms of a marginal distribution and a series of conditional density functions. For example, for a joint distribution of significant wave height and period:

$$f_{H_s T_z}(h, t) = f_{H_s}(h) \cdot f_{T_z|H_s}(t|h) \tag{24}$$

Often, the probability density function for the significant wave height is modelled by a 3-parameter Weibull distribution and the zero-crossing wave period conditional on H_s is modelled by a lognormal distribution. For a joint distribution of significant wave height and wind speed, Bitner-Gregersen and Haver (1989, 1991) use a 2-parameter Weibull distribution which can be applied for the mean wind speed U conditional on H_s.

Other approaches for establishing a joint environmental model exist, such as the Maximum Likelihood Model (MLM) (Prince-Wright 1995), or the Nataf model (Der-Kiureghian and Liu 1986).
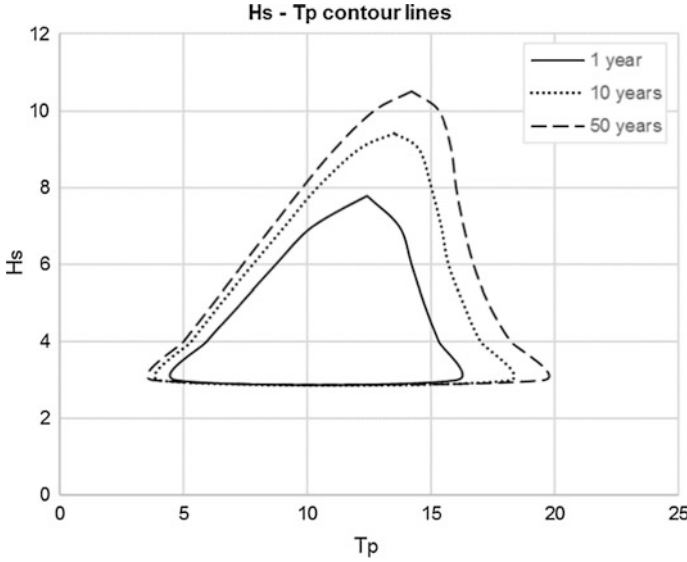
Hs - Tp contour lines

Fig. 24 $H_s - T_p$ probability contour lines for return periods of 1, 10 and 50 years, for omni-directional waves at a specific site (figure based on data presented in Mathiesen et al. 2014)

The environmental contours can then be defined in the environmental space from the joint environmental model of sea state variables (e.g. H_s, T_p, as shown in Fig. 24) (Winterstein et al.1993). A common method to define these contours is to estimate the extreme value for the governing variable for the prescribed return period, e.g. H_s, and associated values for other variables, e.g. T_z. The contour line is then estimated from the joint model or scatter diagram as the contour of constant probability density going through the above mentioned parameter combination.

Following Battjes (1978), the maximum individual wave height in a random sea state can be expressed as:

$$F(H_s) = \frac{1}{\overline{v_0^+}} \iint_0^\infty v_0^+ \left(h_s, t_p\right) F_{H|H_s T_p}\left(h|h_s, t_p\right) f_{H_s T_p}\left(h_s, t_p\right) dh_s dt_p \qquad (25)$$

where $v_0^+ \left(h_s, t_p\right)$ is the expected zero-up-crossing wave frequency for a given sea state and $\overline{v_0^+}$ is the long term average zero-up-crossing wave frequency given by:

$$\overline{v_0^+} = \int \int_0^\infty v_0^+ \left(h_s, t_p\right) f_{H_s T_p}\left(h_s, t_p\right) dh_s dt_p. \qquad (26)$$

The individual wave height with return period T_R (in years) then follows from:

$$1 - F(H_{T_R}) = \frac{1}{T_R \cdot 365 \cdot 24 \cdot 3600 \cdot \overline{v_0^+}} \qquad (27)$$

The extreme sea state characterisation can be made based on measurements of the sea-surface, or using numerical wave models based on wind, tide and seabed topography information. These techniques, and their limitations, are detailed further in the following sections.

2.2 Measuring the Resource

Measurement techniques can be divided in two categories: in situ techniques, where the instrument is deployed in the water, and remote-sensing techniques, where the instrument is deployed at some distance above the water.

When making measurements to determine the wave resource, it is important to have a clear understanding of how representative the measurement is of the area in which the measuring instrument is situated. This depends on the exposure of the measurement site to the prevailing waves in terms of sheltering, and of the bathymetry of the area surrounding the wave measurement site.

In Situ Techniques

Wave Buoys
The most common in situ instruments are wave buoys. Such instruments have been used for measuring waves since the early 1960s. The buoy follows closely the motion of the water particles by floating at the surface, and measures its vertical acceleration with an on-board accelerometer, stabilised on a gravity platform for artificial horizon reference. The sea surface elevation is obtained by integrating twice the vertical acceleration (the small horizontal motion is ignored). Three of the main manufacturers of wave measurement buoys are OCEANOR, Datawell and TRIAXYS. Each produces a range of directional and non-directional buoys for different applications, examples of some available wave buoys are illustrated in Fig. 25.

In order to measure the direction of the wave, the buoy sensor can be refined to also measure its inclination with the horizontal. Two methods are mostly used. The first type calculates the slope of the sea surface from the pitch and roll motions of the buoy. The mean direction is determined from the tilt, measured with incli-nometers, and the direction to the geographic North. Such buoys are usually rela-tively flat, like the WAVEC buoy (Wave-VECtor, a Datawell buoy). The second type uses the sway and surge motions of the buoy to determine its tilt. The Directional WaveRider buoy from Datawell uses the Earth's magnetic field to measure its tilt, and a study conducted by Barstow and Kollstad (1991) showed that

Fig. 25 Seawatch Wavescan buoy (www.oceanor.com) (*left*), Datawell Waverider buoy (http://www.datawell.nl) (*centre*), Seawatch Midi 185 buoy (www.oceanor.com) (*right*)

this leads to reliable data when compared with a Wavescan buoy. Some other wave buoys, like the GPS-WaveRider, use a global positioning system (GPS).

When deploying wave buoys, a compromise must be considered between station keeping and minimal impedance to the buoy motion requirements. Site specific water depth, current and wave climate must be taken into account when designing the moorings that will keep the buoy on station. Aside from mooring compliance and limitation, steep waves also bring bias in the wave buoy motion, with the natural tendency of the buoy to bypass the crest, leading to smaller estimates of the wave height.

The time series data recorded by wave buoys is processed into auto- and cross-spectra, from which the variance density spectrum and the directional distribution can be obtained. It should be noted that integrating acceleration data to obtain displacements is difficult as very low frequencies or offsets are present. Typically, the lower frequencies are amplified with the noise superimposed. A difficulty arises when considering that the use of a high pass filter has the effect of also filtering the second order non-linear part of the waves, and leading to a bias of the measured heights of the wave crests.

Data recorded and post processed by the buoy can be stored on-board, or regularly transmitted to the shore. Data transmission, often used to avoid the weather-window limitation (especially during winter months), can be achieved by standard communication systems such as radio (HF, VHF, GPRS systems) or satellite (ARGOS, ORBCOMM etc.). However, data transmission, especially via radio, can be compromised in for example large waves events. When storing data on-board, manual downloads on a periodic basis, depending on the data storing capacity, will be required. Access to the buoy will also be required typically once to twice a year for battery replacement and check/re-calibration of instrumentation.

Acoustic Doppler Profilers (ADPs)

Although initially developed for current measurements, ADPs have been further developed to enable wave spectrum estimates. Three different technics can be used for sea surface wave measurements.

The first technique leads to a directional spectrum, using the cross-spectra obtained from the along-beam component of the wave orbital velocity. The cross-spectra gives the phase difference between the different beams, which then gives the wave direction and wavelength.

Two other techniques enable the calculation of the omni-directional spectrum. Surface tracking is the echo location, using the ADP beam(s), of the range to the surface. The signal of the inverted echo-sounder is reflected off the water surface, which produces a time series of sea surface elevation. The pressure sensor technique also measures the sea surface elevation via dynamic pressure measurements, but is very sensitive to wave number and is therefore mostly used for redundancy and data quality check.

Two of the most commonly used ADPs for wave measurement are Teledyne RD Instruments' Workhorse Waves Array and Nortek's AWAC with Acoustic Surface Tracking (AST). Both use the three different techniques introduced above to describe the waves.

ADPs can be mounted on the seabed or on a sub-surface buoy. The former is more secured and less vulnerable to damage, but the accuracy at high frequency can potentially be decreased by larger water depths. A compromise must then be considered between accuracy and vulnerability. Furthermore, a bottom mounted ADP can be subject to burying by the bottom soil and compromise the data acquisition; this additional risk should also be taken into account when considering ADP deployment, depending on the bottom soil at the measurement site.

Data recorded and post processed by the ADP can be stored on-board, or regularly transmitted to the shore. Data transmission, often used to avoid the weather-window limitation (especially during winter months), can be achieved by standard communication systems such as radio (HF, VHF, GPRS systems) or satellite (ARGOS, ORBCOMM etc.). However, similar to a wave buoy, data transmission can be compromised in large waves events. When storing data on-board, manual downloads on a periodic basis, depending on the data storing capacity of the instrument, will be required. On top of manual downloads, access to the ADP will also be required typically once to twice a year for battery replacement and check/re-calibration of instrumentation.

Remote-Sensing Techniques

HF and X-Band Radars

HF radar is a shore-based remote sensing system using radio waves in the 3–30 MHz region to measure directional wave spectra and surface currents. It requires two shoreline transmitter/receiver stations to be set up so that the *look* directions are approximately at right angles, with overlapping transmission region.

Subject to a number of limitations, the full directional spectrum can be measured on a grid defined by the intersection of the radar beams with a spatial resolution typically between 300 m at best, for short-range systems, and 5 km. The temporal resolution is typically a maximum of 10-min. The radar operating range, typically between 10 and 100 km, defines the range of H_s that can be observed and the highest wave frequency measurable.

On most occasions the spectrum can be measured accurately using remote sensing systems, but there are occasions when this is not so. This is because the data interpretation (inversion) technique is quite sensitive to imperfections in the radar data. Of the directional parameters, mean direction is reasonably reliable but directional spread may not be very accurate. Comparisons of wave power estimates suggest that differences between buoy and radar measurements are mostly comparable with the (joint) sampling errors associated with the two methods.

Based on the phenomenon of Bragg scattering of the transmitted waves by ocean waves of exactly half their frequency, the Doppler spectrum of the radio backscattered waves is observed. The frequencies of the two discrete peaks of the Doppler spectrum can be used to determine the surface currents. The directional spectrum of the ocean waves is then obtained by inversing techniques.

The main advantages of HF radar compared to in situ measurements such as wave buoys or ADP systems are two-folds: the spatial coverage that a HF radar system is up to 40 by 40 km, which would be very difficult (e.g. in terms of maintenance and costs) to obtain with in situ measurement methods; the easy access to the land-based instrumentation also provides a significant advantage over other in situ or satellite measurements.

The X-band radar is based on a similar technique to that of the HF radar, but uses shorter electromagnetic waves of about three centimetres wavelength. Such short wavelength interacts with surface ripples, which makes the X-band radar valuable for wave measurements in sites with light wind generating ripples on sea surface, where other techniques are unlikely to be successful.

The technique allows high-resolution directional spectra to be derived from radar images over ranges of a few kilometres. The wave information obtained is the average over an area of the order of one half kilometre square, rather than a point measurement.

Satellite Measurements

Satellite-based wave measurement differs significantly from the previous systems discussed due to the extensive coverage available. However, this type of measurement is less suited to short-term, site-specific nearshore wave resource assessment. Due to the satellite's track and revolution time limiting the spatial and temporal resolutions; it is mostly used to obtain long-term datasets for the analysis of longer-term temporal variability. Satellite-borne remote sensors can be divided in two major categories: radar altimeter and synthetic aperture radar (SAR).

Radar altimeters measure the distance between the satellite and the sea surface. The orbit of the satellite is typically 1000 km (Krogstad and Barstow 1999). The distance between the satellite and the reference ellipsoid is derived by using the Doppler effect associated with signals emitted from marker points on the Earth's surface as the satellite orbits overhead. Variations in sea surface height are caused by the combined effect of the geoid and ocean circulation. Tucker and Pitt (2001) proposed a methodology to derive empirically the significant wave height from the rise time measured by the radar. To eliminate random variations in amplitude, results are averaged over a large number of returned pulses, leading to an accuracy of more than ± 0.5 m.

SARs produce a two-dimensional (2-D) image of the sea surface. Using a 2-D Fourier transform, these images are processed to obtain a directional spectrum, with periods typically ranging from 8 to 25 s. SAR is more suited to swell observation because of the limitation in high frequency in the direction perpendicular to the track of the satellite. Typical spatial resolution for SAR images is about 25 m, for a swath of 100 km to up to 500 km wide for some satellites (e.g. RADARSAT).

Quality Control

Quality control is a necessary step in the analysis of the data received by the wave measurement device(s). The objective is to ensure the validity of the data quality, checking for flaws in the data that would lead to potentially significant errors in the resource assessment analysis and/or the determination of extreme events.

Several factors can impair the quality of the data. Faulty electronics, errors in the transmitting process, can for example generate individual spikes in the measurements, that, if large and regular, can introduce bias in the analysis. Faulty electronics can also cause high frequency noise, that potentially affects the calculation of high order spectral moments. Typically, this is solved by introducing a maximum frequency above which any integration is not performed (in general around 0.3–0.4 Hz). The integration process to transform the acceleration measurement to a displacement signal is also often subject to distortion and cause noise, in particular in the low frequency range. This low frequency noise can sometime hide a swell component.

Due to the relatively broad-band form of the wave data, where extremes cannot be automatically assumed to be faulty, the quality control of wave records is typically challenging. However, a variety of tests have been derived and are commonly used to evaluate data quality. These tests can be carried out on the original wave time series (which requires intensive processing for a large number of tests) or on the resulting frequency spectrum. For example, IOOS (2013) provides details on the main type of tests available for quality control of in situ surface wave data. The results are recorded by inserting flags in the data files where data is of low quality. Further description of the problems of wave analysis can be found in Tucker (1993) and Tucker and Pitt (2001).

Typically, the final quality of a particular wave record is determined by visual inspection of the time series or spectra. If there are outliers or suspicious trends, then the corresponding time series or spectral files and plots should be reviewed.

2.3 Resource Mapping

Although measurements of the sea state give a good representation of the wave climate at a site, it is usually too expensive to obtain long term wave climate estimates. Covering this issue, numerical wave propagation models have been developed over the last half century, which can be used in wave resource determination in the following ways:

- To provide long-term time series of wave data from which wave climate statistics can be derived. This is known as hindcasting.
- To allow calculations of wave transformation to be made in coastal areas.
- To allow operational wave forecasting for marine operations.

Since the genesis of wave generation computer simulations, several improvements have been implemented, developing the global wave models from first to third generations. However, their purpose remains the same: to simulate the growth, decay and propagation of ocean waves based on input winds over at a regional or global scale.

The early models focused on modelling wave energy growth and dissipation. Their major limitation lies in that they do not account for the nonlinear interactions between the different wave frequencies. These models are known as first generation models. The next generation of wave models, known as second generation models used parameterised approximations to model the nonlinear spectral interactions. Finally, the third generation of wave models provide a full description of the physical processes governing wave evolution.

Global Model

A number of global wave models exist today, a brief description of some of the main models used by researchers are presented below, along with wave climate studies that have been based on them.

The WAM model (WAMDI Group 1988) is a third generation wave model developed in the 1980s that integrates the basic transport describing the evolution of the wave spectrum. It calculates explicitly the effects of non-linear wave-to-wave interactions. It is routinely run at the European Centre for Medium-Range Weather Forecasts (ECMWF). More information can be found in Gunther et al. (1992) or Komen et al. (1994).

The WERATLAS project, funded by the European Union (EU) under the Joule programme, produced an atlas of annual and seasonal (yearly, Winter and Summer) wave-climate and wave-energy statistics for a set of offshore locations distributed along the European coastline (Pontes et al. 1996). Results from the WAM model were analysed for a total of 85 data points (41 in the Atlantic and 44 in the Mediterranean), using data from the period between 1987 and 1994. A wide range of wave statistical analyses, including power and T_e, are available using an interactive software package. Members of the WERATLAS project team have continued to work on the development of what has become known as WorldWaves (Barstow et al. 2003). WorldWaves is a global database of wind and wave time series data

derived from the ECMWF operational and hindcast models and are calibrated by Fugro OCEANOR against satellite data, and where available in situ buoy data to ensure that the data are as high quality as possible.

WAVEWATCH III is a wave model that was implemented in October 2008 as a replacement for the Met Office second-generation model configuration. The UK Met Office has run and maintained a suite of wave models over the past two decades to provide predictions of wave conditions, globally and around the UK. The WAVEWATCH III model provides forecast and hindcast data for a range of applications extending from predicting offshore vessel motion characteristics to forecasts of coastal overtopping.

Two 5-day forecasts with a 3-hour resolution are run per day for a global model, covering latitude from 80 S to 80 N and longitude from 180 W from 180 E with a 30 km resolution. Two operational forecasts exist for the North Atlantic European seas, covering latitudes from 25 S to 66 N and longitudes from 68 W from 42 E with a 12 km resolution: one 3-day forecast with a 1-h resolution four times a day, and another 5-day forecast with a 3-h resolution twice a day.

Typically, hindcasting requires series of wave data available for a period of at least 10-years to allow the seasonal, year-to-year and longer-term variabilities to be taken into account when deriving wave climate statistics. For this purpose, WorldWaves combines 45-year re-analysis hindcast data with operational data to provide 50-year series of wave parameter and directional spectra. The NCEP Climate Forecast System Reanalysis Reforecast (CFSRR) that uses the WAVEWATCH III model provides a 30-year homogeneous data set of hourly 0.5° spatial resolution winds.

Another use of these global models is as sources of potential wave input data at local model boundaries. Although potentially lacking the accuracy of recorded data, the use of outputs from other models as inputs for a nearshore model can often be a better option because of its spatial distribution. Outputs from other models can be treated in the same way as point measurements, and used to provide input at intervals along the model boundaries—the model will then interpolate between the input points. A second option, depending on the models being used, is nesting. Nesting involves running a larger-scale, coarser resolution model to generate boundary conditions for a finer grid, and can be repeated on decreasing scales until the required scale is attained. These local models are briefly described below.

Local Model

Local models are wave models for coastal and near-shore areas. The purpose of such model is to perform the propagation and associated transformations of the waves from offshore to nearshore, in order to investigate the detailed distribution of the wave climate. Typically, but not always, local models may use the output from a global model for their offshore boundary conditions and calculate the wave conditions at an array of grid points in the near-shore zone. The following paragraphs describe two examples of local models, but there are of course many others.

SWAN is a refraction model developed by the Technical University of Delft (SWAN Team 2006 or SWAN Team 2009) that includes many of the important

shallow water processes as well as generation by the wind. There is thus a lot of overlap between models such as this and the global models; the difference is essentially in the long-term use of the global models by the meteorological agencies. SWAN has been designed so that it can be nested in WAM and WAVEWATCH III, allowing global outputs to feed into the near shore model.

Another local model is the MIKE-21 suite which is available on a commercial basis from the Danish Hydraulics Institute (DHI) (2015). This is a linear refraction/diffraction model based on the mild-slope equation.

These two models are third-generation spectral wave models, developed for the calculation of the propagation of random waves from deep to shallow water, accounting for the different physical processes introduced in Sect. 1.1, such as white capping, bottom friction or wave-to-wave interaction.

Model Validation and Calibration

Wave models can be fine-tuned for different sites and scenarios using a number of model-dependent parameters. The calibration of these parameters can be based on published literature or through comparison to in situ measurements. In the case of calibration using measurements, wave height and wind speed data from satellite altimeter is often used for direct validation of wave models. Wave buoys can also be used, when long-term data sets are available. Figure 26 presents an example of an analysis for a model validation, which compares observed and model data.

If the wave models can bridge gaps in measured data, the wave measurements are still essential to calibration and validation of these models. For detailed site specific assessment this will likely require a dedicated measurement programme. In situ observations obtained from buoys, ships, oil platforms and satellites can be used for this purpose. The following simple statistical parameters (Ris et al. 1999) can be calculated to validate data, with x_i and y_i the measured and model wave parameters respectively:

Bias:

$$bias = \frac{1}{N} \sum_{i=1}^{N} (x_i - y_i) \tag{28}$$

Root Mean Square Error:

$$rms_{error} = \left[\frac{1}{N} \sum_{i=1}^{N} (x_i - y_i)^2 \right]^{\frac{1}{2}} \tag{29}$$

Scatter Index:

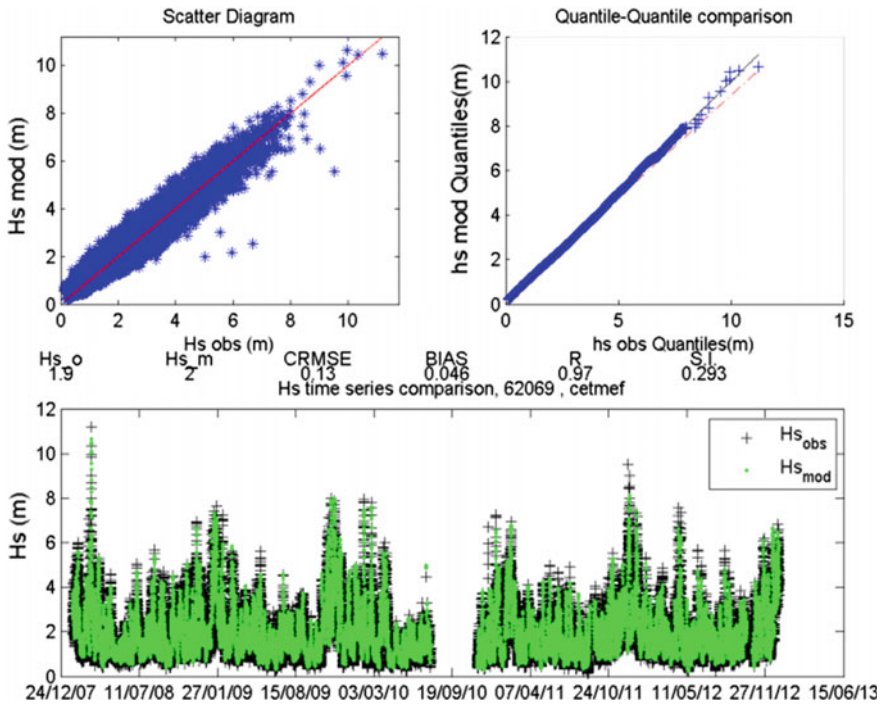$$SI = \frac{rms_{error}}{\bar{x}} \tag{30}$$

Fig. 26 Model validation—cross-comparison between buoy and numerical model output data (Smith and Maisondieu 2014)

Model Performance Index:

$$MPI = 1 - \frac{rms_{error}}{rms_{changes}} \tag{31}$$

Operational Performance Index:

$$OPI = \frac{rms_{error}}{x_i} \tag{32}$$

For example, in the WorldWaves project, satellite data from 1996 to 2002 was used to validate and subsequently calibrate the ECMWF model data. This was found to be worthwhile as there was typically a systematic bias on the raw model data. Removing that bias significantly improves the data quality, particularly in enclosed seas such as the Mediterranean Sea. Barstow et al. (2009) present the correlation coefficient between significant wave height calculated for the validation of the ECMWF wave model. A systematic underestimation of the significant wave height was found and used to calibrate the numerical model (Barstow et al. 2009). As a result, the ECMWF wave model is considered today the lead tool in its field.

2.4 Discussion

In this section a detailed account of the origin and methods to assess the wave climate were given. A knowledge of waves is essential when considering the design and operational safety of offshore structures such as floating wind turbines, and requires the quantification of the wave conditions to establish the relevant environmental conditions for the design of the structure at the proposed location.

Several methods available to estimate the directional spectrum of the waves were described. Sensors such as surface buoys, acoustic Doppler profilers or remote-sensing techniques are commonly used to characterise the sea surface. Careful consideration regarding the local bathymetry is required to ensure that the resource is representative of the target site. For a first selection of suitable areas, numerical models are commonly used and their validation against measurement, is critical.

Overall, the objective of this section has been to present the main parameters to consider to feed into the environmental load calculations and inform the design of a FOWT and its support structure, which are addressed in Chapter "Key Design Considerations".

3 Other Environmental Conditions

Mairéad Atcheson

There are several additional environmental conditions that may be considered when characterising a potential site, leading to their inclusion in a metocean design basis for a FOWT. Section 3.1 overviews the description of local current and water depth variations, including methods of measuring and modelling these variables. Other phenomena which may also be important include seismic activity and ice conditions, which are overviewed in Sects. 3.2 and 3.3 (respectively).

3.1 Currents and Sea Level

Currents
Sea currents vary in space and time, however for design purposes they are generally considered as horizontal uniform flow fields of constant velocity, varying only as a function of depth (IEC 61400-3 2009). The flow of water can be represented mathematically as a velocity vector defining the speed and direction of the current. The following components of sea current velocity should be taken into account when considering the environmental conditions at a proposed installation site:

- Sub-surface currents generated by tides, storm surges, atmospheric pressure variations, etc.,
- Wind-generated, near surface currents, and
- Near shore, wave induced surf currents running parallel to the coast.

The total current at a given location can be calculated by superimposing the vector sum of the relevant current components for the specific site to determine the variation of the current velocity with depth, referred to as the current profile. The current direction is generally described in terms of degrees measured clockwise from geographic north, and the convention is to define the direction the current is flowing in. The DNV offshore standards (DNV-OS-J101 2014) allow for the application of standard current profiles when detailed field measurements are not available to describe the current conditions. The variation in the current velocity with depth may be calculated as:

$$v(z) = v_{tide}(z) + v_{wind}(z) \tag{33}$$

where $v(z)$ is the total current velocity at level z, v_{tide} is the tidal current profile component and v_{wind} is the wind generated current component.

The tidal current profile may be characterised by a recognised power law approximation, where the variation of tidal current with depth, relative to the still water level (SWL) may be taken as:

$$v_{tide}(z) = v_{tide0}\left(\frac{h+z}{h}\right)^{1/7} \quad for \ z \leq 0 \tag{34}$$

where v_{tide0} is the tidal current at the SWL, h is the water depth from the SWL (taken as positive) and z is the vertical coordinate from the SWL (taken as positive).

The wind-generated current can be represented as a linear distribution of velocity reducing from the surface velocity to zero at a reference depth for the wind generated current below the SWL.

$$v_{wind}(z) = v_{wind0}\left(\frac{h_0+z}{h_0}\right) \quad for \ -h_o \leq z \leq 0 \tag{3.35}$$

where v_{wind0} is the wind generated current at the SWL and h_0 is the reference depth for the wind generated current [$h_0 = 20$ m (IEC 61400-3 2009) or 50 m (DNV-OS-J101 2014)].

The wind-generated surface current may be assumed to be aligned with the wind direction, and may be estimated from:

$$v_{wind0} = k \cdot U_0 \tag{36}$$

where U_0 is the 1-hour mean wind speed value at a height of 10 m above the SWL and $k = 0.015$ to 0.03 (DNV-OS-J101 2014) or 0.01 (IEC 61400-3 2009).

Where the currents at a site may vary considerably from the standard profile descriptions, site specific current profile measurements should be made.

Sea Level

The sea level at any location consists of the mean depth, defined as the distance between the seabed and an appropriate datum, and a variable component mainly attributed to astronomical tides and storm surges. Astronomical tides are generated by the gravitational pull of the moon and to a lesser extent the sun on the ocean waters of the rotating earth. Storm surges reflect changes in sea level due to meteorological forcing, including wind and atmospheric pressure effects.

The difference in height between consecutive high and low waters is described as the tidal range. A spring tide is the very highest and very lowest tide (i.e. it has the largest tidal range) which occurs twice a month (approximately every 14/15 days). Neap tides are the opposite of spring tides when the smallest tidal range is observed. The variation in water level due to the tide is described based on the lowest astronomical tide (LAT), which is the lowest level that can be predicted to occur for any combination of astronomical conditions. Similarly, the highest astronomical tide (HAT) is the highest level produced due to astronomical conditions. The best estimates of the mean water level and fluctuation (i.e. HAT, LAT and extreme water levels) are derived from site-specific measurements.

Changes in water depth due to storm surges are superimposed on the tidal variations to define the range of water levels at a site. The highest still water level (HSWL) is defined as a combination of the HAT and positive storm surge, for a given return period. Correspondingly, the lowest still water level (LSWL) is a combination of the LAT and negative storm surge, for a given return period. The relevant water levels that should be considered as a minimum are illustrated in Fig. 27. The mean sea level (MSL) is defined as the arithmetic mean of hourly observed sea levels over a period of at least 1-year, but preferably 19-years to average out the cycles of the 18.6-year nodal tidal cycle (Pugh 1996).
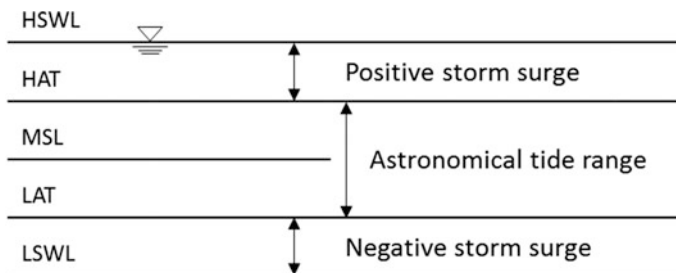

Fig. 27 Definition of water levels

Measurements and Modelling

For the design stages of a FOWT it is necessary to develop accurate and reliable site data as a basis for statistical analyses. The optimal set of data consists of long term, site-specific measurements that accurately describe the currents and sea level conditions that a FOWT would be exposed to at a particular location. However, the availability of such datasets is rare, since the time between the selection of a site and installation may only be a few years, and measurement campaigns usually only commence after a site has been selected. In this situation, hindcast data is commonly used as a supplement to establish a metocean database for a specific site. Once a metocean database has been established, the data can be statistically analysed in various ways to determine values for the metocean parameters required during the design stages.

Types of Sensors

It is important that the correct measurement instruments are used to obtain the level of information required. A thorough understanding of the instrument's measurement range, resolution and accuracy are vital to maximising the instrument's measurement potential. The instrument must also be correctly calibrated and the appropriate deployment options chosen to ensure accurate sampling of the study environment.

Currents can be measured in situ by acoustic Doppler current profilers (ADCPs) or current meters. Current meters provide a measure of flows at a fixed depth in the water column. Often numerous current meters are deployed on a single mooring and the instruments are positions at different intervals throughout the water column. ADCP are increasingly used for in situ current measurements and are capable of making non-intrusive current profile measurements through the water column. The instrument divides the measurement profile into uniform slices called depth cells and a weighted average velocity is calculated for each depth cell. ADCPs may be deployed from ship-mounted and bottom-mounted installations.

Acoustic measurement instruments measure velocity with sound, using a principle of sound waves referred to as the Doppler Effect. The instrument transmits sound at a known frequency into the water and listens for echoes of the sound reflected from particles suspended in the water. The difference between the transmitted pulse and return echo frequencies is referred to as the Doppler shift. If the particles are moving away from the instrument transducer they have a slightly lower frequency than the transmit frequency. Particles moving towards the instrument have a higher frequency. The instrument uses the difference in frequency (the Doppler shift) and the speed of sound in water to calculate the along-beam velocity i.e. the velocity of the particles (and hence the flow speed). A key assumption made by acoustic Doppler measurement instruments is that particles suspended in the water move at the same velocity as the water. ADCPs measure the radial speed of flow along the instruments inclined acoustic beams and the velocity vectors are derived from the along-beam velocity measurements. This method assumes that the flow is homogenous in the horizontal plane over the distance of separation between

the beams. For the purpose of measuring mean current velocities in tidal currents it is sufficient to use averaging periods of 10-min (DNV-RP-C205 2010).

Sea levels are typically measured at tidal stations along the coastline on a long term basis, where they can be levelled to a consistent land datum [i.e. Ordnance Datum Newlyn (ODN)]. Long-term offshore measurements of water level are not as common and more difficult because there are no obvious fixed reference points. One method of observing the offshore sea level is a pressure measuring system. The pressure at some fixed point below the sea surface is measured and converted into a level using the basic hydrostatic relationship, taking into account the water density and atmospheric pressure. Most ADCP instruments include a pressure sensor capable of measuring the water depth.

A data repository for in situ measurements of water level data across the globe is provided by the Global Sea Level Observing System (GLOSS). GLOSS is an international programme that aims to establish high quality global and regional sea level networks through a global core network of 290 sea level stations around the world (GLOSS 2016).

Measured oceanographic data are available from many stations globally and sources of data for a specific region may be identified through the Ocean Data Portal (ODP) held by the International Oceanographic and Data Information Exchange (IODE) programme of the IOC UNESCO (ODP 2016). The ODP hosts oceanographic data from a global network of 80 National Oceanographic Data Centres (NODCs). SeaDataNet and the Marine Data Exchange (by The Crown Estate in the UK) are other databases where current measurement data, as well as other oceanographic data, may be sourced for certain regions and locations. SeaDataNet is a Pan-European network that manages datasets (in situ and remote observations) for all European seas (SeaDataNet 2016). The Marine Data Exchange hosts data collated during the planning, building and operation of offshore renewable energy projects in the UK (Marine Data Exchange 2016).

Hydrodynamic Modelling

Currents and sea levels at a site can be modelled through the application of hydrodynamic models. In general, hydrodynamics models can be split into two categories: a depth averaged current model (2D) and a depth varying current model (3D). Data required to set up hydrodynamic models include the pressure and wind fields, the area bathymetry (water level) and tidal information. The more complex 3D models require additional input data, e.g. temperature, salinity and density variation over the water depth. The hydrodynamic model should be calibrated using site measurements (when available) or data from nearby locations. Another method implemented by global tide models is the assimilation of satellite altimeter data into hydrodynamic models to reduce model uncertainty (Matsumoto et al. 2000; Zijl et al. 2013). A major advantage of using satellite altimeter data is that it provides spatially well-distributed coverage of water level data, including in deep, offshore areas where measurements are less frequently available.

The hydrodynamic regime at a site is defined as the movement of a body of water driven by the actions of the tide and meteorological factors, causing changes

in the currents and sea level. Ideally, the entire sea area affecting the location should be included in the model. Often a series of progressively finer grid models may be used to achieve the required resolution of information across a site for the current and sea level conditions. The atmospheric pressure and wind data (speed and direction) are normally interpolated from a coarser model. The mean water depth is required across the site; this information may be obtained from electronically available bathymetry maps or from a dedicated bathymetric survey of the site. Tidal elevation should be specified at the model boundaries. The model calculates the surface elevation and current as a function of time in each grid point. Data produced by hydrodynamic models may be used to generate hindcast data, which can be analysed to estimate extreme current speed values (see for example Oliver et al. 2012).

Data Analysis

Prior to the analysis of measured data, high quality marine observations require quality control (QC) checks to ensure credibility and quality of the recorded data. Reference may be made to the Integrated Ocean Observing System (IOOS) manual (IOOS 2015) which reflects the present state-of-the-art in QC testing procedures for current observations. The analysis of measured currents and sea level observations has two functions. Firstly, a number of metrics can be derived from current time-series measurements to characterise the current at a development site, including current velocity and directional data with depth (from an ADCP). Secondly, measurements taken over a lunar month enable a tidal current and elevation analysis to be undertaken, which provides the basis for predicting future tides at the site. Data sets that span at least 28 days are required for a tidal analysis to determine the resolution of the primary lunar and solar constituents.

A summary of the current measurement statistic, including the principal flow direction, mean and maximum velocities, may be derived for a variety of depths to decide whether the current conditions at the site are of consequence to the FOWT design or station keeping. A histogram analysis of the processed current speeds may be completed to describe the velocity distribution at the site.

The tidal analysis of current and sea level data typically involves the decomposition of the raw time series data into a tidal and surge (residual) component. Tidal forcing is represented as a set of sinusoids at specific frequencies. Each sinusoid is referred to as a harmonic constituent that has an amplitude and phase. Harmonic analysis is the method of identifying the values of the harmonic constituent that combine to make up the tide at a specific location. The harmonic analysis process decomposes a measured velocity time series into a set of superimposed, periodic forcings, which can be used to predict the tidal current at the site in the future (or make hindcast predictions). The tidal component is deterministic and standard tidal analysis techniques may be applied to predict the tidal current and elevation for any time period over its 18.6-year nodal cycle (Pugh 1996; Pawlowicz et al. 2002). The main tidal harmonic constituents, according to Boon (2004), are: M2 (main lunar semidiurnal—period of 12.42 h); S2 (main solar semidiurnal—period of 12 h); N2 (larger lunar elliptical semidiurnal—period of

12.66 h); K1 (lunar—solar declinational diurnal—period of 23.93 h) and O1 (lunar declinational diurnal—period of 25.82 h).

Unlike deterministic tidal properties, surge events vary from event to event as small variations in weather patterns may produce variable responses in a body of water (Pugh 1996). The prediction of the non-tidal component requires a much longer dataset to reliably estimate the very low probability extreme events. Where there are insufficient observations to make statistical estimates of extreme events, hindcast data from numerical models may be used.

In practice, there are several methods of statistically modelling extreme ocean environments (Jonathan and Ewans 2013), one example is the historical method for calculating low probability values presented in ISO 19901-1 (2005). This method uses either measured or hindcast data, selects a set of the highest occurring current speeds and fits the tail of the probability distribution with an appropriate extreme distribution (i.e. Gumbel or Weibull).

3.2 Seismic Activity

The anticipated seismic activity of an area shall be assessed based on previous records of seismic events, expressed in terms of recurrence intervals and magnitude (DNV-OS-J101 2014). Information on the proximity of a site to active faults, type of faulting and sub-surface soil conditions should also be considered (ABS 2013). A Global Seismographic Network (GSN), formed in partnership with the United States Geological Survey (USGS), the National Science Foundation (NSF) and the Incorporated Research Institutions for Seismology (IRIS), provides worldwide monitoring with over 150 modern seismic stations. Data collected from the GSN are archived, and may be accessed through the IRIS data management centre (IRIS 2016). Other sources of global earthquake event data include the ISC-GEM Global Instrumental Catalogue [1900–2009] (Storchak et al. 2013) and the historical earthquake catalogue and archive [1000–1903] (Albini et al. 2013).

If a region is determined as seismically active, seismic events should be considered by taking into account the maximum ground motion that is likely to occur. Therefore the consideration of seismic events in seismically active regions shall investigate the characteristics of ground motions. Typically, actions arising from earthquakes are not of concern to the design of floating structures (ISO 19904-1 2006), however the effects of earthquake-induced foundation movements on the design of TLP-type floating support structures should be taken into account (DNV-OS-J103 2013). Details of the seismic design procedures and criteria for offshore structures can be found in ISO 19901-2 (2004).

Earthquake ground motions at a site may be described by response spectra or standardised time histories with the peak ground acceleration to characterise maximum motion (NORSOK Standard 2007). Information on the peak ground accelerations for specific annual exceedance probabilities can be found in seismic zonation maps. For example, seismic hazard estimates for the UK Continental Shelf

are presented in Health and Safety Executive (2003) and regional information for offshore areas around the globe is provided in ISO 19901-2 (2004).

In addition to seismically induced ground motions, consideration should also be given to additional seismic hazards including: tsunamis; liquefaction of subsurface soils; submarine slides; fault movement; shock waves and mud volcanoes (ISO 19901-2 2004). Tsunami waves are long with low height when travelling through deep water and pose little hazard to floating structures (ISO 19901-2 2004). A tsunami database is available from the National Oceanic and Atmospheric Administration (NOAA) in the United States, which provides information on historic tsunami events across the global (National Geophysical Data Center/World Data Service 2016). Soil investigations should be carried out to determine the dynamic soil properties and liquefaction potential at seismically active sites (ISO 19901-4 2003). Soil investigation requirements and recommendations for offshore wind turbines located in seismically active regions are given in ISO 19901-2 (2004) and DNV-OS-J101 (2014).

3.3 Ice Conditions

The relevance of sea ice conditions depends on the geographical location of the planned installation site and whether ice may develop or drift at this location. Ice conditions can pose two main threats to the durability of offshore structures, icing on the structure and the mechanical actions of sea ice (Battisti et al. 2006).

The NOAA centre host a wide variety of global ocean climatology data, including the World Ocean Database (WOD13) (Boyer et al. 2013) which presents long-term datasets of oceanographic data (i.e. temperature, salinity). Information from these global databases may provide some guidance on the relevance of ice conditions to a particular region of interest, as well as some indicative values for the relevant metocean parameters that may be suitable for conceptual studies.

Sea Ice

Sea ice is frozen ocean water, which forms and begins to grow whenever the temperature of the ocean reaches freezing point (typically −1.8 °C for seawater of salinity 32 ‰). In contrast to sea ice, icebergs, glacial and shelf ice originate on land and formed from fresh water or snow.

Sea ice can be described in terms of its thickness, its age and its movement with the wind and ocean currents. Ice types can be characterised as first-year, second-year, and multi-year sea ice, shelf ice and glacial ice. Once sea ice develops into sheet ice, it continues to thicken throughout the winter and is referred to as first-year ice. When the temperature increase in the spring the ice begins to melt, but if the ice is thick enough to remain until the following winter, it will begin to thicken again and is now referred to as second-year ice. The descriptor freezing degree-days (FDD) may be used as a measure of the general severity of ice conditions, which is related to how cold it has been for how long. The number of FDDs

during a winter is summed to calculate the frost index K (or accumulated FDD) for a winter using the following equation (ISO 19906 2010):

$$K = \left| \sum T_a - T_b \right| \tag{37}$$

where T_a is the mean daily temperature (degrees Celsius) and T_b is the freezing point of sea water.

Only days with a mean daily temperature below the freezing temperature are included. In order to calculate the actions caused by ice on a structure, values for the thickness of ice floes that are representative of the site should be defined. The ice thickness may be calculated using the frost index or an available ice atlas for the area, and used as a basis for determining design ice loads (DNV-OS-J101 2014). The frost index for a location varies from year to year and may be represented by its probability distribution, which may be used to estimate the frost index with a specified return period. The ice thickness (t) can be estimated by (DNV-OS-J101 2014):

$$t = 0.032\sqrt{0.9K - 50} \tag{38}$$

where t is in units of meters and K is the frost index in units of FDD.

Sea ice data can be obtained from direct observations, interpretation of satellite imagery or historical information available for the region of interest. NOAA provides high-resolution regional climatology information for various regions (e.g. East Asian Seas Regional Climatology (Johnson and Boyer 2015) and the Greenland, Iceland and Norwegian Seas (GINS) (Seidov et al. 2013)). On a national level, ice services (including ice charts) are typically available from national meteorological institutions.

Snow and Ice Accretion

Estimates should be made of the extent to which snow and ice may accumulate on an offshore installation. Icing on an offshore structure requires a combination of water on the offshore structure surfaces above the water level at subfreezing temperatures. Two main types of icing occur on offshore structures: atmospheric icing and icing due to sea spray.

Atmospheric icing is associated with precipitation. Super-cooling occurs in the atmosphere when the liquid phase reaches temperatures below freezing point. Super-cooled droplets can exist in several forms including freezing rain, snow, drizzle and super-cooled fog. Wet snow may freeze to the surface of a structure, but the ice formed is porous and the density of the accumulate snow (100 kg/m^3) is considerable lower than ice (900 kg/m^3) (ISO 19906 2010). Sea spray icing occurs with strong winds in combination with cold air and low sea temperatures, where sub-cooled water hits the structure and the water can freeze instantly. Sea spray is typically generated by the structure as it interacts with waves.

Icing can be measured in terms of thickness, volume or mass of ice adhering to a structure. The uneven distribution of snow or ice accretion should be considered for

buoyancy stabilised structures. Atmospheric icing may form a uniform layer of ice on all surfaces from a few meters above the sea surface, or freezing rain can potentially only cover the windward side of a surface. The ice growth process is highly dependent on both the climatic factors and the wind turbine geometry (Battisti et al. 2006).

The estimation of ice accretion on solid surfaces can be performed through direct measurement, indirect measurement or numerical modelling. Direct measurements are based on the detection of some change in physical property caused by ice accretion (e.g. ice sensors, double anemometer and vane). Indirect measurements are based on the detection of meteorological parameters that lead to icing (e.g. temperature, humidity and wind speed). The International Energy Agency (IEA) Wind Task 19 Wind Energy in Cold Climates was established to address specific issues for wind turbines operating in cold environments. Under this remit, the IEA has produced information on the state-of-the-art of wind energy in cold climates (IEA Wind Task 19, 2012) and recommended practices for wind energy projects in cold climates (IEA Wind 2012).

References

References (1)

American Meteorological Society (2015) Aerodynamic roughness length. Glossary of meteorology. http://glossary.ametsoc.org/wiki/aerodynamic_roughness_length. Accessed 20 May 2015
Ayotte KW (2008) Computational modelling for wind energy assessment. J Wind Eng Ind Aerodyn 96:1571–1590
Barry R, Chorley RJ (1998) Atmopshere, weather and climate, 7th edn. Routledge, London
Barthelmie RJ, Courtney MS, Højstrup J, Larsen SE (1996) Meteorological aspects of offshore wind energy: observations from the Vindeby wind farm. J Wind Eng Ind Aerodyn 62:191–211
Burton T, Sharpe D, Jenkins N, Bossanyi E (2001) Wind energy handbook. Wiley, Chichester
Carta JA, Velázquez S, Cabrera P (2013) A review of measure-correlate-predict (MCP) methods used to estimate long-term wind characteristics at a target site. Renew Sustain Energ Rev 27:362–400
Coelingh JP, Van Wijk AJM, Holtslag AAM (1996) Analysis of wind speed observations over the North Sea. J Wind Eng Ind Aerodyn 61:51–69
Cradden L, Harrison G, Chick J (2012) Will climate change impact on wind power development in the UK? Clim Change 115:837–852

Cradden LC, Restuccia F, Hawkins SL, Harrison GP (2014) Consideration of wind speed variability in creating a regional aggregate wind power time series. Resources 3:215–234

Dee DP, Uppala SM, Simmons AJ et al (2011) The ERA-Interim reanalysis: configuration and performance of the data assimilation system. Quart J Roy Meteorol Soc 137:553–597

DNV-RP-J101 (2011) Use of remote sensing for wind energy assessments. Det Norske Veritas (DNV), Høvik, Norway

EUMETSAT (2015) Jason-2. http://www.eumetsat.int/Jason2/. Accessed 29 May 2015

Fairall CW, Grachev AA, Bedard AJ, Nishiyama RT (1996) Wind, wave, stress, and surface roughness relationships from turbulence measurements made on R/P FLIP in the SCOPE experiment. NOAA Technical Memo. ERL ETL-268. Boulder, CO, USA

Goddard Earth Sciences Data and Information Services Center (2013) MERRA reanalysis

Harrison G, Hawkins S, Eager D, Cradden L (2015) Capacity value of offshore wind in Great Britain. Proc Inst Mech Eng Part O J Risk Reliab 229(5):360–372

Hasager CB (2014) Offshore winds mapped from satellite remote sensing. Wiley Interdiscip Rev Energ Environ 3:594–603

Hasager CB, Barthelmie RJ, Christiansen MB et al (2006) Quantifying offshore wind resources from satellite wind maps: study area the north sea. Wind Energ 9(1–2):63–74

Hasager CB, Pena A, Christiansen MB et al (2008) Remote sensing observation used in offshore wind energy. IEEE J Sel Top Appl Earth Obs Remote Sens 1(1):67–79

Hawkins S (2012) A high resolution reanalysis of wind speeds over the British Isles for wind energy integration. PhD thesis, University of Edinburgh

Hess P, Brezowsky H (1952) Catalogue of european large-scale weather situations (Katalog der Großwetterlagen Europas) (in German). Bad Kissingen, Germany

IEC 61400-1 (2005) Wind turbines—Part 1: design requirements. International Electrotechnical Commission (IEC), Geneva, Switzerland

IEC 61400-3 (2009) Wind turbines—Part 3: design requirements for offshore wind turbines. International Electrotechnical Commission (IEC), Geneva, Switzerland

James PM (2007) An objective classification method for Hess and Brezowsky Grosswetterlagen over Europe. Theoret Appl Climatol 88:17–42

Kendon M, McCarthy M (2015) The UK's wet and stormy winter of 2013/2014. Weather 70 (2):40–47

Lange B, Højstrup J (2001) Evaluation of the wind-resource estimation program WAsP for offshore applications. J Wind Eng Ind Aerodyn 89:271–291

Lange B, Larsen S, Hojstrup J, Barthelmie RJ (2004) Importance of thermal effects and sea surface roughness for offshore wind resource assessment. J Wind Eng Ind Aerodyn 92:959–988

Manwell JF, McGowan JG, Rogers AL (2009) Wind characteristics and resources. In: Wind energy explained, 2nd edn. Wiley, pp 23–89

Met Office (2006a) Global marine meteorological observations data, part of the met office integrated data archive system (MIDAS). NCAS British Atmospheric Data Centre, 21 May 2015. http://catalogue.ceda.ac.uk/uuid/77910bcec71c820d4c92f40d3ed3f249

Met Office (2006b) UK mean wind data, part of the met office integrated data archive system (MIDAS). NCAS British Atmospheric Data Centre, 21 May 2015. http://catalogue.ceda.ac.uk/uuid/a1f65a362c26c9fa667d98c431a1ad38

Met Office (2011) Weather stations. http://www.metoffice.gov.uk/learning/science/first-steps/observations/weather-stations. Accessed 29 May 2015

NASA (2015) Missions: RapidScat. NASA (Jet Propulsion Laboratory). http://www.nasa.gov/rapidscat. Accessed 29 May 2015

National Data Buoy Center (2014) United States voluntary observing ship program. http://www.vos.noaa.gov/. Accessed 1 May 2015

National Data Buoy Center (2015a) National data buoy center. http://www.ndbc.noaa.gov/. Accessed 29 May 2015

National Data Buoy Center (2015b) Station 62107—sevenstones lightship. http://www.ndbc.noaa.gov/station_page.php?station=62107. Accessed 1 May 2015

Palma JMLM, Castro FA, Ribeiro LF et al (2008) Linear and nonlinear models in wind resource assessment and wind turbine micro-siting in complex terrain. J Wind Eng Ind Aerodyn 96:2308–2326

Palutikof JP, Brabson BB, Lister DH, Adcock ST (1999) A review of methods to calculate extreme wind speeds. Meteorol Appl 6:119–132

Peña A, Hasager CB, Gryning SE et al (2009) Offshore wind profiling using light detection and ranging measurements. Wind Energ 12:105–124

Petersen EL, Mortensen NG, Landberg L et al (1998) Wind power meteorology. Part I: climate and turbulence. Wind Energ 1:25–45

Plate EJ (1982) Engineering meteorology: fundamentals of meteorology and their application to problems in environmental and civil engineering. Elsevier Scientific Pub. Co, Amsterdam

Pramod Jain PD (2011) Wind resource assessment. In: Wind energy engineering. The McGraw-Hill Companies, Inc, New York

Pryor SC, Barthelmie RJ, Kjellström E (2005) Potential climate change impact on wind energy resources in northern Europe: analyses using a regional climate model. Clim Dyn 25:815–835

Rienecker MM, Suarez MJ, Gelaro R et al (2011) MERRA: NASA's modern-era retrospective analysis for research and applications. J Clim 24:3624–3648

Risien CM, Chelton DB (2006) A satellite-derived climatology of global ocean winds. Remote Sens Environ 105:221–236

Saha S, Moorthi S, Pan H-L et al (2010) The NCEP climate forecast system reanalysis. Bull Am Meteorol Soc 91:1015–1057

Sempreviva AM, Barthelmie RJ, Pryor SC (2008) Review of methodologies for offshore wind resource assessment in European seas. Surv Geophys 29:471–497

Skamarock WC, Klemp JB, Dudhia J et al (2008) A description of the advanced research WRF version 3. NCAR Techical Note

Smith DA, Harris M, Coffey AS et al (2006) Wind lidar evaluation at the Danish wind test site in Høvsøre. Wind Energ 9:87–93

Strahler AH, Strahler AN (1992) Modern physical geography, 4th edn. Wiley, New York

Stull RB (1988) An introduction to boundary layer meteorology. Springer, Netherlands

Taylor PK, Kent EC, Yelland MJ, Moat BI (1999) The accuracy of marine surface winds from ships and buoys. In: Proceedings of the CLIMAR 99, WMO workshop on advances in marine climatology, Vancouver, Canada, 8–15 Sept 1999

Troen I, Lundtang Petersen E (1989) European wind atlas. Risø Laboratory, Roskilde

Uppala SM, KÅllberg PW, Simmons AJ et al (2005) The ERA-40 re-analysis. Quart J Royal Meteorol Soc 131:2961–3012

Van Wijk AJM, Beljaars ACM, Holtslag AAM, Turkenburg WC (1990) Evaluation of stability corrections in wind speed profiles over the North Sea. J Wind Eng Ind Aerodyn 33:551–566

Watson S, Hughes J (2014) Mesoscale modelling of the UK offshore wind resource. In: Proceedings of the European wind energy association annual event. Barcelona, Spain, 10–3 Mar 2014

Weissman DE, Bourassa MA, Tongue J (2002) Effects of rain rate and wind magnitude on seawinds scatterometer wind speed errors. J Atmos Oceanic Technol 19:738–746

Wilczak JM, Oncley SP, Stage SA (2001) Sonic anemometer tilt correction algorithms. Bound-Layer Meteorol 99:127–150

World Meteorological Organization (2008) Guide to meteorological instruments and methods of observation, 7th edn. WMO-No. 8, Geneva, Switzerland, pp I.15–1 to I.15–11–II.2–10 to II.2–11

References (2)

Barstow SF, Kollstad T (1991) Field trials of the directional waverider. In: Proceedings of the 1st international offshore and polar engineering conference (ISOPE), Edinburgh, UK, 11–16 Aug 1991

Barstow S, Mørk G, Lønseth L et al (2003) WORLDWAVES: fusion of data from many sources in a user-friendly software package for timely calculation of wave statistics in global coastal waters. In: Proceedings of the 13th international offshore and polar engineering conference (ISOPE), Honolulu, Hawaii, USA, 25–30 May 2003

Barstow SF, Mørk G, Lønseth L, Mathisen JP (2009) WorldWaves wave energy resource assessment from the deep ocean to the coast. In: Proceedings of the 8th European wave and tidal energy conference (EWTEC), Uppsala, Sweden, 7–10 Sept 2009

Battjes JA (1978) Engineering aspects of ocean waves and currents. Seminar on safety of structures under dynamic loading. Trondheim, Norway

Benoit M, Frigaard P, Schaffer HA (1997) Analysing multidirectional wave spectra. In: Proceedings of the 27th IAHR congress, IAHR seminar: multidirectional waves and their interaction with structures, San Francisco, USA, 10–15 Aug 1997

Bitner-Gregersen EM, Haver S (1989) Joint long term description of environmental parameters for structural response calculation. In: Proceedings of the 2nd international workshop on wave hindcasting and forecasting, Vancouver, B.C. Canada, 25–28 Apr 1989

Bitner-Gregersen EM, Haver S (1991) Joint environmental model for reliability calculations. In: Proceedings of the 1st international offshore and polar engineering conference (ISOPE), Edinburgh, UK, 11–16 Aug 1991

Challenor PG, Foale S, Webb DJ (1990) Seasonal changes in the global wave climate measured by the Geosat altimeter. Int J Remote Sens 11(12):2205–2213

Danish Hydraulic Institute (DHI) (2015) MIKE 21 wave modelling, MIKE 21 spectral waves FM, short description. DHI, Denmark

Der-Kiureghian A, Liu P-L (1986) Structural reliability under incomplete probability information. J Eng Mech ASCE 112(1):85–104

DNV-RP-C205 (2010) Environmental conditions and environmental loads. Det Norske Veritas (DNV), Høvik, Norway

Forristal GZ (1978) On the statistical distribution of wave heights in a storm. J Geophys Res Oceans 83(C5):2353–2358

Goda Y (2000) Random sea and design of maritime structures, 2nd edn. Advanced Series on Ocean Engineering, World Scientific Publishing Company, Singapore

Guedes Soares C (1984) Representation of double-peaked spectra. Ocean Eng 11:185–207

Gunther H, Hasselmann S, Janssen PAEM (1992) The WAM model cycle 4. DKRZ technical report no. 4, Hamburg, Oct 1992

Hasselmann K (1962) On the non-linear energy transfer in a gravity-wave spectrum, Part 1: general theory. J Fluid Mech 12:481–500

Hasselmann K (1963) On the non-linear energy transfer in a gravity-wave spectrum, Part 2: conservation laws, wave-particle correspondence, irreversibility. J Fluid Mech 15:273–281

Hasselman K, Barnett TP, Bouws E et al (1973) Measurements of wind-wave growth and swell decay during the Joint North Sea Wave Project (JONSWAP). Dtsch Hydrogr Z, Suppl 12:A8

Integrated Ocean Observing System (IOOS) (2013) Manual for real-time quality control of in-situ surface wave data: a guide to quality control and quality assurance of in-situ surface wave observations, ver. 1.0. June 2013

Komen GJ, Cavaleri L, Donelan M et al (1994) Dynamics and modelling of ocean waves. Cambridge University Press, Cambridge

Krogstad HE, Barstow SF (1999) Satellite wave measurements for coastal engineering applications. Coast Eng 37:283–307

Mathiesen M, Mayer AK, Kvingedal B (2014) Hywind Buchan deep—Metocean design basis, rev. 2. Statoil document number RE2014-002, May 2014

Munk WH (1950) Origin and generation of waves. In: Proceedings of the 1st international conference on coastal engineering, long beach, California. ASCE, pp 1–4

Ochi MK, Hubble EN (1976) Six-parameters wave spectra. In: Proceedings of the 15th coastal engineering conference, Honolulu, Hawaii, USA, 1–17 July 1976

Pierson WJ, Moskowitz L (1964) A proposed spectral form for fully developed wind seas based on the similarity theory of S.A. Kitaigorodskii. J Geophys Res 69(24):5181–5190

Pontes MT, Athanassoulis GA, Barstow S et al (1996) An atlas of the wave energy resource in Europe. J Offshore Mech Arct Eng 118(4):307–309

Prince-Wright R (1995) Maximum likelihood models of joint environmental data for TLP design, In: Proceedings of the 14th international conference in offshore mechanics and arctic engineering, vol 2, ASME, New York, USA, pp 535–445

Ris RC, Holthuijsen LH, Booij N (1999) A third-generation wave model for coastal regions: 2. Verification. J Geophys Res 104(C4):7667–7681

Sarpkaya T, Isaacson M (1981) Mechanics of wave forces on offshore structures. Van Nostrand Reinhold Company, Melbourne

Smith H, Maisondieu C (2014) Resource assessment for Cornwall, Isles of Scilly and PNMI—Task 1.2 of WP3 from the MERiFIC Project: marine energy in far peripheral and island communities. MERiFIC Project, University of Exeter and Ifremer, Apr 2014

Strekalov SS, Tsyploukhin VP, Massel SR (1972) Structure of sea wave frequency spectrum. In: Proceedings of the 13th international conference on coastal engineering, vol 1. ASCE, pp 307–314

SWAN Team (2006) SWAN technical documentation, SWAN cycle III version 40.51. [Online]. Available at: www.swan.tudelft.nl. Accessed 18 Mar 2016

SWAN Team (2009) SWAN user manual, SWAN cycle III version 40.72ABCDE [Online]. Available at: www.swan.tudelft.nl. Accessed 18 Mar 2016

Torsethaugen K (1993) A two peaked wave spectrum model. In: Proceedings of the 12th international conference on offshore mechanics and arctic engineering (OMAE), Glasgow, UK, 20–24 June 1993

Tucker MJ (1993) Recommended standard for wave data sampling and near real-time processing. Ocean Eng 20:459–474

Tucker MJ, Pitt EG (2001) Waves in ocean engineering. In: Bhattacharyya R, McCormick ME (eds) Elsevier ocean engineering series, vol 5. Elsevier Science & Technology, Oxford

WAMDI Group (1988) The WAM model—a third generation ocean wave prediction model. J Phys Oceanogr 18(12):1775–1810

Winterstein S, Ude TC, Cornell CA et al (1993) Environmental parameters for extreme response: inverse FORM with omission sensitivity. In: Proceedings of the ICOSSAR-93, Innsbruck, Austria, 9–13 Aug 1993

Young IR (1999) Wind generated ocean waves. In: Bhattacharyya R, McCormick ME (eds) Elsevier ocean engineering series, vol 2. Elsevier Science & Technology, Oxford

References (3)

Albini P, Musson RMW, Gomez Capera AA et al (2013) Global historical earthquake archive and catalogue (1000-1903). GEM technical report 2013-01 V1.0.0, GEM Foundation, Pavia, Italy

American Bureau of Shipping (ABS) (2013) Guide for building and classing floating offshore wind turbine installations. ABS Guideline #195. Houston, TX, USA

Battisti L, Fedrizzi R, Brighenti A, Laakso T (2006) Sea ice and icing risk for offshore wind turbines. In: Proceedings of the OWEMES 2006, Civitavecchia, Italy, 20–22 Apr 2006

Boon J (2004) Secrets of the tide: tide and tidal current analysis and predictions, storm surges and sea level trends. Horwood Publishing Ltd, Chichester

Boyer TP, Antonov JI, Baranova OK et al (2013) World ocean database 2013. NOAA Atlas NESDIS 72, Ed. Levitus S, Technical Ed. Mishonov A. Silver Spring, MD, USA, 209 pp

DNV-OS-J101 (2014) Design of offshore wind turbine structures. Det Norske Veritas (DNV), Høvik, Norway

DNV-OS-J103 (2013) Design of floating wind turbine structures. Det Norske Veritas (DNV), Høvik, Norway

DNV-RP-C205 (2010) Environmental conditions and environmental loads. Det Norske Veritas (DNV), Høvik, Norway

GLOSS (2016) GLOSS station handbook. http://www.gloss-sealevel.org/station_handbook/. Accessed 28 Mar 2016

Health and Safety Executive (2003) An appraisal of existing seismic hazard estimates for the UK continental shelf. Research report 166. ISBN 0 7176 2778 0

IEA Wind (2012) Expert group study on recommended practices, 13. Wind energy projects in cold climates, edn 1. International Energy Agency, May 2012

IEA Wind Task 19 (2012) State-of-the-art of wind energy in cold climates. International Energy Agency, Oct 2012

IEC 61400-3 (2009) Wind turbines—part 3: design requirements for offshore wind turbines. International Electrotechnical Commission (IEC), Geneva, Switzerland

Integrated Ocean Observing System (IOOS) (2015) Manual for real-time quality control of in-situ current observations: a guide to quality control and quality assurance of acoustic Doppler current profiler observations, Version 2.0. Oct 2015

IRIS (2016) IRIS earthquake browser, incorporated reasearch institutions for seismology (IRIS). http://ds.iris.edu/ieb. Accessed 28 Mar 2016

ISO 19901-1 (2005) Petroleum and natural gas industries—specific requirements for offshore structures part 1: Metocean design and operating considerations. International Organization for Standardization (ISO), Geneva, Switzerland

ISO 19901-2 (2004) Petroleum and natural gas industries—specific requirements for offshore structures part 2: seismic design procedures and criteria. International Organization for Standardization (ISO), Geneva, Switzerland

ISO 19901-4 (2003) Petroleum and natural gas industries—specific requirements for offshore structures part 3: geotechnical and foundation design considerations. International Organization for Standardization (ISO), Geneva, Switzerland

ISO 19904-1 (2006) Petroleum and natural gas industries—floating offshore structures and mobile offshore units. International Organization for Standardization (ISO), Geneva, Switzerland

ISO 19906 (2010) Petroleum and natural gas industries—artic offshore structures. International Organization for Standardization (ISO), Geneva, Switzerland

Johnson DR, Boyer TP (2015) Regional climatology of the East Asian seas: an introduction. NOAA Atlas NESDIS 79. Silver Spring, MD, USA, pp 37

Jonathan P, Ewans K (2013) Statistical modelling of extreme ocean environments for marine design: a review. Ocean Eng 62:91–109

Marine Data Exchange (2016) Marine data exchange. The crown estate. http://www.marinedataexchange.co.uk/. Accessed 28 Mar 2016

Matsumoto K, Takanezawa T, Ooe M (2000) Ocean tide models developed by assimilating TOPEX/POSEIDON altimeter data into hydrodynamical model: a global model and a regional model around Japan. J Oceanogr 56:567–581

National Geophysical Data Center/World Data Service (NGDC/WDS) (2016) Global historical tsunamic database. National Geophysical Data Center, NOAA. doi:10.7289/V5PN93H7. Accessed 28 Mar 2016

NORSOK Standard (2007) N-003 action and action effects, edn 2. Sept 2007

Ocean Data Portal (2016) Ocean data portal. http://www.oceandataportal.org/. Accessed 28 Mar 2016

Oliver EC, Sheng J, Thompson KR, Urrego Blanco JR (2012) Extreme surface and near-bottom currents in the northwest Atlantic. Nat Hazards 64:1425–1446

Pawlowicz R, Beardsley B, Lentz S (2002) Classical tidal harmonic analysis including error estimates in MATLAB using T TIDE. Comput Geosci 28:929–937

Pugh DT (1996) Tides, surges and mean sea-level (reprinted with corrections). Wiley, Chichester

SeaDataNet (2016) SeaDataNet. Pan-European infrastructure for ocean and marine data management. http://www.seadatanet.org/. Accessed 28 Mar 2016

Seidov D, Baranova OK, Biddle M et al (2013) Greenland-Iceland-Norwegian seas regional climatology, Regional Climatology Team. NOAA/NCEI

Storchak DA, Di Giacomo D, Bondár I et al (2013) Public release of the ISC-GEM global instrumental earthquake catalogue (1900-2009). Seismol Res Lett 84(5):810–815

Zijl F, Verlaan M, Gerritsen H (2013) Improved water-level forecasting for the Northwest European Shelf and North Sea through direct modelling of tide, surge and non-linear interactions. Ocean Dyn 63:823–847

Overview of Floating Offshore Wind Technologies

Andrew Henderson, Maurizio Collu and Marco Masciola

In this chapter a review of the key technology components that can be directly associated with FOWTs is presented. The main options for the key technology component that make up a FOWT are discussed in detail, namely the types of support structures (Sect. 1), wind turbines (Sect. 2) and mooring systems (Sect. 3). The main objective of this chapter is to provide the reader with a clear overview of the relative advantages and disadvantages of each key design option.

1 Support Structures for Floating Wind Turbines

Andrew Henderson

Similar to the bottom-fixed case, there is a wide range of candidate types of floating foundations, this being liberally demonstrated by the variety of full-scale prototype units in the water or under construction today, in Norway, Portugal and Japan with a further unit under assembly for the German Baltic Sea.

A. Henderson (✉)
DONG Energy Wind Power, 33 Grosvenor Pl, London, SW1X 7HY, UK
e-mail: ANHEN@DONGEnergy.co.uk

M. Collu
Offshore Renewable Energy Engineering Centre, Cranfield University,
School of Energy, Environment and Agrifood, Building Whittle Building,
Ground Floor, G113 Cranfield, UK
e-mail: maurizio.collu@cranfield.ac.uk

M. Masciola
ABS Consulting, 16855, North chase Drive, Houston, TX 77060, USA
e-mail: mmasciola@eagle.org

This section explores the fundamental diversity of floater concept designs, and explains some of the considerations that drive the engineering decisions, with the section being laid out as follows:

- *Floater Concept Identification*: how do the different types of concepts arise? Why are they so different?
- *Floater Concept Selection*: how can the foundation types be assessed? Why might one concept be more suitable for a particular site?
- *Floater Concept Description*: understanding the strengths and weaknesses of each foundation type.

How the foundation counters the wind turbine overturning thrust load and achieves stability is arguably the primary design driver and hence foundation types can be conveniently classified accordingly:

- Spar concepts, which use gravity in the form of ballast,
- Semi-submersible concepts, which use distributed buoyancy, similar to a catamaran,
- Tensioned-moored concepts, which use taut moorings.

In reality, any floater type will use a combination of the above to achieve stability, and there is a *continuum* of intermediate designs. However, usually one method for achieving stability will dominate, leading to clear differences in how the floater concepts are constructed and installed.

Water depth arguably will have the greatest influence on the selection of floater concept, however ground conditions will determine the choice of anchoring methods, which might have a knock-on effect on the floater type, whilst design and fabrication experience, including from the offshore oil and gas sector, risk appetite, and IP (intellectual property) considerations will also affect the selection.

The weight and cost of bottom-mounted wind turbine foundation structures for deeper waters generally increases exponentially with depth, thus challenging the offshore wind energy industry's cost reduction goals. Similarly, floating foundations are larger and costlier than the foundations at the shallowest water sites originally developed in the industry's earliest years. However, the current generation of very large wind turbines should deliver lower foundation costs for floating platforms, in the same manner as such wind turbines do for bottom-mounted monopiles, jackets and GBSs (gravity base structures).

On another positive note, compared with bottom-mounted designs, costs of floating platforms are less sensitive to increases in water depth, since only the mooring costs are sensitive to water depth, with the platform structure costs being mainly unaffected by depth. This can be understood by considering how the wind turbine loads are transferred. For a conventional bottom-fixed foundation, the loads are transferred deep within the seabed through a rigid structure. Whilst this does provide a stable platform and is now well understood by wind turbine and foundation design engineers, the load path is lengthy and bending loads can be severe. In contrast, a floating platform transfers the primary wind turbine loads to the water,

which has two important advantages: firstly, the water is closer, hence the load path is shorter and in particular, the bending moments will be commensurately lower; and secondly, water is compliant, hence there is dynamic flexibility and the peak forces can potentially be lower.

However, the dynamics of a floating foundation does introduce some new challenges, including:

- minimising the wind turbine and wave induced motion;
- minimising the wind turbine and wave induced static displacement, i.e. heel (fore-aft rotation) and surge (horizontal displacement);
- modelling the complete system and the effect that the additional motion will have on the wind turbine;

    – including understanding and modelling the coupling between the support structure (including moorings) and the wind turbine (including controller);

- understanding what the design limits should be; relaxing specific design limits could prove beneficial for the foundation, hence each design driver should be carefully examined, challenged and justified;
- understanding the dynamic effects on the electrical cable exporting the power from the platform.

In summary, utilisation of floating support structures can deliver a number of important benefits, principally:

- greater choice of sites and countries, as well as reduced penalty for variability in water depth and ground conditions across a site;
- wide and flexible choice of concepts; as evidence view the wide variety of technology solutions proposed and being demonstrated;
- the most cost optimal foundation concept for deeper water; the future will show where the transition water depth is;
- good flexibility of construction and installation procedures;
- easier removal, relocation and decommissioning.

1.1 Concept Identification

A floating support structure can be broken down into the following systems:

- Structure (floater, platform): maintain buoyancy and structural integrity;
- Mooring: connect the floater to the seabed, typically chain or cables;
- Anchoring: attach the mooring lines to the seabed;
- Electrical cable: export of power.

The focus of this section is the first item: the main structure or platform. In essence, the foundation concept must support the wind turbine. It needs to react to and transmit loads whilst maintain stability and station-keeping. Examining these

Fig. 1 Principal design loads
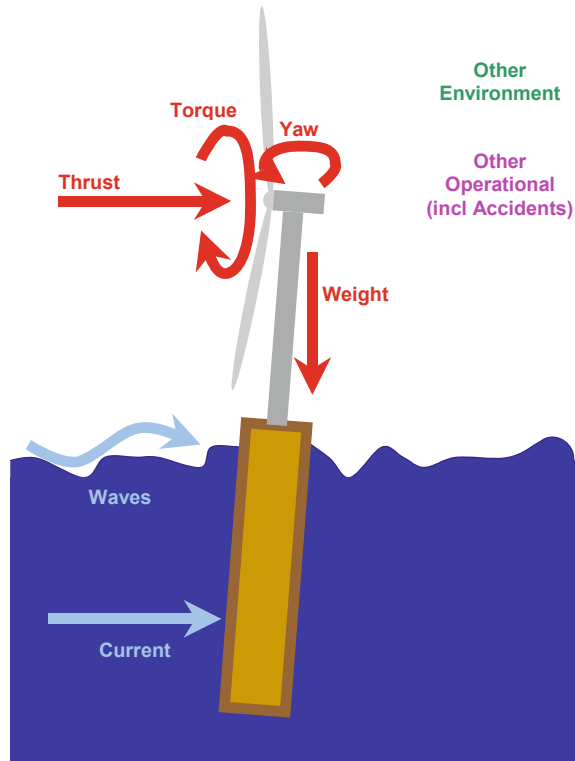
technical aspects in more detail, a floating foundation will experience the following types of loads (see also Fig. 1; further details on design loads for FOWTs are also presented in Sect. 1 in Chapter "Key Design Considerations"):

- Wind-induced loads on the wind turbine rotor,

  – Considering both the mean and the dynamic components,
  – Considering both shear and bending moments,
  – Considering the thrust, torque and yaw axes;

- Wave-induced loads on the floater as well as associated secondary structures, such as landing platforms and J-tubes,

  – Considering both the static (drift force) and the dynamic components,
  – Considering both shear and bending moments;

- Ocean current induced loads on the floater,

  – Including vortex shedding loads,
  – Consider misalignment between wind, waves and currents;

- Sea-level induced loads on the floater, for example due to tides;
- Weight of the wind turbine and floater;

- Other environmental loads, such as icing;
- Accident and fault loads, for example:

    – Wind turbine fault conditions,
    – Water-tightness failure of buoyancy chambers;

- And finally other incidental and miscellaneous loads, such as:

    – dynamic response of the export cable,
    – wind loading on the tower.

Of the sources of loading listed, the *mean wind turbine thrust overturning moment* can be considered the primary design driver. Consequentially the basic structure of the floater will be developed to counter this load and the method taken to do so will determine the basic shape. There are three methods (see Fig. 2):

- Ballast stabilised: leads to a slender vertical structure, i.e. the spar platform,
- Buoyancy-stabilised, through hydrostatics: leads to a large surface structure, i.e. the semi-submersible platform,
- Mooring-stabilised, through taut lines: leads to a slender highly loaded submerged structure, i.e. the tensioned-moored or tension-leg platform (TLP).

The geometry of the floating platform will depend on which method is chosen to counter the wind turbine loads, thus driving the multiplicity in designs that is evident in the floating wind sector.

All the above design approaches are technically and practically viable and indeed all are being actively pursued. Each class of platform has different characteristics and strengths: the spar and semi-submersible type floater has the benefit of
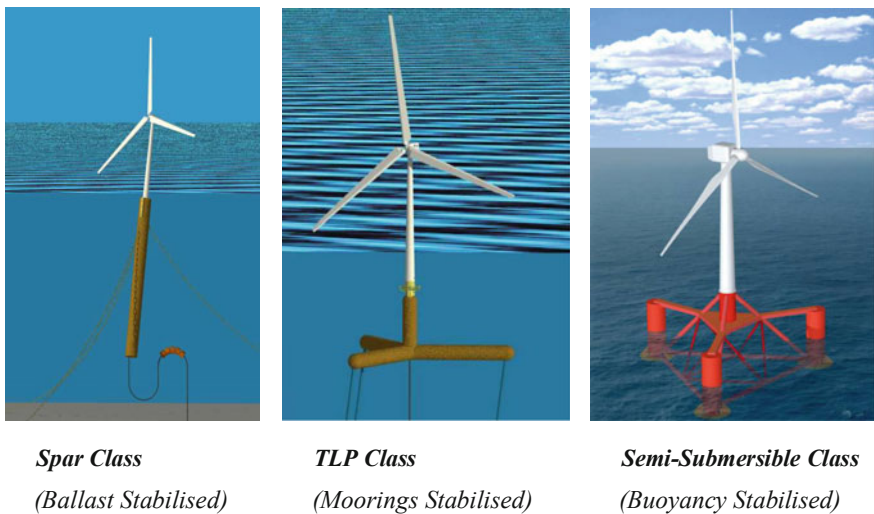

| *Spar Class* | *TLP Class* | *Semi-Submersible Class* |
| *(Ballast Stabilised)* | *(Moorings Stabilised)* | *(Buoyancy Stabilised)* |

Fig. 2 Support structure classes

using predominantly widely used and proven technology, while the tensioned and semi-submersible type floater can be used in shallower waters than the spar and for the tensioned floater, a lightweight elegant design may be ultimately achievable.

Concepts Comparison and Selection

The key criteria for the evaluation and selection of floating foundation platforms will be:

- Motion response and Station-keeping,
  - Ability to maintain the wind turbine within operating and extreme envelope.

- Structural loading,
  - Ability to withstand extreme conditions at the site.

- Maturity of the design,
  - Including credible and comprehensive modelling capability, calibrated against scale and full size platforms.

- Fabrication and Installation,
  - Ease and confidence in manufacturing techniques as well as installation methods.

- Safety,
  - Building on experience in the onshore and offshore wind sectors as well as other marine sectors.

  Examining each criterion to greater detail in turn:

- Motion response needs to remain within the envelope acceptable to the wind turbine, however firstly it needs to be acknowledged that this is a novel question for the wind turbine suppliers and hence cannot be answered without analytical effort and cautious testing thus building up practical experience. In general, an appropriately designed floating platform will experience predominantly low accelerations and hence manageable wave-motion-induced loads; this is because the largest amplitude waves inevitably have long periods with associated slower movements and accelerations; conversely, the short period waves, which could cause high accelerations to very small floating structures, are short as well as with relatively low heights, due to breaking wave height-limits; the short lengths mean the platform will move less in response, since the waves will have a similar dimension as the structure itself. As a result, the accelerations and loads experienced by the wind turbines on a floating platform are not exceptionally severe and indeed are broadly similar to those experienced by onshore and fixed-offshore wind turbines; this has been demonstrated by prototypes and matches well with conclusions from modelling work. It should be appreciated that onshore wind turbines can experience very high accelerations and loads, for example due to extreme gusts at turbulent sites in mountainous terrain, or

emergency shut-down events, hence wind turbines are designed for such conditions.

- Many platform designs, specifically spars and semi-submersible structures, use the restoring forces generated by the platform heel (leaning backwards) to counter the turbine thrust load, hence the wind turbine will be at an angle of a few degrees during normal operations; this never occurs for an onshore or bottom-fixed offshore wind turbine of course, hence there is no experience to guide setting appropriate design limits, bearing in mind that this design criteria will directly impact the size and hence cost of the floating foundation, indicatively in a linear manner. The wind turbine industry does have experience of the resulting misalignment of the wind inflow, firstly since rotors are invariable tilted by a few degrees and secondly since flow directions in complex terrain can deviate by an order of magnitude higher;

- Some platform designs, specifically spar and TLP concepts, provide very little upwind yaw-stability; it should be born in mind that conventional three-bladed upwind turbines are stable, i.e. for small misalignments with the wind direction, the net yaw forces will cause the wind turbine rotor to restore back into the wind; unfortunately it does need to be acknowledged that this yaw moment is challenging to accurately calculate using state-of-the-art methods and models hence some conservatism and contingency planning (for example, anticipation to tune the wind turbine controller) will be required; the yaw restoring moment itself needs to be provided by the moorings, requiring a non-negligible misalignment in the case of slack moorings;

- Waves induce both a dynamic as well as a mean or static force on a structure, this later being smaller but significant and called the drift force, hence the moorings will need to generate a restoring force;

- Coupling between modes of motion will occur, for both the floater and the wind turbine; an interesting example is the yaw moment generated from the rotor torque when the wind turbine drive train is inclined. The inclination due to the rotor tilt will be increased if the floater heels to counter the thrust force. It is noted that larger turbines have slower rotational speeds, hence generate proportionately higher torque loads;

- Any additional inclination of the rotor caused by the platform heeling over during operation could cause a small reduction to power production due to the further misalignment with the wind direction; however, this is likely to be non-material.

- The loads on the floater and wind turbine structure need to be accurately calculated and designed for; a number of coupled software suites are capable of modelling seabed-fixed offshore wind turbines with some models also able to simulate the low-frequency high-amplitude motion that is unique to floating wind turbines (see also Sect. 5 in chapter "Modelling of Floating Offshore Wind Technologies" for a review of numerical modelling design codes for FOWT applications):

- – Regarding modelling of the wind turbine, key challenges include modelling the wind-field and the controller; the wind-field is modelled in a statistical rather than a deterministic manner, of course, making validation of new floating-specific features of the code more difficult; to date validation has focused on code-to-code comparisons however for the floater design to be fully optimised, code-to-measurements validation will be required; installing a full suite of calibrated instruments on the demonstration units and employing suitable technical expertise can achieve this goal;
- – Regarding modelling of the floater, key challenges include diffraction coupled with surface effects as well as mooring line dynamics; diffraction modelling will mainly be required for floaters with a large structure at or near the water surface, specifically semi-submersible platforms though TLP floaters in shallow water could include elements at a short distance below the surface; diffraction analysis is usually run in a linear manner, assuming infinitesimal wave heights and hence ignoring wave run up and temporary submergence of parts of the structure; mooring line dynamics is arguably the most challenging feature for offshore software, specifically for slack moorings;
- – For the foreseeable future, wind turbine design adjustments for the benefit of floating deployments will likely be limited to controller design and tuning and possible some O&M (operation and maintenance) processes however in the longer term there may be benefits of including floating wind energy drivers as priorities in the fundamental wind turbine design; the key objective is minimising nacelle weight: depending on the floater concept, for each tonne saved in the nacelle, several tonnes will be saved in the platform; more sophisticated wind turbine design adaptations could include design for horizontal transport and ballast-driven horizontal-to-vertical installation methods;
- – In general, it can be assumed that the additional loads on the wind turbine itself caused by the motion of the floating platform will be minimal and unlikely to require any material design changes to the wind turbine rotor-nacelle assembly (RNA), such as requirements for a more robust wind turbine class; this will not be the case for the wind turbine tower, which will require a site and platform specific design; reinforcements will be necessary to mitigate additional fatigue loading as well as the default inclined operating orientation of spar buoy and some semi-sub concepts.

- Maturity of the design:

  - – Floating wind turbine foundations are novel and indeed the degree of novelty can be accentuated by a desire to achieve step changes in performance and cost and to stake out patentable IP (intellectual property), irrespective of overall technology risk; however there will be many aspects similar to existing wind energy and offshore engineering technologies where existing design, fabrication, installation and operation experience can be utilised; a suitable balance needs to be found between incorporating necessary novel

features, in order to achieve a successful design and to lower the cost of energy, and deploying existing proven technologies, in order to manage overall risk; arguably, during this stage of industry immaturity, floating wind energy projects should be inclined towards the latter;

– For the novel design aspects, a comprehensive programme of credible modelling and testing is necessary, including scale testing for the floater assembly (noting that wind turbines do not scale successfully, hence there will be no benefits from scale tests to the wind turbines themselves) and simulation-model development for the turbine and the complete system, calibration against full-scale prototypes and a wide-ranging programme of simulations, preferably extending well beyond current standards the risks that need to be minimised include unexpected phenomena as the operational envelope is extended; such phenomena have affected both the wind energy and offshore industries in the past and can be expensive and time-consuming to resolve in the field, historic examples include wind turbine blade edge-wise vibration and spar and mooring line VIV (vortex-induced vibrations);

– The offshore engineering industry has a long history of developing and implementing novel fixed and floating concepts; the functional specifications to support a drilling rig or well service plant at a new development field can be unique and unusual compared with traditional marine engineering requirements, for example in terms of anchoring water depth, survival wave climates, payloads, processing of flammable liquids, manning levels etc. there have been many successes from which floating wind is already bene-fitting from, in terms of the technologies themselves as well as the processes used to mature new platforms;

– Finally, the design process should prioritise fabrication and installation equally as the more obvious objective of optimal in-field performance.

- Fabrication and Installation:

  – The issues elaborated within the previous paragraphs on design also relate to fabrication and installation; for fabrication, standardised processes should be available, for example monopile fabrication methods for spar buoys (which in turn originated at high pressure boiler manufacturers), fabrication-optimised jacket methods for more complex steel structures whilst marine and coastal assembly methods could be suitable for concrete platform types;

  – Monopiles are most successfully assembled in efficient and well laid-out facilities, where automated processes, material flow and quality control is prominent; the cost of raw material will be a similar order of magnitude as the cost of fabrication;

  – For more complex steel structures, such as bottom-mounted jackets or floating semi-sub platforms, the costs of fabrication and assembly will dominate the costs of the raw materials, hence a *fabrication-optimised* design will deliver a lower cost of energy compared with a *weight-optimised* design;

   this could focus on welding types, weld geometry, material handling, fab-
   rication of sub-assemblies as well as the platform itself, effectiveness of
   quality control, general automation amongst other factors;
– Installation should be an integral platform design objective, and indeed for
   some platform concepts, in particular spar buoys and TLPs, installation may
   prove to be the primary objective for successful platforms; credibility of
   installation methods will depend on metocean climate at site and en-route, in
   particular wave climate, but in some cases also currents and wind regime;
– For spar buoys, the key installation challenge is transporting a deep-draft
   platform from the shallow assembly harbour (the deep and enclosed
   Norwegian fjords being a notable and worldwide unique exception) to the
   deeper windfarm site and then upending the platform; the oil and gas
   industry has typically achieved this by transferring ballast to the spar-base,
   thus changing the stability of the spar and causing it to upend; in the oil and
   gas industry, this will be undertaken without the topside, which would
   require a suitable very-calm weather window to complete; for offshore
   windfarms, it might be possible to pre-install the wind turbine in the hori-
   zontal and upend the fully assembled structure at site;
– For TLPs, the key installation challenge is the transition from a stable
   float-out where the main horizontal structure is at the sea-surface to the stable
   in-service configuration where the main horizontal structure has been pulled
   down below the sea surface and the structure is under tension; both start and
   end situation are reasonably stable, however the transition itself will not be
   stable;
– However perhaps installation can also be considered an opportunity; whilst
   the challenges are significant, credible if costly installation methods are
   available and engineering ingenuity may propose successful novel solutions
   from the apparently infinite range of opportunities that the blank canvass of a
   flexible platform topology, experience within the offshore industry of a
   myriad of platform concepts and an open sea offers.

• Safety:

– For a successful birth of the floating offshore wind industry, safety must be
   paramount and should reflect the professionalism and diligence required to
   achieve such a challenging goal of establishing a new renewable energy
   sector; much experience can be transferred from the existing onshore and
   offshore wind sectors as well as other marine sectors, such as coastal engi-
   neering and oil and gas.

   In summary, design objectives for floating wind energy platforms need to
encompass fabrication and installation and not just in-service operation; factors for
evaluation of candidate platform types could include:

• Site conditions, in particular water depth and sea climate;
• Controlling turbine and wave induced motion;

Table 1 Assessment of floating platform classes

	Spar	TLP	Semi-Sub
Stability	Ballast	Moorings	Hydrostatics
Min depth [a]	Deeper	Shallower	Shallower
Periods	Good	Good	Acceptable
Cost	Uncertain	Uncertain	Uncertain
Yaw and torque	Acceptable	Probably good	Good
Fabrication	Potentially simple structure	More complex structure	More complex structure
Installation	More complex operation	More complex operation	Good

[a]However greater depths will typically allow a better performing and lower cost design to be deployed

- Managing the greater complexity of the design process, including understanding and modelling the coupling between the support structure and the wind turbine (in particular moorings & control);
- The electrical infrastructure design and costs, in particular the flexible cable;
- The construction, installation and O&M procedures, in particular similar attention should be paid to installation as to the operation.

Table 1 presents a high-level evaluation of the three offshore floating platform classes. It can be seen that each has advantages and disadvantages, hence it is likely that more than one type of foundation platform will become established, in particular one concept for shallower and another for deeper waters.

1.2 Spar Buoy Class of Platforms

Examining the spar concept first in greater detail, Fig. 3 shows the key characteristics and components.

Due to the fact that the platform must support a major horizontal load at a significant height above the sea level, designing a successful floating offshore wind
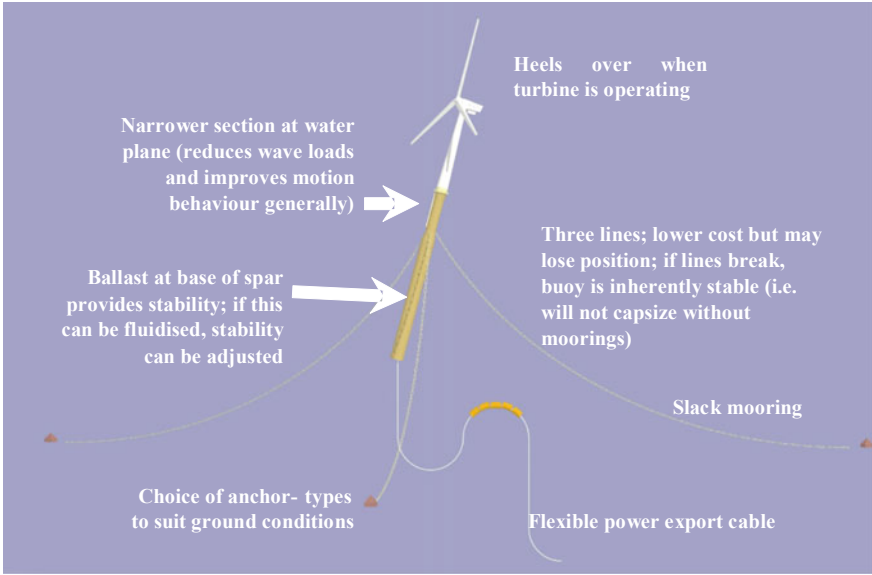
Fig. 3 Spar buoy—summary of the technical details

spar concept is arguably a more interesting engineering challenge compared with oil and gas designs. Figures 4 and 5 illustrate this, starting with the process of balancing the conflicting requirements from selected principal design drivers.

Figure 4 shows how three design drivers:

(i) maximising pitch stiffness in order to minimise vessel heel,
(ii) maximising the natural heave period in order to reduce wave induced motion and
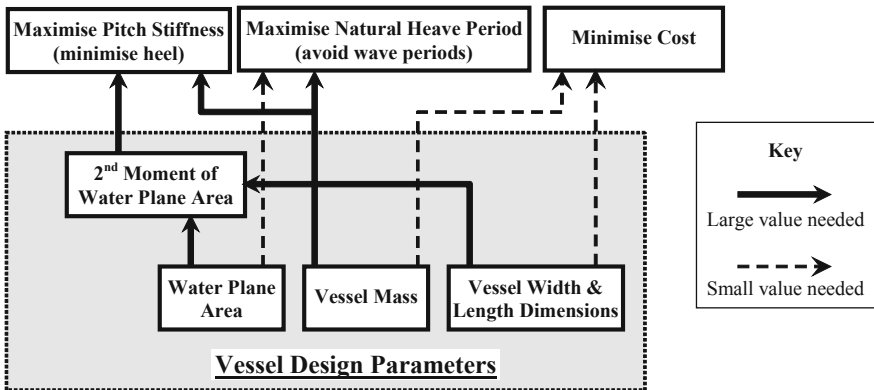(iii) minimising cost

Fig. 4 Conflict between design drivers

drive conflicting demands on the vessel design parameters. There are demands on the water plane area, vessel mass and vessel dimensions to be simultaneously as large as possible and as small as possible.

The consequence of these conflicting design drivers is that the suitable design space is very limited and involves compromise; Fig. 5 illustrates this graphically for a matrix of all configurations of spar length and spar diameter, i.e. the extremes in terms of spar length and diameter are shown in each corner of the figure. The overwhelming majority of spar configurations are not technically viable for a wide range of differing reasons.

The viable design-space is small and is bounded by design limiting criteria for:

   (i)   stability;
  (ii)   vertical motion (heave natural period);
 (iii)   pitching motion (fore-aft rotational natural period);
 (iv)   cost (overall size of the spar), and
  (v)   fatigue criteria.

Invariable a certain degree of compromise with these criteria will be necessary. If larger wind turbines are used, the size of the acceptable design-space does increase, in particular since the larger spar will have longer natural periods in heave and roll/pitch. However, a disadvantage for larger wind turbines is that the minimum water depth also increases hence some windfarm project opportunities might be lost.

Figure 5 provides a visual presentation of the viability of a matrix of conceptual designs, for increasing spar buoy diameter (left-to-right) and increasing spar buoy length (top-to-bottom). The diagram shows the viable design space and why other designs are not feasible, due to excessive motion, instability, fatigue and cost.

Fig. 5 Identifying the optimal design space
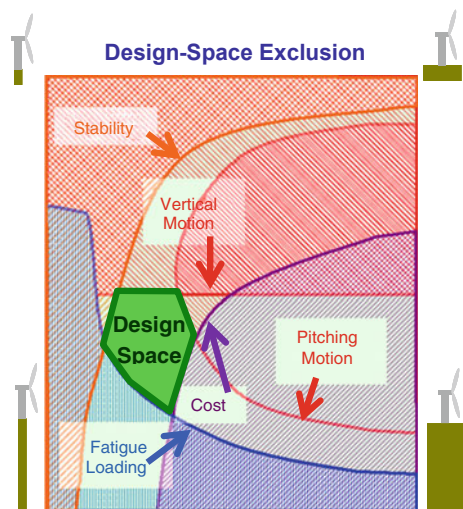
In summary, the principal challenges in delivering a successful spar buoy concept are anticipated to be:

- controlling the size of the spar buoy structure;
  - negotiating the static and dynamic motion limits required for the wind turbine;

- strengthening the wind turbine tower to cope with the bending moment induced by the heel during normal operation, as well additional loading due to motion during transport, installation and operation;
- assembly of the wind turbine on to the spar buoy; in the enclosed deep waters of the Norwegian fjords, this can be done in the vertical, but most locations will not allow this off-site; in such cases horizontal tow-out and upending will be necessary, this being the conventional approach in the offshore engineering industry; waiting for weather-windows at the inevitably exposed and windy project site will involve lengthy delays to installation.

1.3 Tensioned Moored Class of Platforms

Turning to the TLP (Tensioned Leg Platform) concept and examining this in greater detail, Fig. 6 shows the key characteristics and components. The concept is also known as a TBP (Tensioned Buoyant Platform).
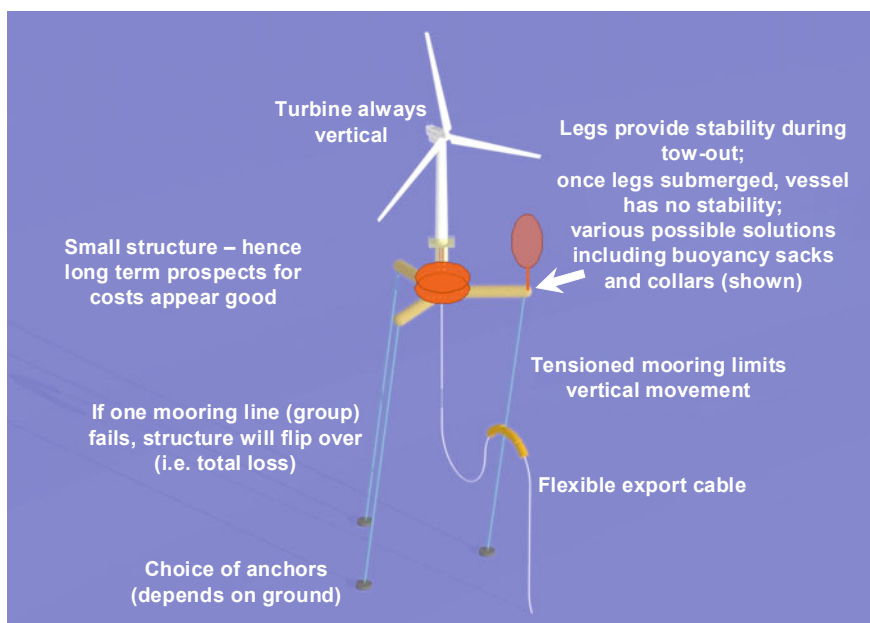

Turbine always vertical

**Legs provide stability during tow-out;
once legs submerged, vessel has no stability;
various possible solutions including buoyancy sacks and collars (shown)**

Small structure – hence long term prospects for costs appear good

Tensioned mooring limits vertical movement

If one mooring line (group) fails, structure will flip over (i.e. total loss)

Flexible export cable

Choice of anchors (depends on ground)

Fig. 6 TLP—summary of the technical details

Due to the unextendable mooring lines, TLPs are the most stable platform-class, once in the fully installed position. Since the mooring lines are designed to be axially rigid, there is typically no significant heave (vertical) motion, nor roll (forward inclination) and pitch (sideways inclination). There will be surge (forward) and sway (sideways) translational motion as well as yaw motion.

Assuming that the wind turbine will be installed at the quayside, the installation of the complete structure at site will be more challenging than the alternative concepts. Although the fully-assembled TLP can be designed to float stably on the sea-surface during tow-out, and will also be stable once installed, TLPs will be vulnerable to instability during the installation process on site. During tow-out, buoyancy aids may be required to avoid capsizing in waves, with such aids being imperative during the installation process, as the structure is tensioned downwards to its operating configuration. Buoyancy and stability could be provided by buoyancy collars, sacks or chambers, which should be removed once installed to reduce operational wave loading. Alternatively, a vessel-assisted installation operation could be mounted, using a specialist barge or offshore service vessel, noting that bespoke modification can be expensive and can reduce the attractiveness of the vessel to other customers.

The concept has low stiffness against surge and sway forces, with the reactive force being generated by inclination of the mooring lines. However, this inclination of the mooring line will cause the platform to drop downwards further into the water, the exact response being dependant on the water depth and mooring design details. This response is termed *set-down*.

Since the vertical position of the platform is fixed by the mooring tendons, the structure is unable to move vertically in response to changes in sea-level in particular caused by tides. Tidal ranges are highly site dependent, with some seas such as the Baltic and the Mediterranean experiencing negligible tides, whilst other locations observe tidal ranges as high as 10 m, for example where local and regional seabed topology funnels tidal flows from major oceans towards particular bays and channels. A mooring system that responds dynamically to this change in sea level is not practical for reliability and safety reasons.

Related to this is a key operational risk suffered by TLP structures, in that the mooring lines are designed to be taut and straight and must remain so. If the tension is removed, the lines will flex temporarily and when the tension is restored will experience snap loads, likely to result in instant or eventual failure. Loss of one tendon in a three or four tendon system will be catastrophic.

Loss of tension in the mooring lines is caused by changes in the instantaneous water surface level, which might most commonly be caused by tidal variations or extreme waves. Hence waves that exceed design limits might cause the complete loss of the TLP platform and wind turbine rather than repairable damage. Failure of mooring lines will typically result in capsizing of the vessel and hence complete loss. Whilst spar and semi-submersible platforms are themselves inherently stable, the TLP structure is inherently unstable and entirely dependent on the mooring lines to provide stability.

TLP mooring lines impose vertical loads on the anchor points, which differs from forces associated with slack mooring lines which can be either entirely horizontal or a combination of horizontal and vertical loads. The vertical loading will require particular types of anchoring, with gravity-type, suction-caissons and piles being the leading candidates and all arguably being less attractive than further options available only to spar and semi-submersible platforms, such as drag anchors. Gravity anchors will inevitably be massive and expensive to fabricate, transport and install, whilst suction-caisson and piled anchors are challenging to design, are sensitive to and restricted to certain soil conditions and have a limited operational track record at the depths being considered.

As is elaborated in the preceding paragraphs, the challenges in developing a successful TLP design are significant and involve greater risks than spar and semi-submersible platforms. It is not clear at this stage whether this design challenge will be surmountable in a cost effective manner. However, if a successful TLP design can be found for offshore wind turbines, there is potential for a light-weight, elegant and hence low-cost offshore wind foundation, deployable across a very wide range of water depths, including relatively shallow sites and being able to successfully compete against the alternative of bottom-mounted foundations.

1.4 Semi-Submersible Class of Platforms

Turning to the semi-submersible class of platforms, which typically can be described as a floating jacket or space-frame and examining this in greater detail, Fig. 7 shows the key characteristics and components of a four column floater.

There are numerous variations of this concept, for example:

- With either three of four primary columns;
- With the turbine either at the centre or over one of the columns;
- Fabricated either from steel, specifically the floating jacket or space-frame concept with this being the more common, or from concrete;
- Incorporating heave suppression discs, at the base of the columns;
- Incorporating variable numbers and configurations of catenary mooring lines.

This concept can also potentially be deployed in the shallowest waters, arguably down to 25 m for small wind turbines in benign wave climates; however, this does cause the design of the catenary mooring to become challenging. Contrary to instinctive impressions, it is hardest to design catenary moorings in the shallowest waters, since the lines become taut with relatively little horizontal movement of the floater.

A large part of this structure lies at the water's surface, inevitably leading to greater structural loads and higher amplitudes of motion. The primary columns provide the buoyancy and reactive moments to the wind turbine thrust, hence need
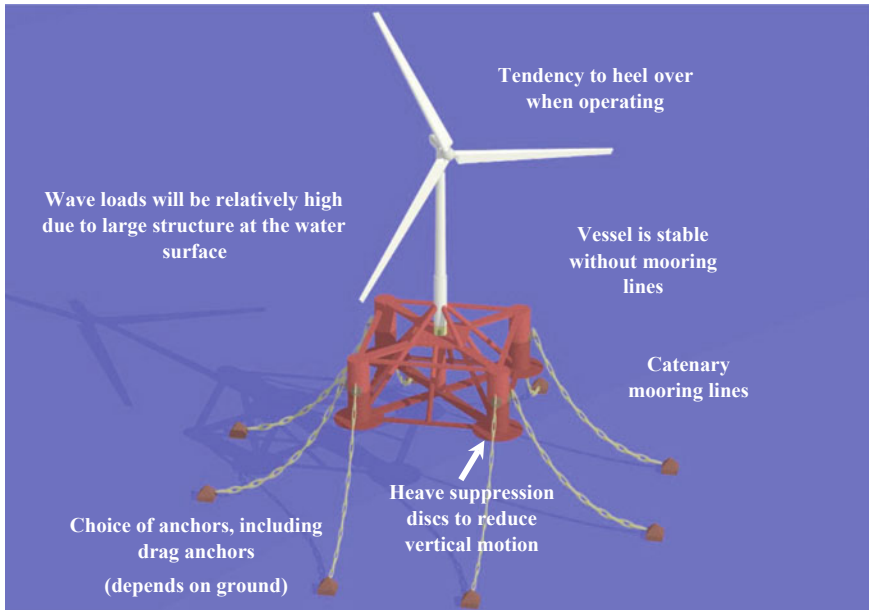
Fig. 7 Floating jacket—summary of the technical details

to be substantial. Elsewhere in the platform, slender lattice structural members for bracing will reduce wave loads.

An alternative configuration is with a concrete structure; this will have a significant impact on the motion response, hence requiring a full redesign including optimisation of the floater.

Motion response can be mitigated by applying advanced design features to the structure, including of relevance to semi-submersible platforms:

- Positioning of the largest structural members so that wave loading is out-of-phase for the predominant and design critical waves at the site; this might involve a site specific design;
- Introducing heave-damping plates, i.e. at the base of the primary columns; wave motion reduces rapidly with water depth and such plates synchronise the vessel movement towards the lower amplitudes of wave motion at depth;
- Incorporating a moon-pool; this is an unusual and rarely utilised device but in theory changes natural frequencies and provides damping; it requires a sophisticated approach for the modelling, diffraction will be insufficient and advanced CFD will be required, together with extensive tank test trials;
- Structural geometry can also provide damping, such as shape of the structure and sharp edges.

Similar to bottom-mounted offshore wind turbine jacket foundations, the fabrication effort required to build a steel semi-submersible is immense and requires

advanced assembly techniques. Cost of fabrication will greatly exceed the cost of material, hence a fabrication-optimised design will be required, as opposed to focusing design efforts on saving steel tonnage. The obvious approach would be to build on any techniques currently being developed by the offshore wind industry for bottom-mounted jackets.

Similarly, the manufacturing methods for concrete semi-submersibles will be critical to achieving attractive cost levels. The same challenges that currently face concrete offshore wind GBS foundations apply, in terms of finding suitable sites and the costs of setting up the assembly facilities. It should be appreciated that the lack of suitable floating crane vessels for GBS foundations will not affect floating foundations (noting that self-buoyant GBS foundation designs would also avoid the need for an installation vessel).

Like the spar, this concept can be assembled from proven subsystems however the initial size and hence cost of the concept can appear prohibitive. A successful implementation of floating jackets will require optimisation of the complete system, for example in terms of the number of columns (three appears to have the edge), minimising wave induced motion (through heave plates and semi-taut moorings) as well as other more original solutions being proposed.

1.5 Summary of Support Structure Options

To summarise this section, a few final remarks on floating platforms for offshore wind turbines can be made:

- There is a wide range of floating foundation concepts that can be used for offshore windfarms;
  - foundation concepts can be classified according to three broad types, where the geometry of the structure is driven by how the platform counters the overturning moment generated by the wind turbine rotor thrust force;
  - the three foundation classes are:

    firstly spar buoys, long slender vertical structures where ballast counters the turbine thrust,
    secondly semi-submersibles, shallow and wide lattice-type structures floating on the surface, where distributed buoyancy counters the turbine thrust, and thirdly tension-buoyant platforms, horizontal structure held below the surface by taut vertical mooring lines, where the tension in the mooring lines counters the turbine thrust.

- Technically viable water depths start at sites where monopiles and jackets are currently being deployed, however the great advantage of floating foundations are to allow much deeper sites to be exploited, the most attractive being those

with good wind resources and which are suitably close to both the shore and a suitable grid connection point, as well as a local demand for power;

- Suitable integrated wind turbine-floating-platform software is available, able to model critical aspects of both the wind turbine and the floater, in particular the wind turbine control and the slack mooring line dynamics; validation against demonstration units will increase confidence in design capabilities and allow further optimisation, thus saving weight and cost (for further information on software packages available to model FOWTs, see Sect. 5 in chapter "Modelling of Floating Offshore Wind Technologies");
- Several demonstration units are in the water in Europe and Japan, with the wind turbines performing well under characteristic floating conditions: i.e. that long-period motion.

2 Wind Turbine Options

Maurizio Collu

This section presents a high level comparison of the wind turbine options considered for offshore floating wind turbines. In particular, it considers Horizontal Axis Wind Turbines (HAWTs) and Vertical Axis Wind Turbines (VAWTs), comparing their main characteristics in view of the very different nature of the offshore metocean conditions.

The onshore wind industry has reached a relatively mature level, and a large majority of large scale wind turbines share the same configuration: horizontal axis of rotation, three blades, upwind, variable-speed, variable blade pitch (with feathering capability). This has been the result of several decades of research and development, and originally several configurations had been considered, including HAWT with a different number of blades, but also VAWT configurations. For example, Éole (shown in Fig. 8) is the largest VAWT built, with a height of 110 m and a rated power of 3.8 MW. It had been operating for six years (1986–1993), with availability equal to 94 %. The conventional HAWT design eventually emerged as the optimum techno-economic trade-off for the onshore large scale wind market (Tangler 2000).

The same evolutionary process did not take place for the offshore wind market, substituted by a *marinisation* of the configurations used for the onshore market. It has been implicitly assumed that, despite the very different environmental conditions of an offshore environment, the optimum configuration for the wind turbine is the same: the conventional three bladed, upwind, horizontal axis wind turbine. This has been implicitly assumed not only for the seabed-fixed offshore wind turbine configurations, but also for the proposed floating systems. The National Renewable Energy Laboratory (NREL) proposed a reference wind turbine to be used to compare different fixed and floating support structures for offshore wind turbines

Fig. 8 Éole, the largest
VAWT, 110 m height, 60 m
diameter, Cap-Chat, Québec.
Source Spiritrock4u at en.
wikipedia

(Jonkman and Butterfield 2009). It is widely used, and the configuration is basically
the same as a conventional onshore large wind turbine. But recently there has been
a resurgence of interest for VAWT (Shires 2013; Borg et al. 2014).

In the following sections, HAWT and VAWT configurations are compared and
contrasted highlighting some of the key aspects in terms of advantages and dis-
advantages for a floating wind turbine application, referring not only to the R&D
state-of-the-art, but also to recent and ongoing projects.

2.1   HAWT and VAWT: High Level Comparison

Aerodynamics

The aerodynamics of HAWT and VAWT are substantially different, and in this
section only the main characteristics of both, which can simply illustrate the
resultant differences in aerodynamic efficiency, are considered. For more details on
the aerodynamics of VAWT and its modelling see Borg et al. (2014), while for
HAWT further details are presented in Sect. 1 in Chapter "Modelling of Floating
Offshore Wind Technologies".

Assuming a uniform and steady wind field (simplified conditions), it can be easily
seen that a section of a blade of a VAWT and of a HAWT operate in very different
flow regimes. For a HAWT, each blade section operates at a constant angle of
attack, and therefore it can be designed, for a given RPM, to operate at optimum
conditions (i.e. optimum angle of attack to generate the highest torque). As a
consequence, the aerodynamic forces acting on the HAWT rotor are constant,
including the torque produced by the rotor, transmitted eventually to the generator
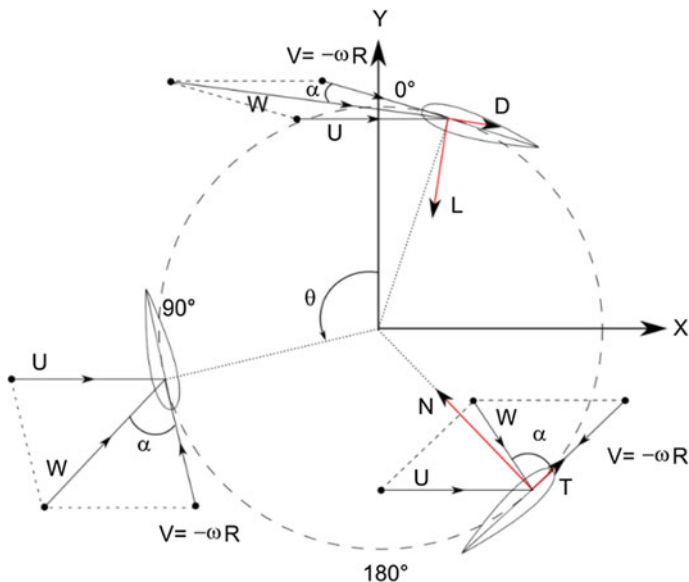to produce electric power.

Fig. 9 Illustration of the variation of the angle of attack (α) with the blade angular position (θ) for a VAWT section (U = wind speed, V = tangential speed due to the angular rotation velocity ω, R = radius of the wind turbine, W = vectorial wind speed resultant) (Jamieson 2011)

Differently, for the same conditions, each section of a VAWT blade operates at an angle varying with the blade angular position, as illustrated in Fig. 9, and therefore the aerodynamic forces acting on this wind turbine are oscillatory in nature. For example, in Fig. 10, it can be seen the difference between the constant (not taking into account the effect of the tower) thrust force acting at rated power on a 5 MW HAWT versus the oscillating thrust force acting on a 5 MW VAWT (Borg and Collu 2015). This implies that the VAWT blade section cannot operate at the optimum angle of attack over the whole cycle, and therefore from this point of view the aerodynamics of VAWTs is inherently inferior to that of HAWTs. Recently there have been a number of projects trying to overcome this weakness adopting periodically pitching blades, even if it is still unclear if the added costs associated with the additional necessary systems and the lower reliability is paid off by the higher aerodynamic efficiency: the simplicity of stall-regulated VAWTs is often claimed as one of its major benefit. Nonetheless, in this case the theoretical power coefficient limit for VAWTs would be the same Betz limit (C_p < 16/27) that applies for HAWTs, and some authors (Newman 1986) even suggest a higher value if in the aerodynamic analysis the *upwind* blades (the blades in the angular positions $0° < \theta < 180°$) and the *downwind blades* ($180° < \theta < 360°$) are considered acting on two different actuator disc, for which it can be derived an equivalent Betz limit of C_p = 16/25.

The power coefficient is the percentage of kinetic power in the wind that is harvested by the wind turbine, and can be considered as the reference measure of
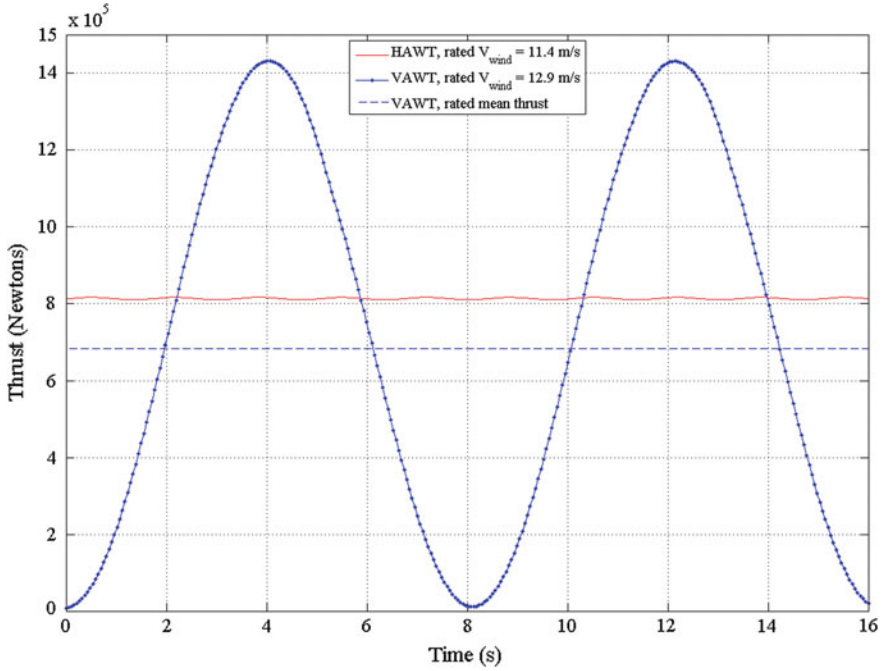
Fig. 10 Comparison between the thrust forces acting on a 5 MW HAWT and a 5 MW VAWT (Borg and Collu 2015)

the wind turbine aerodynamic efficiency. In Fig. 11 are compared the power coefficients of different typologies of wind turbine against the tip speed ratio λ, defined as the ratio between the tangential speed of the rotor blades and the undisturbed wind velocity. For modern three bladed, variable pitch, variable rotational speed, upwind HAWTs, the maximum C_p can reach values around 0.5 and above (Hau 2013), while for VAWT (fixed pitch blades) the maximum C_p demonstrated is around 0.4.

Considering their lower power coefficient, one may ask what is the reason behind the recent resurgence in interest in VAWTs: one key aspect is the inclining moment generated by the wind turbine, especially when considering floating support structures. When a wind turbine, HAWT or VAWT, is operating, it will be subject to a thrust force, parallel and in the same direction of the wind. This thrust force can be considered to act at a point, the centre of thrust pressure (C_T). In a recent work, Borg and Collu compared the dynamics of a reference 5 MW offshore HAWT against a 5 MW offshore VAWT concept (Borg and Collu 2015), and in Fig. 12 is shown the comparison between the two C_T positions. The inclining moment acting on the wind turbine and transmitted to the support structure can be estimated by multiplying the thrust force by the arm equal to the distance between the C_T and the point where the thrust force is counteracted (for a floating wind
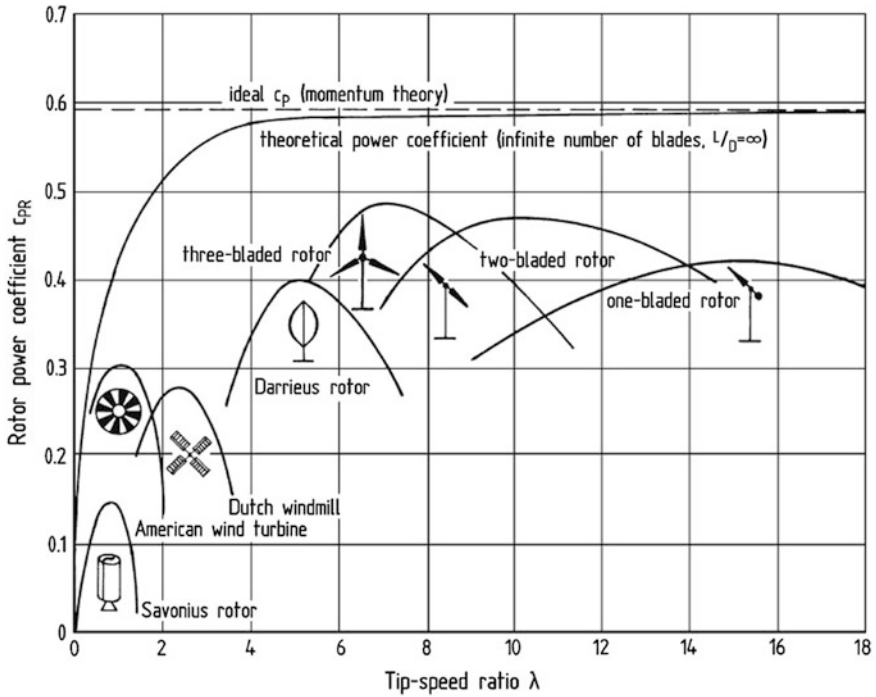
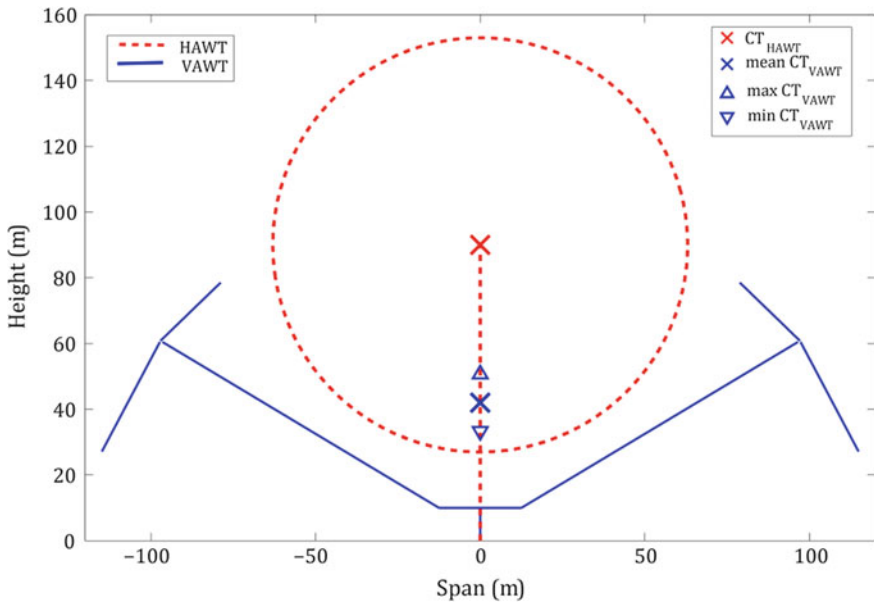**Fig. 11** Wind turbines' power coefficients vs. tip-speed ratio (Hau 2013)

Fig. 12 Front view schematic of HAWT (NREL 5 MW) and VAWT (NOVA 5 MW), with the centre of thrust pressure, C_T, indicated. Note that the height of the VAWT C_T varies as the turbine rotates, with maximum and minimum values indicated (Borg and Collu 2015)

turbine, this typically coincides with the mooring lines attachment point). As illustrated in Fig. 10, the average VAWT thrust for this configuration, at rated wind speed, is slightly lower than the HAWT thrust force but, similarly to the other aerodynamic forces acting on the VAWT, it oscillates around this value, up to thrust forces almost double than the HAWT one. Nonetheless, the position of the VAWT C_T can be much lower than the HAWT C_T, resulting in a final VAWT inclining moment much lower than the HAWT inclining moment, as illustrated in Fig. 13. As illustrated in more detail in the following sub-section *static stability*, since the VAWT has a lower inclining moment for the same rated power, the floating support structure has the potential to be smaller and, consequently, potentially less expensive. It has to be noted that this effect depends on the VAWT configuration, and for the V-shaped VAWT considered in the Borg and Collu (2015) study this effect is particularly enhanced. Nonetheless, it is a good example to illustrate one of the potential advantages of VAWT configurations for offshore floating applications.

Another important aspect to be considered is the aerodynamic behaviour of the wind turbine when operating in *skewed flow* conditions. For HAWTs, the optimum condition is when the wind direction is perpendicular to the rotor disc, and therefore parallel to the axis of rotation. In order to satisfy this condition, when the wind direction is parallel to the ground but not perpendicular to the rotor disc, modern HAWTs are equipped with a yaw control system (NB. due to the axisymmetric
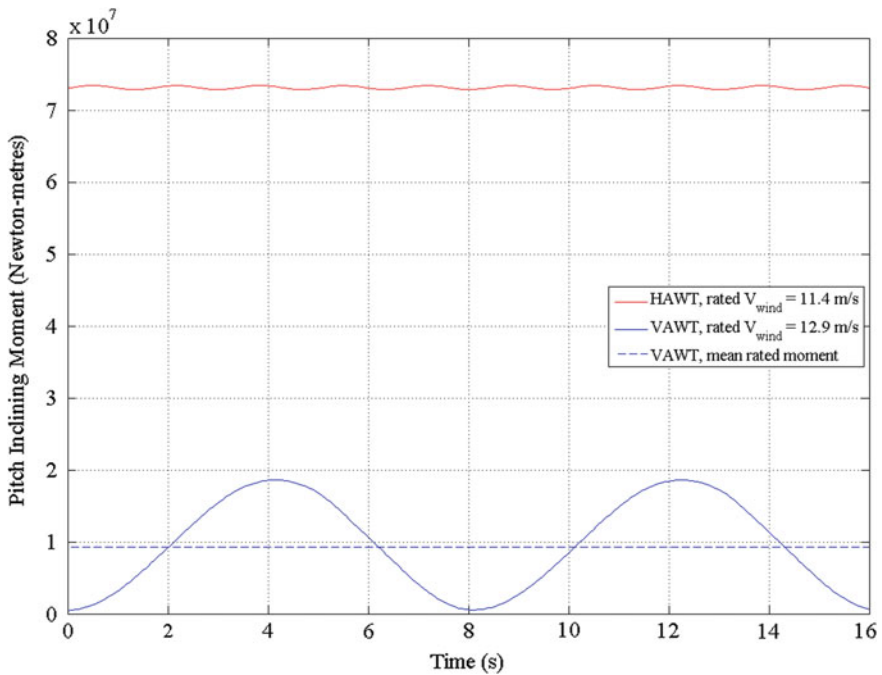

Fig. 13 VAWT and HAWT rotor inclining moments at the relative rated wind speeds (Borg and Collu 2015)

configuration of VAWTs, they are insensitive to the yaw angle of the wind, so no yaw control system is required). When a floating support structure is considered, due to the inclining moment transmitted by the rotor to the support structure, and due to the action of the wave loads, the wind turbine can be operating inclined toward the wind or away from the wind, in a so-called *skewed flow* condition. Theoretical studies and experimental measurements have shown that the skewed flow condition is detrimental for HAWTs (Tongchitpakdee et al. 2005), while for some VAWT configurations it can not only be less detrimental, but even beneficial. If H-VAWT configurations are considered, as shown by theoretical and experimental studies (Mertens et al. 2003; Ferreira et al. 2006), the coefficient of power in skewed conditions can be higher than the coefficient of power in upright conditions (i.e. for a VAWT with axis of rotation perpendicular to the wind direction): the main reason proposed to justify this phenomenon is that when the wind turbine is inclined toward the wind or away from the wind, a fraction of the blade/s in the downwind cycle ($180° < \theta < 360°$ in Fig. 9) is exposed to a wind flow no longer disturbed by the blade/s in the upwind cycle, and therefore can extract more energy from it, as it can be seen from Fig. 14. In an offshore environment, floating wind turbine systems will be oscillating most of the time, and therefore the wind turbine will be very often operating in a skewed flow condition, making the H-VAWT configuration more suitable from this point of view.
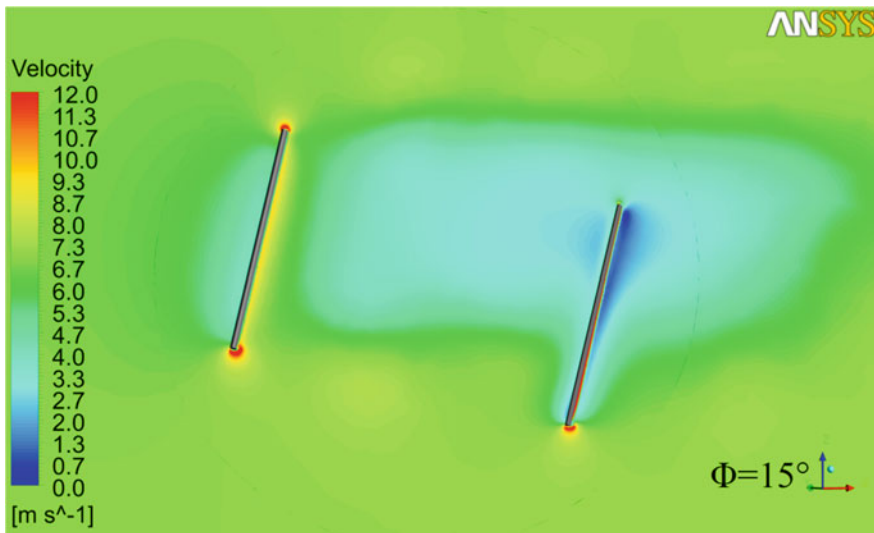
Drive Train

Fig. 14 Velocity field for an inclined H-VAWT, angle of inclination $\Phi = 15°$, positive if away from the wind, wind direction *left* to *right*, parallel to *x*-axis. The downwind blade, on the right, is not completely in the lower speed region (*blue*) due to the upwind blade, and therefore the bottom part is exposed to higher wind speeds (Orlandi et al. 2015)

A consequence of the different aerodynamics of VAWTs with respect to HAWTs is that, in general, the optimum tip-speed ratio λ for VAWTs is lower than the one for HAWTs (Jamieson 2011), as also illustrated by Fig. 11. Since the power generated by a wind turbine can be derived as:

$$P = T\omega \tag{1}$$

where T is the torque and ω is the rotational speed, it can be seen that, for the same rated power P, lowering ω will augment T.

Due to the previous consideration, VAWTs tend to have lower rotational speeds than HAWTs, and therefore the average torque transmitted is higher for the same output power. As for the other aerodynamic forces, also the torque for a VAWT is oscillatory in nature, and this means that the maximum torque will be even higher than the average torque. Since the driving parameter for the weight and the cost of a drive train is the maximum torque, for the same rated power, a typical VAWT needs a heavier and costlier drive train. This challenge can be reduced if the height-to-radius VAWT aspect ratio is increased: in fact, for the same λ, ω is augmented, and therefore the maximum torque is diminished, with beneficial effects on the weight and cost of the drive train.

The oscillating nature of the torque for VAWTs, compared to the (at constant wind and rotational speed of the rotor) constant torque of HAWTs, constitutes a disadvantage for the VAWT configuration. For example, while for HAWTs the drive turbine systems can be optimised for the rated torque, linked to the rated power, for VAWTs the design need to take into account a wide oscillatory variation of the torque.

Other aspects also need to be taken into account. For offshore wind turbines in general, and for floating wind turbines in particular, the position of the drive train assembly is an important aspect of the design, and one where VAWT design may claim some advantages over the HAWT counterpart. The most suitable location of the drive train for a HAWT is the nacelle, on top of the tower: this can be at around 100 m above the waterline level for modern 5 MW + HAWTs, and the nacelle can weight around 400 t. These heights and weights can pose serious challenges in terms of installation and maintenance, impacting on the costs of these operations and on the availability of the wind turbine. Furthermore, they drive the structural design of the tower, which needs to withstand such large bending moments. In addition to this, the high position shifts the centre of gravity (CoG) of the whole structure upward, having a negative effect on the stability of floating wind turbines (see the following sub-section *static stability*).

One of the potential advantages of VAWTs with respect to HAWTs is the possibility to transmit the torque along the rotational axis down to the ground level (seawater level), and therefore have all the main drive train systems at this level. This not only facilitates the installation and the maintenance of these systems, since it is much simpler, especially in an offshore environment, to have access to a system at ground level rather than at a height ~ 100 m, but will also lower the CoG of the whole system, with a beneficial effect on the overall stability. Furthermore, being at

ground level, upscaling the drive train assembly for higher rated powers will have a lower impact on the wind turbine structure: for a HAWT, the drive train upscaling has an impact on the structural design of the tower sustaining the rotor and the drive train. On the other hand, to transmit the torque down to the ground level it is necessary to adopt a VAWT tower-less design, such the V-shaped VAWT (e.g. the Energy Technologies Institute (ETI) NOVA project), or a rotating tower approach, like in the FP7 EU-funded DeepWind project, or to have a shaft able to transmit the aerodynamic torque down to the basement, where the drive train is located. For these reasons, some of the VAWT designs have their drive train on top of the tower similarly to the HAWT.

Static Stability

Referring to Fig. 15, for a floating wind turbine system, under the small angle of inclination approximation, the equilibrium between the inclining moment
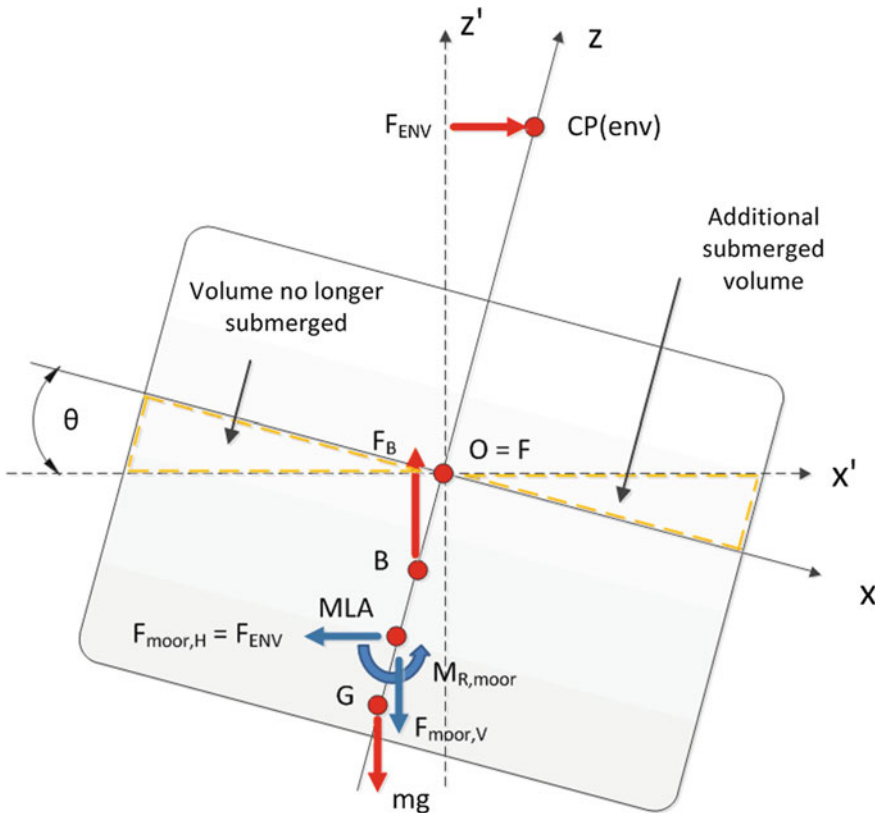

Fig. 15 Diagram of forces and moments acting on a floating wind turbine system, longitudinal plane (pitch degree of freedom/rotations around *y*-axis, *x*-axis aligned with wind speed direction) (Collu and Borg 2016)

transmitted by the wind turbine and the restoring moment generated by the floating support structure can be written as (Borg and Collu 2015):

$$M_I = M_R \tag{2}$$

$$M_I = F_{env}\left(z_{CP(env)} - z_{MLA}\right)\cos\theta \approx T(z_{CT} - z_{MLA}) \tag{3}$$

$$M_R = \left(\rho g I_x + F_B z_{CB} - mg z_{CG} + C_{55,moor}\right)\theta = C_{55,tot}\theta \tag{4}$$

where $C_{55,moor}$ (Nm/rad) = rotational stiffness provided by the mooring system (e.g. TLP); F_B (N) = buoyancy force; F_{env} (N) = sum of environmental forces (wind, wave, currents) along the x-axis (in the present simplified analysis, this is represented by the aerodynamic thrust force T only); g (m/s^2) = gravitational acceleration; I_x (m^4) = second moment of waterplane area with respect to the y-axis; m (kg) = total mass of the floating wind turbine system; M_I (Nm) = inclining moment around y-axis (wind parallel to axis y, z perpendicular to x and y, positive upward); M_R (Nm) = restoring moment around axis y; $z_{CP(env)}$ (m) = vertical position of the centre of pressure of environmental forces, defined as the point on which the sum of the environmental forces (in the present simplified analysis, it coincides with the vertical position of the centre of aerodynamic thrust pressure, z_{CT}); z_{CG} (m) = centre of gravity of the whole floating wind turbine system; z_{MLA} (m) = centre of mooring line action, i.e. the intersection of the line of action of the horizontal component of the mooring force with the z axis; θ (rad) = inclination angle, rotation around the y-axis; ρ (kg/m^3) = seawater density.

In the design phase of a floating wind turbine system, one of the requirements is to limit the maximum angle of inclination (θ_{max}) of the whole system, in order to limit the loss of power produced due to the skewed flow condition, as previously mentioned. This can be translated in a requirement to have a minimum rotational stiffness C_{55}, or:

$$C_{55,min} = \frac{M_I}{\theta_{max}} \tag{5}$$

In general, the higher the rotational stiffness required, the more expensive the floating support structure will be, and therefore the aim is to reduce it as much as possible. With regard to θ_{max}, the aerodynamic performances of floating HAWT and VAWT systems operating with their axis of rotation not parallel (HAWT) or perpendicular (VAWT) to the wind direction is still a relatively unexplored research field. According to Zambrano et al. (2006), a maximum mean pitch/roll angle of 5° plus ±15° of dynamic amplitude should be imposed. Referring to Eq. (3), as previously mentioned in the section on aerodynamics, for the same rated power, the inclining moment of a VAWT configuration can be much smaller than the one of an HAWT configuration, and this has a beneficial effect since it reduces $C_{55,min}$ with a positive impact on the final cost of the floating support structure.

Referring to Eq. (4), it can be seen as a higher position of the CoG (higher z_{CG}) has a detrimental effect on the restoring capability of the floating support structure. In order to compensate this destabilising effect, the other terms composing the total restoring moment should be augmented, augmenting I_x (i.e. for a Trifloater floating support structure, it means larger columns and/or a larger distance between the columns), and/or augmenting the stiffness provided by the mooring system: both solutions will result in a costlier floating support structure. Depending on the VAWT configuration, for the same power, a lower CoG can be achieved, especially if the drive train systems are located at ground (seawater) level.

2.1.1 Maturity of the Technology

The majority of the state-of-the-art offshore floating wind turbines prototypes, some of which are illustrated in Chap. 6, have adopted HAWTs. These wind turbines, due to their superiority for the onshore market, have been intensively studied, analysed, developed and optimised over the past decades, and the design has now converged toward relatively few options, with the so-called *Danish design*, the three-bladed, upwind, variable pitch, variable rpm, horizontal axis wind turbine, having the lion share of the market. On the other hand, despite major research and development efforts on VAWTs mainly in Canada, in USA, and in UK during the 1980s and 1990s, and even taking into account the recent resurgence of interest in VAWT for the offshore wind market over the past years (Shires 2013; Borg et al. 2014), VAWT technology is still lagging behind in terms of maturity with respect to HAWT.

In Chap. "State-of-the-Art" an up-to-date overview of current floating HAWT projects are presented. For completion a brief description of some of the main floating VAWT projects is given below, together with some references on where to find more information.

The DeepWind Project
The DeepWind project had been funded by the European Union through the Framework Programme 7 (FP7), and started on the 1st of October 2010, with a length of 4 years. The consortium consisted of twelve partners, including several universities and some major offshore wind companies, as well as research institutes, coordinated by the Technical University of Denmark (DTU). The aim of the project was to develop a novel offshore floating VAWT concept, specific for deep water sites, which could substantially reduce the cost of electricity of floating offshore wind energy (Paulsen et al. 2014). The concept was based on a Darrieus type rotor, with the main novelty being the fact that it was installed on a rotating spar platform, moored to the seabed through torque arms and catenary mooring lines. The project produced a 1 kW prototype, which has been manufactured and experimentally tried in real sea conditions. This prototype has been used for refining the conceptual and preliminary design of the 5 MW floating VAWT concept. A comprehensive set of analytical and numerical analyses has been carried out in order to not only estimate

the power production, but also to evaluate the loads acting on the system and to perform a first structural design of the main components. The drive train system is positioned underwater, at the bottom of the spar platform (this is another novelty of the project), with the main aim of substantially reducing the inclining moment acting on the bearing system of the wind turbine. This has been recognised as one of the main challenges for large VAWTs, requiring large bearing system not currently available at commercial level, and therefore significantly impacting on the final cost of electricity. The project has also delivered a conceptual design of a 20 MW floating VAWT, in order to show the potential to further reduce the cost of offshore floating wind electricity.

Several economic analyses have been conducted in order to estimate the Levelised Cost of Electricity (LCOE),[1] showing that for a 500 MW wind farm, considering a lifetime of 25 years, the estimated reference cost would be around 63 €/MWh, with a lower estimate of 59€/MWh and an upper estimate of 75€/MWh (Paulsen et al. 2015). To have a comparison, in the United Kingdom from the first offshore wind farms (~2000) until 2011, the LCOE has been increasing, levelling out at around 175€/MWh during the period 2011–13 (The Crown Estate 2012).

The main outcomes of the project are summarised by Paulsen et al. (2015), and the main numerical simulation challenges have been illustrated by Verelst et al. (2015).

The Nénuphar-Led VAWT Project

In 2009, with the first project VERTIFLOAT, the French start-up company Nenuphar led the development and manufacturing of the first 35 kW onshore prototype. This project seems to be the first step toward the development of the first offshore floating VAWT wind farm, through several projects co-funded by the French government, the EU and some of the big industries in the field (project VERTIWIND, project INFLOW, project VERTIMED) (IWES 2013). In May 2014, the first stage of a 2 MW onshore prototype of this VAWT configuration started to be operative, as part of the VERTIWIND project activities, and the objective is to be used as test-bed to further develop and optimise the wind turbine in view of the first floating wind turbine version of this concept.

Scalability

One of the advantages of moving wind turbines offshore is the potential to scale them up to very large rated power: in general, the larger the wind turbine, the lower will be the final cost of electricity produced. The trend toward larger wind turbines offshore has been clearly observed over the past years, from the 0.45 MW wind

---

[1]In simple terms, LCOE can be seen as the lifetime cost of the project, per unit of energy generated. It is defined as the sum of discounted lifetime generation costs (£) divided by the sum of discounted lifetime electricity output (MWh). Generation costs include all capital, operating, and decommissioning costs incurred by the generator/developer over the lifetime of the project, including transmission costs (The Crown Estate 2012).

turbines adopted for the world's first offshore wind farm, Vindeby, in Denmark, to the Westermost Rough wind farm, under construction (2015) in the UK, adopting 35 Siemens SWT-6.0-154 (6 MW).

With the offshore wind farm moving to further and deeper sites, the floating wind turbine solution is becoming more and more economically viable, but even considering the lower costs of a floating solution rather than a fixed support structure, the overall costs are likely to increase. This will reinforce even more the need to accelerate the development of bigger, higher rated power wind turbines.

Comparing HAWTs and VAWTs from the upscaling potential point of view, Clare and Mays observed in 1989 that (Clare and Mays 1989):

> The cyclically varying gravity stresses of a HAWT become progressively more dominant as the overall turbine size is increased and could limit the size to which a horizontal axis rotor can be economically constructed. Although the blades of a VAWT experience fluctuating aerodynamic loads, the stresses that result from these do not increase with the size of the wind turbine and gravity stresses do not fluctuate. Consequently, there is potential for development of VAWTs to sizes significantly larger than HAWTs and for improvement in the economics of offshore wind energy systems

It has to be observed that the previous statement is certainly a valid point, but it is difficult to estimate what would be the related rated power limit for HAWT. At the moment (2015), there are already 7 MW offshore HAWT commercially available (e.g. Siemens SWT-7.0-154), and 8 MW ones close to commercial maturity (e.g. Vestas V164-8.0 MW), while there are several projects looking at 10 MW and beyond HAWTs (Project HiPRWind). In particular, the EU funded FP6 project UpWind (2006–2011) and its successor, the EU funded FP7 project InnWind.EU (2012–2017) are looking at innovative solutions for offshore HAWTs from 10 to 20 MW. In the final report of the project UpWind (UpWind Consortium 2011) it is mentioned that:

> UpWind did not seek the optimal wind turbine size, but investigated the limits of upscaling, up to, approximately, 20 MW/250 m rotor diameter

and it is claimed that

> UpWind demonstrates that a 20 MW design is feasible. No significant problems have been found when upscaling wind turbines to that scale, provided some key innovations are developed and integrated. These innovations come with extra cost, and the cost /benefit ratio depends on a complex set of parameters.

Nonetheless, in principle VAWTs have the potential to be scaled up to higher rated powers, with the potential to further lower the cost of offshore wind electricity. In the UK, the Energy Technology Institute (ETI) funded a 1 year and half project, NOVA (Collu et al. 2014), aimed to demonstrate the feasibility of a large VAWT. Based on a novel V-shaped VAWT configuration, having as a main advantage the minimisation of the inclining moment, and therefore enhancing its suitability for floating support structures, the project investigated a 5 MW and a 10 MW offshore VAWT solution, from the conceptual and preliminary design to the evaluation of the final LCOE.

2.2   Summary of Wind Turbine Options

As regard the onshore wind industry, during the 1980s the need to lower the cost of energy led to the demise of many VAWT concepts, perceived as less cost effective compared with HAWTs (Tangler 2000). Attracted mainly by the higher and more consistent winds, the lower visual impact, and the upscaling potential, the wind industry has progressively moved toward offshore sites: at first near-shore, in relatively shallow waters, and now further offshore, in deeper water sites. At which depth a floating wind turbine becomes more cost effective than a fixed one? The debate is still open, but eventually in the range between 50 and 100 m it is very probable that a floating wind turbine is economically advantageous with respect to a fixed to seabed solution.

If the offshore, deep water environmental conditions are compared to the onshore environmental conditions, where the HAWT concepts have competed and prevailed against the VAWT concepts, it appears immediately evident that they are substantially different. Therefore, the question arises: is the HAWT configuration the most suitable for this novel environmental conditions still, or do we need to take a step back and compare again the HAWT configurations to some of the alternative concepts initially considered even onshore? The fact that the HAWTs are being adopted also for the first floating prototypes is the result of a systematic and detailed design space investigation, comparing alternative concepts, or is more due to a legacy from the onshore wind industry?

Even if inherently less efficient from an aerodynamics point of view, VAWTs can have, if compared to a HAWT with the same rated power, a substantially lower inclining moment, and this advantage can be translated into a smaller and cheaper floating support structure, lowering the final cost of electricity. Furthermore, while for a HAWT configuration there is a loss of aerodynamic efficiency in skewed flow conditions, a condition very common for floating wind turbines due to the wave loads, for certain VAWT configurations (H-VAWT) it seems not only that these conditions are not detrimental, but also beneficial.

From a drive train system point of view, due to the lower rotational speed VAWTs need larger, heavier and therefore costlier drive train systems than HAWTs. Nonetheless, while for HAWTs the drive train systems are usually located in the nacelle, on top of the tower, for VAWTs there is the possibility to locate the drive train assembly at ground (seawater line) level, with advantages in terms of installation, accessibility and maintenance, as well as upscaling potential. Having a drive train system at ground level also lowers the vertical position of the CoG of the whole system, that is beneficial for its stability. Again, together with the lower inclining moment, the enhanced stability can be instead used toward a smaller, less costly floating support structure, lowering the final cost of the offshore wind electricity.

In terms of technological and economic maturity, VAWTs are still lagging behind HAWTs, and need to be further investigated before determining if their potential advantages can be implemented at a practical level. Recently there have

been a number of projects co-funded by the industry and various national and international governments, aimed at pushing forward the Technology Readiness Level (TRL) of floating VAWT technology: these will hopefully help in assessing their potential. Due to inherent limits of HAWTs configuration, there are some potential barrier to their further upscaling beyond 15–20 MW, and VAWT could eventually emerge as economically more viable for very large powers (15–20 MW +), as they do not suffer from the same limitations.

To conclude, while for the onshore and near-shore wind market the wind turbine configuration options seem to be limited to a narrow set, the substantially different nature of the challenges posed by the offshore, deep water environment can reopen the design space toward a number of alternative wind turbine configurations.

3   Mooring Systems

Marco Masciola

Mooring systems are the facilitators that allow floating structures to be used in deep waters where conventional jacket foundations are economically prohibitive or technically challenging. In combination with the platform buoyancy, mooring lines emulate the role of the tower substructure to maintain the position and orientation of the wind turbine. It is the goal of the designer to implement a mooring with the durability to resist external forces, yet exhibit stiffness properties for the FOWT platform to operate outside of the wave excitation frequencies. Many design variables help fulfil the goal, though the design process begins with a set of constraints.

Converging on a mooring system radial footprint, anchor type, and line properties is an iterative process. The design process begins with anchor selection based on a soil's holding capacity, which leads to the number of anchors required to oppose the total environmental forces. The total required anchor holding capacity is balanced against the external forces applied on the FOWT. The total anchor holding capacity should be sufficient to oppose the design environment loads. This holding capacity then relates to choosing a line's *minimum breaking strength*, or MBS (Ruinen and Gijs 2001; API RP 2SK 2005). Mooring properties, such as the line material, line length, and clump weights are then selected based on meeting a desired performance criterion. Simulations are subsequently run to determine if the line meets the necessary safety margins. Design iterations are performed as necessary. This synopsis describes the common design spiral for moorings.

Over the past two decades, the offshore industry has expanded into deeper waters with the introduction of synthetic fibre rope materials. FOWTs, however, usher in new and unique challenges due to a combination of shallow water depths and large wind thrust loads. This combination may lead to a need for greater mooring scope traditionally used in conventional deepwater floating production systems. Despite foreseeable challenges, the latest international standards remain applicable and are

an important resource for FOWT permanent moorings. The referenced standards include:

- ISO 19901-7 (2013): Station keeping systems for floating offshore structures and mobile offshore units.
- API RP 2SK (2005): Design and Analysis of Station keeping Systems for Floating Structures.
- API RP 2SM (2014): Design, Manufacture, Installation, and Maintenance of Synthetic Fibre Ropes for Offshore Mooring.

The practices described in these standards are adopted in the forthcoming IEC 61400-3-2 international standard on floating offshore wind turbines.

3.1   Common Materials

The adopted mooring design is a compromise of many factors, including: anchor holding strength, material fatigue properties, breaking loads, seabed clearance and between other subsystems, tower and wind turbine motion limitation, special considerations for fibre ropes (such as compression fatigue, and creep characteristics), and permissible platform offset, all of which should balance to oppose environmental loads. With floating production units, the platform displacement is restricted by the risers, the conduit carrying fluid from the seafloor to the floating production unit. Although FOWTs lack risers, other factors may restrict FOWT displacement watch circles, such as bending restrictions on the power umbilical or to limit rotor waking effects to maximise capacity factor. Spacing between adjacent units is another factor the FOWT system may need to contend with for damaged line conditions.

A mooring line can be decomposed into several sections with different line types to improve the restoring force characteristics or system durability. Chain is commonly used on the lowest section of line closest to the seabed, not only because is exhibits excellent abrasion resistance, but also because the chain weight acts as a medium to bolster system stiffness through the action of raising mass off the seafloor. Wire rope is an alternative to chain exhibiting similar stiffness and weight characteristics, but with improved shock absorption properties. The cross-sectional strand pattern can affect strength by a significant degree between two steel ropes with equal nominal diameters. A third line material, known as synthetic fibre rope, has emerged in recent years allowing deep water to be reachable. Although polyester ropes are recommended for permanent installations (API RP 2SK 2005), other materials such as aramid and high modulus polyethylene (HMPE), show promise for future applications. Figure 16 compares Young's modulus for various rope types that have been studied for permanent moorings.

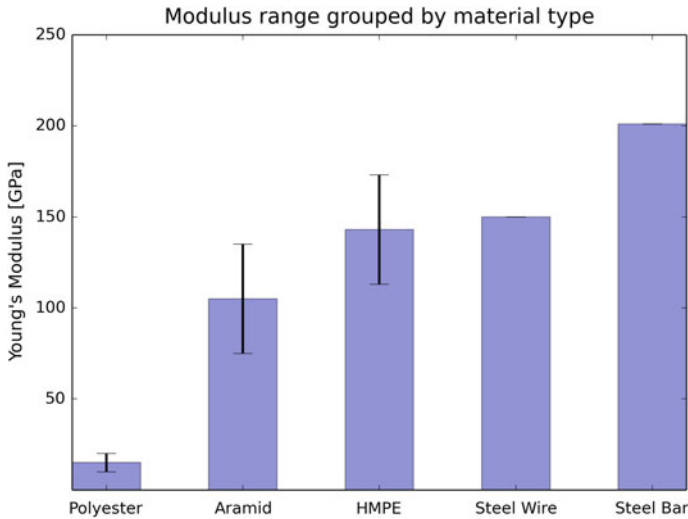A mooring system may be comprised of a combination of the following components:

Fig. 16 Average Young's modulus for various materials for mooring systems. The *upper* and *lower* modulus bounds are given. Material properties are derived from Ayers and Renzi (2010)

- Mooring line
  - Chain
  - Wire rope
  - Fibre (synthetic) rope

- Anchor
  - Drag embedment anchor
  - Plate anchor
  - Suction pile
  - Pile and screw anchor
  - Gravity anchor

- Clump weights and buoyancy modules
- Connection equipment and hardware
  - Triplate
  - Shackle
  - Splices

Power umbilical's normally do not constitute as part of the mooring system since they are not designed to enhance the station keeping characteristics, though their strength analysis may follow design guidelines for moorings and risers. None the less, their analysis is vital for global performance studies. Power umbilicals serve an analogous purpose as to the risers used in oil and gas platforms, but instead of

Chain Grade	Yield Stress [N/m²]	Elongation (%)
R3	410×10^6	17
R3S	490×10^6	15
R4	580×10^6	12
R4S	700×10^6	12
R5	760×10^6	12

Table 2 Yield stress and elongation characteristics of different chain grades Values are procured from API RP 2F (1997)

carrying fluid, the power cable transfers electricity. As with risers, the FOWT range of motion can be restricted by bending radius limitation on the power umbilicals.

Chain and Wire-Rope

Chain is prominently used throughout the offshore industry for station keeping applications either in studlink or studless construction. Marine chain is graded according to material strength scaled by R3, R3S, R4, R4S, and R5 as described in Table 2 (API RP 2F 1997). Chain is graded to promote consistency across various manufactures and ensure that minimum strength characteristics are guaranteed. This assurance is based on industry standard qualification testing that manufacturers submit to.

The strength of steel wire rope, on the other hand, must be judged carefully and on a case-by-case basis. The strength depends on several factors ranging from the use of cathodic protection to the type of stand pattern used. Steel wire rope lifespan can range from six to 35 years. The lifetime ranges are estimated to be (API RP 2SK 2005):

- 6–8 years for 6-strand galvanised steel wire line.
- 10–17 years for spiral-galvanised strand.

  - 10–12 years without corrosion protection.
  - 15–17 years with corrosion protection.

- 20–35 years for spiral-galvanised with protective sheathing.

  - 20–25 years without corrosion protection.
  - 30–35 years with corrosion protection.

As indicated, the strand, sheathing, and corrosion protection all combine to influence the rope life span. While designing a mooring, it is common to work with the chain or rope manufacturer to ensure the simulated properties reflect real-life properties. The life span is roughly estimated based on past experiences, though in practice, routine inspections are required to monitor life cycle.

3.1.1 Fibre Rope

Over the past 20 years, fibre ropes have demonstrated versatility in permanent deep water, station keeping applications (Kwan and Bruen 1991; Flory and Banfield

Table 3 Variation of stiffness for fibre ropes. Properties are taken from Ayers and Renzi (2010)

Rope family	Intermediate stiffness	Storm stiffness	Elongation characteristic
Polyester	15 × (MBS)	30 × (MBS)	Log
Aramid	35 × (MBS)	70 × (MBS)	Log
HMPE	60 × (MBS)	90 × (MBS)	Proportional

2006). Their near-neutral buoyant properties diminish negative effects from self-weight and permit deep waters to be reached. Despite the use of polyester fibre rope in deepwater oil and gas applications, little research has been applied towards fibre ropes in shallow-water FOWT designs. Undoubtedly, fibre ropes will see increased activity as FOWTs venture into deeper waters. The transition point where fibre ropes reach economic parity with conventional chain and wire rope installations is a question of not only water depth, but also platform type (tension leg platform (TLP) versus semisubmersible versus spar), deployment time, length of line, and effect on the platform natural periods.

Weller et al. (2012) characterises the long-term durability properties of synthetic lines to propose a testing/measurement protocol for ocean energy mooing applications. The authors find tensions peak at approximately 11 % of MBS, and most load measurements remain within 3 % of MBS; this region is important for fatigue analysis (Lechat et al. 2008; Weller et al. 2012). The study shows long term potential for synthetic lines if tension magnitude can be managed, but fatigue analysis is essential, as this could be a governing case for the mooring design.

Although the study demonstrates promise for fibre ropes in the offshore renewable energy sector, it also alludes to special accommodations needed due to the unique properties synthetic material possesses. Unlike steel wire strand or chain, synthetic ropes are susceptible to non-linear elongation (creep) and variable stiffness properties. Axial stiffness depends on the rope material and load range, Table 3, also depicted in Fig. 16. Aramid and HMPE occupy a large stiffness range compared to polyester, although polyester fibre rope is a proven technology for permanent moorings. Certain fibre ropes are sensitive to loss of load, such as aramids, which can succumb to wear when compressed. Given the wide variability of material properties and strength characteristics, it is common to defer to manufacturer specifications based on qualification testing.

Fibre Rope Permanent Elongation and Non-Linear Stiffness

Fibre ropes are susceptible to permanent elongation, which results in decreased mooring stiffness. Line length increases are a natural occurrence and are inevitable with synthetic materials, and engineers must accommodate and plan for permanent elongation in the mooring design. Permanent elongation properties can vary depending on the fibre rope material. Creep properties can either be linearly proportional to time or logarithmic functions of time. Polyester fibre rope is generally preferred for permanent installations because of elongation characteristics and demonstrable track record, Fig. 17 (Huntley 2006). Load history is the primary driver affecting elongation, as synthetic ropes are aware of the previous loading

Fig. 17 Permanent
elongation, or creep, results in
an increase in line length
relative to the original
installation length. Elongation
can be linearly proportional to
the length of period a load is
applied to the line (such as
HMPE) or expressed as a
logarithmic of the load history
(as is the case for aramid and
polyester fibre ropes)
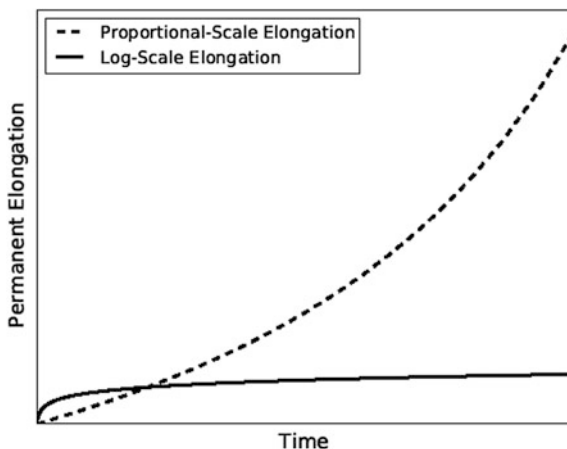
regimes and respond by elongating as a new maximum load is encountered (Flory
and Banfield 2006). Although HMPE possess proportional creep characteristics,
new chemical compounds demonstrate a possibility to decrease creep coefficients to
low values competing with log-proportional properties typically found in polyester
ropes.

The lack of constant stiffness is a second contributor that the designer must
contend with. Unlike chain and wire rope, the axial stiffness of synthetic varies
depending on load amplitude (A), loading period, and average load (L). These
factors can be combined to model the non-linear axial stiffness parameters (Flory
1999; Tahar and Kim 2008):

$$K = \alpha + \beta L + \gamma A \tag{6}$$

where the coefficients α, β, and γ are specified in rope qualification tests. An extra
term can be included in Eq. (6) to account for permanent elongation, which is
particularly important for analysis in storms. Numerical models can accommodate
Eq. (6) to include the non-linear stiffness attributes (Tahar and Kim 2008). If the
model is incapable of including a variable stiffness model, then the designer may
have to resort to an upper and lower bound stiffness model (Wibner et al. 2003).

3.2 Composite Mooring Systems

Many applications may benefit from mixing various line properties in series to
maintain adequate stiffness margins while decreasing static and dead weight loads.
One such rendition is given in Fig. 18 to show the mooring profile for three lines,
one of which has a composite construction. Line 1 is comprised entirely of chain,
and Line 2 uses a synthetic material. A mixture of the chain and fibre rope is used in
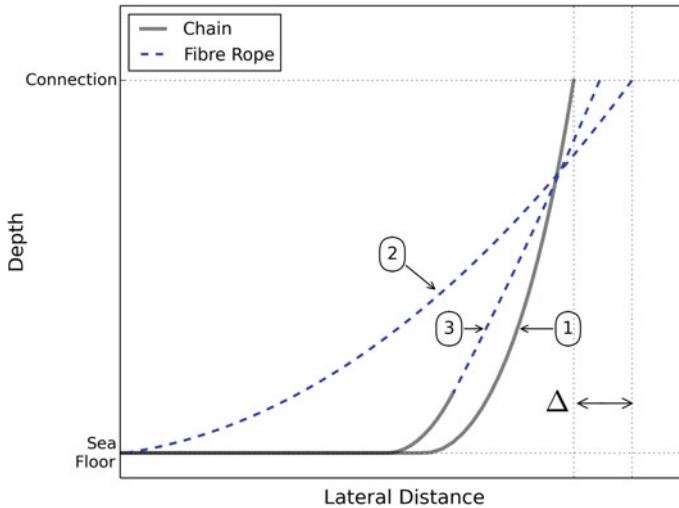
Fig. 18 The horizontal restoring force of a slack line mooring depends on the submerged weight property. This illustration demonstrates the mooring profile for three different compositions to yield equivalent mean horizontal forces at the upper terminal. The vertical force is different, since each line has a different weight. (*1*) is for chain; (*2*) is fibre rope; and (*3*) is composed of chain and fibre rope

Line 3. In this conceptual example, the fairlead for Lines 2 and 3 are extended outward until their horizontal force equals that of Line 1. One finds the all-fibre rope mooring stretches the furthest to match the restoring force of Line 1. The offset gap Δ is due to the absence of the chain weight. In effect, the presence of weight enhances the mooring stiffness. To reword this: catenary-shaped moorings derived most of their restoring stiffness from geometric non-linearities (i.e. the shape of the mooring) rather than from axial strain. The restoring force for Line 3, the line using both chain and fibre rope, lies between the two systems because a proportion of the chain weight is preserved. As more chain is lifted off the seabed, the restoring force increases by the action of raising weight.

There are repercussions to using an all-chain mooring in deep waters. Effects from self-weight eventually become a design constraint as depth increases because of growing static loads. This increasing static load may eventually require a larger chain size to meet safety factor thresholds. Under these circumstances, the benefits of fibre ropes become apparent. By placing synthetic lines in series at the upper terminal, the static loads are decreased. Note that although the horizontal force for Lines 1, 2 and 3 are equal, the vertical force static loads do not match. The applied vertical force for this statically arranged lines correlates to the submerged weight of the chain. In other words, fibre ropes can also be used as a mechanism to moderate the upper terminal vertical loads. Chain resting on the seabed also serves as a purpose of averting fibre rope soil ingress. Penetrating soil particles can exacerbate abrasion within the fibre yarn, though a protective barrier can delay or prevent premature failure (Majhi and D'Souza 2013).

3.3 Design Methodology and Applicable Standards

API RP 2SK (2005) defines the practices for designing permanent station keeping systems for floating platforms, which is the methodology adopted into ISO 19901-7 (2013). Special provisions pertaining to fibre ropes are addressed in API RP 2SM (2014). Collectively, these standards form the basis of the mooring design process accepted into the forthcoming IEC 61400-3-2 international standard for floating wind turbines.

As described in Kwan (2015), mooring design procedures are constantly evolving as new challenges are addressed with industry consensus. The first API mooring design standards were published with API RP 2P (1984) for drilling units and API RP 2FP1 (1993) for production units. Both API RP 2P and API RP 2FPI spawned the first edition of API RP 2SK (released in 1995). The latest release of API RP 2SK is currently on the third edition (API RP 2SK 2005), with the impending release of a fourth edition. Among the many differences between the first-generation mooring standard API RP 2P and the latest API RP 2SK edition, Kwan (2015) notes the following significant changes:

- Drilling units initially relied on a return period of 1-year. This is increased to larger non-exceedance probability thresholds.
- The use dynamic-based mooring simulation tools is advocated over quasi-static methodologies.
- Cyclic loading can reduce lifespan of the mooring, and fatigue analysis is introduced as an additional factor to assess.

As floating offshore wind continues to gain traction, new processes or modifications to existing procedures may come to light. A similar direction was experienced for the predecessors to API RP 2SK: API RP 2P and API RP 2FP1. Irrespective of the platform type and purpose, there are many mooring design factors that will continue to remain constant. Following the procedure in the latest mooring design standards, which are based on working stress design (WSD), the mooring system can be designed using time-domain, frequency-domain, or a combined approach (Kwan and Bruen 1991; Fitzgerald and Bergdahl 2008). Ensuring longevity and suitability of the mooring design requires the maximum tension T_{max} to remain within the allowable safety margins. The maximum tension is typically based on the maximum line terminal excursion in calm water (x_{max}).

Maximum FOWT Offset
The maximum offset is determined by combining the mean FOWT excursion from steady loads with the amplitude motion range from the time-varying cyclical loads. Steady loads include the mean rotor thrust force, wind drag from exposed surfaces, current drag, and the mean second-order drift force. Cyclical loading arises from dynamic contributions from wave-induced drag loads, frequency-dependent added mass, atmospheric turbulence, and sum-difference and sum-sum second-order wave loads.

Following the relevant standards (API RP 2SK 2005; ISO 19901-7 2013), time domain, frequency domain, and a hybrid of time and frequency domain procedures can be applied to find the maximum line tension and maximum vessel offset. A statistical distribution model is applied in the case of the time domain simulation to calculate tension values that have a very low probability of exceedance using a Weibull, Gumbel, or other extreme-value probability model (Nadarajah and Kotz 2006). The maximum offset can be calculated in the frequency domain by virtue of:

$$x_{max} = x_{mean} + \text{MAX}\left(x_{dyn_1}, x_{dyn_2}\right) \tag{7}$$

$$x_{min} = x_{mean} - \text{MAX}\left(x_{dyn_1}, x_{dyn_2}\right) \tag{8}$$

Each dynamic term above is determined by filtering the vessel motion frequency to find the FOWT response from 1) the wave frequency excitation range and 2) the low frequency excitation range. The mean offset, x_{mean}, is decided based on the distance the FOWT must offset for the mooring system to balance the applied environmental load.

The dynamic offset is defined as $x_{dyn_1} = \left(x_{lf_{max}} + x_{wf_{sig}}\right)$ and $x_{dyn_2} = \left(x_{wf_{max}} + x_{lf_{sig}}\right)$ with the following definitions provided:

- $x_{lf_{max}}$—maximum low-frequency motion
- $x_{lf_{sig}}$—significant low-frequency motion
- $x_{wf_{max}}$—maximum wave-frequency motion
- $x_{wf_{sig}}$—significant wave-frequency motion

The larger value of Eq. (7) or Eq. (8) is used to assess tension loads based on offsets.

Combining the mean offset x_{mean} and dynamic offset x_{dyn} to result in the maximum offset is demonstrated in Fig. 19. This offset, x_{max} is used to find the line tension based on quasi-static procedures. The mean offset can be large in FOWT systems during normal operation due to the exceptionally large thrust force in power generation mode. Although this is contingent on individual designs, the combined rotor thrust and exposed area drag force are likely to be large at two wind speeds. The first is at the rated wind speeds, where rotor thrust force is usually high. The second is at the N-year return period wind speeds, where the platform exposed area drag force can dominate the rotor thrust for the idling turbine. This imposes two conditions where wind drag loads are significant: one is with a low probability of exceedance (the N-year return period), and the second is during normal operation in power productions mode. Hence, it would not be surprising if Eq. (7)/(8) peaks during the operational load cases.

Figure 20 demonstrates the application of Eq. (7)/(8). The displacement x_{mean} is indicative of the required offset to balance the mean horizontal environmental force. This results in an average line tension magnitude of T_{mean}. With the addition of a dynamic offset x_{dyn}, the maximum line tension $T_{x_{max}}$ is achieved. Although the curve in Fig. 20 represents tension in a single line for pedagogical reasons, the collective
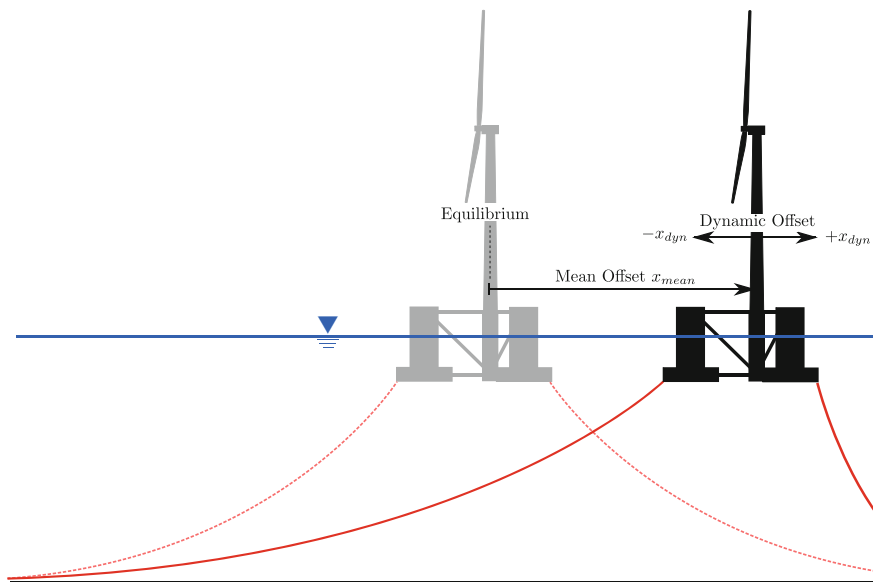
Fig. 19 Contribution of the frequency-independent mean offset x_{mean} and frequency-dependent dynamic offset x_{dyn} to result in the maximum vessel offset x_{max}. A large portion of the FOWT offset may derive from the rotor thrust force during normal operation modes. This creates a possibility for a peak x_{mean} condition to occur during normal power production modes. This aspect sets FOWTs apart from conventional offshore systems

restoring force of the entire intact (or damaged) mooring system should be assessed when calculating x_{mean} offsets. Strength analysis should be performed on individual lines, anchors, shackles, and other mooring components using the axial tension magnitude.

The procedure discussed in Fig. 20 represents the force/displacement relationship for a line with constant properties during its deployment life—a valid assumption for chain and wire rope. Fibre rope properties will vary throughout its life span. When determining the maximum offsets and peak tension loads, it is necessary to repeat the analysis to consider variability in the rope stiffness and elongation.

Similarly, ISO 19901-7 (2013) adopts the following analogy to Eq. (7) and (8) for maximum frequency-domain tension analysis:

$$T_{extreme} = T_{static} \pm T_{wf_{max}} \tag{9}$$

The static tension T_{static} in Eq. (9) is calculated based on the tension measured at relevant offset $\left(x_{max} - x_{wf_{max}}\right)$ or $\left(x_{min} - x_{wf_{max}}\right)$, which is different from the definition of T_{mean} (ISO 19901-7 2013). In contrast, the tension analysis in API RP 2SM (2014) is given as:
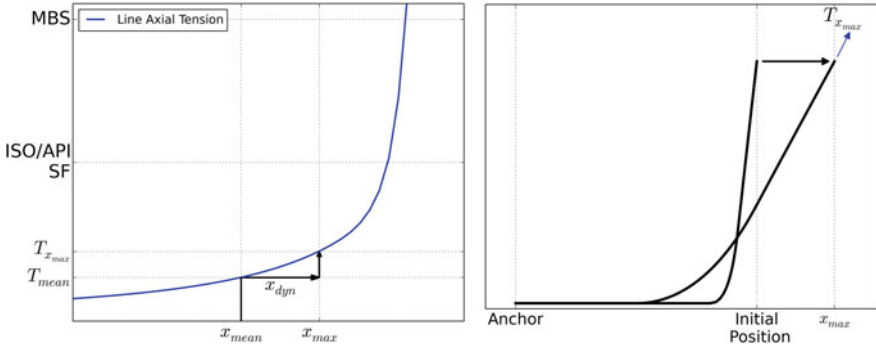
Fig. 20 Interpretation of Eq. (7)/(8) applied to a mooring system. The mean offset x_{mean} presents the offset due to steady forces from current, drift loads, and the average wind thrust. x_{mean} contributions can be significant because the rotor thrust loads are large in FOWTs. The dynamic offset, x_{dyn} are derived from cyclical loads combined from low-frequency and wave-frequency content

$$T_{max} = T_{mean} + \text{MAX}\left(T_{dyn_1}, T_{dyn_2}\right) \tag{10}$$

where the mean tension T_{mean} represents the axial line force at the mean vessel displacement, i.e. at x_{mean}. The dynamic tensions $T_{dyn_1} = \left(T_{lf_{max}} + T_{wf_{sig}}\right)$ and $T_{dyn_2} = \left(T_{wf_{max}} + T_{lf_{sig}}\right)$ are defined as:

- $T_{lf_{max}}$—maximum low-frequency tension
- $T_{lf_{sig}}$—significant low-frequency tension
- $T_{wf_{max}}$—maximum wave-frequency tension
- $T_{wf_{sig}}$—significant wave-frequency tension

Note that $T_{x_{max}}$, $T_{extreme}$ in Eq. (9), and T_{max} in Eq. (10) are not necessarily identical. Equation (9) and/or Eq. (10) can be utilised as alternative design criteria, but it is often used in parallel with Eqs. (7) and (8). Although the demonstrated procedure is performed using a quasi-static method, the analysis should be followed up with a dynamic simulation studies. The rigors offered by dynamic, fully-coupled simulations entrust that non-linearities are captured and resonance matching between the platform, tethers, and environment is not overlooked.

3.4 Design Challenges

Although there are many facets to investigate when designing permanent moorings, the nucleus of the design is initiated with the anchor selection based on soil holding capacity. Strength analysis follows next to ensure mooring components and line

tensions remain below acceptable safety factors. If design fails to meet the acceptance criteria, designers have the option to increase the material diameter or other viable alternatives to augment strength. As the mooring design matures, follow-up studies could be required in other areas, including but not limited to:

- Fatigue life and limit states
- VIV (vortex-induced-vibration) damage
- Damage conditions
- Anchor holding strength
- Installation tolerances
- Component strength
- Touchdown point
- If applicable, creep rupture and abrasion

Installation tolerance and sensitivity to anchor positioning errors should be assessed (Majhi and D'Souza 2013). Incorrect anchor placement or deviations in the line length from the assessed conditions could trigger failures, which can be exacerbated by the shallow waters FOWTs are deployed in. The shallow water poses a design challenge due to the large horizontal FOWT offset as a ratio of water depth.

References

References (2)

Borg M, Shires A, Collu M (2014) Offshore floating vertical axis wind turbines, dynamics modelling state of the art, part I: aerodynamics. Renew Sustain Energy Rev 39:1214–1225

Borg M, Collu M (2015) A comparison between the dynamics of horizontal and vertical axis offshore floating wind turbines. Philosophical Transactions A: Mathematical, Physical and Engineering Sciences, 373 (2035)

Clare R, Mays ID (1989) Development of vertical axis wind turbine. Proc Inst Civ Eng 86(5):857–878

Collu M, Brennan FP, Patel MH (2014) Conceptual design of a floating support structure for an offshore vertical axis wind turbine: the lessons learnt. Ships Offshore Struct 9(1):3–21

Collu M, Borg M (2016) Design of floating offshore wind turbines. In: Ng C, Ran L (eds) Offshore wind farms, technologies, design and operation. Woodhead Publishing Series in Energy, Cambridge

Ferreira C, van Kuik G, van Bussel (2006) Wind tunnel hotwire measurements, flow visualization and thrust measurement of a VAWT in skew. In: Proceedings of the 44th AIAA aerospace sciences meeting and exhibit, Reno, Nevada, 9–12 Jan 2006

Hau E (2013) Wind turbines: fundamentals, technologies, application, economics, 3rd edn. Springer-Verlag, Berlin, Heidelberg

IWES (2013) INFLOW project. Fraunhofer Institute for wind energy and energy system technology IWES. Accessed 3 Apr 2015

Jamieson P (2011) Innovation in wind turbine design, 1st edn. Wiley, Chichester

Jonkman JM, Butterfield S (2009) Definition of a 5 MW reference wind turbine for offshore system development. Technical report NREL/TP-500-38060, National Renewable Energy Laboratory (NREL), Golden, CO, USA, February 2009

Mertens S, van Kuik G, van Bussel G (2003) Performance of an H-Darrieus in the skewed flow on a roof. J Sol Energy Eng 125:433–440

Newman BG (1986) Multiple actuator-disc theory for wind turbines. J Wind Eng Ind Aerodyn 24 (3):215–225

Orlandi A, Collu M, Zanforlin S et al (2015) 3D URANS analysis of a vertical axis wind turbine in skewed flows. J Wind Eng Ind Aerodyn 147:77–84

Paulsen US, Madsen HA, Kragh KA et al (2014) DeepWind—from idea to 5 MW concept. Energy Procedia 53:23–33

Paulsen US, Borg M, Madsen HA et al (2015) Outcomes of the DeepWind conceptual design. Energy Procedia 80:329–341

Shires A (2013) Design optimisation of an offshore vertical axis wind turbine. Proc ICE Energy 166:7–18

Spiritrock 4u at en.wikipedia (2015) Quebec turbine. In: Licens. under CC BY-SA 3.0 via Wikimedia Commons. https://commons.wikimedia.org/wiki/File:Quebecturbine.JPG#/media/File:Quebecturbine.JPG. Accessed 30 Mar 2015

Tangler JL (2000) The evolution of rotor and blade design. NREL/CP-500-28410, National Renewable Energy Laboratory (NREL), Golden CO, USA, July 2000

The Crown Estate (2012) Offshore wind cost reduction—pathways study. The Crown Estate, London

Tongchitpakdee C, Benjanirat S, Sankar LN (2005) Numerical simulation of the aerodynamics of horizontal axis wind turbines under yawed flow conditions. J Solar Energy Eng 127(4):464–474

UpWind Consortium (2011) UpWind—Design limits and solutions for very large wind turbines—A 20 MW turbine is feasible. UpWind Project, Sixth Framework Programme (019945 (SES6))

Verelst D, Madsen HA, Borg M et al (2015) Integrated simulation challenges with the DeepWind floating vertical axis wind turbine concept. In: Proceedings of the 12th deep sea offshore wind R&D conference, EERA DeepWind'2015, Trondheim Norway, 4–6 Feb 2015

Zambrano T, MacCready T, Kiceniuk TJ et al (2006) Dynamic modeling of deepwater offshore wind turbine structures in Gulf of Mexico storm conditions. In: Proceedings of the 25th international conference on offshore mechanics and artic engineering (OMAE). Hamburg, Germany, 4–9 June 2006

References (3)

API RP 2F (1997) Specification for mooring chain. American Petroleum Institute (API), Washington D.C.

API RP 2FPI (1993) Design, analysis, and maintenance of moorings for floating production systems. American Petroleum Institute (API), Washington D.C.

API RP 2P (1984) Analysis of spread mooring systems for floating drilling units. American Petroleum Institute (API), Washington D.C.

API RP 2SK (2005) Design and analysis of stationkeeping systems for floating structures, 3rd edn. American Petroleum Institute (API), Washington D.C.

API RP 2SM (2014) Design, manufacture, installation, and maintenance of synthetic fiber ropes for offshore mooring, 2nd edn. American Petroleum Institute (API), Washington D.C.

Ayers RR, Renzi DT (2010) Evaluate new materials for deepwater synthetic mooring systems. Technical Report. U.S. Department of Interior, Mineral Management Service, Contract No. M09PC00005

Fitzgerald J, Bergdahl L (2008) Including moorings in the assessment of a generic offshore wave energy converter: a frequency domain approach. Mar Struct 21(1):23–46

Flory J (1999) Taut leg mooring polyester rope test program. DeepStar–CTR4400 Technical Report

Flory J, Banfield S (2006) Durability of polyester ropes used as deepwater mooring lines. In: Proceedings of the IEEE OCEANS 2006 conference, pp 1–5, Boston, MA, 18–21 Sept 2006

Huntley MB (2006) Polyester mooring rope: length determination and static modulus. In: Proceedings of the IEEE OCEANS 2006 conference, pp 1–6, Boston, MA, 18–21 Sept 2006

ISO 19901-7 (2013) Petroleum and natural gas industries–specific requirements for offshore structures–Part 7: Station keeping systems for floating offshore structures and mobile offshore units, 2nd edn. International Standards Organization (ISO), Geneva, Switzerland

Kwan C (2015) Mooring design standards—the past, present, and future. In: Proceedings of the 20th SNAME offshore symposium, Houston, TX, USA, 17 Feb 2015

Kwan C, Bruen F (1991) Mooring line dynamics: comparison of time domain frequency domain and quasi-static analyses. In: Proceedings of the offshore technology conference, Houston, TX, USA, 6–9 May 1991

Lechat C, Bunsell A, Davies P, Burgoyne C (2008) Characterisation of long term behaviour of polyester fibres and fibre assemblies for offshore mooring lines. In: Proceedings of the oilfield eng. with polymers, Cavendish Conference Centre, London, UK, 7–8 Oct 2008

Majhi S, D'Souza R (2013) Application of lessons learned from field experience to design, installation and maintenance of FPS moorings. In: Proceedings of the offshore technology conference, Houston, TX, 6–9 May 2013

Nadarajah S, Kotz S (2006) The exponentiated type distributions. Acta Applicandae Math 92 (2):97–111

Ruinen R, Gijs D (2001) Anchor selection and installation for shallow and deepwater mooring systems. In: Proceedings of the international offshore and polar engineering conference (ISOPE), pp 17–22, Stavanger, Norway, 17–22 June 2001

Tahar A, Kim M (2008) Coupled–dynamic analysis of floating structures with polyester mooring lines. Ocean Eng 35(17):1676–1685

Weller S, Davies P, Thies P et al (2012) Durability of synthetic mooring lines for ocean energy devices. In: Proceedings of the 4th international conference on ocean energy (ICOE), Dublin, Ireland, 17–19 Oct 2012

Wibner C, Versavel T, Masetti I (2003) Specifying and testing polyester mooring rope for the barracuda and Caratinga FPSO deepwater mooring systems. In: Proceedings of the offshore technology conference, Houston, TX, 5–8 May 2003

Modelling of Floating Offshore Wind Technologies

Denis Matha, Joao Cruz, Marco Masciola, Erin E. Bachynski, Mairéad Atcheson, Andrew J. Goupee, Sébastien M.H. Gueydon and Amy N. Robertson

The modelling of FOWT forms a critical stage of the design process, as it allows a fully coupled dynamic assessment of the response of the concept while accounting for blade-rotor dynamics, support structure motions and mooring dynamics. For both new and for existing concepts, modelling offers the potential to test, in controlled environments, a series of assumptions and scenarios at a relatively minor cost. Two fundamental modelling approaches can be followed: numerical and

D. Matha
Ramboll Wind, Hamburg, Germany
e-mail: denis.matha@ramboll.com

J. Cruz (✉) · M. Atcheson
Cruz Atcheson Consulting Engineers Lda, Lisbon, Portugal
e-mail: Joao.cruz@cruzatcheson.com

M. Atcheson
e-mail: Mairead.atcheson@cruzatcheson.com

M. Masciola
ABS Consulting, Houston, TX, USA
e-mail: mmasciola@eagle.org

E.E. Bachynski
Marine Technology Centre, MARINTEK, NO-7491, Trondheim, Norway
e-mail: erin.bachynski@ntnu.no

A.J. Goupee
University of Maine, Orono, ME, USA
e-mail: agoupe91@maine.edu

S.M.H. Gueydon
Maritime Research Institute of the Netherlands, Wageningen, The Netherlands
e-mail: S.Gueydon@marin.nl

A.N. Robertson
National Renewable Energy Laboratory, Golden, CO, USA
e-mail: Amy.Robertson@nrel.gov

experimental. The former carries the potential to allow a wider range of design iterations and design situations to be tested at a low cost and under a potentially shorter timeframe, while the latter may prove useful for specific physical tests outside the remit of existing numerical tools and/or to validate early numerical estimates. In this chapter the main physical aspects to be modelled are described in detail: firstly, the key considerations regarding aerodynamics (Sect. 1) and hydro-dynamics (Sect. 2) are described, in an effort to overview the main options that a design engineer may wish follow when considering the modelling of FOWT. In addition, specific aspects related to the assessment of the mooring dynamics and the structural design of FOWTs are also detailed in Sects. 3 and 4, respectively. Finally, the chapter is concluded with a brief overview of the available numerical tools that specifically address FOWT modelling (Sect. 5), and with a detailed case study related to the experimental testing of a FOWT (Sect. 6).

1 Aerodynamics

Denis Matha

1.1 Introduction

The primary purpose of a wind turbine on a floating support structure is to extract kinetic energy from the incoming wind by the rotor to generate electricity, as it is the case for bottom-fixed and onshore wind turbines. While the aerodynamic principles and mechanisms are the same, the additional degrees of freedom of a FOWT may influence the aerodynamics of the rotor and of the airfoil sections along the blade. This section will provide an introduction into wind turbine aerodynamics and common methodologies to calculate the aerodynamic forces on rotor blades in general and will be concluded by a summary of the particular challenges in aerodynamics of FOWTs.

1.2 Wind Turbine Rotor Aerodynamics Basics

The energy P_{max} that can be extracted by a wind turbine rotor is given by the expression:

$$P_{max} = \frac{1}{2} C_p \rho A U_\infty^3 \tag{1}$$

where ρ is the air density, A the rotor swept area, U_∞ the wind speed perpendicular to the rotor plane far in front of the rotor and C_p the power coefficient, which is

limited by the Betz limit $C_{P_{max}} = \frac{16}{27} \approx 0.593$. The Betz limit can be derived by application of classical momentum theory applied on a 1D control volume as depicted in Fig. 1:

$$\frac{\partial}{\partial t} \iiint_{CV} \rho \vec{v} dV + \iint_{S} \rho \vec{v}(\vec{v} \cdot \vec{n}) dS = \vec{F} \tag{2}$$

Assuming stationary flow $\frac{\partial}{\partial t} = 0$ and considering that net external pressure force on the control volume is zero because the control volume is surrounded by ambient pressure p_∞, the equation simplifies to:

$$-\rho U_\infty^2 A_1 + \rho U_w^2 A_2 = -T \tag{3}$$

By application of the Bernoulli equation in front of and after the pressure drop Δp at the rotor disc (Eq. 4) and utilizing the law of conservation of mass (Eq. 5), one can derive the thrust (Eq. 6) and power output (Eq. 7) (from the integral energy balance of the control volume) of the turbine as:

$$\Delta p = \frac{1}{2} \rho \left(U_\infty^2 - U_w^2 \right) \tag{4}$$

$$\dot{m} = \rho UA = \rho U_\infty A_1 = \rho U_w A_2 \tag{5}$$

$$T = \rho UA (U_\infty - U_w) \tag{6}$$

$$P = T \cdot U = \frac{1}{2} \rho UA \left(U_\infty^2 - U_w^2 \right) \tag{7}$$

In wind energy the axial induction factor a is introduced to describe the velocity deficit caused by the flow deceleration in the rotor plane:

$$u_i = a U_\infty \tag{8}$$
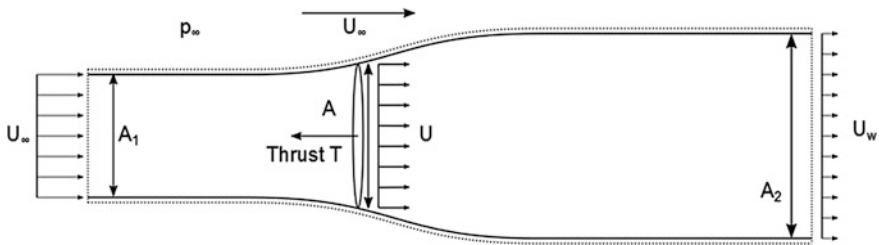
Fig. 1 Control volume of an idealised wind turbine used in 1D-momentum theory analysis, assuming momentum balance and stationary flow

with u_i denominated as the induced velocity. Using the induction factor relationships from Eqs. (9) and (10) below, Eq. (7) can be rewritten as Eq. (11):

$$U = (1 - a)U_\infty \tag{9}$$

$$U_w = (1 - 2a)U_\infty \tag{10}$$

$$P = T \cdot U = 2\rho U_\infty^3 A \cdot a(1 - a)^2 \tag{11}$$

It is important to note in particular with regard to floating wind turbines as described in the next section, that Eq. (11) assumes momentum balance, which is only valid up to an induction factor, an induced velocity of

$$a \leq 0.5, \quad \text{respectively} \quad U_\infty \geq 2|u_i| \tag{12}$$

If $a > 0.5$, then Eq. (10) predicts $U_w < 0$ which would mean an unphysical flow reversal in the wake. In reality, additional air is sucked into the wake from the surrounding flow by developing eddies; i.e. momentum is transported from the outer flow into the control volume rendering the momentum balance assumption invalid.

When the air passes through the rotor and part of its kinetic energy is transformed into the electricity-producing shaft torque, the basic laws of Newtonian Mechanics imply that an opposite and equal reaction torque must be imposed on the wake. This wake rotation velocity component V_Ω at a radial rotor distance r, which is directed tangential to the rotor rotation, is expressed in terms of a tangential induction factor a':

$$V_\Omega = 2r\Omega a' \tag{13}$$

The torque ΔQ on a rotor annulus (annular ring) at radius r and width Δr generated by the change of the angular momentum in the wake can be expressed as:

$$\Delta Q = \rho 2\pi r^2 U_\infty(1 - a)V_\Omega \Delta r \tag{14}$$

Equating the resulting rotor shaft power (Eq. 14) with the power derived from the axial momentum analysis (Eq. 11) yields a relationship between axial and tangential induction factor with the so-called dimensionless local tip-speed ratio TSR_{local} (for completeness, the often used global tip-speed ratio TSR, computed for the outer rotor radius R is also given here):

$$\Delta P = \Delta Q \cdot \Omega \tag{15}$$

$$TSR_{local} = \frac{r\Omega}{U_\infty}, \quad TSR = \frac{R\Omega}{U_\infty} \tag{16}$$

$$a(1 - a) = TSR^2_{local}a' \tag{17}$$

1.3 Blade Element Momentum Method

The most widely used technique to compute the aerodynamic power of a wind turbine rotor is the blade element momentum method, commonly abbreviated by BEM. It combines the previously outlined momentum analysis in axial and tangential direction with the local blade element theory, which relates the aerodynamic lift $\vec{L}$ and drag $\vec{D}$ forces acting on a blade element of width Δr and chord length c to the incoming flow velocity $\vec{V}$:

$$\Delta\vec{L} = \frac{1}{2}C_l\rho\vec{V}^2c\Delta r, \quad \vec{L} \parallel \vec{V} \tag{18}$$

$$\Delta\vec{D} = \frac{1}{2}C_d\rho\vec{V}^2c\Delta r, \quad \vec{D}\perp\vec{V} \tag{19}$$

The lift coefficient C_l and drag coefficient C_d are functions of the angle of attack α and the Reynolds number Re and are also sensitive to surface roughness, i.e. pollution and deterioration of the blade surface e.g. by salt water. They are typically known from wind tunnel measurements or computations for 2D airfoils.

$$C_l, C_d = f(\alpha, Re) \tag{20}$$

Figure 2 depicts the geometric relationships at a blade element, with the angle of attack $\alpha = \varphi - \beta$, blade chord angle β (typically the of sum built-in blade twist and current pitch angle) and the inflow angle φ.

Fig. 2 Blade element inflow velocities from wind and rotor rotation, associated angles and lift and drag forces
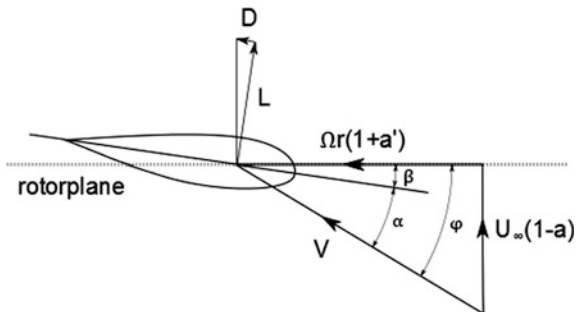
From Fig. 1 it follows, that for a blade element at radius r, the inflow angle can be computed as:

$$\tan \varphi = \frac{U_\infty(1 - a)}{\Omega r(1 + a')} \tag{21}$$

Dividing the rotor into multiple annuli of width Δr, i.e. discretising the blade into multiple elements, the basic BEM algorithm can be derived by balancing the following thrust and torque equations on each annulus derived from the blade element method (BE) and from the momentum analysis (MA):

$$\Delta T_{MA} = 4\pi r \rho U_\infty^2 a(1 - a)\Delta r \tag{22}$$

$$\Delta Q_{MA} = 4\pi r^3 \rho U_\infty \Omega a'(1 - a)\Delta r \tag{23}$$

$$\Delta T_{BE} = n(L(C_l) \cos \varphi + D(C_d) \sin \varphi)\Delta r \tag{24}$$

$$\Delta Q_{BE} = n(L(C_l) \sin \varphi - D(C_d) \cos \varphi)r\Delta r \tag{25}$$

With these equations, the classical BEM algorithm can be established. In Table 1, a scheme for a typical BEM algorithm is described (steps 1–6 without the steps marked with superscript *). In addition to the previously described basic relations, most modern BEM implementations account for aerodynamic effects that are not captured with the outlined underlying basic theory by applying engineering correction models. These empirical or semi-empirical models are also included in Table 1. Further details on these correction models, as well as the BEM method in general is found e.g. in Sant (2007) and Moriarty and Hansen (2005).

1.4 Potential Flow and CFD Methods

So far the focus was on BEM theory, because it is by far the most widely used aerodynamic method to compute aerodynamic loads on wind turbine rotors. Nevertheless, there are certain limitation in BEM theory that can only be addressed by application of engineering correction models, as presented in Table 1. With increasing computational power available, more computationally expensive aerodynamic models are developed and applied to overcome BEM limitations. The most important two methods are:

- Potential flow, and
- Computational fluid dynamics (CFD) based methods.

Potential flow methods are based on the assumptions of incompressible, irrotational, inviscid flow. The most fundamental equations for potential flow methods

Table 1 BEM algorithm with correction models (note that the position of the correction models in the stepwise algorithm may be different than shown here depending on the specific software implementation and correction model used)

1	Initialisation of the induction factors a and a'
2	Computation of the inflow angle φ with Eq. (21) and the local angle of attack $\alpha = \varphi - \beta$
2.1*	Account for tip and hub loss by calculation of the Prandtl tip and hub loss factors F_{tip} and F_{Hub} (to be used in step 4 when calculating a, a')
3	Look-up $C_l, C_d = f(\alpha)$
3.1*	Account for Stall-Delay and 3D rotational effects by adjusting the C_l, C_d tables with empirical models, such as models developed
3.2*	Account for local unsteady 2D dynamic stall effects by dynamically modifying the lift and drag coefficients from the airfoil tables: $C_l, C_d = f(\alpha, \dot{\alpha})$
4	Compute a, a' from the blade element momentum balances for torque and thrust $\Delta T_{MA} = \Delta T_{BE}$ and $\Delta Q_{MA} = \Delta Q_{BE}$
4.1*	Correct for skewed wake effect in case the rotorplane is not perpendicular to the incoming flow due to yaw and tilt
4.2*	Correct for turbulent wake state (Glauert correction), usually applied when $a > 0.4$
4.3*	Account for the dynamic inflow effect by introduction of unsteady terms into the thrust force equations $\Delta T_{MA,dynamic} = \Delta T_{MA} + f(\dot{a}, U_\infty)$
5	If a, a' have changed beyond a defined tolerance, repeat steps 2–4 with the obtained induction factors
6	After the BEM iteration has finished, compute the local blade forces with the final values of a, a'

are the Laplace equation (Eq. 26) for the velocity potential φ; the Biot Savart law (Eq. 27) establishing a relation for the induced velocity from a vortex filament dl with circulation strength Γ to an arbitrary point at distance r; the Kutta-Joukowski theorem (Eq. 28), linking the lift force from blade element theory to the circulation strength and Kelvin's circulation theorem (Eq. 29) stating that the circulation in the domain must remain constant in time. In addition, the Helmholtz theorem needs to be fulfilled which demands that a bound vortex filament cannot start or end abruptly in the domain, resulting in the typical horseshoe shaped lattice structure.

$$\nabla^2 \varphi = 0 \tag{26}$$

$$dU = -\frac{\Gamma}{4\pi} \frac{r \times dl}{|r|^3} \tag{27}$$

$$\Delta \vec{L}(r) = \frac{1}{2} C_l \rho \vec{V}^2 c \Delta r = \rho V \Gamma(r) \tag{28}$$

$$\frac{D\Gamma}{DT} = 0 \tag{29}$$

In the most widely applied potential flow method for wind turbine applications based on the lifting line free vortex wake theory, the rotor blade is discretised into several segments, each with its individual bound circulation strength. From these nodes at the blade, over time vortex filaments are evolving into a vortex lattice representing the complex wake structure, with trailing filaments (directed in the local velocity direction) related to the spanwise spatial bound circulation gradients $\partial\Gamma/\partial x$ and shed filaments (parallel to the bound filaments) related to temporal variation of bound circulation strength $\partial\Gamma/\partial t$. The Biot-Savart law is used to compute the velocity induced by the wake on each node, while the Kutta-Joukowski theorem is applied to compute the bound vorticity strength along the blade span depending on the current inflow velocity and direction at each blade segment. In Leishman (2006), Sebastian (2012) detailed information on the approach can be found. The advantage of this method compared to BEM is that the rotor wake is physically modeled in space and time and phenomena like tip roll-up, the dynamic inflow effect and rotor motions into and out of the wake as potentially present for FOWTs are represented without additional engineering correction models.

Computational fluid dynamics (CFD) models are based on the Navier Stokes Equations (NSE) for which no analytical solution has been found yet and which therefore need to be solved numerically (for brevity the NSE are not presented here, see e.g. Anderson (2007) for further details). The most widely used approximation of the NSE for wind turbine rotor aerodynamic load calculations is based on the Reynolds averaged NSE (RANS) for modelling of turbulent flows. By decomposing the NSE into time-averaged and fluctuating quantities, a nonlinear Reynolds stress term is generated that requires additional turbulence models to close the RANS equation for solving. The RANS equations are typically discretised by either finite differences, finite volumes or finite elements methods, with the computational domain spatially discretised by structured or unstructured meshes. Another approach that is also applied for wind turbine rotors is to use detached eddy simulations, where the regions near to the boundary layers at the turbine and ground surface with small turbulent length scales are resolved using RANS while the regions in the flowfield with larger turbulent length scales are solved with large eddy simulation (LES). LES is a method to directly resolve the turbulence at large scales while low-pass filtering the NSE to eliminate small scales of the solution and thus reduce computational effort. The advantage of CFD is that the entire flowfield with the turbulent wind inflow, the boundary layer at the blades and the turbine wake is physically resolved. Nevertheless, CFD is less robust than BEM and potential flow methods because the quality of the solution is significantly depending on the selection of the applied turbulence models (common is e.g. the k-ω-SST model), the discretisation of the blade boundary layer (y+ values below 1 are recommended) and resolution of the rotor wake (particular the tip vortex wake should be discretised with an appropriately fine mesh). Currently CFD is primarily applied for detailed rotor blade design and for isolated single load case simulation

of limited time (Bekiropoulos et al. 2012; Quallen et al. 2013) and is not used within coupled aero-servo-hydro-elastic load simulation codes for typical load simulations due to its high computational cost. Nevertheless, some studies on FOWTs have been performed using CFD that provide some indication to the shortcomings of the simpler methods such as BEM and potential flow approaches (Matha et al. 2013).

1.5 Aerodynamic Considerations for Floating Wind Turbines

The primary differences in terms of aerodynamics of FOWTs with its fixed counterparts are caused by the floating platform motions. Before elaborating on possible special aerodynamic effects for FOWTs, it must be noted that there is a wide variety of different floating platform concepts and some types of substructure concepts proposed exhibit only very small motions, with some TLP concepts even designed in such a manner that the motion is comparable to fixed-bottom offshore structures. Therefore, the following aerodynamic considerations may not be valid for all platform concepts but only to concepts such as spars or semi-submersibles that are usually designed to allow motions in extreme cases with amplitudes in the range of 5°–10° in platform pitch and surge excursions in the range of 20–40 m. The trend to large offshore wind turbines up to 10 MW also leads to increased hub heights and rotor diameters. The demand to lower the cost of energy requires economic floating support structure designs, which may lead to lighter, smaller platform concepts with potentially more dynamic motion. Additionally, modern large blades are of increased flexibility allowing for larger tip deflections. Advanced turbine controls can reduce these increased dynamics by a certain degree, but overall these developments lead to increased velocities and accelerations at the rotor blade sections during floating platform operation compared to fixed-bottom systems, especially for platform pitch and surge motions. Additionally, far offshore the environmental conditions are different in the atmospheric boundary layer, with higher average wind speeds, lower turbulence levels and the blades may exhibit increased roughness due to sea salt and erosion combined with less maintenance than onshore.

The additional motions of FOWTs affect the aerodynamics in terms of:

- additional mean rotor tilt angle,
- time-varying geometric angle of attack along the blade sections,
- possibility of occurrence of vortex ring state,
- time-varying rotor induction (dynamic inflow),
- other effects, such as increased occurrence of rotor misalignment (skewed inflow), and blade-vortex interactions.

Additional Mean Rotor Tilt Angle

On FOWTs the aerodynamic thrust force acting at the rotor is balanced by the restoring stiffness in pitch from the platform itself and the mooring system. Depending on the concept this can cause a significant additional mean platform tilt angle of several degrees. In some platform concepts there are countermeasures implemented such as dynamic ballasting to decrease the mean rotor tilt angle. Figure 3 shows the percentages of annual energy production (AEP) losses (computed according to the IEC 61400-12 (2005) Standard) for a 5 MW wind turbine for different static mean platform pitch angles, where until about $\theta_{pitch} \approx 4.5°$ the losses are below 1 %.

An approximation describing the effect of the additional tilt on the generated power output can be derived from Eq. (1), assuming that the inflow velocity is reduced by the platform pitch angle θ_{pitch} (note that here it is implied that $C_{p,onshore}$ already accounts for any built-in tilt angle of the rotor shaft of the onshore wind turbine):

$$P_{FOWT} = \frac{1}{2} C_{p,onshore} \rho A \left(U_\infty \cdot \cos \theta_{pitch} \right)^3 \tag{30}$$

Time Varying Geometric Angle of Attack

The 6-DOF platform translational and rotational motions introduce changes in the incoming velocity and its direction at the blade sections, leading to variations in the geometric angle of attack α_{geo}. These variations occur at the platform motion frequencies. A useful analysis to identify the relevance of this additional variation of
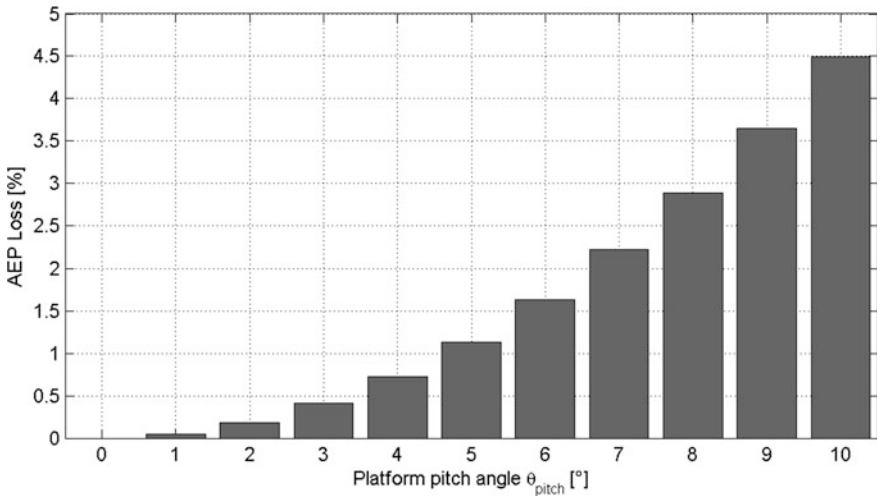
Fig. 3 AEP losses due to different mean platform pitch angles

FOWTs is reduced frequency approach. The reduced frequency k is a dimensionless parameter used in aerodynamics for an airfoil with chord length c to identify the unsteadiness of a flow due to a variation of the inflow velocity $\vec{V}$ at some frequency ω. According to Theodorsen's theory the flow can be categorised as unsteady if $k > 0.05$. For a FOWT rotor blade segment i, a first-order approximation for steady inflow (without accounting of the induction factors) and with the platform oscillating at frequency ω_{ptfm} yields:

$$k_i = \frac{\omega c}{2|\vec{V}|} = \frac{\omega_{ptfm} c_i}{2\sqrt{U_\infty^2 + (r_i \Omega)^2}} \qquad (31)$$

Applying the criteria of $k > 0.05$ to Eq. (31), the platform periods where flow unsteadiness is likely to occur can be identified in Fig. 4 along a rotor blade for the example of a 5 MW wind turbine. The grey areas indicate the regions where $k > 0.05$. That means that flow unsteadiness is more likely to occur in the inboard sections of a blade and at lower wind speeds. The hatched areas indicate the regions where typically natural periods of TLP and semi-submersible or spar designs are placed, with the area in-between from 3 to 30 s being the region where typical sea states have their peak spectral periods.

From Fig. 4, for a platform operating at rated wind speed in a sea state with a period of 15 s, one would expect additional unsteady aerodynamic flow effects due to platform motion at the wave period for the first 20 % of the inboard blade. The platform degree of freedom that is most relevant for the unsteady flow effects is primarily pitch, but yaw and surge may also be relevant. It shall be noted that the
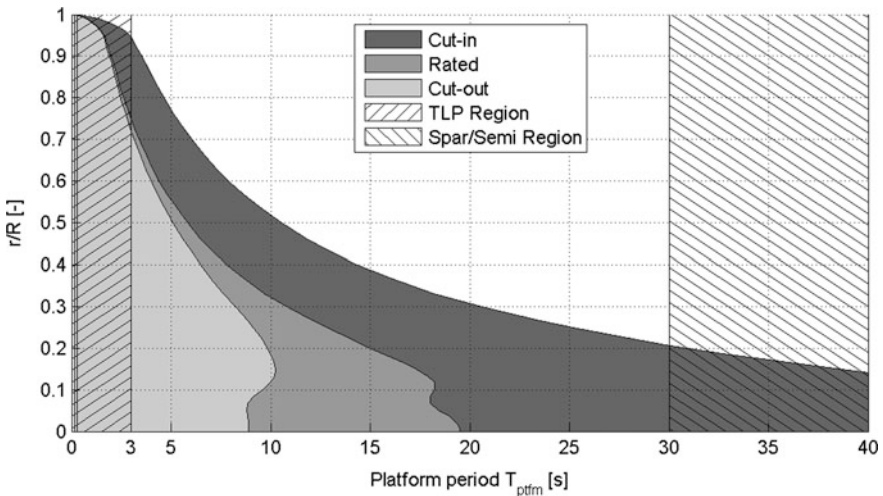
Fig. 4 Regions with increased possibility of flow unsteadiness ($k > 0.05$)

importance of these additional unsteady effects due to platform motion depend also on the amplitude of the oscillation and if and to what extent unsteadiness e.g. due to turbulence, effective shear is also present.

Turbulent Wake State

In the previous section it was introduced that the momentum balance assumption used in BEM breaks down for high induction factors. When accounting for the additional axial velocity U_{ptfm} from platform motion Eq. (12) becomes:

$$U_\infty - U_{ptfm} \geq 2|u_i| \tag{32}$$

During platform pitch motions at lower wind speeds that are in the same direction as the incoming wind inflow, i.e. downwind, Eq. (32) may become violated and the rotor may enter a transient condition called vortex ring state (VRS). The VRS leads to recirculation in the blade tip region and generate highly unsteady loads; eventually the rotor may act as a propeller. Analyses (Sebastian 2012) have shown that particularly at lower wind speeds the outer regions of the rotor blade are prone to operate in a condition that violates the momentum balance assumption and leads to differences in load predictions between BEM and potential flow or CFD codes.

Time-Varying Rotor Induction (Dynamic Inflow)

Dynamic inflow is an aerodynamic effect that occurs if the rotor loading condition (i.e. thrust) is quickly changed e.g. due to pitching of the blades, wind gusts and floating platform motion. The rotor does not reach the new equilibrium state corresponding to the new load condition immediately but gradually, resulting in an overshoot of instantaneous angle of attack which results in an overshoot of thrust loading. Engineering models for BEM exist to model that delay in load response, but they often assume momentum balance in their derivation and therefore may lead to deviations in load predictions for FOWTs.

Comparisons (Sebastian 2012; Matha et al. 2013) of potential flow and CFD results with BEM models indicate that BEM is unable to accurately model the lag response. Particularly for platform pitch motions. The engineering models appear to react at a higher rate leading to lower load amplitudes during larger platform pitch motions. The reason for that underestimation is likely the omission of circulatory contributions in the estimation of flow acceleration. De Vaal et al. (2012) investigated the applicability of BEM dynamic inflow models for FOWT surge motions with an actuator disc model. Differences in local induced velocity were identified leading to a wake geometry not resembling exactly the momentum theory idealised stream tube model, but according to de Vaal, the frequency of the surge motions are typically well above the dynamic inflow model time constants. This indicates that the platform pitch motion may be of greater importance regarding the dynamic inflow effect than surge motion, but de Vaal's actuator disc approach did not investigate local effects on the blades and was limited to one specific wind turbine rotor, which renders it difficult to come to a general conclusion regarding surge.

Other Effects

In addition to the previous effects, FOWTs are also more likely to operate in oblique inflow conditions with high angles of misalignment, rendering the BEM engineering models accounting for that effect more important.

Another effect that may occur due to platform motion is blade-vortex interaction (BVI) that is typically a problem for helicopters. BVI may occur if the airfoil is passing a vortex during a platform motion which then may lead to rapidly changing angle of attack at the airfoil due to the change of directions of induced velocity from the vortex during the blade passage. This effect can only be represented by potential flow or CFD models physically resolving the wake vortex structure.

1.6   Discussion

The FOWT platform motions lead to more dynamic inflow conditions and influence the aerodynamics of the rotor. The additional mean rotor tilt angle leads to losses in AEP, while unsteady aerodynamic effects such as the time-varying geometric angle of attack along the blade sections, the possibility of occurrence of vortex ring state conditions, time-varying rotor induction (dynamic inflow), and other effects, such as increased occurrence of rotor misalignment (skewed inflow), and blade-vortex interactions may lead to different loads and load fluctuations at the rotor. Currently primarily blade-element/momentum theory based methods are used in design codes capable of simulating FOWTs, which model the mentioned aerodynamic effects by usage of engineering correction models, since BEM inherently is not capable of representing these. The correction models are originally not designed for FOWT operating conditions and have known limitations for load predictions in certain load situations. Nevertheless, there is currently no clear picture in research on how significant these aerodynamic effects for FOWTs are and the available studies have primarily dealt with a limited number of platform concepts and rotor configurations rendering it difficult to draw general conclusions. Therefore, to quantify the uncertainty of load calculations for a given FOWT based on BEM aerodynamic models, it may be beneficial to investigate these additional aerodynamic effects and their relative importance with more advanced aerodynamic methods than BEM such as potential flow and CFD methods.

2   Hydrodynamics

Joao Cruz

As overviewed in Sect. 1 of Chapter "Overview of Floating Offshore Wind Technologies", multiple types of support structures can be envisaged for FOWT

concepts. Pending on key design variables such as size and shape of the support structure, different numerical formulations may be more or less adjusted for the estimation of the relevant hydrodynamic characteristics of a given design. This section provides an overview of the most commonly used hydrodynamic theories and the associated methodologies to estimate the hydrodynamic forces on the multiple types of support structures of FOWTs, and discusses their main assumptions and limitations. Where applicable, specific details related to the numerical implementation of the overlying theories are also discussed.

2.1 Numerical Modelling Challenges

To fulfil the potential of providing a credible option for the assessment of the dynamic response of a FOWT, numerical methods must offer a reliable compromise between accuracy and speed (computational time). The correct balance between these two variables if often a function of the design situations under consideration, but in rough terms it can be proposed that:

- Linear (or quasi-linear) methods that are capable of performing calculations for many load cases at an acceptable computational time are required for initial investigations. Depending on their accuracy, such methods may be more or less utilised at a detailed design stage.
- Nonlinear methods may be more suitable for calculations related to non-moderate design situations (e.g. wave-structure interaction under extreme events). These methods also provide a means to verify the accuracy and limitations of linear methods.

From a hydrodynamic perspective, one of the challenges that a numerical model faces is the ability to deal with arbitrary geometries. Generally speaking, this requires an approach that explicitly solves the radiation and diffraction problems, which may be particularly relevant for large support structures. A non-exhaustive list of challenges that a numerical model may need to address is provided below, and includes:

- The necessity to account for radiation and diffraction forces, namely when these are of the same order of magnitude as the inertial forces.
- The need to recognise and incorporate the frequency dependence of the above forces, in addition to memory effects.
- Estimation of the mean and slow drift varying forces.
- When relevant, consider shallow water effects, current and wave-current interactions in the calculations.

- Estimation of the mooring dynamics and their effect on the overall system response.
- When relevant, account for dissipative phenomena such as slamming loads and vortex induced vibrations (VIV).

Given the range and depth of these challenges, it is not surprising that related industries such as offshore oil and gas and the maritime shipping sector have helped to develop a series of numerical methods that address the above challenges and potentially more complex problems. The nature of the numerical methods developed to address these challenges may be explicit, i.e. they address the physics of the problem from a theoretical perspective and explicitly solve the equations that dominate the device response; or empirical, i.e. based on experimental evidence, a parametric set of equations is devised and used to estimate the relevant forces in similar conditions.

From the long list of explicit methods—linear strip, nonlinear strip, linear panel, nonlinear panel, finite-volume, etc.—linear panel methods are the most widely used. These have the potential to address, under certain limitations, the majority of the challenges outlined above, and are addressed in detail in Sect. 2.2. Practical examples of the application of linear panel methods are provided in Sect. 2.3. In some situations, empirical methods may yield similar results to explicit techniques. One of these methods, based on Morison's equation, has been extensively used in offshore engineering, and is thus overviewed in detail in Sect. 2.4. Finally, Sect. 2 is concluded in Sect. 2.5 with an overview of more advanced numerical methods that may prove useful when targeting design situations and environmental conditions that defy the limits of the assumptions behind the more simplistic numerical formulations.

2.2 Principles of Linear Wave-Structure Interaction

Linear (or Airy) wave theory remains a common starting point when considering solutions for a wave-structure interaction problem. The theory is documented in a vast number of references, where it is presented to several target audiences using different levels of mathematical complexity. Classical texts that provide a thorough review of the underlying theoretical principles associated with wave-structure interactions include Lé Mehauté (1976), Newman (1977) and Mei (1989; revised and extended edition in 2005 (Mei et al. 2005), among many others. For the interested reader, Le Méhauté (1976) provides a survey of wave theories and general hydrodynamic aspects, while waves and wave effects are discussed in Newman (1977), with particular emphasis on the definitions of damping and added mass, exciting force and moment, and also the response/motion of floating bodies.

Other texts specifically address the effects of wave forces on offshore structures, for both large and small bodies, and can be considered a good introduction to those

aiming to increase their knowledge in offshore structural engineering design. A subset of available texts in this area is reviewed next. In an application relevant to FOWT support structures, cylindrical structures have been the subject of extensive research. A complete review of the hydrodynamics around cylindrical structures is presented in Sumer and Fredsøe (1997), including a detailed description of the flow regimes and forces on cylinders in the presence of steady currents and oscillatory flows, along with an introduction to VIV. The treatment and description of the force coefficients is particularly useful when planning comparisons with experimental work. More generic approaches to offshore engineering, valuable when conducting design exercises, are presented in Faltinsen (1990), where emphasis is given to wave-induced motions and loads on floating structures. Among many other similar references, Sarpkaya and Isaacson (1981) distinguishes itself based on the level of detail and the chapter dedicated to scale model testing and experimental techniques. The authors also derive a guideline threshold for which that diffraction effects can be considered relevant: $kD > 1.3$, where k is the wavenumber and D is the characteristic dimension of the body. Knowing that the wavelength λ is equal to $2\pi/k$, this relation can be converted in $D/\lambda > 0.2$.

It is beyond the scope of this section to present a thorough review of linear wave theory. Such exercise can be found in one of the references mentioned in the previous paragraph. However, it is relevant to briefly summarise the equations that define the boundary value problem and the main simplifying assumptions that are implemented in (linear) potential flow solvers, which may be used to estimate the solutions of the wave-structure interaction problem. Firstly, it is important to acknowledge the underlying principles of linear wave theory that apply if (pure) linear solvers are to be used. In particular:

1. The free-surface and the body boundary conditions are linearised;
2. The fluid is incompressible and the flow is irrotational (potential flow): $\nabla^2\Phi = 0$, where Φ is the velocity potential;
3. Viscous effects like shear stresses and flow separation are not considered;
4. The bottom is assumed to be flat (and uniform);
5. Under these assumptions all variables can be expressed as a complex amplitude times e^{iwt} (regular waves, sinusoidal motions).

The starting point for estimating the solution of the wave-structure interaction problem is the definition of a Cartesian coordinate system (x, y, z) which is fixed with the body (body fixed coordinate system), in a way that the input geometry is defined with regard to this system (see Fig. 5). Under the above described assumptions, the velocity potential Φ at any point in the fluid domain can be given by

$$\Phi = \text{Re}\{\phi e^{i\omega t}\} \tag{33}$$

Fig. 5 Mathematical notation
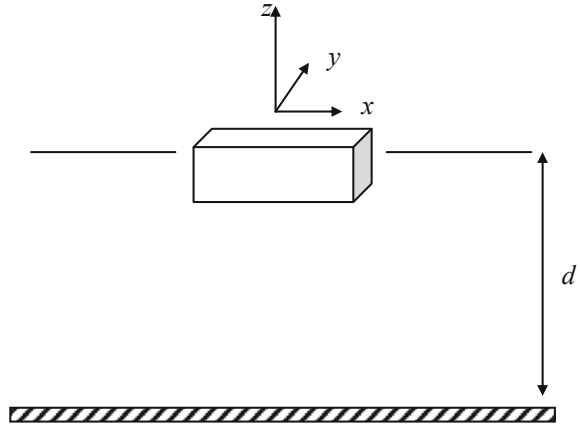
where ϕ is the complex velocity potential, Re denotes the real part, ω is the angular frequency of the incident wave and t is time. The first boundary condition can be expressed in the frequency domain by

$$\frac{\partial \phi}{\partial z} - K\phi = 0 \tag{34}$$

at $z = 0$ (free-surface) corresponding to the dynamic and kinematic boundary conditions. In Eq. (34) $K = \omega^2/g$ is the deep water wavenumber, with g being the modulus of the acceleration of gravity.

Under the previously mentioned assumptions the complex amplitude of the velocity potential of a 2D incident wave is given by (e.g. Mei 1989)

$$\phi_0 = \frac{igA}{\omega} \frac{\cosh k(z+d)}{\cosh kd} e^{-ikx \cos \beta - iky \sin \beta} \tag{35}$$

where d is the water depth, β is the angle between the direction of propagation of the incident wave and the positive x-axis, A is the incident wave amplitude and k is the local wavenumber, obtained from the dispersion relation:

$$\frac{\omega^2}{g} = k \tanh kd. \tag{36}$$

By assuming a linear decomposition of the problem, the velocity potential can be obtained by the sum of the radiation and the wave exciting components,

$$\phi = \phi_R + \phi_S, \tag{37}$$

where ϕ_R is the radiation potential and ϕ_S the exciting potential, respectively given by

$$\phi_R = \sum_{j=1}^{6} \xi_j \phi_j, \tag{38}$$

and

$$\phi_S = \phi_0 + \phi_D. \tag{39}$$

In Eq. (38) ξ_i are the complex amplitudes of oscillation in the six degrees-of-freedom (j) and ϕ_j is the corresponding unit-amplitude radiation potentials (those resulting from the body motion in the absence of an incident wave). These potentials must satisfy the impermeability condition over the body surface:

$$\frac{\partial \phi_j}{\partial n} = u_j = (\mathbf{u} \cdot \mathbf{n})_j \tag{40}$$

where $(n_1, n_2, n_3) = \mathbf{n}$ and $(n_4, n_5, n_6) = \mathbf{x} \times \mathbf{n}$, with $\mathbf{x} = (x, y, z)$. Note that $\mathbf{n}$ is the normal direction to the boundary and $\mathbf{u}$ is the velocity of the boundary surface. In this definition, $\mathbf{n}$ points out into the fluid domain.

In Eq. (39) the velocity potential ϕ_D reflects the perturbation induced by incident wave when the body is held fixed (diffraction). The exciting potential ϕ_S is obtained by the sum of ϕ_D with ϕ_0, the velocity potential of the incident wave. When the diffraction contribution (ϕ_D) is much smaller than the one related to the incident wave field (ϕ_0)—typically for $D/\lambda \leq 0.2$ as per Sarpkaya and Isaacson (1981)—ϕ_D can be neglected and the exciting contribution equals ϕ_0. This result is also known as the Froude-Krylov approximation. Note that the radiation and the diffraction problems reflect the most basic physical situations: a body forced to oscillate in otherwise undisturbed water and a fixed body subject to a regular wave field, respectively. With regard to ϕ_S it must also satisfy the impermeability condition which in this case (no body motion) is given by

$$\frac{\partial \phi_S}{\partial n} = 0. \tag{41}$$

Both ϕ_D and ϕ_j additionally obey a far-field radiation condition of the form (e.g. Linton 1991):

$$\lim_{kr \to \infty} r^{1/2} \left(\frac{\partial \phi_{D,j}}{\partial r} + ik\phi_{D,j} \right) = 0 \tag{42}$$

where r is the distance to the body. Finally, the impermeability boundary condition on the seabed (assuming a non-porous surface) must be satisfied by both ϕ_D and ϕ_j [similar condition to Eq. (41)].

To conclude this section, additional details regarding the most typical methods are given. This summary is based on the results firstly presented in Lamb (1932) and Havelock (1942), and in a review provided in Faltinsen (1990). Equations (33)–(42) define the boundary value problem, which can be solved using Green's function, $G(\mathbf{x}, \mathbf{x}')$. The integral equations related to the radiation and diffraction potential are:

$$2\pi\phi_j(\mathbf{x}) + \iint_{S_b} \phi_j(\mathbf{x}') \frac{\partial G(\mathbf{x}, \mathbf{x}')}{\partial n_{x'}} dS = \iint_{S_b} n_j G(\mathbf{x}, \mathbf{x}') dS \qquad (43)$$

and

$$2\pi\phi_S(\mathbf{x}) + \iint_{S_b} \phi_S(\mathbf{x}') \frac{\partial G(\mathbf{x}, \mathbf{x}')}{\partial n_{x'}} dS = 4\pi\phi_0(\mathbf{x}) \qquad (44)$$

respectively. Note that S_b is the body surface and that in linear methods S_b is calculated from a mean profile, while nonlinear methods may update S_b at every time step (see Sect. 2.5).

The Green function was originally derived by Havelock (1942), describing the source potential for infinite water depth (hence the common designation of wave source potential). The velocity potential at $\mathbf{x}$ due to a point source of strength -4π located at $\mathbf{x}'$ is given by

$$G(\mathbf{x}, \mathbf{x}') = \frac{1}{r} + \frac{1}{r'} + \frac{2\gamma}{\pi} \int_0^\infty \frac{\mathrm{e}^{k(z+z')}}{k - \gamma} J_0(kR) dk. \qquad (45)$$

where $J_0(kR)$ is the zero order Bessel function

$$\begin{cases} r^2 = (x - x')^2 + (y - y')^2 + (z - z')^2 \\ r'^2 = (x - x')^2 + (y - y')^2 + (z + z')^2 \\ R^2 = (x - x')^2 + (y - y')^2 \\ \gamma = \frac{\omega^2}{g} = k \tanh kh \end{cases}. \qquad (46)$$

and for finite water depth d, Wehausen and Laitone (1960) obtained

$$G(\mathbf{x}, \mathbf{x}') = \frac{1}{r} + \frac{1}{r''} + 2 \int_0^\infty \frac{(k + \gamma) \cosh k(z + d) \cosh k(z' + d)}{k \sinh kd - k \cosh kd} e^{-kd} J_0(kR) dk. \qquad (47)$$

with

$$r''^2 = (x - x')^2 + (y - y')^2 + (z + z' + 2d)^2. \tag{48}$$

To conclude, it is relevant to point out that two different representations can be considered to estimate the velocity potential, following Lamb (1932): the potential or the source formulation. In the former, Green's theorem is used, and the source strength is set equal to normal velocity, leaving the dipole moment, which is equal to the potential, unknown. Alternatively, the source formulation relies solely on source terms with unknown strength to describe the potential, discretising the surface with panels with constant source strength on each panel.

Numerical techniques have been developed to solve such integral equations in both formulations for arbitrary geometries. Typically, panel methods are used for such task (these are also referred to as Boundary Element Methods, or BEM). There are two main versions of the methods: a low-order method, where flat panels are used to discretise the geometry and the velocity potential, and a high-order method, which uses curved panels, allowing (in theory) a more accurate description of the problem. The high-order method has inherent advantages and disadvantages when compared with the low-order equivalent. For example, Lee et al. (1996) and Maniar (1995) showed the increase in computational efficiency, i.e., the method converges faster to the same solution when the number of panels is increased in both. The possibility of using different inputs for the geometry, like an explicit representation, can also contribute to an increase in accuracy. Another significant advantage relies on the continuity of the pressure and velocity on the body surface, which is mainly relevant for structural design. A potential disadvantage is linked to a lack of robustness of the method, for example when a field point is in the vicinity of a panel or near sharp corners, at times this may prevent the convergence of the numerical solution. It is beyond the scope of this section to present a detailed review of panels methods, and although not directly related to offshore engineering such review can be found in e.g. Hess (1990). In Sect. 2.3 practical details on the implementation of linear panel methods in the modelling of FOWT are presented alongside representative examples from previous relevant projects.

2.3 Linear Panel Methods: Key Features and Examples

Panel methods, also described as Boundary Element Methods (BEM) in a more general engineering context, can be defined as computational methods used to solve partial differential equations which can in turn be expressed as integral equations. BEM are often applicable to problems where the Green function can be calculated. An overview of panel methods in computational fluid dynamics can be found presented in Hess (1990). In this section, and based on the review originally presented in Cruz (2009), the work of Newman is used as a guideline for illustrating

the evolution and application of linear panel methods to offshore engineering problems that are relevant for the development of FOWTs.

A review of the principles that define the application of panel methods in marine hydrodynamics is given in Newman (1992). Newman stresses that many of the common problems, such as wave resistance, motions of ships and offshore platforms, and wave-structure interaction can be addressed following potential flow theory, where viscous effects are not taken into account. As per Sect. 2.2, the main objective is to solve the Laplace equation with multiple restrictions imposed by boundary conditions. The domain is unbounded (with the solution being specified at infinity), so a numerical approach that arranges sources and (optionally) normal dipoles along the body surface can be used to solve the hydrodynamic problem.

The pioneer work of Hess and Smith (1964), in which the source formulation was used for three-dimensional bodies of arbitrary shape, is also mentioned in Newman (1992). Hess and Smith (1964) were the first to derive a linear system of n algebraic equations by establishing boundary conditions at a collocation point on each of the n panels that were used to describe the fluid domain. The authors also produced the analytical expressions for the potential and velocity induced by a unit density source distribution on a flat quadrilateral panel, avoiding numerical integration that could lead to erroneous results when the calculation point is in the vicinity (or on) the panel. The basic differences between the two main calculation formulations—the source and the potential formulations—are also overviewed in Newman (1992). Although the computational effort required for both approaches is roughly equivalent, differences may include e.g. issues linked with thin bodies (where normal dipoles prove to be more stable than sources), and the lack of robustness of the potential formulation when using flat panels to discretise a curved surface, given that the velocity field induced by the dipoles changes quickly over distances similar to the panel dimensions.

With the evolution of computational power some of the issues and concerns associated with the computational burden related to panel methods have lost practical importance. However, such issues remain clear when developing a new code, particularly when studying complex problems. It is also clear that the pre-processing, linked with the calculation of the panel representation and relevant parameters, like areas and moments, and the solution of the linear system itself, are the steps which require the majority of effort. Newman and Lee (1992) performed a numerical sensitivity study on the influence that the discretisation has on the calculation of wave loads. The effects of the number of panels and their layout were investigated. Typically, increasing the number of panels used in the geometric and hydrodynamic representations will lead to an increase in accuracy. One important exercise that should never be neglected when developing a code is the numerical verification of the results, ensuring that the solution is not diverging, or converging to the wrong solution. Naturally validation, i.e., the comparison with experimental results, is also a key. The computational time required to solve the problem also increases with the number of panels, so an optimal ratio between accuracy and the number of panels can be derived. Also relevant is the panel layout, which can be

responsible for invalid solutions. A few basic qualitative guidelines were pointed out by Newman and Lee (1992), and can be summarised as follows:

- Near the free-surface, short wavelengths demand a proportionately fine discretisation;
- Local singularities, induced by (e.g.) sharp corners, tend to require fine local discretisation;
- Discontinuities on the characteristic dimension of the panels should be avoided; ideally a cosine spacing function should be used for the panel layout (where the width of the panels is proportional to the cosine of equally-spaced increments along a circular arc);
- Problems involving complex geometries can require a high number of panels even for simple calculations (e.g. volume).

At present there are numerous commercial and open-source BEM solvers that can be used to estimate key hydrodynamic parameters related to FOWT support structures. Some of these solvers allow extensions to the linear formulations described in this section (e.g. generalised modes, second-order approximations, etc.) which may be relevant for particular problems, such as the design of the mooring system (see Sect. 3).

A relevant example of the application of BEM solvers in FOWT modelling can be found in a recent European project aimed at framing the design limits of very large wind turbines (UpWind). In one of its deliverables (D4.3.6; see UpWind 2011), design methods related to offshore foundations and support structures were overviewed. In particular, comparisons between linear and second-order potential flow hydrodynamic models that characterise the support structure loading and motion response FOWTs were presented. Two FOWT support structures were considered:

- A spar-buoy, originally developed by Statoil ASA (see also Sect. 2 of Chapter "State-of-the-Art") and modified to accommodate a NREL-5 MW offshore wind turbine. This concept (OC3-Hywind) is described in detail in Jonkman (2009).
- A semi-submersible platform, geometrically similar to the WindFloat platform (Aubault et al. 2009).

Figure 6 illustrates both concepts, whereas numerical discretisations used in the calculations are presented in Fig. 7. Some of the key design features of each support structure are clear in both figures: for example, the heave plates at the bottom of each column of the semi-submersible platform, designed to provide high added-mass and viscous damping to decrease the motions in this mode of motion, were included in the analysis.

First and second-order calculations were performed using a commercial BEM solver (WAMIT V6.1s). The output variables compared included:

- The first and second-order excitation forces.
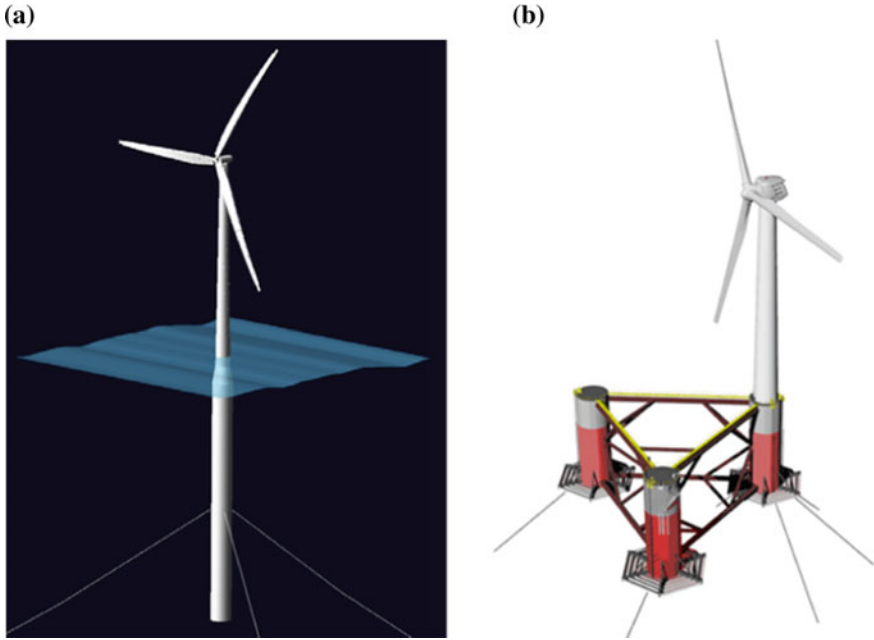- The first and second-order Response Amplitude Operators (RAOs) for unconstrained motions.

Fig. 6 Example FOWT support structures: **a** OC3-Hywind, **b** WindFloat (UpWind 2011)
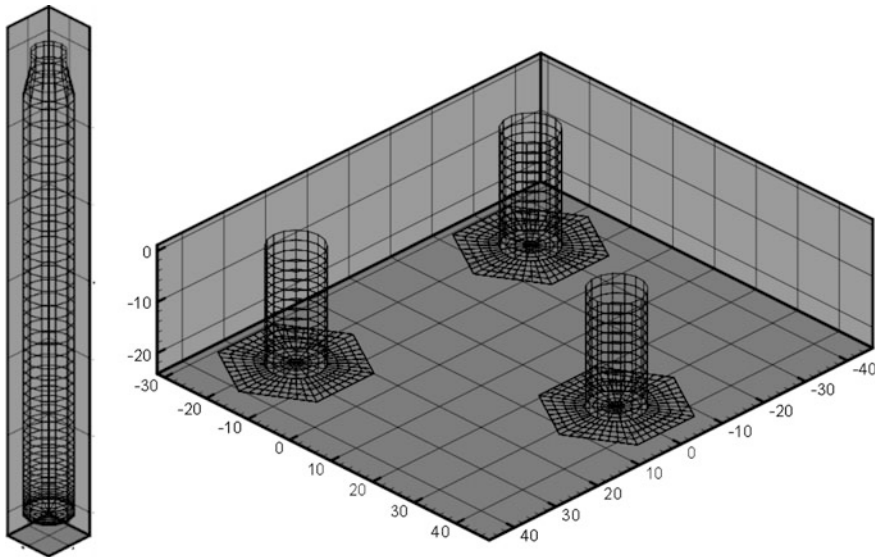

Fig. 7 Numerical discretisations of the example FOWT support structures: OC3-Hywind (*left*) WindFloat (*right*) (UpWind 2011)

The first and second-order responses to three distinct regular waves and three unidirectional Pierson-Moskowitz spectra were derived and compared. These incident waves are defined in Table 2.

Comparisons between the first and second-order unrestrained motions associated with the OC3-Hywind for regular waves defined in Table 2 are presented in Fig. 8 for the surge mode. As it can be observed, for the three incident waves studied, the unrestrained motions are small and the second-order effects are in turn very small when compared with the first-order effects.

For irregular waves, comparisons between first and second-order excitation forces in surge, heave and pitch mode for the OC3-Hywind associated one of the Pierson Moskowitz (PM) spectrum defined in Table 2 (H_s = 5.0 m) are presented in Fig. 9. It is clear in Fig. 9 that the second-order components of the exciting force are of the same order of magnitude as the first-order components for the three modes of motion. In addition, the phasing of the second-order components contributes to an overall increase in the peak values of the exciting force. In Fig. 10 the unrestrained motions of the OC3-Hywind concept for the same input spectrum are presented, where it is clear that second-order effects are mostly relevant in heave, where the second-order contribution exceeds the first-order equivalent.

In UpWind (2011) similar first and second-order comparisons were derived for the semi-submersible platform. For regular waves, first-order components were found to be dominant, in particular for the longer waves (7 and 9 s). However, for irregular waves this pattern can be reversed. In Fig. 11, the excitation force associated with the Pierson-Moskowitz spectrum with H_s = 2.5 m (see Table 2) is presented for all degrees-of-freedom. The second-order excitation forces are dominant relative to the first-order excitation forces for all modes except for heave, due to the dominance of the sum-frequency force quadratic transfer functions (QTFs). However, it should be noted that the associated motions are small in all degrees-of-freedom except in heave.

The output variables illustrated in this section can be considered standard outputs from BEM solvers. Additional relevant outputs include the added-mass and radiation damping coefficients. Combined with the excitation force, these offer a description of the two basic hydrodynamic problems (diffraction and radiation), and thus the possibility of using BEM outputs to create a more complex global model of hydrodynamic loading affecting the support structure of a FOWT (see also Sect. 2.5).

Table 2 Regular and waves and Pierson-Moskowitz spectra used for the comparisons between first and second-order hydrodynamic quantities (UpWind 2011)

Regular waves	
H = 1.0 m	T = 5.0 s
H = 2.0 m	T = 7.0 s
H = 4.0 m	T = 9.0 s
Pierson Moskowitz spectra	
H_s = 0.5 m	T_p = 3.5 s
H_s = 2.5 m	T_p = 7.9 s
H_s = 5.0 m	T_p = 11.2 s

Fig. 8 Comparisons between
first and second-order
unrestrained surge response to
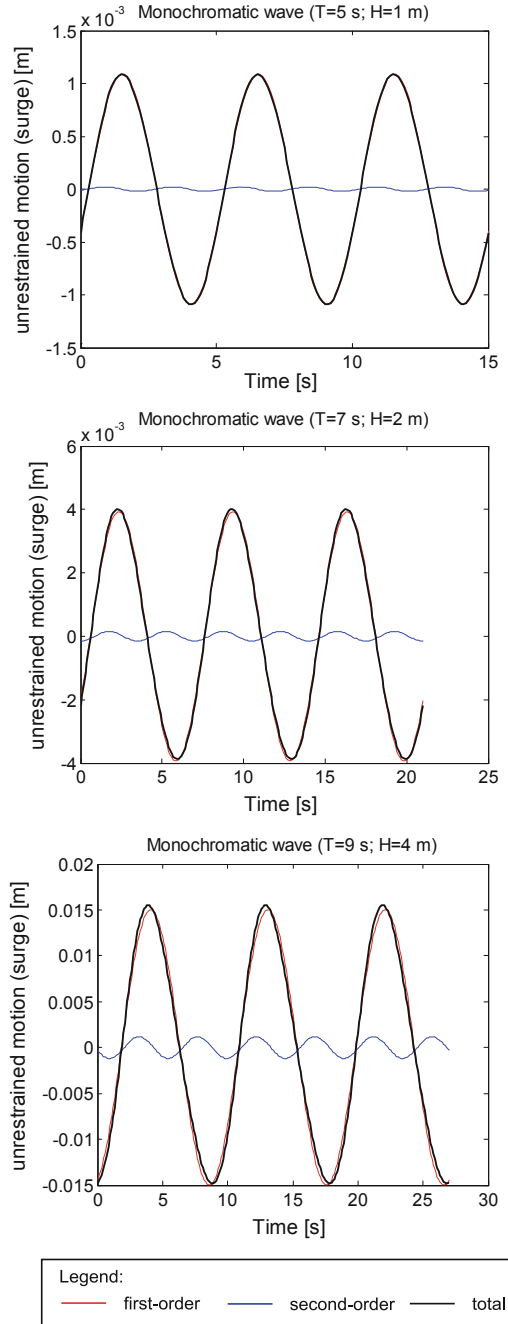regular waves: OC3-Hywind
(UpWind 2011)

Fig. 9 Comparisons between first and second-order unrestrained surge response to irregular waves (PM, H_s = 5 m): OC3-Hywind (UpWind 2011)
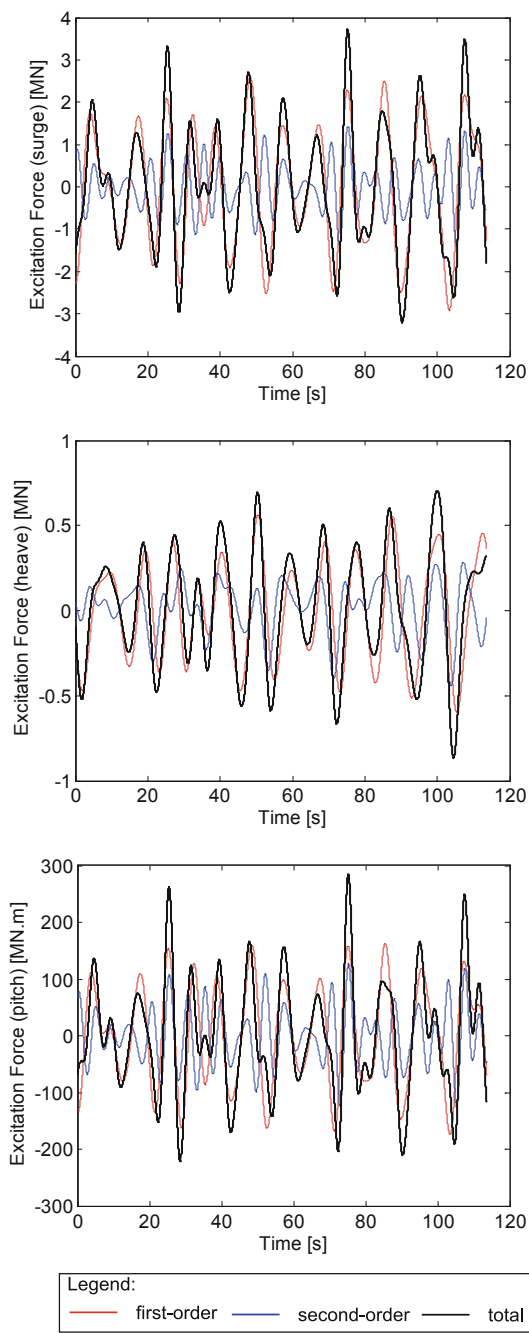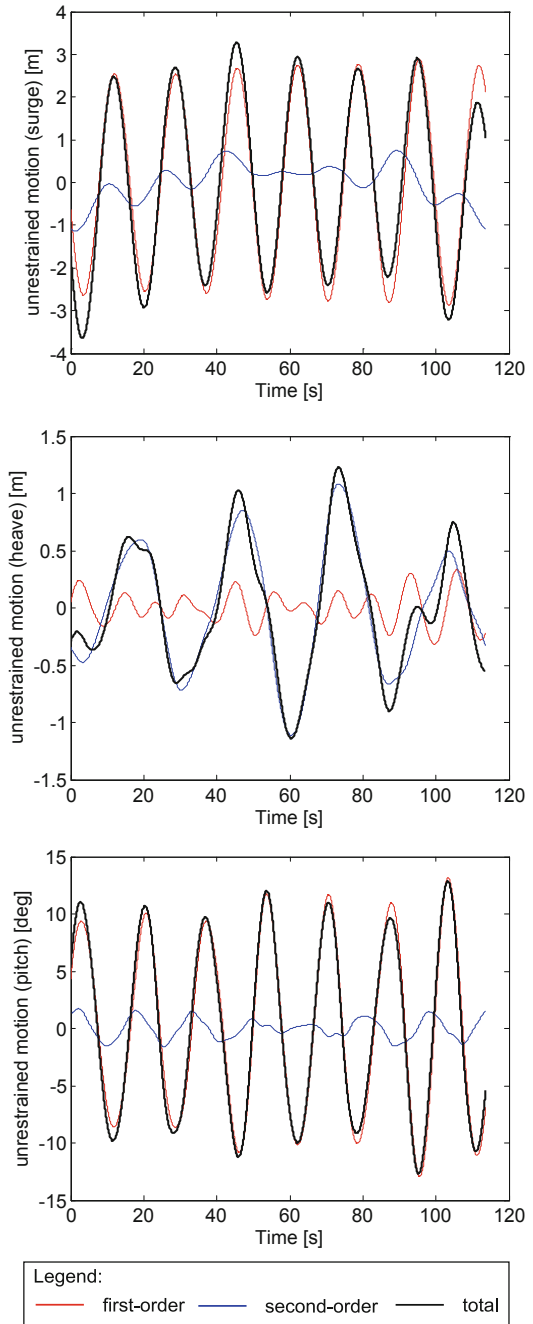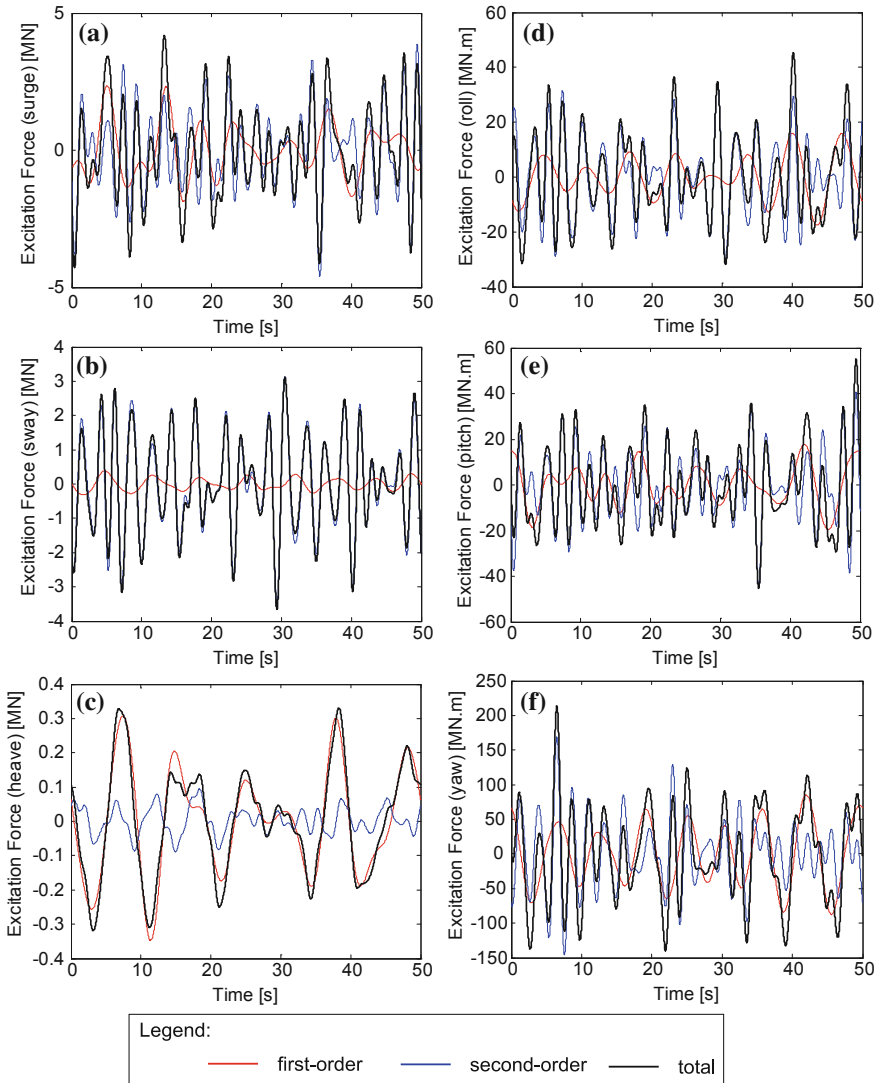
Fig. 11 Comparisons between first and second-order response to irregular waves (PM, H_s = 2.5 m): Semi-submersible platform (UpWind 2011). Excitation forces in **a** Surge; **b** Sway; **c** Heave; **d** Roll; **e** Pitch; **f** Yaw

2.4 Morison's Equation

As discussed in Sect. 2.2, the nature of the numerical methods developed to address the key challenges associated with estimating the hydrodynamic loading on a FOWT may be explicit, i.e. they may address the physics of the problem from a

theoretical perspective and explicit solve the equations that dominate the device response; or empirical, i.e. based on experimental evidence, a parametric set of equations is devised and used to estimate the relevant forces in similar conditions. Having reviewed in Sect. 2.3 the most widely used explicit method (linear panel methods), the most commonly used empirical method, Morison's equation, is overview in this section.

Morison's equation was first conceptualised in Morison et al. (1950), and has been extensively used in offshore engineering. It was originally derived to estimate the loading exerted by surface waves on circular cylinders/piles, although it has since been applied in a wider context including in oscillatory flows and for alternative geometries. Unlike panel methods, it aims to address viscous effects in addition to inertial loads via an empirically derived equation.

In short, Morison's equation can be summarised as:

$$F(t) = \rho C_m \frac{\pi}{4} D^2 \dot{u}(t) + \frac{1}{2} \rho C_D D u(t) |u(t)|. \tag{49}$$

where $F(t)$ is the total wave induced force, C_m is the inertial coefficient (note that the added mass coefficient C_A is given by $1 - C_M$); D is the cylinder diameter; $\dot{u}$ is the flow acceleration; C_D is the drag coefficient and u is the flow velocity.

When Morison's equation is used to calculate the hydrodynamic forces acting on a support structure, the variation of the hydrodynamic coefficients (C_A and C_D), as a function of the Reynolds number, Keulegen-Carpenter number and the surface roughness, need to be considered. Detailed guidance is provided in e.g. Sarpkaya and Isaacson (1981).

Despite its empirical nature and although it was originally formulated for slender, non-diffracting structures, it has been extensively applied to assess the loads acting on multiple types of offshore structures. For floating wind turbine applications, a recent example can be found in Sethuraman and Venugopal (2013), where the hydrodynamic response of a floating spar under regular and irregular waves were estimated using a Morison based formulation and compared with results from 1:100 scale model experiments. The support structure was modelled using 47 circular cylinders, the physical properties of which were defined by the experimental modelling of the spar. The commercial code used in Sethuraman and Venugopal (2013) computes the forces on each segment individually using Morison's equation relative velocity formulation. The hydrodynamic properties (drag, inertia and damping) were discretised in six dimensions with user supplied coefficients, chosen empirically. The numerical model used to describe the spar is illustrated in Fig. 12 and the surge response to an irregular sea (at model scale) are presented in Fig. 13.

Suitable extensions to Morison's equation may involve e.g. the use of frequency dependent C_D estimates for a range of environmental conditions. For generic shapes, these may in turn be derived from more advanced numerical formulations such as those described in Sect. 2.5. Such hybrid approach may prove critical for a more rapid assessment of a wide range of design situations, which is a testament to the usefulness of Morison's equation.
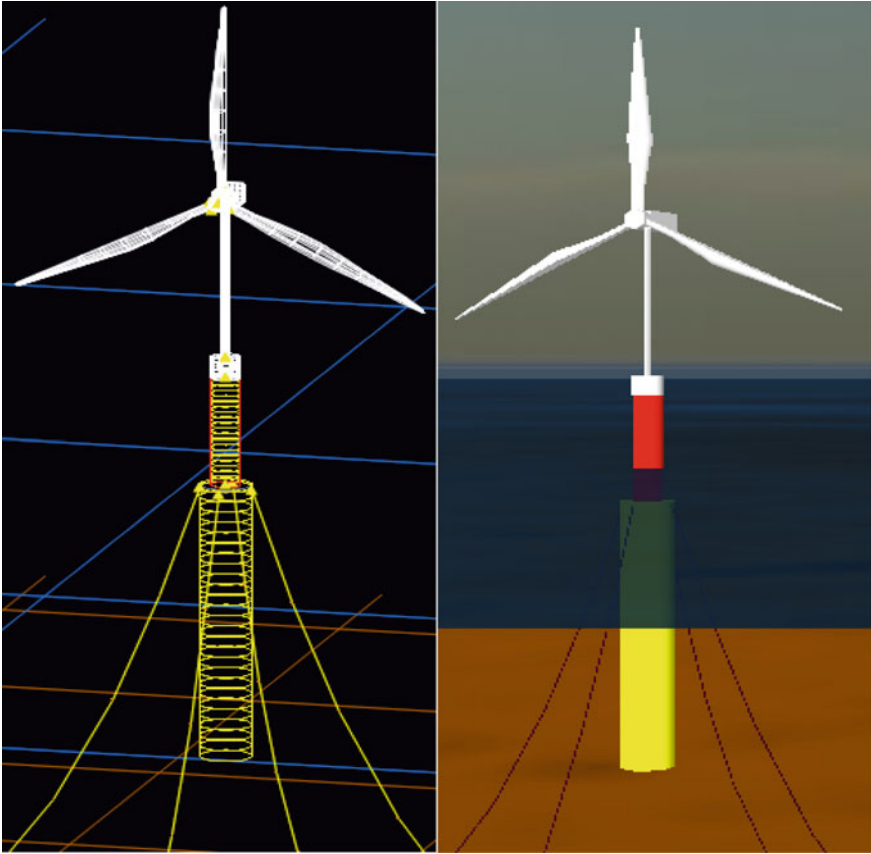
Fig. 12 Model of a spar floating wind turbine, discretisation of the elements (*left*) and complete model (*right*) (Sethuraman and Venugopal 2013)

2.5 Moving Forward: Advanced Methods

The challenge of reducing the overall cost of floating offshore wind will continuously push for new, advanced design methods to reduce the risk and uncertainty when estimating the design driving loads acting on floating support structures. In most situations, such loads may in turn be related to ULS (Ultimate Limit State) design situations and extreme environmental conditions. The conceptualisation of probabilistic based methods that include evaluation procedures that rely on nonlinear wave kinematics, validated load models and their interface to detailed structural response estimation tools remains an open research topic in the present day.
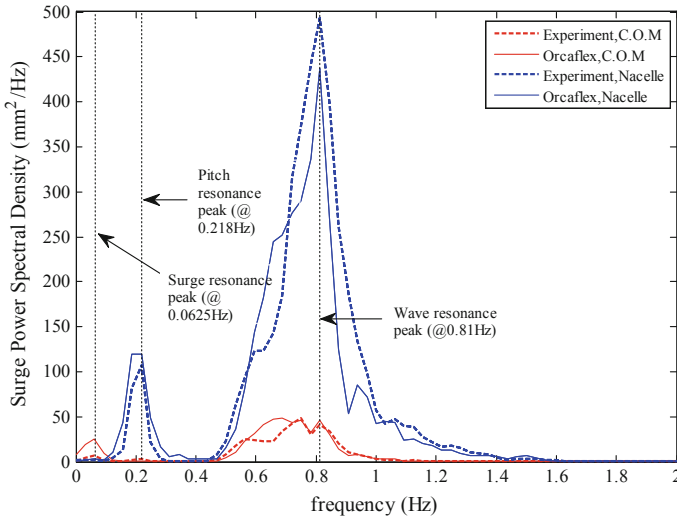
Fig. 13 Surge response spectrum for a H_s = 30 mm, f_p = 0.8 Hz sea state (Sethuraman and Venugopal 2013)

Although the above challenges are clear, current design practices do not necessarily address them. In Day et al. (2015) a review of hydrodynamic modelling methodologies applied to marine renewable energy devices is presented. The vast majority of the examples presented, including all of the numerical codes documented in the Offshore Code Comparison Collaboration, Continuation, with Correlation (OC5) project (see Sect. 5.2 and also Robertson et al. 2014a, b), are based on methods outlined in the previous subsections of Sect. 2. Therefore, the main simplifying assumptions detailed in Sects. 2.2 and 2.4 apply to the calculations, and from a hydrodynamic perspective may contribute to high levels of uncertainty when design situations associated with ultimate loading are to be addressed.

When nonlinear effects are judged to be significant, time-domain solutions need to be derived and implemented. In some cases, especially for large, diffracting support structures, the nonlinear analysis may need to be based on direct pressure integration over the body surface at each time step of the simulation. A first additional level of complexity may therefore be obtained by calculating certain components of the wave induced force (such as e.g. the Froude-Krylov) over each time step, or by using databases of linear solutions for different mean wetted profiles (and interpolating between them). Recently, this baseline approach has been extended to incorporate viscous loading sources, mostly using Reynolds Averaged Navier-Stokes Equations (RANSE) solvers. Studies comparing wave induced pressures (forces) derived via potential flow, RANSE and experimental

data can be found in the literature. For example, Lopez-Pavon and Souto-Iglesias (2015) who estimate the hydrodynamic coefficients and pressure loads on heave plates for a semi-submersible floating support structure (see Fig. 14). Particular attention was given to the pressure field around the heave plate attached to the bottom of a cylindrical column, which as Fig. 15 illustrates led to detailed discretisations of the geometry. The added-mass comparisons were possible via forced oscillation (radiation) trials. The RANSE derived estimations showed closer agreement with the experimental results when compared to the potential flow estimates, although the authors note that the potential flow solver applied did not allow the assessment of the flow around thin plates using dipoles.

When considering advanced numerical methods, a key aspect not to be neglected is the computational effort involved. As highlighted in Bunnik et al. (2008), and although the evolution of parallel processing and the increased ease of access to supercomputers partly diminishes such concerns, the large computational effort involved in CFD time-domain simulations should not be overlooked, as it can limit the practical application of such techniques. The ULS related load calculations that advanced methods can address are often associated in offshore standards with long-duration sea states (e.g. 3-h), which may not be practical to implement in a CFD solver. Alternative methods to generate extreme waves in CFD therefore need to be considered, with focused wave groups being a first candidate. The comparisons

Fig. 14 Photograph of the experimental model used in Lopez-Pavon and Souto-Iglesias (2015)
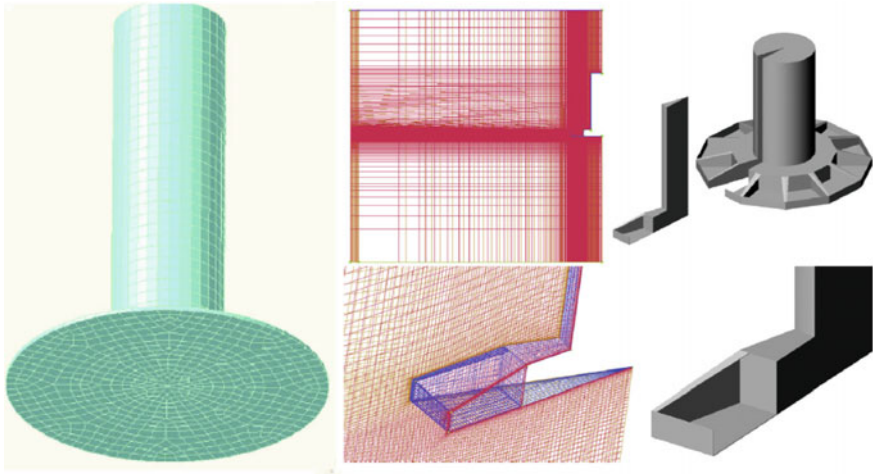
Fig. 15 Potential flow mesh and RANSE mesh used in Lopez-Pavon and Souto-Iglesias (2015)

between numerical and experimental data presented in Bunnik et al. (2008) show good agreement, which is encouraging. However, the relationship between the estimated loads using both type of inputs remains an open research topic.

Moving forward, hybrid approaches using wave kinematics derived from fully nonlinear potential flow solvers and Morison-type wave induced force models may offer a means to mitigate some of the practical concerns regarding more advanced methods. RANSE methods can also be used to create databases of e.g. drag coefficients as a function of the environmental inputs and geometrical shape that can be used to inform approaches such as the one outlined in Sect. 2.4. However, it is the generalised use of open-source solvers, such as OpenFOAM (Open Field Operation and Manipulation), that is more likely to facilitate the dissemination of novel methodologies, and multiple ongoing (and future) projects may benefit from the findings. As an example, the *Wave Loads* project (see Bredmose et al. 2013) presents an extensive set of comparisons between ultimate and fatigue loads on fixed offshore wind turbine support structures. Complex simulations including directional sea states (see Figs. 16 and 17) were assessed, with particular attention given to impact loads and pressures. Further validation of breaking wave loads,

Fig. 16 Details of the free-surface elevation around a fixed cylinder as calculated by a RANSE solver (Bredmose et al. 2013)
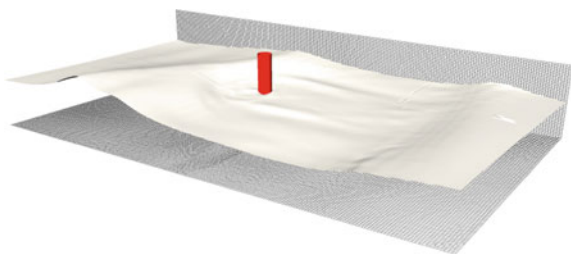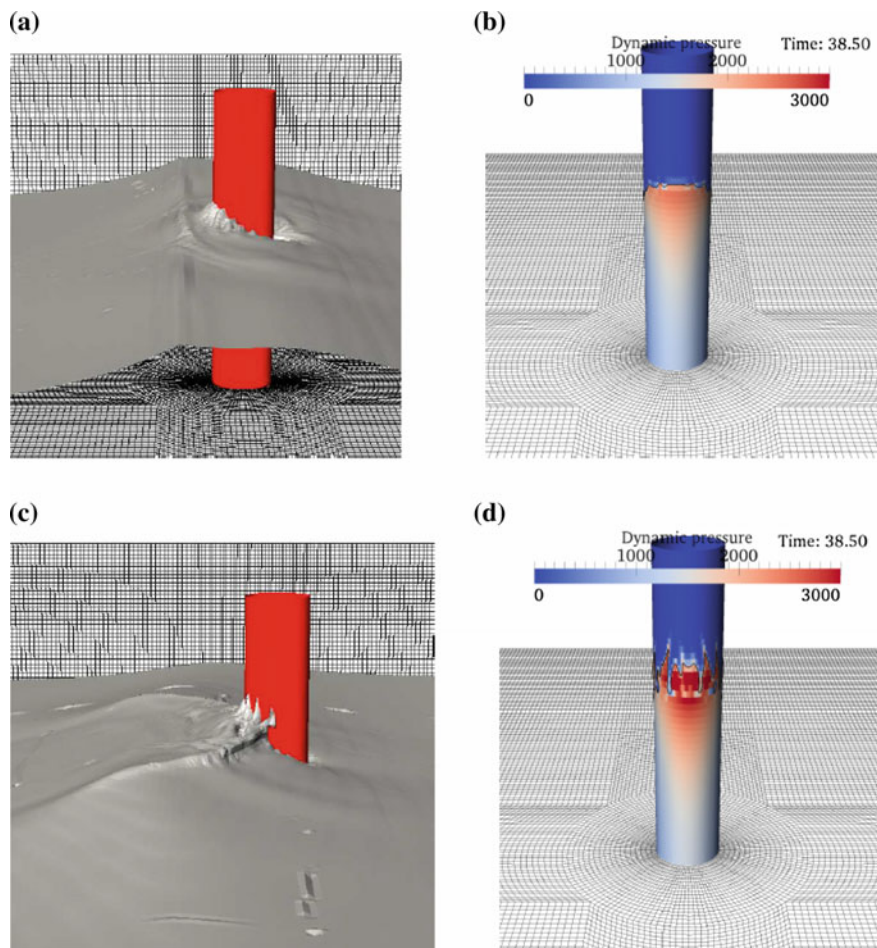
Fig. 17 Wave impact pressures as calculated by a RANSE solver (Bredmose et al. 2013). **a** Unidirectional wave impact: free surface. **b** Unidirectional wave impact: dynamic presure. **c** Bi directional wave impact: free surface. **d** Bi-directional wave impact: dynamic presure

including detailed comparisons with the measure pressure fields, are recommended by the authors for future work—and should be particular relevant when considering larger, floating support structures.

Finally, and although not specifically targeted at floating support structures, a project that may addresses some of the key challenges described in this section is the DeRisk project. Initiated in 2015, this is a joint research project involving nine partners (DTU Wind Energy, DTU Mechanical Engineering, DTU Compute, DHI, DONG Energy, University of Oxford, University of Stavanger, Statkraft and Statoil) that is scheduled to be completed in 2019. The overall objective of the DeRisk project is to contribute to the creation of new computational methods and

design procedures for estimating ULS loads in offshore wind support structures. Follow up extensions for large, floating support structures may allow the complete range of support structures for offshore wind turbines to be addressed, and can therefore be suggested as a future research topic.

3 Mooring Dynamics

Marco Masciola

The choice of mooring model used in the numerical simulation relates to level of accuracy and the information required to advance the design to the next phase. Two mooring model conventions are widely applied. Under one assumption, the restoring force is supplied based on the statics of a line held in equilibrium between the anchor and vessel attachment point. This leads to the so-called *quasi-static* model. In practice, the line is not stationary and succumbs to effects from fluid-drag, inertial forces, and nonlinear loads associated with touching a boundary. A *dynamic* mooring model, by design, captures these effects by modelling the line as a kinematic chain of elements subjected to different loads. Each line is effectively linear-elastic element that can stretch incapable of compressing. Through this method, short-lived dynamic excitation loads attributed to nonlinear effects can be implemented into the model.

Cermelli and Bhat (2002) reported on the effects of various modelling procedures according to the applicable standards (API RP 2SK 2005; ISO 19901-7 2013; API RP 2SM 2014) have on the design. Quasi-static generally under predicts the mooring tension, and to account for greater uncertainty, larger safety factors are used. Despite their limitations, quasi-static models have the capability to model the mean force-displacement relationship, making them an ideal surrogate for prototyping a design (Mekha et al. 1996; Masciola et al. 2013). Where a dynamic mooring model and a quasi-static model diverge is in the tension load magnitude and how the line interacts with the surrounding environment (Nordgren 1987; Oran 1983). For example, Fig. 18 demonstrates a line tension using two mooring line theories with prescribed motion. Although both models capture the snap-load event at time = A, the dynamic model emerges with the larger tension. A loss of tension episodes such as that depicted in Fig. 18 should be avoided at the risk of damaging the mooring infrastructure. In advance stages, dynamic models are necessary to capture peak tension in extreme events.

Other physical effects captured in dynamic mooring model are visualised in Fig. 19 to show the second longitudinal $u(s,t)$ and transverse $w(s,t)$ vibration mode. The vibration mode can be estimated for a pinned-pinned boundary condition through (Inman and Singh 1994):

Fig. 18 Comparison of the tension time series for quasi-static (*dashed line*) and dynamic (*solid line*) mooring models. Although the snap-load instances are caught by both models at time = A, the dynamic model captures high-frequency oscillation and results in a larger peak tension compared to the static model. This extreme example differentiates one characteristic between a quasi-static and dynamic mooring model
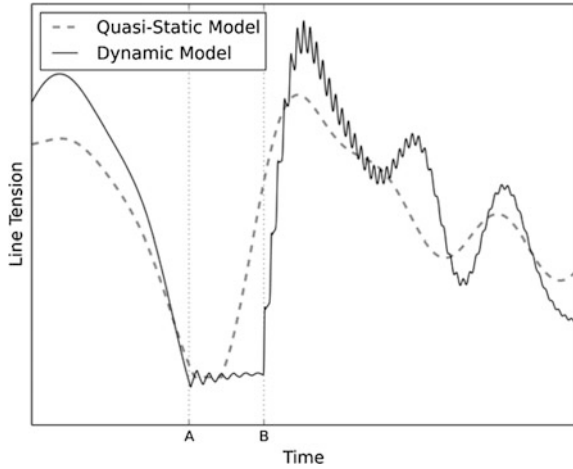
Fig. 19 The longitudinal $w(s,t)$ and transverse $u(s,t)$ wave forms represent the structural deformation considered in dynamic mooring models. The 2nd vibration mode is illustrated, though multiple frequencies are often present. The modal frequencies depend on the boundary conditions used, but are usually outside the wave band spectrum. Variable s_a represents a position (distance) on the mooring line, where $L > s_a$
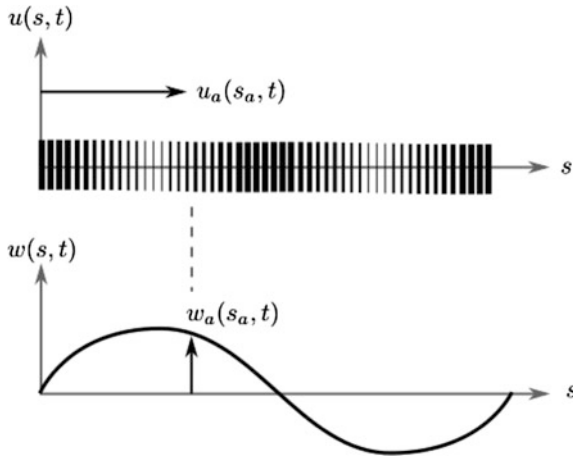
$$f_u^n = \frac{n}{2L}\sqrt{\frac{EA}{\mu}} \tag{50}$$

for the longitudinal direction, and:

$$f_W^n = \frac{n}{2L}\sqrt{\frac{T}{\mu}} \tag{51}$$

for the transverse direction. Variable L is the unstretched cable length, μ is the mass-per-unit length, EA is the cross-sectional stiffness, T is the line tension, and

n is an integer corresponding to the nth vibration mode. Equations (50) and (51) are linearised values assuming constant cable pretension T and cross-sectional properties, although practical mooring systems may have significant portions touching the seabed with varying internal tension. Added discussions on mooring line theories can be referenced in Choo and Casarella (1973).

3.1 Quasi-Static Mooring Model

Quasi-static models provide an efficient means to relay the mean restoring force in a line. This model includes effects from gravity and axial strain, though bending stiffness is typically left out. Two interpretations of a quasi-static model are provided herein. One is based on linearising the mooring restoring force about an equilibrium position to determine equivalent stiffness coefficients. A second method is based on solving a pair of nonlinear equations to determine the applied horizontal and vertical fairlead forces (Bauduin and Naciri 2000; Jonkman 2007; Quallen et al. 2013). A third quasi-static variant is based on the dynamic models presented in Sect. 3.2 by omitting the time integration procedure and solving the statically determinate force-balance equations. The benefit of the approach is the cable profile in the presence of viscous drag can be obtained.

Linear Spring

A simple linear spring model can be employed to produce a force proportional to the vessel displacement. One common use is in frequency-domain hydrodynamic analysis to establish vessel Response Amplitude Operations (RAOs). In conventional time-domain simulations, linear spring models are used with less regularity because the small motion limitations are often exceeded. Vessel displacements should remain small for the linear spring model to yield reliable results. Slack-line moorings should be scrutinised well to determine the restoring force sensitivity to a range of offsets. As demonstrated in Sect. 3.2 of Chapter "Overview of Floating Offshore Wind Technologies", slack-line moorings derive their restoring force from changes in geometry and the action of lifting mass off the seabed. In contrast, a larger portion of the restoring force is derived from axial stiffness, EA as the line becomes tauter (Malaeb 1983). The linear stiffness matrix is invoked simply by using:

$$F = Kx \tag{52}$$

where F is the restoring force, x is the generalised global FOWT displacements, and K is the matrix of linearised stiffness coefficients. The size of F is $N \times N$, where N is the number of platform degrees-of-freedom. Linear spring moorings are inclined to be used in taut systems where axial strain dominates, such as a tension leg platform. Linearised force-displacement models have been applied widely to tension leg platforms as demonstrated in Morgan (1983), Malaeb (1983),

Chandrasekaran and Jain (2002) and Low (2009). Notably, a 6×6 stiffness matrix was derived for a TLP with vertical tethers (Malaeb 1983). The process can be re-derived to find the equivalent stiffness for non-vertical taut lines at equilibrium. A second common approach is to linearise the forces through finite-differencing using closed-form analytical solutions (Jain 1980; Liu and Bergdahl 1997), which are specialised adaptations of the model presented in the next section. In many cases, Eq. (52) is paired with a constant coefficient in the direction of gravity to account for the mooring weight if it is not included in the platform mass matrix.

Closed-Form Algebraic Solution

Closed-form algebraic models are structured to provide the anchor-to-fairlead displacement based on a combination of fairlead horizontal H and vertical V forces. In most practical applications, particularly with time-domain simulations, H and V are unknown quantities. Iterative methods are invoked to converge on the mooring terminal force based on the prescribed vessel displacement. As demonstrated in Veselic (1995), the solution to a hanging cable is unique provided the net weight of the cable in immersed fluid is not zero (i.e. the cable is not neutrally buoyant). The equation roots are notoriously more difficult to find as the line density approached that of sea water. The closed-form algebraic model is derived assuming the cable possesses constant properties along its length. The well-known solution for a hanging chain is presented in Irvine (1992). A novel, albeit a lesser-known solution, was derived by Jonkman (2007) to include friction effects of the line touching the sea floor. Both models are derived assuming constant material properties along the line. Thus, Hooke's Law is a convenient apparatus to describe how the line terminal force and axial stiffness influence the catenary shape (Irvine 1992; Wilson 2003):

$$dx = \left(1 + \frac{T}{EA}\right)ds \tag{53}$$

Although outside the scope of the models presented herein, others have developed and applied multisegmented variants of closed-form algebraic models to equip a simulation with discontinuous line properties or bridle/triplate/delta joints (Peyrot and Goulois 1979; Masciola et al. 2013; Quallen et al. 2013).

Freely Hanging Chain

A pedagogical treatment deriving of algebraic equations for a free-hanging is given in (Irvine 1992; Wilson 2003). Required definitions to obtain the shape and end forces for a suspended line are illustrated in Fig. 20. Given a combination of fairlead horizontal l and vertical h offsets relative to the x, z cable origin, the corresponding reaction force at the cable end points can be solved. H_a and V_a constitute the horizontal and vertical anchor forces, respectively.

Fig. 20 Definition of geometry and parameters used in constructing a single mooring line suspended in fluid and freely hanging
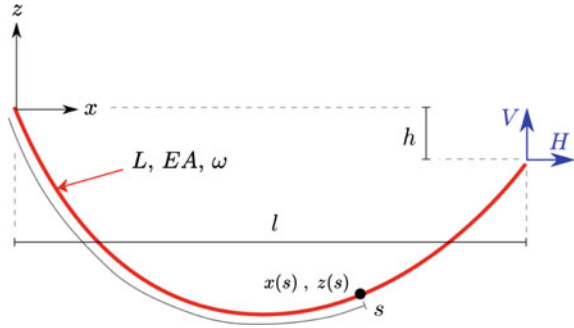
The line geometry can be expressed as a function of the forces exerted at the end of the line[1]:

$$l = \frac{H}{\omega}\left[\sinh^{-1}\left(\frac{V}{H}\right) - \sinh^{-1}\left(\frac{V - \omega L}{H}\right)\right] + \frac{HL}{EA} \tag{54}$$

$$h = \frac{H}{\omega}\left[\sqrt{1 + \left(\frac{V}{H}\right)^2} - \sqrt{1 + \left(\frac{V - \omega L}{H}\right)}\right] + \frac{1}{EA}\left(VL - \frac{\omega L^2}{2}\right) \tag{55}$$

where:

$$\omega = gA(\rho_c - \rho) \tag{56}$$

is the net weight-per-unit length of the cable in sea water, with ρ being the density of seawater, and ρ_c is the cable density; Eqs. (54) and (55) both describe the catenary reactions provided all entries on the right side of the equations are known. In practice, the force terms H and V are sought, and the known entities are the material properties and fairlead excursion dimensions, l and h. In this case, the forces H and V are found using a root-finding algorithm. The following expressions are defined for the anchor reaction force to guarantee static equilibrium:

$$H_a = H \tag{57}$$

$$V_a = V - \omega L \tag{58}$$

which simply states the decrease in the vertical anchor force component is proportional to the mass of the suspended line. By virtue of Eq. (58), the difference of

---

[1]Note that $\sinh^{-1}(x) = \ln\left(x + \sqrt{1 + x^2}\right)$, and Eq. (54) can have a different appearance in various text books, although the equations are equivalent.

the vertical end force $V - V_a$ should equate to the line weight in fluid to conform to the static-equilibrium requirement. The line profile can be sought using:

$$x(s) = \frac{H}{\omega}\left[\sinh^{-1}\left(\frac{V_a + \omega s}{H}\right) - \sinh^{-1}\left(\frac{V_a}{H}\right)\right] + \frac{H_s}{EA} \tag{59}$$

$$z(s) = \frac{H}{\omega}\left[\sqrt{1 + \left(\frac{V_a + \omega s}{H}\right)^2} - \sqrt{1 + \left(\frac{V_a}{H}\right)^2}\right] + \frac{1}{EA}\left(V_a s + \frac{\omega s^2}{2}\right) \tag{60}$$

Lastly, the tension in the line is determined using the following relationship:

$$T(s) = \sqrt{H^s + (V_a + \omega s)^2} \tag{61}$$

As outlined previously, Eqs. (54)–(61) are applicable to the case of a cable suspending freely in a fluid with no portion of the line touching a surface. This condition is determined by virtue of Eq. (58) indicating a catenary must be supported by a vertical force larger than the submerged weight:

$$V - \omega L > 0 \tag{62}$$

Contact with Horizontal Bottom Boundary

A new closed-form algebraic solution evolves when additional forces are considered on a finite cable section touching a bottom boundary with friction as depicted in Fig. 21 based on the study in Jonkman (2007). The origin of the equations describing a cable resting on the seabed follows a similar derivation process for the suspended case as described in Irvine (1992). The following assumptions are observed in this derivation:

- Effects from bending, torsion, and shear stiffness are neglected.
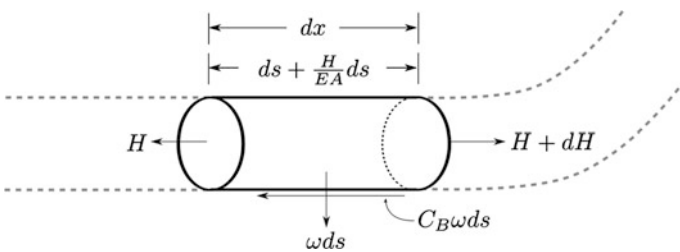- Mass, elastic and cross-sectional properties along the line are constant.

Fig. 21 Free-body diagram for an infinitesimal cable section in contact with the seabed

- The seabed contact friction force is directed tangential to the element and only exists on the portion of line resting on the seabed.
- The seabed is perfectly horizontal (not inclined).
- The cable touch-down point is noted as B in Fig. 22.
- The entire cable (on the seabed and hanging in the fluid) lies in a vertical plane. Transverse seabed friction is neglected.

Figure 22 is dissected into three segments. Points a (the anchor position) and f (the fairlead position) are typically known entities based on the FOWT motions. The touch-down point B that is a parameter that is calculated in the course of iteratively solving for H and V. The displacement x_0 identifies the transition point where $H(x_0^+) > 0$ and $H(x_0^-) = 0$. The length of line resting on the seabed, L_B, is a linear function proportional to the vertical force V magnitude. If the vertical force is not sufficient to suspend the cable, then $V < \omega L$, which implies a portion of the line rests on the seabed. The difference between V and ωL accounts for the total weight of cable resting on the seabed. This is recognised with the following expression:

$$L_B = L - \frac{V}{\omega} \tag{63}$$

When $L_B > 0$, then Eq. (58) is violated, and the line is no longer fully suspended. Although L_B is useful in describing the mooring line geometry and juncture of the touch-down point, it is an essential component for determining the transition point x_0, which is necessary to advance towards the final solution. Because the line is in static equilibrium, the horizontal forces on the line due to friction must equate to the horizontal applied force at the fairlead:
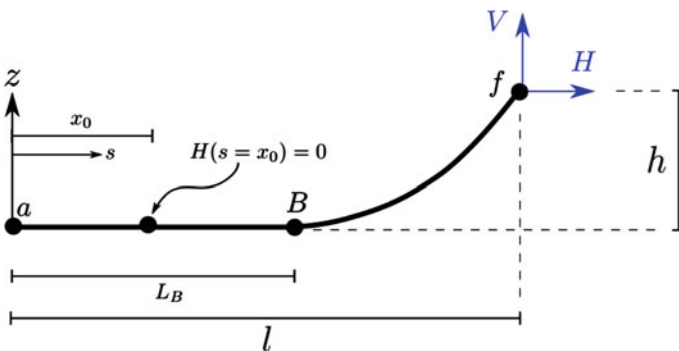
$$H = C_B \omega (L_B - x_0) \tag{64}$$

Fig. 22 Definition of geometry and parameters used in constructing a single mooring line suspended in fluid and touching a horizontal bottom boundary

With the fundamental geometric components defined, the derivation for the closed-form analytical cable model with seabed contact proceeds by defining the governing differential equations. The next step is to determine the horizontal force $H(s)$ along the portion touching the seabed. The expression for $H(s)$ is a prerequisite to determine the equivalent forms of Eqs. (54) and (55) for the cable/seabed contact problem.

Horizontal Force

For the case of a cable resting on the seabed, the rate of change in the element horizontal direction will be proportional to $C_B\omega$. Through a summation of force in the x direction, as depicted in Fig. 21, one obtains:

$$\sum F_x = 0 \rightarrow H + C_B\omega ds = H + ds$$
$$\rightarrow dH = C_B\omega ds \tag{65}$$

The horizontal force $H(s)$ is found by integration Eq. (65) from a to B, Fig. 22, where the expression for the horizontal then becomes:

$$H(s) = \begin{cases} C_B\omega(s - x_0) & \text{if} \quad s \leq x_0 \\ 0 & \text{otherwise} \end{cases} \tag{66}$$

Given the tension component T is exclusively in the x direction at the cable/seabed interface, Fig. 22, the substitution $T = H$ can be made in Eq. (53).

Cable Profile

The line geometry can be sought by integrating Eq. (53):

$$\int_0^{x(s)} dx = \int_0^s \left[1 + \frac{H(s)}{EA}\right] ds' \tag{67}$$

Equation (67) leads to a series of conditional algebraic expressions based on the section of line in contact with the boundary:

$$x(s) = \begin{cases} s & \text{if} \quad 0 \leq s \leq x_0 \\ s + \frac{C_B\omega}{2EA}\left(s^2 - 2x_0s + x_0\lambda\right) & \text{if} \quad x_0 < s \leq L_B \\ L_B + \frac{Hs}{EA} + \frac{C_B\omega}{2EA}\left(x_0\lambda - L_B^2\right) + \frac{H}{\omega}\sinh^{-1}\left[\frac{\omega(s-L_B)}{H}\right] & \text{if} \quad L_B < s \leq L \end{cases} \tag{68}$$

with λ equal to:

$$\lambda = \begin{cases} L_B - \frac{H}{C_B\omega} & \text{if} \quad x_0 > 0 \\ 0 & \text{otherwise} \end{cases} \tag{69}$$

The expression $z(s)$ is found by continuing Eq. (55) beyond point B. Between the range $0 \leq s \leq L_B$, the vertical height is zero since the line is resting on the seabed and forces can only occur parallel to the horizontal plane. This produces:

$$z(s) = \begin{cases} 0 & \text{if} \quad 0 \leq s \leq L_B \\ \frac{H}{\omega}\left[\sqrt{1 + \left(\frac{\omega(s-L_B)^2}{H}\right)} - 1\right] + \frac{\omega(s-L_B)^2}{2EA} & \text{if} \quad L_B < s \leq L \end{cases} \quad (70)$$

Equations (68) and (70) produce the mooring line profile as a function of s. Ideally, a closed-form solution for l and h is sought to permit simultaneous solves for H and V, similar to Eqs. (54) and (55). This is obtained by substituting $s = L$ into Eqs. (68) and (70) to yield:

$$l = L_B + \frac{H}{\omega}\sinh^{-1}\left(\frac{V}{H}\right) + \frac{HL}{EA} + \frac{C_B\omega}{2EA}\left(x_0\lambda - L_B^2\right) \quad (71)$$

$$h = \frac{H}{\omega}\left[\sqrt{1 + \left(\frac{V}{H}\right)^2} - 1\right] + \frac{V^2}{2EA\omega} \quad (72)$$

Finally, a useful quantity that is often evaluated is the tension as a function of s along the line. This is given using:

$$T(s) = \begin{cases} \text{MAX}[H + C_B\omega(s - L_B); 0] & \text{if} \quad 0 \leq s \leq L_B \\ \sqrt{H^2 + [\omega(s - L_B)]^2} & \text{if} \quad L_B < s \leq L \end{cases} \quad (73)$$

3.2 Dynamic Mooring Models

The previous derivations resulted in models providing the static equilibrium forces. A different method is considered next relying on numerical integration. Convincing arguments for dynamic mooring models where provided earlier in the section through Eqs. (50) and (51); though not all dynamic cable models can capture longitudinal excitations in Eq. (50), as this depends if the model is inextensible or not (i.e. the *EA* cable property) (Rupe and Thresher 1975).

Choo and Casarella (1973) presented a summary of qualities various dynamic mooring models possesses, including those with inextensible elements. These early cable models were derived heuristically as a kinematic mass-spring-damper chain, akin to the system in Fig. 23 (Walton and Polachek 1960; Schram and Reyle 1968; Merchant and Kelf 1973; Ketchman and Lou 1975). The focus of this era was geared towards defining various theories and practices to simulate mooring
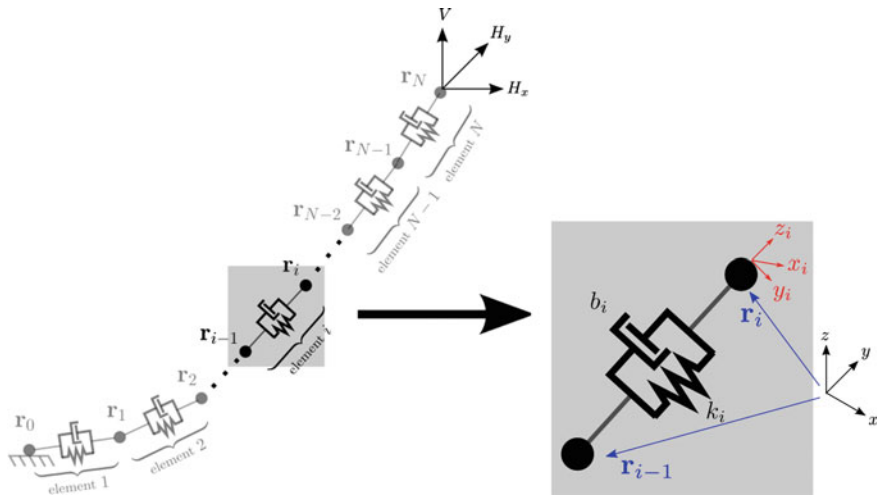
Fig. 23 Dynamic mooring models can be represented as a kinematic chain of discrete elastic elements. The illustration above defines various kinematic parameters and element properties commonly encountered and used in dynamic mooring formulations

dynamic responses. These early dynamic models lead to the progress allowing deeper waters to be reached with confidence (Skop 1988). By the late 1980s, theory fundamentals were in place. It is not coincidental that as computers became more powerful, dynamic mooring models increased in complexity, leading to rapid progress in standard design practices.

The modern era has ushered in inexpensive computational resources to render sophisticated dynamic models highly accessible features for FOWT applications. With expanded computational resources, the research envelope has shifted from developing dynamic model theories to advancing simulation features to closely replicate real-life conditions, such as contoured seabed-cable interaction, integration strategies, and fully-coupled aero-elastic-hydro-mooring dynamic analysis (Sun et al. 1994; Kamman and Huston 1999; Gobat and Grosenbaugh 2001; Gatti-Bono and Perkins 2004; Williams and Trivailo 2007; Bae et al. 2011). Dynamic mooring models can be classified into three main groups:

- Lumped-mass model
- Finite element model
- Finite-difference model

In general, each of these models converges on nearly identical results given sufficient resolution (Ketchman and Lou 1975; Leonard and Nath 1981). The models described herein are adequate for design code checks categorised as *dynamic analysis*.

Fundamentals

The constituting equation describing the foundation for discretised dynamic cable models can be summarised as:

$$\mathbf{M}_i \ddot{\mathbf{r}}_i = \sum \mathbf{f}_{i_{ext}} + \sum \mathbf{f}_{i_{int}} \tag{74}$$

where $\mathbf{M}_i$ is the mass matrix, $\mathbf{r}_i$ is the node position, and $\mathbf{f}_{i_{ext}}$ and $\mathbf{f}_{i_{int}}$ represent external and internal forces, respectively. This equation is provided purely for demonstration purposes of how components of the model come together, though formulations may vary depending how the theory is applied. Nodes represent $N+1$ discrete points on the line, Fig. 23, where each node acceleration and velocity must be integrated to determine position. Internal forces are those defined by the element properties, and may comprise of:

- Tension
- Damping
- Bending
- Torsion

External forces are those defined by interactions with the environment, and may be comprised of:

- Gravity loads from weight and buoyancy
- Hydrodynamic loads
- Vortex-Induced-Vibrations (VIV)
- Seabed interaction
- Collision with adjacent bodies

For demonstration purposes, the following vectors are defined: $\mathbf{t}_i$ is tension, $\mathbf{b}_i$ is structural damping, $\mathbf{n}_i$ is the internal bending moment, $\mathbf{w}_i$ are the gravity loads, and $\mathbf{h}_i$ are hydrodynamic forces. Contrasting Eq. (74) to continuous models found in (Garrett 1982; Nordgren 1987):

$$\mu \ddot{\mathbf{q}}(s,t) = \underbrace{(\mathbf{h}+\mathbf{w})}_{\text{external force}} + \underbrace{(\mathbf{t}+\mathbf{b})}_{\text{internal force}} \tag{75}$$

the resemblance is apparent. Equation (74) is the continuous interpretation of the discretised form for Eq. (75), where the units are in force-per-length. Boundary conditions are applied at the end points, nodes $\mathbf{r}_0$ and $\mathbf{r}_N$, which usually are not integrated since the positions are prescribed (or fixed in the case of an anchor). Although derived heuristically, this is the basis of where the three dynamic mooring model classes can trace their origins to. This fundamental representation can be expanded to include contributions from bending and torsion. Among the three dynamic models presented, the lumped-mass, finite element, and finite-difference rely on a comparable kinematic description given in Fig. 23. The size of N directly relates to the number of longitudinal and transverse vibration modes the dynamics model can capture.

Forces arising from strain, damping, gravitational loads, and hydrodynamic forces, will be the targets of this abridged presentation for the purpose of describing the lumped-mass, finite element, and finite-difference model formulations are arranged. References will be provided pointing to the relevant literature with elaborately detailed derivations. Essential differences between the three classes of dynamic mooring models are how the forces and mass matrix are discretised. Other differences among the three model classes are also described in Masciola et al. (2011).

Lumped-Mass Model

The lumped-mass model is a straightforward model to implement, making it a popular tool in the offshore community (Huang 1994; Chai et al. 2002; Buckham et al. 2004; Nicoll 2006; Williams and Trivailo 2007). Borrowing concepts from Fig. 23 and Eq. (74), the ith element is adjacent to nodes $\mathbf{r}_{i-1}$ and $\mathbf{r}_i$, implying the element tension $\mathbf{t}_i$ can found using:

$$\mathbf{t}_i = k_i \Delta_i \widehat{\mathbf{k}}_i \tag{76}$$

where $k_i = \frac{EA}{L_i}$ is the element stiffness and $\Delta_i = \|\mathbf{r}_{i-1} - \mathbf{r}_i\|$ is the stretched length. The unit vector $\widehat{\mathbf{k}}_i = [0, 0, 1]^T$ is the local element frame as depicted in Fig. 23. Equation (76) is assigned zero if $L_i > \|\mathbf{r}_{i-1} - \mathbf{r}_i\|$ since mooring cannot support compressive loads. Line forces are solved in a local frame fixed to the element for convenience of deriving the forcing functions, but are eventually transformed into a global orientation which the platform equation of motion is defined in. Equation (76) is an essential component of dynamic mooring models to capture dynamic tension variations, particularly those associated with Eq. (50).

The internal (structural) damping model can be incorporated based on the stretched length rate of change:

$$\mathbf{b}_i = b_i \dot{\Delta}_i \widehat{\mathbf{k}}_i \tag{77}$$

Bending moments can be implemented on a strategy of solving the spatial derivative of a spline curve, $\mathbf{q}(s)$, fitted through the node points (Buckham et al. 2004). In a three dimensional domain, the spline function at the ith element is:

$$\mathbf{q}_i(s) = \mathbf{A}_i + \mathbf{B}_i s + \mathbf{C}_i s^2 + \mathbf{D}_i s^3 \tag{78}$$

The line/element slope arises from the spatial derivative $\frac{d\mathbf{q}_i}{ds}$, the decisive ingredient for determining the bending moment:

$$\mathbf{n}_i = \left[\frac{EI}{L_i} (\boldsymbol{\kappa}_{i-1} - \boldsymbol{\kappa}_i) \right] \tag{79}$$

with $\boldsymbol{\kappa}_i$ being a vector describing the radius of curvature derived from $\mathbf{q}_i(s)$ in Eq. (78).

Hydrodynamic $\mathbf{h}_i$ loads are commonly included by treating the element as a Morison element to consider the relative fluid velocity. There are various methods to derive this force (Merchant and Kelf 1973; Buckham et al. 2004; Gatti-Bono and Perkins 2004), but most approaches follow a precedent of arranging the relative fluid velocity/acceleration in components parallel and perpendicular to the element. The perpendicular relative fluid velocity/acceleration contributes quadratic drag and cross-flow added mass effects. The component parallel to the line may also provide skin friction and, in the case of chain, added mass. Directness of the lumped-mass model evolves from treating the mooring line as a discretised system as its inception. This inherently leads to a diagonal mass matrix $\mathbf{M}_i = \mathrm{diag}(m_i, m_i, m_i)$. Other dynamic models, such as the finite element and finite-difference, proceed by discretizing the continuous partial differential equations in Eq. (75) using the method of weighted residuals or a differencing stencil to approximate gradients and time derivatives.

Consistent Finite Element Formulation

Fundamental differences between the lumped-mass model and a finite element mooring model include the following (Garrett 1982; Ran 2000):

- Model initiates with the continuous model in Eq. (75).
- Mass matrix discretisation: Consistent finite element model yield off-diagonal terms in $\mathbf{M}_i$. This may couple the motion of nonadjacent nodes.
- Force, boundary, and constraint discretisation.

A finite element representation for a structural cable system can be described in abridged form as (Garrett 1982; Ran 2000; Zienkiewicz and Taylor 2000):

$$\underbrace{\rho_c \int_0^L A_j \ddot{\mathbf{r}}_i ds}_{\mathbf{M}_i} + \underbrace{\int_0^L \left(EI A_j'' \mathbf{r}_i'' + \lambda A_j' \mathbf{r}_i' \right) ds}_{\text{stiffness matrix}} = \underbrace{\int_0^L A_j F_i ds}_{\text{external force}} \qquad (80)$$

where A_j is the cubic interpolation (shape) function based on the node arrangement pattern on the line, and λ is the Lagrange multiplier to resolve the axial line tension constraint:

$$\int_0^L P_j \left[\left(\frac{1}{2} \mathbf{r}_i' \cdot \mathbf{r}_i' - 1 \right) - \frac{\lambda}{EA} \right] ds = 0 \qquad (81)$$

where P_j is a quadratic interpolation coefficient. Both Garrett (1982) and Ran (2000) cultivate a finite element dynamic mooring model based on Eq. (75) with bending and torsion effects to result in Eqs. (80) and (81). This practice parallels Eqs. (78)/(79) for the lumped-mass model.

With the finite element model being a more rigorous formulation, it can improve the model fidelity with fewer elements compared to a lumped-mass model (Leonard and Nath 1981). This discretisation method also guarantees L^2 stability and conservation of energy due to Galerkin orthogonality (Hughes 1977; Liu et al. 2008). The finite element model also permits external forces to be decomposed as a series of Gauss points along an element. This effectively maintains continuity and smoothness of the applied forces even if a coarse element resolution is used.

Finite-Difference Model

The finite-difference model proceeds as a Taylor series expansion of the governing partial differential equation in Eq. (74). Seminal works in this area include Van den Boom (1985) and Gobat (2000). Parallels between the finite-difference model and the method of lumped-masses is explained in Huang (1994). A distinction between finite-difference models and other dynamic mooring lines derivation is that both the time and spatial derivatives are preserved in the domain discretisation. Unlike the finite element, which computes piece-wise derivatives explicitly, the finite-difference model approximates these functions. Although the spatial and time discretisation can take many forms, one finite-difference mooring model is based on a backward difference (box) stencil and first-order Taylor expansion of Eq. (74) (Gobat 2000; Gobat and Grosenbaugh 2001):

$$
\begin{aligned}
\mathbf{f}_j^i + \mathbf{f}_{j-1}^i &+ \mathbf{f}_j^{i-1} + \mathbf{f}_{j-1}^{i-1} \\
&= \frac{\left(\mu_j^i + \mu_j^{i-1}\right)\left(\dot{\mathbf{q}}_j^i - \dot{\mathbf{q}}_j^{i-1}\right)}{\Delta t} + \frac{\left(\mu_{j-1}^i + \mu_{j-1}^{i-1}\right)\left(\dot{\mathbf{q}}_{j-1}^i - \dot{\mathbf{q}}_{j-1}^{i-1}\right)}{\Delta t} \\
&\quad \frac{(\mathbf{t}_{j-1}^i + \mathbf{t}_j^i)(\mathbf{q}_j^i - \mathbf{q}_{j-1}^i)}{\Delta s} + \frac{\left(\mathbf{t}_{j-1}^{i-1} + \mathbf{t}_j^{i-1}\right)(\mathbf{q}_j^{i-1} - \mathbf{q}_{j-1}^{i-1})}{\Delta s}
\end{aligned}
\tag{82}
$$

where i is the spatial derivative, j is the time variable, and $\mathbf{f}$ is the applied external forces. The choice of differencing stencil implicates the equation format. By incrementing the time variable forward as opposed to backward, a forward-differencing scheme is produced (Mehrabi and Tabatabai 1998). In other words, the integration strategy is central to the application of the finite-difference model. This makes it relatively straightforward to translate a mathematical model into a computer algorithm. Unlike the finite element model, the finite-difference model does not guarantee energy flux is conserved due to approximating the derivatives. As a result, stability needs can influence the number of elements, the discretisation stencil, discretisation size (both Δt and Δs), and boundary condition resolution. Although this assessment also pertains to the finite element and lumped-mass models, numerical stability is less ominous with those models and can be achieved by modifying fewer parameters—such as using a coarser discretisation (i.e., increasing element size) or reducing time-step size. Finite-difference models have a proven track record providing high-fidelity modelling capabilities on par with finite element representations.

Other Caveats

Although the theory for translating a mooring system into computer code is well documented, there are several nuances with limited exposure. Tool developers new to this field commonly encounter these challenges as the model is created. The purpose here is to highlight these common challenges and provide references offering solutions to numerical instability and static convergence issues.

Numerical Stability

As with all structural models, maintaining numerical stability is essential. Instability can be controlled through adding damping, either as a structural component (Rayleigh damping) or skin drag. Cross-flow hydrodynamic damping (such as that applied using Morison's equation) is also crucial to limit amplitude of the transverse oscillation governed by Eq. (51). Including the local line velocity in the fluid drag calculation is vital to limit transverse oscillations to within reasonable values.

Artificial numerical damping is a viable means to limit instabilities arising from high-frequency longitudinal excitations. This is introduced in few implicit numerical integration methods (Chung and Hulbert 1993). Though, when artificial damping is present, additional structural damping might not be necessary, and Eq. (77) can be omitted depending on the numerical integration strategy. There are discussions within the structural modelling community as to how reasonable and realistic damping values should be derived. There is an agreement, however, that structural damping should be sufficient to promote numerical stability, but not large enough to foster noticeable changes in the system dynamics (Balzola 1999). An additional means to promote numerical stability is by introducing bending stiffness in the model (Choo and Casarella 1973; Gobat and Grosenbaugh 2001; Buckham et al. 2004; Williams and Trivailo 2007).

Static Convergence

Numerical instability from static convergence failures is an issue many cable model developers encounter with consternation; the purpose of a dynamic mooring model is to solve the dynamic response of the line, not necessarily to solve a statics problem. But to satisfy the dynamics equation, the model must start in an equilibrium configuration to avoid excessive start-up transients. Static convergence is achieved when the $\ddot{\mathbf{r}}_i$ term in Eq. (74) and $\ddot{\mathbf{q}}_i$ term in Eq. (75) are zero, i.e., the no acceleration and the node forces balance. This reduces the respective equations of motion into a static equation. To the surprise of many, this can be a difficult problem to solve (De Zoysa 1978; Webster 1980; Powell and Simons 1981; Shugar 1991; Wu 1995; Zueck and Powell 1995; Masciola et al. 2011). Fortunately, solution strategies are numerous, and the choice of approach is a matter of preference. Note that the continuous analytical model given by Eqs. (59) and (60) do not result in a static equilibrium solution for the discretised model; though the results can be used as initial estimates to the solution. Simply solving the resulting statics equation using conventional nonlinear iterative solvers proves to be difficult

due to the large condition number of the Jacobian matrix (Strang 1988). Methods to solve the discretised cable statics problem include:

- Dynamic relaxation: a preliminary simulation is executed with a fixed or adaptive damping term to softly arrive at the statics solution (Webster 1980; Shugar 1991; Wu 1995).
- Shooting method: the method relies on iterating boundary conditions until a targeted solution is achieved (De Zoysa 1978; Friswell 1995; Masciola et al. 2011).
- Modified root-finding methods: the step size advancing the solved variable is reduced based on iteration history to avoid exceeding the radius of convergence (Powell and Simons 1981; Zueck and Powell 1995).

4 Structural Design

Erin E Bachynski

Various types of structural analysis may be performed in order to assess the safety of a FOWT design with respect to the fatigue limit state (FLS), ultimate limit state (ULS), and accidental limit state (ALS) which are described in standards such as DNV-OS-J103 (2013). A typical design process includes a progression from simplified frequency-domain models, to global models which can capture some cross-sectional loads, to detailed local models for evaluation of stress concentration factors and local strength. The simple frequency-domain models are used to obtain first estimates of the motions in waves, which can then be used in preliminary mooring system design. More detailed global analysis models include more interaction between the structure, waves, wind, wind turbine control system, as well as accounting for flexibility in selected components. Such global analysis models must be accurate enough to capture important effects, but also computationally efficient in order to be able to simulate a wide range of design load cases within a reasonable amount of time.

Global analysis models are used to provide information about the overall structural strength and system behaviour as well as to provide input for local analysis models. The structure is subjected to static loads (gravity, buoyancy, and hydrostatic pressure) as well as dynamic loads from the environment, inertia, and operation. In general, time-varying loads will give time-dependent responses (displacements, strains, stresses). For loading of frequency less than about 1/4 of the lowest structural natural frequency, quasi-static analysis may be appropriate. In the case of floating wind turbines, the range of excitation frequencies generally includes frequencies well above this lower limit, such that dynamic analysis is needed. Dynamic response may be greater or less than the corresponding static response.

Global analysis models using beam or shell elements may not, however, be able to capture stress concentration factors in welded joints or scantlings, or to verify local pressure loads. Local final element analysis (FEA) using solid elements may therefore be needed. The boundary conditions for local FEA may be obtained from the global analysis model and applied in a more detailed model.

For any type of numerical structural analysis, the key is physical and theoretical understanding of the mathematical model as well as its limits. It is therefore recommended to start with relatively small and simple models, and then refine as needed. One should also take care to use reliable, well-understood finite elements, and to check that the solution has converged before examining the results.

4.1 Linear Rigid Body Dynamics

The simplest dynamic structural model of a FOWT is a single rigid body. One can define up to six traditional global motions about a given inertial reference point: surge ζ_1, sway ζ_2, heave ζ_3, roll ζ_4, pitch ζ_5, and yaw ζ_6. These global motions can be represented mathematically by the motion vector, $\vec{\zeta}$, where

$$\vec{\zeta} = [\zeta_1(t), \zeta_2(t), \zeta_3(t), \zeta_4(t), \zeta_5(t), \zeta_6(t)]^T \tag{83}$$

and t represents time. Newton's second law is then applied in an inertial reference frame as:

$$\mathbf{M}\ddot{\vec{\zeta}} = \vec{F} \tag{84}$$

where $\mathbf{M}$ is a 6×6 matrix containing the entries $\mathbf{M_{ij}}$ representing the dry mass of the structure, with the inertia computed about the body reference point; $\vec{F}$ is a time-dependent vector of all of the forces acting on the body; and the double dot represents two differentiations with respect to time.

For a moored floating body subjected to waves, a linear analysis of the global motions can be carried out by separating the force vector into several components: an added mass component which opposes the body acceleration, a linear damping component which is proportional to the body velocity, a linear stiffness due to hydrostatics which is proportional to the body motion, a linear stiffness due to the mooring system, and external wave excitation loads. By collecting the added mass, damping, and stiffness terms on the left hand side, the equation of motion becomes:

$$[\mathbf{M} + \mathbf{A}]\ddot{\vec{\zeta}} + \mathbf{B}\dot{\vec{\zeta}} + [\mathbf{C} + \mathbf{K}]\vec{\zeta} = \vec{X} \tag{85}$$

where $\mathbf{A}$ represents added mass coefficients, $\mathbf{B}$ represents damping coefficients, and $\mathbf{C}$ and $\mathbf{K}$ represent linear stiffness coefficients due to hydrostatics and the mooring

system, respectively. **A**, **B**, **C**, and **K** are 6×6 matrices, including coupling terms, and **A** and **B** are generally frequency-dependent. The 6×1 frequency- and amplitude-dependent vector $\vec{X}$ contains the external wave excitation force for each mode of motion.

For a linear wave-only analysis of a floating body, it is then convenient to consider the problem in the frequency domain (Faltinsen 1990). For a floating offshore wind turbine, such an approach can be extended with linearised approximations of the aerodynamic loads (Bachynski 2014; Kvittem 2014). In order to include nonlinear load effects in a rigid body model, the equations of motion should, however, be solved in the time domain. In that case, the frequency-dependence can be included through a convolution integral or by a state-space representation of the time-dependent coefficients (Taghipour et al. 2008). A rigid body model does not provide sufficient information for structural strength analysis, and one must therefore examine alternative methods.

4.2 Finite Element Methods

Rather than limiting the analysis to six rigid body motions, the structure may be discretised using a number of *finite elements*. These elements have approximate representations of the mass and stiffness properties of the structure. By combining the mass, damping, and stiffness matrices corresponding to all of the degrees of freedom of many individual elements in a consistent manner, the static and dynamic structural responses of a physical structure can be estimated. Finite element analysis (FEA) provides a piecewise approximation of field quantities such as stress and strain.

Beam elements can capture the overall behaviour of long, slender structures. Shell elements, which remove a level of abstraction from the beam element model, can capture flexural stresses which are not considered in a beam model. A solid element model removes another level of abstraction, but requires even greater computational effort.

In FEA, regardless of the element type, the governing equation for structural dynamics can be formulated by requiring that the virtual work done by externally applied loads be equal to the sum of the virtual work absorbed by inertial, dissipative, and internal forces. The global form of the governing equation can be written as in Eq. (86), assuming that the element mass ($\mathbf{M_g}$) and damping ($\mathbf{B_g}$) matrices follow from the discretisation and use the same shape function as the stiffness matrix.

$$\mathbf{M_g}\ddot{\vec{D}} + \mathbf{B_g}\dot{\vec{D}} + \vec{R}^{\text{int}} = \vec{R}^{ext} \tag{86}$$

In Eq. (86), $\vec{D}$ is the system displacement vector, $\vec{R}^{\text{int}}$ are the internal reaction forces and $\vec{R}^{ext}$ are the external loads. For a linear elastic material, the internal forces can be written:

$$\vec{R}^{\text{int}} = \mathbf{K_g}\vec{D}. \tag{87}$$

In practice, however, the stiffness matrix is not necessarily linear: $\mathbf{K_g}$ is, in general, a function of $\vec{D}$. For FOWTs, nonlinearities in the physical problem can be related to geometrical nonlinearities (such as the large deflections of the blades or mooring lines), nonlinear force boundary conditions (such as the generator torque which is applied by the turbine controller), displacement boundary condition nonlinearity (such as contact), or in some cases by material nonlinearities.

Equation (86) is a system of coupled second-order differential equations that are continuous in time (and discretised in space). The formulation of the mass, damping, and stiffness matrices, as well as the load and displacement vectors depends on the type of elements to be used. A brief review of classical and Timoshenko beam theories, and the formulation of beam element stiffness, mass, and damping matrices is given here. Traditional structural mechanics (Hibbeler 2011) and finite element textbooks (Cook et al. 2002) should be consulted for greater detail.

Beam Theory

Classical beam theory, also known as Euler-Bernoulli beam theory, is a mathematical description of the relationship between the applied load and the deflection of a slender beam. The theory is applicable for long slender beams and relatively small deflections. The shear deformation is assumed to be much smaller than the transverse deformation. Consider the beam in Fig. 24, which has its long axis along the x-axis and deflects in the y-direction, and the corresponding cross section in Fig. 25.

From the mechanics of materials, the time-varying bending moment sustained by the beam $M(x, t)$ is related to the bending deformation $w(x, t)$ as in Eq. (88), where
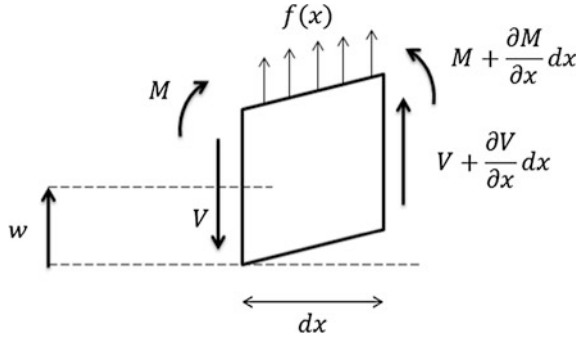

Fig. 24 Beam in bending about the z axis
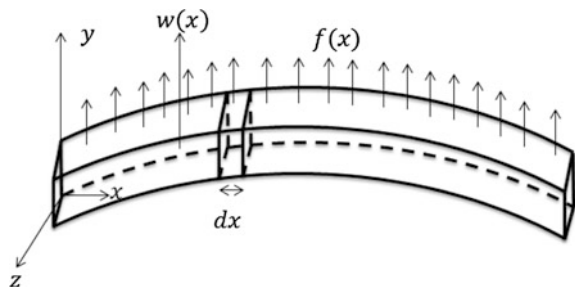
Fig. 25 Cross-section of the beam in Fig. 24 Note that w is measured from the undeformed *x*-axis

E is the Young's modulus, and I is the cross-sectional area moment of inertia about the z axis.

$$M(x,t) = EI(x)\frac{\partial^2 w(x,t)}{\partial x^2} \tag{88}$$

By considering the summation of forces (Eq. 89) and of moments (Eq. 90) on an infinitesimal element (Fig. 25), the shear force V is found to be related to the moment as in Eq. (91) for Euler-Bernoulli beams. The cross sectional area is denoted A and the total external force per unit length is f. In Eq. (90), the rotational inertia of the infinitesimal element is assumed to be very small, which results in the right hand side of the equation being zero. In order to obtain Eq. (91), terms with $(dx)^2$ are neglected, as these are much smaller than the terms which are proportional to dx.

$$\left(V(x,t) + \frac{\partial V(x,t)}{\partial x}dx\right) - V(x,t) + f(x,t)dx = \rho A(x)dx\frac{\partial^2 w(x,t)}{\partial t^2} \tag{89}$$

$$\begin{aligned}\left[M(x,t) + \frac{\partial M(x,t)}{\partial x}dx\right] - M(x,t) \\ + \left[V(x,t) + \frac{\partial V(x,t)}{\partial x}dx\right]dx + [f(x,t)dx]\frac{dx}{2} = 0\end{aligned} \tag{90}$$

$$V(x,t) = -\frac{\partial M(x,t)}{\partial x} \tag{91}$$

Equation (92) gives the final dynamic Euler-Bernoulli beam equation, obtained by substituting Eq. (88) into Eq. (91).

$$\rho A(x)\frac{\partial^2 w(x,t)}{\partial t^2} + \frac{\partial^2}{\partial x^2}\left[EI(x)\frac{\partial^2 w(x,t)}{\partial x^2}\right] = f(x,t) \tag{92}$$

The Euler-Bernoulli formulation is a special case of Timoshenko beam theory. Timoshenko beam elements account for the deformation due to shear and are appropriate for thicker beams. The corresponding relationship between the shear and moment for a Timoshenko beam is given in Eq. (93).

$$V(x,t) = \kappa^2 AG \left[\psi(x,t) - \frac{dw(x,t)}{dx} \right] \qquad (93)$$

In Eq. (93), κ^2 is a dimensionless shear coefficient which depends on the shape of the cross section, and G is the shear modulus. The deformation denoted $\psi(x,t)$ includes the effects of bending and shear deformation. The resulting coupled dynamic beam equations for a Timoshenko beam, including rotational inertia, are given in Eqs. (94) and (95). Note that, for the sake of space, the dependence on x and t is not shown explicitly in Eqs. (94) and (95).

$$\frac{\partial}{\partial x} \left[EI \frac{\partial \psi}{\partial x} \right] + \kappa^2 AG \left(\frac{\partial w}{\partial x} - \psi \right) = \rho I \frac{\partial^2 \psi}{\partial t^2} \qquad (94)$$

$$\frac{\partial}{\partial x} \left[\kappa^2 AG \left(\frac{\partial w}{\partial x} - \psi \right) \right] + f = \rho A \frac{\partial^2 w}{\partial t^2} \qquad (95)$$

Stiffness Matrix for Beam Elements

In order to apply the beam theory in the finite element formulation, one must develop the formulation for a beam element. The formulation of the mass and stiffness matrix for beam elements can be illustrated by examining a two-dimensional beam along the x-axis, disregarding the axial degrees of freedom. This simple beam, shown in Fig. 26, therefore has two nodes, and each node has two degrees of freedom: lateral translation v and rotation θ.

The stiffness matrix for our simple beam can be obtained by applied a unit deformation in each degree of freedom—one by one—and computing the resulting internal forces in the element in order to achieve force and moment balance. For example, if one applies a unit deformation $v_1 = 1$ and zero deformations in the other degrees of freedom, the beam now takes the form of Fig. 27.
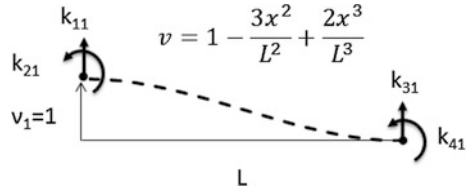
By considering the element as cantilevered at node 2 and loaded by the force k_{11} and moment k_{21} at node 1, in order to obtain the desired deflections, one finds:

$$\frac{k_{11}L^3}{3EI} - \frac{k_{21}L^2}{2EI} = 1 \qquad (96)$$

Fig. 26 Simple 2D beam element

Fig. 27 Deformed simple
beam element

$$\frac{k_{21}L}{EI} - \frac{k_{11}L^2}{2EI} = 0 \tag{97}$$

By solving the set of Eqs. (96) and (97) and requiring force and moment equilibrium, the resulting components of the first column of the element stiffness matrix become $k_{11} = \frac{12EI}{L^3}$, $k_{21} = \frac{6EI}{L^2}$, $k_{31} = -\frac{12EI}{L^3}$, $k_{41} = \frac{6EI}{L^2}$. A similar approach can be used to obtain the full stiffness matrix for this simple example.

For more general beam elements, additional degrees of freedom should be considered. Often, 12 degrees of freedom (6 at each node) are included for beams, and either Euler-Bernoulli or Timoshenko beam theories are used in the development of the stiffness matrix. Furthermore, for more general elements, the stiffness matrix is established based on stress-strain relations, strain-displacement relations, and energy considerations.

An important concept in the more general formulation of the stiffness matrix is the shape function. In order to provide a representation of a continuous function over an element, a polynomial shape function provides a basis for interpolation which is continues and differentiable. For beam elements, a cubic curve is a typical basis for the shape function.

Mass Matrix
There are several ways to formulate the mass matrix for FEA: lumped, consistent, combined, HRZ lumping, or optimal lumping (Cook et al. 2002). A lumped mass model, which places particle masses at nodes, yields a diagonal mass matrix, which is convenient for explicit time domain integration. A consistent mass matrix uses the same shape function as the stiffness matrix. For implicit time domain integration, commonly employed for dynamic analysis of FOWTs, it is less important to obtain a diagonal mass matrix, as non-diagonal terms in the stiffness matrix are also present on the left hand side of the equation. Therefore, it is typical to describe the mass of a beam element using cubic shape functions.

Structural Damping
The damping term in Eq. (86) accounts for the dissipation of energy, which is important for limiting the structural response. Real sources of damping include viscous damping (proportional to velocity), hysteresis damping in the material, Coulomb damping (dry friction), and radiation damping (the generation of waves in another medium such as soil or water). In a FOWT analysis, the hydrodynamic viscous and radiation damping may be accounted for in the damping or excitation loads, but one often also models the remaining "structural" damping through a

small viscous term. Rayleigh damping is a convenient formulation for the structural damping in finite element analysis. The structural damping $\mathbf{B_{Rayleigh}}$ can be specified as a linear combination of the mass and stiffness matrices, as in Eq. (98). (More precisely, the tangential damping matrix is a function of the tangential mass and stiffness matrices.) In Eq. (98), a_1 is the mass-proportional coefficient, and a_2 is the stiffness proportional coefficient.

$$\mathbf{B_{Rayleigh}} = a_1\mathbf{M_g} + a_2\mathbf{K_g} \qquad (98)$$

If global coefficients a_1 and a_2 are used, the Rayleigh damping formulation gives an orthogonal structural damping matrix. Mass-proportional damping is effective for low frequencies, while stiffness-proportional damping is effective for high frequencies. For a floating system, which may have important rigid-body motions, it is typical to set $a_1 = 0$. The damping ratio then becomes a linear function of frequency.

4.3 Modal Methods

As an alternative to finite element methods, modal methods use a reduced number of degrees of freedom. That is, certain structural deformation patterns are defined, and the time-varying structural deformations are found from the sum of a combination of these patterns (or mode shapes). If the mode shapes are determined accurately, modal analysis is reasonably accurate and computationally efficient for wind turbine analysis. The well-known FAST software from NREL is based on a combination of modal and multibody dynamics formulations. Nonlinearity on the load side of the equation can be accounted for, though material nonlinearity (elasto-plastic behaviour) and geometrical stiffening due to large deformations cannot be considered. The key advantage to such analysis is its computational efficiency. An important disadvantage of modal analysis is that it requires accurate pre-processing of the system modes, and can only capture the modes which are identified and included.

An example of modal decomposition is shown in Fig. 28. The fore-aft (FA) tower modes are shown for different frequencies for two different platforms. These modes include the low-frequency surge mode, as well as a mode which is considered platform pitch for the spar and includes bending for the TLP. Although some of the mode shapes are similar, there are differences in the frequencies: even though the tower structure is identical, the base support has a significant effect. In a modal analysis, the displacement of the tower would be computed as a superposition of these modes combined with several side-side and twist modes, such that the tower could easily be modelled with very few degrees of freedom. It is important to note that these frequencies and mode shapes are dependent on the
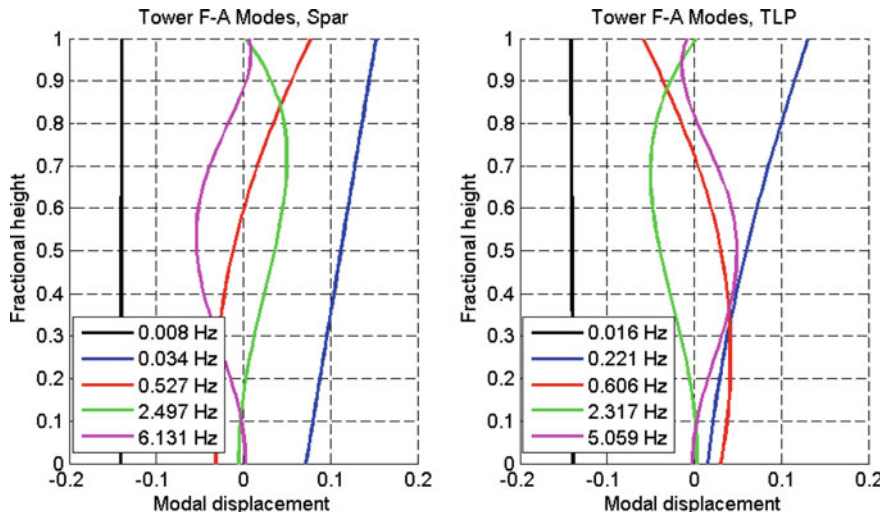
Fig. 28 Fore-aft tower modes of the OC3-Hywind spar and MIT-NREL TLP, computed using BModes (NREL)

substructure which supports the tower and must be recomputed for a new substructure.

The mass, stiffness, and damping matrices for modal decomposition are formulated slightly differently than in a pure finite element formulation, but the same principles for global analysis apply.

4.4 Global Analysis Procedure

Static Equilibrium

Before carrying out any dynamic analyses of a FOWT, one must first determine the deformations and stresses in the structure under gravity, buoyancy, and other constant loads. For a FOWT, the constant loads might include current-induced drag, mean wave drift forces, or mean thrust at a given mean wind speed.

A static equilibrium calculation may be performed by incrementally increasing the applied loads from zero up to their nominal value. During each incremental step, an iterative procedure, such as Newton-Raphson, may be applied. The Newton-Raphson algorithm uses predictor-corrector steps: the displacement under the new loads is computed based on the present tangential stiffness matrix, convergence is checked, and one computes a new tangential stiffness matrix and displacement if convergence criteria are not met. Figure 29 shows the results of a static equilibrium calculation of a spar FOWT.
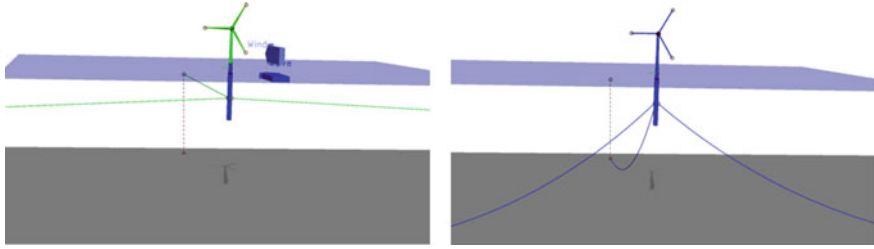
Fig. 29 Spar FOWT before and after static equilibrium calculations (SIMA software, MARINTEK)

Decay and Eigenvalue Analysis

After the mathematical model of the FOWT structure is established and static equilibrium achieved, determining the natural frequencies of the system is an important step.

If the rigid body motions are of primary interest, a decay analysis may be used to establish the damped natural frequencies. In a decay analysis, the structure is displaced in one of the rigid body motions and then allowed to freely return to its equilibrium position. The resulting time series of the displacement can be analysed to determine the damped natural frequencies and the linear and quadratic damping in the model (Hoff 2001).

For flexible structures, however, a more complete eigenvalue analysis may be needed in order to determine the natural frequencies including structural deformations. Some important frequencies in the structural model include the first and second tower bending modes, the collective and individual blade modes, flexural modes within the hull, and for tension leg platform FOWTs, the tendon transverse and axial frequencies.

An eigenvalue analysis is performed by identifying the solutions to the homogeneous, undamped, linearised form of Eq. (86):

$$\mathbf{M_g}\ddot{\vec{D}} + \mathbf{K_g}\vec{D} = \vec{0} \tag{99}$$

for harmonic displacements, $\vec{D} = \ddot{\vec{D}}\sin(\omega t)$. The eigenvector problem then becomes:

$$\left[\mathbf{K_g} - \omega^2\mathbf{M_g}\right]\ddot{\vec{D}} = 0 \tag{100}$$

Equation (100) may be solved for nonzero displacement vectors ($\ddot{\vec{D}}$, the eigenmodes of the structure) in combination with particular frequencies (ω, the eigenfrequencies). If these modes are lightly damped, any excitation at the eigenfrequencies can result in significant and potentially damaging responses. For FOWTs, an important consideration is the interaction between the tower bending frequency and the blade passing (3p) frequency: the tower bending frequency on a

floating platform differs from that of the same tower on a different platform or on land due to the change in the boundary conditions. As such, designers must exercise caution to avoid any potential operations during which the blades provide excitation at the tower natural frequency for the particular platform. This problem may be avoided by modifying the stiffness or mass of the tower and rotor, or by modifying the operation of the turbine.

Time Domain Response Analysis

The majority of the analyses carried out for checking the structural strength of a FOWT are dynamic analyses. That is, the governing FE equations (Eq. 86) are solved step-by-step in time: the response is computed at discrete time instants ($t = \Delta t, 2\Delta t, \ldots, n\Delta t$).

In general, explicit or implicit methods can be used for time integration. An explicit method relies only on historical data to compute the response $\vec{D}_{n+1}$, while an implicit method contains the terms $\dot{\vec{D}}_{n+1}$ and $\ddot{\vec{D}}_{n+1}$ on the right hand side of the equation. Explicit algorithms require a smaller time increment Δt for stability, but the computation for each time step is more efficient. Implicit algorithms require more computational time per step, but fewer total steps (Cook et al. 2002). Furthermore, implicit algorithms are better suited to structural dynamics problems, such as the analysis of FOWTs.

A commonly used family of implicit algorithms is the Newmark-Beta family. The Newmark relations are:

$$\vec{D}_{n+1} = \vec{D}_n + \Delta t \left[\gamma \ddot{\vec{D}}_{n+1} + (1 - \gamma) \ddot{\vec{D}}_n \right] \tag{101}$$

$$\vec{D}_{n+1} = \vec{D}_n + \Delta t \dot{\vec{D}}_n + \frac{1}{2} \Delta t^2 \left[2\beta \ddot{\vec{D}}_{n+1} + (1 - 2\beta) \ddot{\vec{D}}_n \right] \tag{102}$$

where γ and β are numerical factors which control the accuracy, numerical stability, and the amount of algorithmic (numerical) damping (Cook et al. 2002). By applying the Newmark relations to Eq. (86) and eliminating terms including $\dot{\vec{D}}_{n+1}$ and $\ddot{\vec{D}}_{n+1}$, one obtains:

$$\begin{aligned} \mathbf{K}^{\text{eff}} \vec{D}_{n+t} = \vec{R}_{n+1}^{ext} + \mathbf{M_g} \left[\frac{1}{\beta \Delta t^2} \vec{D}_n + \frac{1}{\beta \Delta t} \dot{\vec{D}}_n + \left(\frac{1}{2\beta} - 1 \right) \ddot{\vec{D}}_n \right] \\ + \mathbf{B_g} \left[\frac{\gamma}{\beta \Delta t} \vec{D}_n + \left(\frac{\gamma}{\beta} - 1 \right) \dot{\vec{D}}_n + \Delta t \left(\frac{\gamma}{2\beta} - 1 \right) \ddot{\vec{D}}_n \right]. \end{aligned} \tag{103}$$

The Newmark-Beta algorithm of Eq. (103) is unconditionally stable for $2\beta \geq \gamma \geq 0.5$. Algorithmic damping is introduced for $\gamma > 0.5$, but the accuracy is then reduced from $O(\Delta t^2)$ to $O(\Delta t)$. Algorithmic damping is desirable for dissipating energy in high-frequency components of the response that are related to discretisation, but undesirable for the frequencies of interest (Krenk 2009).

For a linear stiffness matrix $\mathbf{K_g}$, the effective stiffness matrix ($\mathbf{K^{eff}}$) is given by Eq. (104).

$$\mathbf{K^{eff}} = \frac{1}{\beta \Delta t^2} \mathbf{M_g} + \frac{\beta}{\gamma \Delta t} \mathbf{B_g} + \mathbf{K_g} \tag{104}$$

In order to account for geometric nonlinearities, $\mathbf{K_g}$ may be replaced by the tangential stiffness matrix and a Newton-Raphson iteration procedure may be used. As in the static equilibrium calculation, the displacements are computed iteratively during each time step, and the tangential stiffness matrix is updated.

Example: Beam Element Model of a Tension Leg Platform Wind Turbine

Consider the tension leg platform (TLP) FOWT designs in Fig. 30. In order to determine which (if any) of these designs is feasible, how should one carry out an efficient initial screening of the static, extreme, and fatigue loads in the tower and tendons?

A common error in this type of analysis is to begin by building a complete model and simply running a computer program. The first step in global analysis should be a *simple preliminary analysis* which gives insight into the expected results. For TLP FOWTs, a spreadsheet analysis is useful for estimating the natural periods and mean offset. Frequency-domain rigid body analysis can be used to quickly estimate the standard deviations of the motions and tendon tension in many sea states (Bachynski 2014).

After conducting the preliminary simplified analyses and eliminating any problematic designs, one may begin to carefully construct a global analysis model.

One of the first choices that the analyst must make is the *element type* to be used in the model. In the stated problem description, the tendons and tower are of
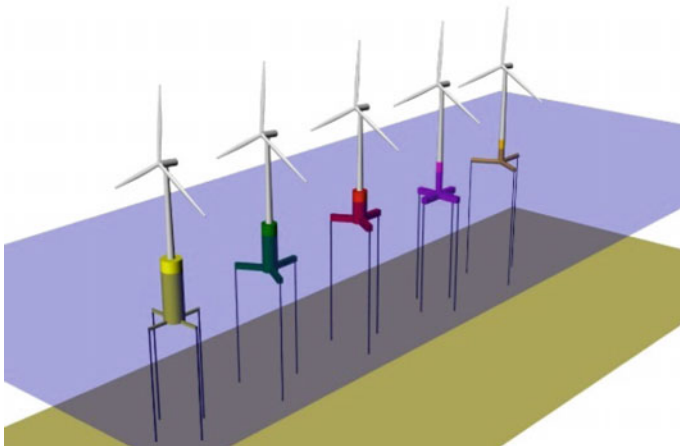
Fig. 30 Tension leg platform wind turbine designs (Bachynski 2014)

interest, so it is logical to choose flexible elements for those components. Beam elements are an appropriate choice, since the tower and tendons are long and slender. The blades are even more flexible than the tower and tendons, so it would be reasonable to model them with flexible beam elements as well. On the other hand, the hull itself is likely to be stiffer than the tower and tendons, so one may consider using a rigid body in order to improve the speed of the simulation. In that case, however, the connection between the hull and tower in the global model should be carefully considered in order to avoid a sudden change of stiffness at the point of interest.

The *boundary conditions* in the model are another important consideration. If the FOWT is anchored to the seabed, what are the boundary conditions at the anchors? How are different elements in the FEA connected to each other? For anchors (or piles), the connection at the seabed depends on the physical conditions. Pinned connections, which allow rotation but not translation, may be appropriate for the tendons if the connection to the soil can be considered relatively rigid. Springs and friction models to represent soil behaviour may be needed for other models. The connection between the tower and the hull may similarly require thought in order to appropriately model the physical structure.

Once the elements of the model are set, the first calculation is to obtain *static equilibrium*. The analyst should not only verify that the still water position of the structure matches his or her expectations, but also that the solution has converged numerically within the chosen tolerances and that the loads in the different components are sensible and in agreement with each other. For the TLP FOWT example, it is especially important to check that the compression in the base of the tower matches the expected weight that should be carried and that the tendon tension values are correct at both the fairlead and the seabed. The output of the computer program should also be understood in light of the finite element model: there may be differences in the reported internal forces and moments based on the shape factors used for the mass distribution.

Before carrying out dynamic analyses in wind and waves, it is also expected that the analyst will carefully *check the model*. Important types of analysis for checking the model include eigenvalue calculation, decay tests, wave-only tests, and wind-only tests. In addition to these checks, one should ensure that the time-stepping parameters are appropriate: the numerical solution should converge at each time step, the results should not change when the time step is reduced, and the amount of numerical damping in the numerical algorithm should be known and understood. The size of the elements should also be investigated. In general, it is recommended to avoid sudden changes in element size, and the element size should be appropriate for the type of element and loading.

After the model has been checked, the analyst will likely perform extensive dynamic analysis. The results of such analyses should be carefully investigated and checked. During the *results check*, one must also *account for the limitations* of the numerical model. For example, buckling loads and the limits of linear material behaviour may occur without the computer program identifying these events. It is the analyst's responsibility to critically examine the results. The limits of the

numerical model may also include the load models themselves: for the TLP FOWTs shown above, ringing loads may be critical, but a hydrodynamic load model for ringing may not be present in all software (Bachynski and Moan 2014).

4.5 Local Finite Element Analysis

Structural failure often occurs due to local stress raisers (welds, doorways, connections). The details of such stress raisers cannot generally be captured in the global finite element analysis. In some cases, a stress concentration factor (SCF) for a given design detail may be tabulated in standards such as DNV-RP-C203, such that the calculated stress in the global model can be related to the local stress. In other cases, the stress concentration factor may be unavailable, or one may simply desire a better understanding of the stress distribution in the material. In those cases, a detailed local finite element analysis may be carried out.

A local FEA may be carried out with boundary conditions provided by the global FEA, or with unit loading in different directions in order to calibrate SCFs for fatigue design. For FOWTs, typical details for local analysis include connections between bracings and columns on semi-submersibles, joints in TLP concepts, fairlead attachment points, and ladders and doors. The extent of the local model should be chosen such that effects due to the boundaries are sufficiently small. An example of stress calculation for a brace-to-column connection is shown in Fig. 31.

If the local analysis is carried out based on the boundary conditions from the global analysis model, it is important to keep in mind that the global analysis is
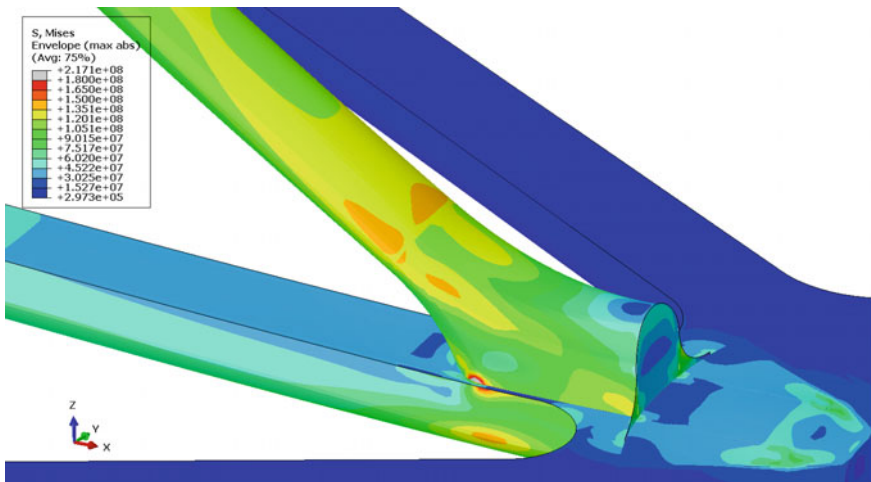
Fig. 31 Local stress in brace connection to column of a semi-submersible wind turbine (Dr.techn. OLAVOLSEN 2012)

unaffected by the local analysis. That is, one should check that the global analysis mesh is sufficiently refined and that the stresses along the cut match between the two analyses. A common problem is that the global mesh is effectively too stiff near joints and cuts, which may lead to underestimation of the local stress.

If the hot spot stress is to be computed using a refined local mesh with unit loading, several different types of elements may be used. For plated structures, thick plate and shell elements (arranged in the mid-plane of the structural components) may be appropriate. 8-noded hot spot shell elements give reliable hot spot stresses at points $0.5t$ and $1.5t$ from the intersection of interest (where t is the thickness) and the stress concentration may be interpolated using an appropriate curve (DNV-RP-C203 2010).

Three-dimensional solid elements are another option, and are well-suited for complex structures. The number of elements required to capture the stress distribution depends on the type of element. For 20-node hexahedral elements, one element over the thickness may be sufficient to capture a linear stress distribution, while four times as many 8-node elements could be required. In the solid element model, the fillet weld will likely be included, which will naturally limit the size of the mesh.

Local finite element analysis is also important for checking the detailed design of plates and stiffeners. Pressure loads (hydrostatic and hydrodynamic) are important for determining initial plate thicknesses and stiffener arrangements for FOWT hulls, while loads due to ship collisions or ice typically require additional local analysis.

5   Review of Numerical Modelling Design Codes

Mairéad Atcheson

The design of FOWTs is a relatively new topic, with only a few prototype FOWT devices deployed in recent years. In order to progress the development of the FOWT industry it is necessary create numerical modelling tools to inform the design process and predict the structural integrity of devices, ensuring the survivability and performance of a device once deployed. A key objective of a FOWT model is to find the net force of a fluid(s) on a structure, to inform the design loads required for structural analysis and detailed design stages (see Sect. 1 of Chapter "Key Design Considerations").

Numerical modelling simulations can be carried out in the time or frequency domain. The decision on which method to use depends on the required model outputs, as method has advantages and limitations. Initial FOWT studies carried out in the frequency domain proved useful in the demonstration of the technical feasibility of FOWTs. However, frequency-domain models are not capable of capturing the nonlinear dynamic characteristics or transient loading events which are important to the dynamic response of FOWTs. Matha et al. (2009) showed that the use of a frequency domain model may lead to natural frequencies being wrongly

predicted because some couplings between the platform motion and the flexible tower and blades were not accounted for these results highlighted the necessity of undertaking FOWT calculations in the time domain. Numerous time domain numerical analysis codes have been developed to simulate the aero-hydro-servo-elastic response of FOWTs, and an overview of many of these design tools is presented in Cordle and Jonkman (2011).

Section 5.1 will provide an overview of some of the design codes currently available for FOWT applications. A number of code comparison studies have also been completed to compare the different codes under development and are presented in Sect. 5.2.

5.1 Floating Offshore Wind Design Codes

Several simulation codes capable of modelling FOWTs are presently under development by FOWT device developers, commercial consultancy companies and research institutes. In general, code developers have approached the task in two manners. Many of the codes were originally developed for the design of onshore wind turbine devices and additional modules have been added to these codes to model floating platforms and mooring systems. Others have approached the task with a code capable of modelling floating platforms, and in this case the developers have included additional modules to represent the wind turbine, including the aerodynamics loading on the support structure and a control module for the turbine.

Design tools capable of modelling FOWTs currently available include (but are not limited to): FAST, SIMPACK, Bladed, SIMA workbench and HAWC2. Table 3 provides an overview of the existing modelling capabilities used by each code to model the structural dynamics, aerodynamics, hydrodynamics and mooring system. For a more complete list of simulation tools used to model FOWTs see Robertson et al. (2014a, b).

A brief description of the different design codes listed in Table 3 are presented in the following section. The description includes some background information on the codes and describes the methods applied to simulate the aerodynamics, hydrodynamics, mooring lines and structural dynamics for FOWTs. The information on the individual code capabilities is based on the most recent version of the code available at the time of writing, however it should be noted that most numerical modelling codes are continuously being developed to expand their capabilities.

FAST (Fatigue, Aerodynamics, Structures and Turbulence) (NREL)
FAST is an open-source design tool capable of modelling the dynamic response of two- and three-bladed horizontal axis wind turbines. It was originally developed by National Renewable Energy Laboratory (NREL) and Oregon State University, but post 1996 further code development has been completed by NREL alone. FAST was originally developed for predicting loads on land-based and offshore

Table 3 Summary table of numerical modelling code capabilities (adapted from Robertson et al. 2014a, b)

Code	Developer	Structural dynamics	Aerodynamics	Hydrodynamics	Mooring model
FAST v8	NREL	T: Mod/MB P: Rigid	(BEM or GDW) + DS	PF + ME	QS
SIMPACK + HydroDyn	SIMPACK	T: Mod/MB P: Rigid	BEM or GDW	PF + QD	QS
Bladed (Advanced Hydro Beta)	DNV GL	T: Mod/MB P: Rigid	(BEM or GDW) + DS	PF + ME + (IWL)	QS
Simo, Riflex + AeroDyn	MARINTEK, NREL	T: FE P: FE	(BEM or GDW) + DS	PF + ME	FE/Dyn
HAWC2	DTU Wind	T: MB/FE P: MB/FE	(BEM or GDW) + DS	ME	FE/Dyn

T turbine, *P* platform. *Mod* modal, *MB* multi-body, *FE* finite element, *BEM* blade element/momentum, *GDW* generalised dynamic wake, *DS* dynamic stall, *PF* potential flow *ME* Morison's equation, *QD* quadratic drag, *IWL* instantaneous water level, *QS* quasi-static, *Dyn* dynamic

bottom-mounted wind turbines, but the code capabilities were extended with additional modules added to permit the modelling of FOWTs. The code comprises of modules representing different aspects of a FOWT to enable coupled nonlinear aero-hydro-servo-elastic analysis in the time domain. Further development of FAST code continues at NREL, with the introduction of a new modularisation framework in FAST v8 (Jonkman 2013). The new modularisation framework supports module-independent inputs and aims to improve numerical performance and robustness, as well as increasing module sharing and code development within the wind energy community. Various modules of FAST have also been coupled with other dynamic analysis programs to model the dynamics of FOWTs (i.e. Simo, Riflex and AeroDyn as presented in Robertson et al. 2014a, b).

FAST v8 incorporates major changes from the previous versions with several new capabilities introduced, most significantly the ability to incorporate new functionalities in the form of modules (Jonkman and Jonkman 2015). All of the modules are open source and available on the NREL website. Figure 32 illustrates the core modules of FASTv8 for floating wind turbine systems.

The wind turbine aerodynamics module (AeroDyn) uses a quasi-static blade element/momentum (BEM) theory with dynamic stall and an optional dynamic inflow theory. The latest version of the code released by NREL is AeroDyn v.15, the source code for version 15 was entirely rewritten to be fully compatible with the FAST modularisation framework (Jonkman et al. 2015a).

Improvements made for the modelling of FOWTs include changes to the hydrodynamic load calculations algorithms in HydroDyn. HydroDyn is a time domain hydrodynamics module. It is capable of modelling the hydrodynamic loading on multi-member structures and can be coupled to FAST v8 or driven as a
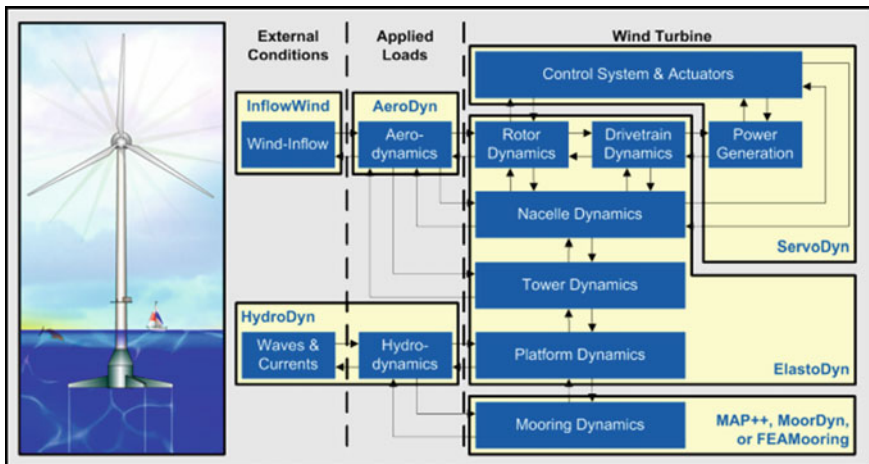
Fig. 32 FAST v8 core modules for floating wind turbine systems (Illustration by Al Hicks, NREL; Flowchart by Jason Jonkman, NREL)

standalone code. HydroDyn can simulate regular or irregular waves and currents and solves for the hydrostatic, radiation, diffraction and viscous loads on the wind turbine platform. Multiple approaches to calculate the hydrodynamic loads on a structure can be applied in HydroDyn, including potential flow theory, strip theory or a hybrid combination of the two. HydroDyn can describe the wave climate using first-order and second-order wave theory, with the option to include directional spreading (Jonkman et al. 2015b).

Different mooring modules are available for use with FAST v8, including a quasi-static mooring line model MoorDyn (Hall 2015) and FEAMooring (Bae 2014) a finite-element based mooring dynamics module. The structural dynamics are simulated using the ElastoDyn module and the control and electrical system can be modelled in the ServoDyn module.

SIMPACK (SIMPACK AG)

SIMPACK is a general purpose multibody system (MBS) code developed by SIMPACK AG, which is used by the automotive, railway, aerospace and robotics industries. SIMPACK Wind provides an extension to the code that allows integrated wind turbine modelling. An interface between the Energy Research Centre of the Netherlands' (ECN) Aero-Module and SIMPACK has also been developed (Bulk 2012). The ECN Aero-Module is a BEM code with advanced correction models and is based on the BEM implementation in PHATAS (Lindenburg and Schepers 2000).

Researchers at Stuttgart's Chair of Wind Energy (SWE) at the University of Stuttgart added an extension to the SIMPACK code to simulate FOWTs. In order to support the simulation of FOWTs in SIMPACK, two hydrodynamic modelling methodologies developed by SWE (SIMorison and SIMHydro Force Elements) were implemented. The SIMHydro module couples HydroDyn to SIMPACK (Matha and Beyer 2013). In order to enable coupling of the codes, the original input file for HydroDyn is modified allowing users to select between the SIMorison and linear hydrodynamics module, and to define the properties of the mooring system.

For mooring systems, SIMorison may be used to model the hydrodynamic loads on mooring lines of FOWTs. The original HydroDyn quasi-static mooring line module is replaced by an MBS-mooring-line model where each line is discretised into separate rigid or flexible bodies connected by spring-damper elements (Matha et al. 2011). The MBS representation implemented by SIMPACK enables a large number of structural configurations and degrees of freedom to be modelling, including flexible FEM bodies of arbitrary geometry. Drivetrain models can also be implemented to account for flexibility of the mounting plate and other components.

Bladed (DNV GL)

Bladed is a commercial software package originally developed for on-shore fixed bottom mounted wind turbines by DNV GL (previously Garrad Hassan), but has more recently been extended to model FOWTs. The Bladed package provides integrated modelling of floating wind turbine platform motions along with blade and platform dynamics, wind and wave loading and controller actions.

The Bladed software uses a modal representation to model the structural dynamics of a wind turbine. This approach is accurate, reliable and well validated for onshore fixed wind turbines, however for FOWTs additional modelling issues arise. Further developments of Bladed introduce a new multibody code, which enables a structure to be modelled in a number of separate bodies, each with separate properties and coupled together using the equations of motion (Cordle 2010).

Aerodynamic forces on a rotor are calculated using a combined blade element and momentum model, including tip and hub losses based on Prandtl's method. The dynamic wake model used within Bladed is based on the work of Pitt and Peters, and the Beddoes model has been adopted to account for dynamic stall (Bossanyi 2003). Two hydrodynamic models are available within Bladed, the Morison's equation approach and a panel method (Buils Urbano et al. 2013). A fully dynamic mooring line model, which uses multibody dynamics to represent the mooring lines has also been developed in Bladed, further details of the modelling approach adopted can be found in Buils Urbano et al. (2013). Figures 33 and 34 illustrate screenshots of a FOWT being modelled in Bladed.

SIMA Workbench (MARINTEK)

SIMA is an integrated simulation workbench for MARINTEK's software suite for the analysis of marine operations and floating systems. The SIMA workbench includes numerical codes developed at MARINTEK, including SIMO and RIFLEX which can be coupled to determine the dynamic behaviour of a floating platform. SIMO (Simulation of Marine Operations) is a general-purpose time domain program for the modelling of offshore structures. RIFLEX is a nonlinear finite element model (FEM) code used to model the static and dynamic analysis of slender marine
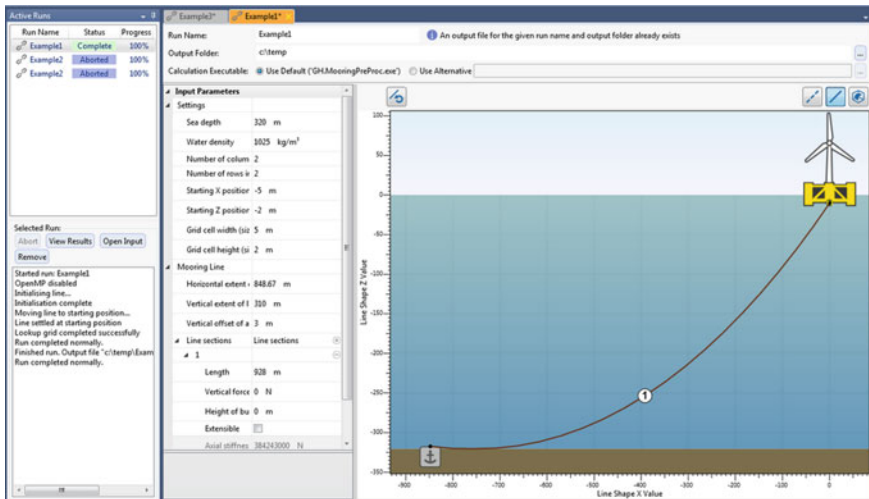
Fig. 33 Screenshot of a FOWT example in Bladed (courtesy of DNV GL)
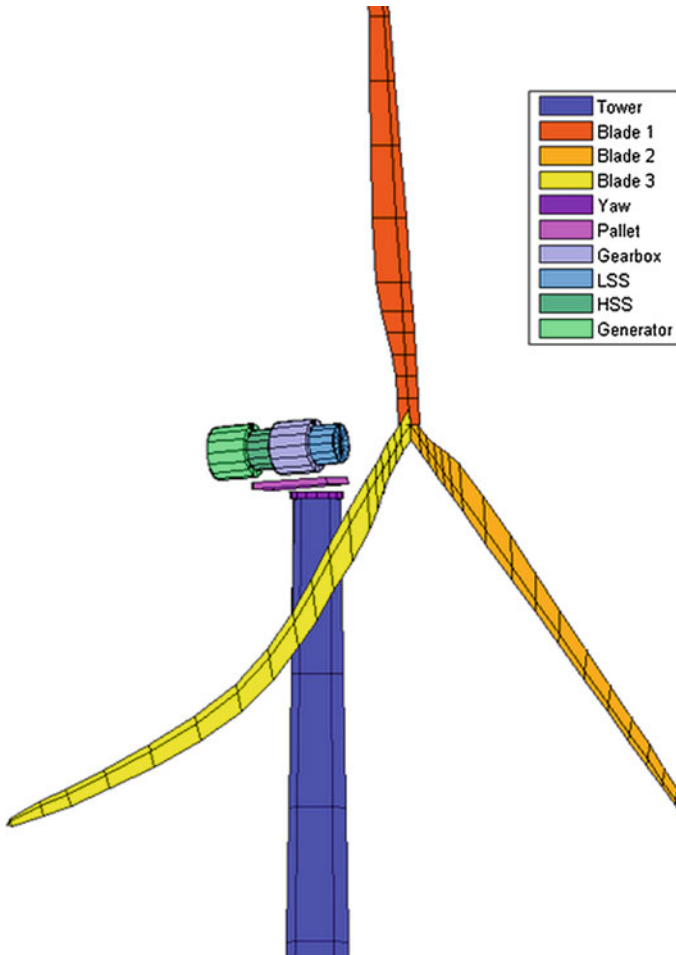
Fig. 34 Screenshot of a turbine configuration in Bladed (courtesy of DNV GL)

bodies, such as risers and mooring lines, as well as wind turbine blades and towers. SIMO and RIFLEX can be coupled to take advantage of all of the hydrodynamic and structural options in order to model FOWTs, both in operational conditions and during the installation process. Figure 35 illustrates a screenshot of a semi-submersible FOWT example in SIMA.

The aerodynamic forces in the SIMA workbench are calculated using BEM theory, including dynamic stall and dynamic wake corrections. The hydrodynamic forces on large-volume rigid bodies are modelled using the standard SIMO code, taking into account linear and quadratic potential forces, while slender flexible elements may be subjected to hydrodynamic loads from Morison's equation.
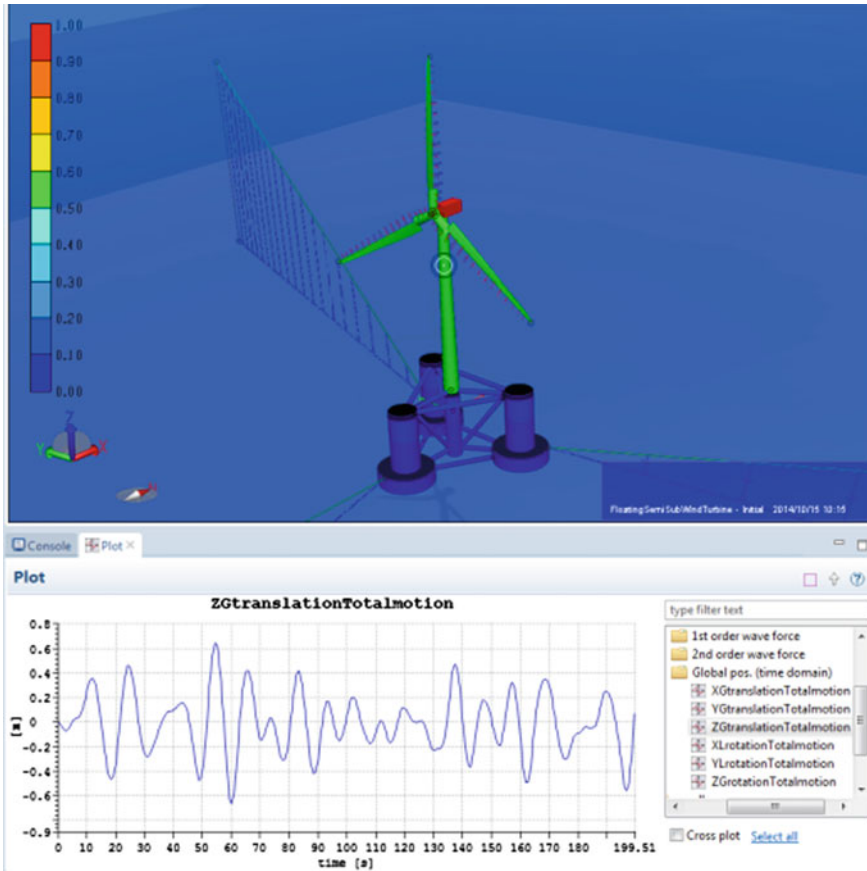
Fig. 35 Semi-submersible wind turbine modelling in SIMA (courtesy of MARINTEK)

Irregular wave time series with first or second order Stokes' waves kinematics may be applied, while turbulent wind time series are read from files generated by programs such as TurbSim or IEC Turbulence Simulator. The coupling scheme is numerically stable due to the use of a single structural solver, and both user-defined and internal options for the wind turbine control system are included. SIMA is continually validated against hydrodynamic model tests, and has been benchmarked against other simulation tools for FOWTs (Ormberg and Bachynski 2012; Jonkman et al. 2010; Aksnes et al. 2015).

SIMO/RIFLEX with HAW2 (MARINTEK and DTU)

HAWC2 (Horizontal axis wind turbine code 2nd generation) is an aero-elastic simulation tool for the dynamic analysis of fixed bottom mounted wind turbines, subjected to aerodynamic loads and control action. The code was mainly developed between 2003 and 2007 by the Aeroelastic Design Research Program at the Technical University of Denmark (DTU), Department of Wind Energy at the Risø

Campus in Denmark, but it is continuously updated and improved (Larsen and Hansen 2015). HAWC2 is part of the commercially available codes from DTU Wind Energy.

The HAWC2 code consists of models describing the environmental conditions (wind, waves and soil), applied loads (aerodynamics, hydrodynamics and soil models), structural dynamics and control system. The structural formulation of the code is based on a multibody system using Timoshenko beam elements. The aerodynamic forces on the rotor are calculated using BEM theory. The code has also been extended to include dynamic inflow, dynamic stall, skewed inflow, shear effects on induction and effects from large deflections. The wind turbine can be controlled through external DLL's (Dynamic Link Library) that operates the system under different conditions.

The SIMO/RIFLEX code has been coupled with the HAWC2 code in Skaare et al. (2007) to simulate the response of a FOWT. The two independent codes were coupled and each program was used for modelling separate parts of the FOWT system. The HAWC2 code modelled the rotor and nacelle, and the mooring lines and submerged hull of the platform were modelling in SIMO/RIFLEX. More recently Bellew et al. (2014) presented an extension of the HAWC2 code with a special external system the reads output files directly generated by WAMIT and generates a system with the same response, named by the authors the HAWC2-WAMIT model.

5.2   Code Comparison Studies

The majority of codes have yet to be validated due to a lack of available FOWT data. In order to compare and verify offshore wind turbine design codes an international collaborative effort was established to perform code-to-code comparisons. The Offshore Code Comparison Collaboration (OC3) was established within Subtask 2 of the International Energy Agency (IEA) Wind Task 23 Offshore Wind Technology and Deployment (Jonkman and Musial 2010). The OC3 project was an international forum for offshore wind energy software developers to compare their design codes, which took place between 2005 and 2009. The objectives of OC3 were to examine simulation accuracy and reliability, investigate the capability of theories currently implemented by models and to identify further research and development requirements. OC3 was divided into four different phases, each representative of a different wind turbine support structure:

- Phase I: NREL 5 MW wind turbine on a monopile and rigid foundation in 20 m of water.
- Phase II: Monopile and flexible foundation—the same foundation as Phase I with different models to represent soil/pile interactions.
- Phase III: NREL 5 MW wind turbine on a tripod structure in 45 m of water.
- Phase IV: NREL 5 MW wind turbine on a floating spar buoy in deep water (320 m), the OC3-Hywind spar buoy (Jonkman 2010).

The results from OC3 are summarised in Jonkman and Musial (2010), with additional papers published summarising the results from each phase of work (Passon et al. 2007; Jonkman et al. 2007, 2010; Nichols et al. 2008). Further research needs identified in OC3 triggered a follow-on project which was established under the IEA Wind Task 30 to continue the work that had begun in Task 23. The Offshore Code Comparison Collaboration, Continued (OC4) started in 2010 through to 2013. The OC4 project was split into two work packages, and similar to OC3, all simulations used the NREL 5 MW offshore turbine but the turbine support structures differed for each phase:

- Phase I was led by Fraunhofer-IWES and focused on the verification of simulation codes for jacket-supported fixed bottom structure in 50 m of water. The reference jacket structure design was based on that used in work package 4 of the UpWind project (Vorpahl et al. 2011).
- Phase II was led by NREL and focussed on comparing codes used to model a floating semisubmersible in 200 m of water. A semi-submersible floating offshore wind system developed for the DeepCwind project (Goupee et al. 2012) was modelled.

The OC3 and OC4 projects were performed through technical exchange among a group of international participants from universities, research institutions and industries across the United States of America, Germany, Denmark, the United Kingdom, Spain, the Netherlands, Norway, Sweden and Korea. Two additional countries participated in the OC4 project, Portugal and Japan. Figure 36 illustrates the offshore wind turbine configurations modelled in the OC3 and OC4 projects.

The modelling of offshore wind turbine models under stochastic aerodynamic and hydrodynamic loading is a complex process. In order to conduct a fair comparison between OC3 and OC4 participant models, the model inputs were controlled and a stepwise approach to simulation load cases was applied, increasing complexity one step at a time. The NREL offshore 5 MW wind turbine (including control system) (Jonkman et al. 2009) was chosen as the wind turbine model for all simulations.

In order to compare the results obtained by different modelling codes, a range of different load cases simulations were performed for a variety of cases with increasing complexity (i.e. wind only, wave only, wind and wave combined). The simulation output parameters were also prescribed and included: loads and deflections from the rotor blade, tower and drivetrain and generator; platform displacement; mooring system (tension) and the environmental conditions (wind and waves). Results from OC4 Phase 1 for coupled simulations of an offshore wind turbine with jacket support structure are published in Popko et al. (2012) and OC4 Phase II results regarding a floating semisubmersible wind system are published in Robertson et al. (2014).

An extension of the IEA Wind Task 30, OC5 (Offshore Code Comparison Collaboration, Continued, with Correlation) is currently underway and will continue until 2018. The OC5 project consists of three phases examining different offshore wind turbine systems: monopiles, semi-submersibles and jacket/tripod.
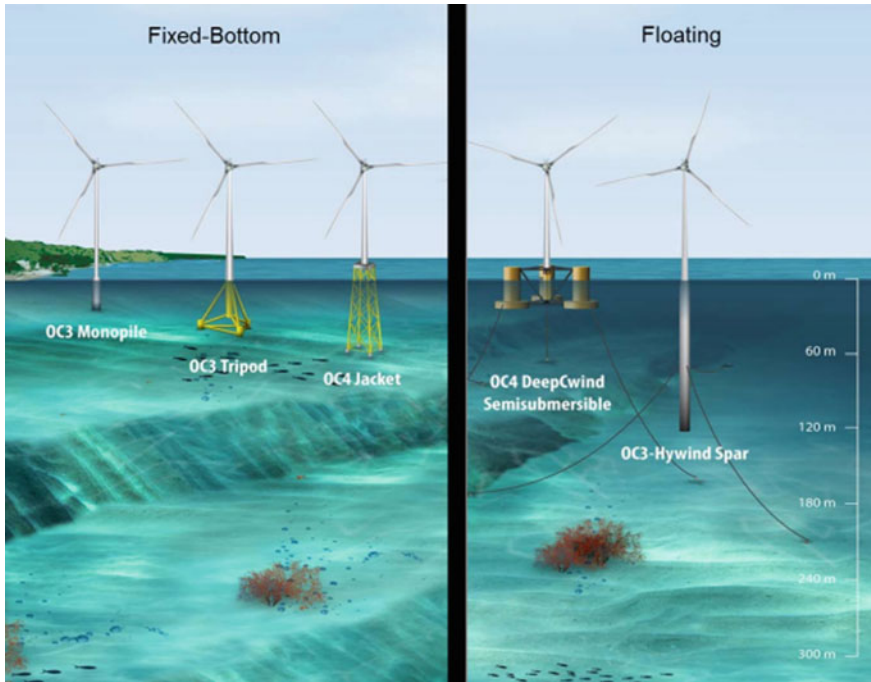
Fig. 36 Offshore wind turbine system systems modelled in OC3 and OC4 (illustration by Joshua Bauer, NREL)

A set of experimental tests is conducted within each phase. Phase one examines monopiles and two tank testing campaigns will be conducted to obtain experimental data, phase 2 focuses on semisubmersible tank tests and phase 3 will involve open ocean testing.

6 Floating Wind Turbine Tank Testing

Andrew J. Goupee, **Sébastien M. H. Gueydon** and
Amy N. Robertson

6.1 Model Testing: An Overview

Wave basin model testing is a refined science that is commonly used to test designs of large scale offshore vessels and structures by the oil and gas, military, and marine industries (e.g. see Chakrabarti 1994). A basin model test can be advantageous

compared to a full-scale, open-ocean test as it requires less time, resources and risk, while providing real and accurate data on system global response. However, even though basin testing is well refined for many types of offshore configurations, protocol for properly modelling coupled wind and wave loads on a FOWT in a wave basin test environment have started to take shape only recently.

Floating wind turbines are complex structures with numerous variables contributing to their complicated dynamic behaviour. Simultaneous wind and wave loading, turbine aerodynamics and control methods, and flexible structural components make execution of an accurate scale model test a significant challenge. Performing meaningful tests in a basin requires overcoming many challenges. Chief among them is the desire to preserve the Froude number for the hydrodynamics and Reynolds number for the aerodynamics at model scale, which cannot be done simultaneously. Ultimately, Froude scaling is required to perform a floating body model test and the Reynolds number must be significantly reduced, and as a result, aerodynamic performance of a Froude-scaled rotor suffers greatly. Other difficulties include creating quality wind environments in a wave basin without interfering with the waves and assembling a sufficiently functional model wind turbine with the appropriate mass and structural properties at small scales.

Despite the aforementioned difficulties, several floating wind turbine basin model tests have been performed (e.g. see Nielsen et al. 2006; Roddier et al. 2010; Windsea AS 2010; Ren et al. 2012). Each of these model tests provided valuable information to respective stake holders and advanced knowledge of floating wind turbine dynamics. However, the methodologies and techniques used during these model tests differed significantly, with many of the tests simplifying the turbine and associated aerodynamics. These tests do not provide the necessary information to fully investigate the coupled dynamic behaviour of FOWTs nor do they provide a comprehensive enough data set to validate the computer-aided-engineering tools used to design the systems.

In an effort to overcome these shortcomings, research was performed by the DeepCwind Consortium to advance model testing techniques for floating wind turbines as well as to generate data for use in validating computer-aided-engineering tools for these systems. These tests, which were conducted in 2011, enlightened researchers on the unique coupled dynamic behaviour of floating wind turbines (e.g. see Weller and Gueydon 2012) and have laid the foundation for further advancements in model testing techniques (e.g. see Gueydon and Fernandes 2013; Huijs et al. 2014; Kimball et al. 2014; de Ridder et al. 2014) and numerical model validation (e.g. see Browning et al. 2012; Stewart et al. 2012; Prowell et al. 2013; Coulling et al. 2013; Robertson et al. 2013) for these complex floating systems. The 2011 DeepCwind model test program constituted a major step in the evolution of FOWT model testing, and as such, the remainder of this section reviews the design, execution and results obtained from these pioneering tests.

6.2 Case Study: DeepCwind Testing at MARIN

The DeepCwind consortium is a group of universities, national labs, and companies funded under a research initiative by the U.S. Department of Energy to support the research and development of floating offshore wind power. The two main objectives of the project are to better understand the complex dynamic behaviour of floating offshore wind systems and to create experimental data for validating the tools used in modelling these systems. In support of these objectives, the DeepCwind consortium conducted a model test campaign in 2011 of three generic floating wind systems: a tension-leg platform (TLP), a spar buoy and a semi-submersible platform. Each of the three platforms was designed to support a 1:50 scale model of a 5 MW wind turbine and was tested under a variety of wind/wave conditions.

The DeepCwind experiments were hosted by the Maritime Research Institute of The Netherlands (MARIN), one of the leading hydrodynamic testing laboratory for the maritime and offshore industries. MARIN supports projects from the design phase to the operational phase through simulations, model tests and full-scale measurements. In 2009, MARIN had formed a team to support the development of marine renewable energy (MRE). The main motivation of MARIN in hosting the DeepCwind consortium was to quickly develop a unique knowledge and expertise in testing FOWTs in combined waves and wind in a basin. This project, and following research activities on FOWTs, resulted in the development of state-of-the art techniques for performing model tests of these structures. Chief among them was the development of a methodology to scale down the rotor of a wind turbine in such a manner that appropriate aerodynamic forces can be achieved with active blade pitch control in the Froude-scaled wind environment of the wave basin.

Model Testing Approach

To perform tests oN a FOWT in a wave basin, the system must be scaled to a size that can fit in the basin, with an appropriately scaled wind and wave environment. For offshore structure testing, a Froude scaling approach is typically employed, which means that the Froude number (ratio of inertia to gravity forces) does not change in the scaling. However, the drawback of following Froude scaling is that the Reynolds number is not maintained in the process. The incompatibility between Froude scaling and Reynolds number causes errors in modelling the fluid-structure interaction. One way to address this challenge is to use a hybrid testing approach, where the wind turbine is not modelled at all. Instead, either a fan or some other actuator is placed at the top of the tower to emulate the thrust force produced by the wind turbine. The DeepCwind program considered utilising a hybrid testing approach, but this approach does not capture all of the dynamics present in an offshore wind system and appeared to defeat the objective of providing a comprehensive dataset for model validation. Therefore, the choice was made to create a

fully-functional wind turbine model and test it under Froude-scaled conditions in a wave basin equipped with wind generation capabilities. This choice presented new challenges for testing wind turbines in Froude-scaled wind environments that had to be overcome to conduct a successful model test program.

Aside from choosing to physically model the wind environment and turbine, care was taken to design a test program that would provide data that would be well suited to understanding the unique behaviours of FOWTs as well as provide data ideal for computer-aided-engineering tool validation studies. A program was selected to study three different platforms, each based on viable offshore oil and gas platform technology with vastly different means for achieving stability (see Sect. 1 of Chapter "Overview of Floating Offshore Wind Technologies"). The test program was also crafted to build step-by-step, from very simplistic tests to complex coupled dynamic wind and irregular wave environments. Tests types included static offset tests, hammer tests, free-decay tests, wind only tests (steady and dynamic), wave only tests, (regular and irregular), and combinations of wind and wave environments, some with turbine yaw errors. This choice to systematically build the complexity of the test environment helped to single out the root cause of unique coupled response behaviours, as well as facilitated the identification of weaknesses in computer-aided-engineering tools during validation studies.

Froude Scaling Overview

Offshore platform wave basin tests are typically scaled using Froude number and geometric similarity. Although a Froude model does not scale all parameters properly, the dominant factors in the hydrodynamic problem, gravity and inertia, are appropriately scaled (Chakrabarti 1994). For a FOWT, this covers most properties of interest which influence the global dynamic response of the system, excepting the aerodynamic wind forces. This approach also allowed for consistent scaling of the tower bending frequency, which was critical for ensuring the proper coupling between the wind turbine and floating platform response.

Employing a Reynolds number scaling scheme, common for model aerodynamic experiments, is impractical for a floating body subjected to wave forcing. Therefore, Froude scaling is best suited for model testing of floating wind turbines. The Froude number for a free surface wave is:

$$Fr_{wave} = C/\sqrt{gL} \tag{105}$$

where C is the wave celerity, or propagation speed, g is the local acceleration due to gravity and L is a characteristic length.

The scaling relationship maintained from model scale to the full-scale prototype is expressed as:

$$Fr_p = Fr_m \qquad (106)$$

where p and m stand for prototype (full-scale) and model scale, respectively. Defining the scale parameter λ as the ratio of the prototype to model length scales, one can determine the scaling factors for Froude-scaled testing in Table 4.

Wave Basin

The DeepCwind testing campaign was carried out in the Offshore Basin of MARIN. This basin offers a number of unique possibilities for the modelling of current, waves and wind. The basin measures 46 m × 36 m and has a movable floor, which is used to adjust the water depth. The maximum water depth measures 10 m at model scale. The basin also has a deep pit, with a maximum depth of 30 m. For these tests, the scale was 1:50 and the floor of the basin was lifted to 4 m below the still water line, corresponding to a water depth of 200 m at full scale. The dimension of the basin made it possible to model all mooring systems of the 3 floating wind turbine concepts without truncation. Wave generators are positioned at two adjacent sides of the basin and consist of hinged flaps. Each segment has its own driving motor, which is controlled separately. The wave generators are able to simulate various wave types, such as short crested wave patterns. The system is equipped with compensation of wave reflection from the model and the wave absorbers. A plan view of the basin is shown in Fig. 37.

Table 4 Scaling factors for floating wind turbine model testing

Parameter	Scale factor
Length (e.g. displacement, wave height)	λ
Area	λ^2
Volume	λ^3
Angle	1
Density	1
Mass	λ^3
Time (e.g. wave period)	$\lambda^{0.5}$
Frequency (e.g. rotor rotational speed)	$\lambda^{-0.5}$
Velocity (e.g. wind speed, wave celerity)	$\lambda^{0.5}$
Acceleration	1
Force (e.g. wind, wave, structural)	λ^3
Moment (e.g. structural, rotor torque)	λ^4
Power	$\lambda^{3.5}$
Area moment of inertia	λ^4
Mass moment of inertia	λ^5
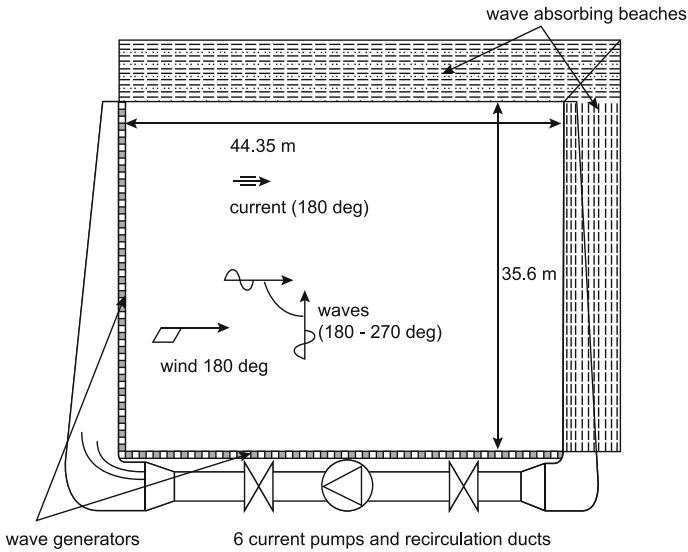
**Fig. 37** Top view of the offshore basin of MARIN

Regular and irregular waves in combination with wind were applied to the three different wind turbine floaters during the test program. Design waves (100-year condition) in combination with and without constant wind were applied to test the behaviour of the floaters in extreme conditions. Operational waves (operational wave and 1-year wave condition) with and without constant wind were applied to investigate the responses of the floaters in operational conditions. These were also repeated in combination with a stochastic wind, to investigate the dynamic coupling between the wind turbine and the floater. Furthermore, tests in regular and white noise waves with and without wind were performed to develop response amplitude operators (RAOs) that show the general wave response behaviour of the systems.

The requested wave conditions were calibrated without the models present in the basin prior to the actual model tests for duration of 3.5-h full-scale. The generated waves were measured by two immobile wave probes and three wave probes around the centre line of the floaters. Since the wave realisations might be different at different locations in the basin the waves were calibrated at the expected mean location of the floaters during the tests. Waves were generated in two directions in the basin representing the 180° and 225° wave directions. Figure 38 shows the comparison of a calibrated wave and requested theoretical waves for survival conditions.

Wind Generation

A major challenge for the DeepCwind model test campaign was the issue of manufacturing a quality Froude scale wind environment for the wind turbine to operate in. The wind environment was to be of a high quality with little evidence of fan generated swirl and low turbulence intensity. This required a dedicated wind

Fig. 38 Spectral density of the design wave (measured spectrum in *plain line* against the theoretical spectrum in *dashed line*)
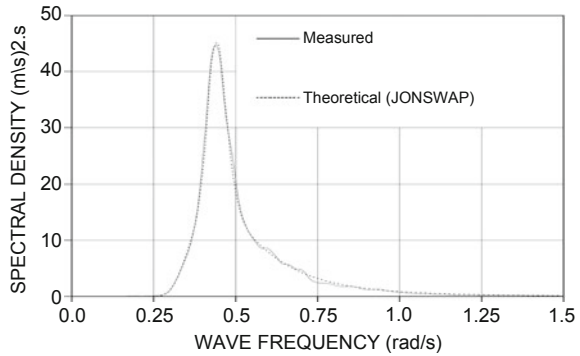
generator consisting of a series of fans and screens, as well as a contracting nozzle. In addition, the output area of the nozzle needed to cover the entire wind turbine rotor in quality wind, even as the floating system moved through its expected range of motion. Therefore, a large wind generation system was ideal. However, too large a system would be impractical as it would be very costly to build, maintain and operate. Therefore, a balance was struck in choosing a size for the model wind turbine and wind generation system. A scale parameter of $\lambda = 50$ was chosen and dictated the size of the wind generation system to permit testing of a 1:50 scale 5 MW wind turbine.

An exploded image of the wind generation machine, which utilised a bank of 35 fans, honeycomb screens and a contracting nozzle is shown in Fig. 39. An image of the wind machine as installed in the basin is given in Fig. 40. As shown in the figure, the wind machine was suspended from an aluminum frame affixed to the ceiling that allowed the scaled 100-year extreme waves to pass underneath the wind machine unimpeded. The outlet of the nozzle was elliptical in shape with full-scale dimensions of 200 m in width and 150 m in height. These dimensions ensured reasonably good wind coverage for the 1:50 scale model rotor which possessed a 126 m rotor diameter at full scale. The wind machine was rotated down 2.16° to better cover the rotor area at the test section 225 m downwind as lowering the wind machine further would have impeded passage of the waves.

Within the projected area of the nozzle, the turbulence intensity was approximately 3–5 % with little to no observed swirl. At locations outside of nozzle outlet, the turbulence intensity rose significantly to 11–40 % depending on location. Spatial uniformity of the wind field over a majority of the rotor area was fairly good, as shown in Fig. 41. Uniformity was poorest at the bottom of the rotor plane as it was the point on the rotor nearest the boundary of the of the wind machine outlet nozzle. For temporally dynamic winds, which were used extensively in the DeepCwind test campaign, the wind generation machine yielded wind spectra at hub height very close to the target NPD[2] spectrum as shown in Fig. 42.
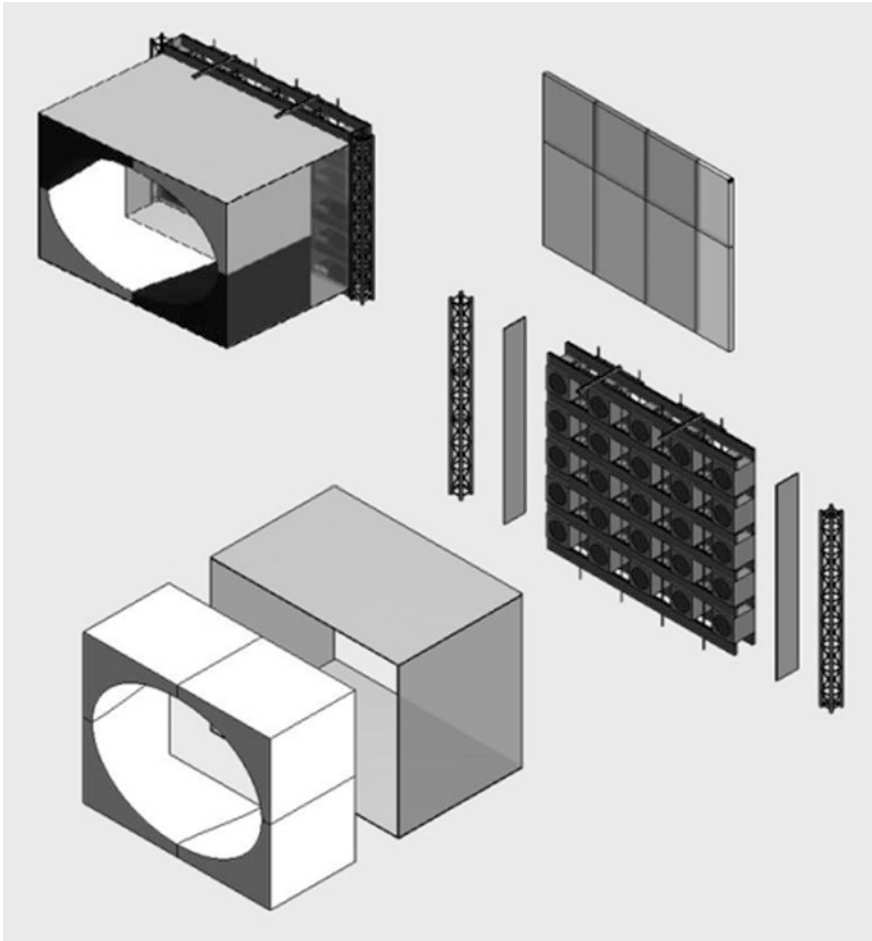
---

[2]Norwegian Pertoleum Directorate.

Fig. 39 Exploded view of MARIN offshore basin wind generation machine

Wind Turbine and Tower

For the model tests, the horizontal-axis wind turbine chosen for scale model construction was the National Renewable Energy Laboratory (NREL) 5 MW reference wind turbine (Jonkman et al. 2009a, b). An image of the scale model wind turbine, which employs geometrically-scaled blades as is customary for strict Froude scaling, is shown in Fig. 43. The wind turbine possessed a 126 m rotor diameter and was located with a hub height of 90 m above the still water line (all values are given at full-scale rather than model scale). The flexible tower, which began 10 m above the still water line, was designed to emulate the fundamental bending
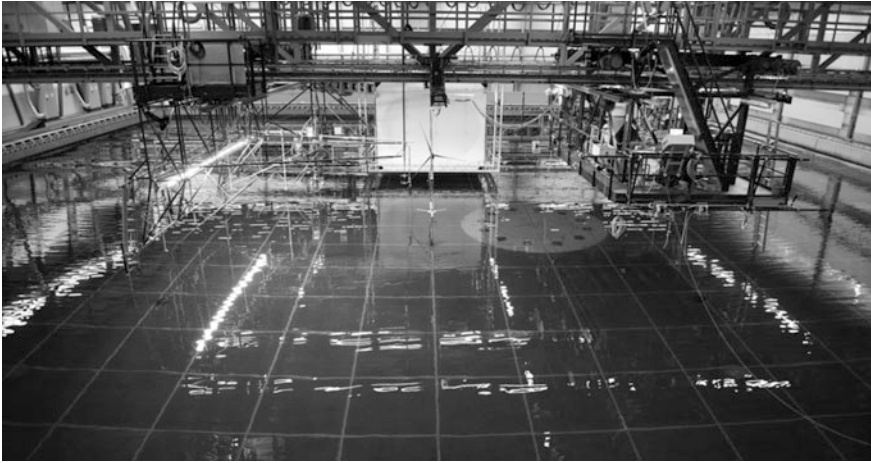
Fig. 40 Wind machine installed in MARIN offshore basin for DeepCwind model tests

Fig. 41 Normalised mean wind velocity at rotor plane
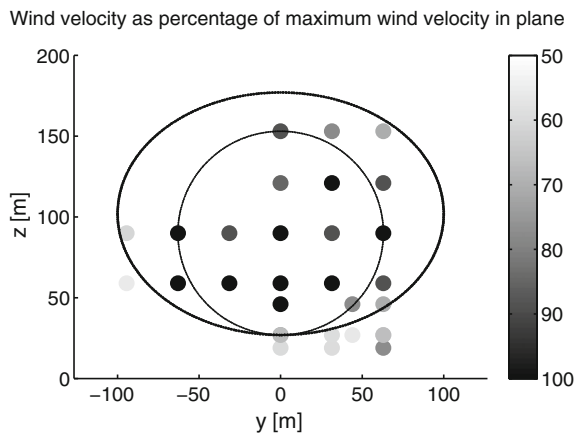
frequency of the OC3 Hywind tower (Jonkman 2010a, b). The wind turbine deviates from the standard NREL 5 MW reference wind turbine in a few notable areas (Martin 2011). For the model wind turbine, the shaft tilt was 0°, the blade precone was 0° and the blades were for all practical purposes rigid. The last difference was the result of two factors. First, fabricating the 17.7 t blades at 1:50 scale requires a very light woven carbon fiber construction which is inherently stiff. Second, eliminating the added aeroelastic dynamic phenomena associated with a flexible rotor was deemed to be desirable as these effects were perceived as being beyond the scope of these tests. To mimic the first bending frequency of the OC3 Hywind tower, the tower was constructed from specifically sized aluminum tubing.

Fig. 42 Comparison of
theoretical target and
achieved wind spectrum at
hub height for a mean wind
speed of 16.98 m/s at 10 m
above the still water line
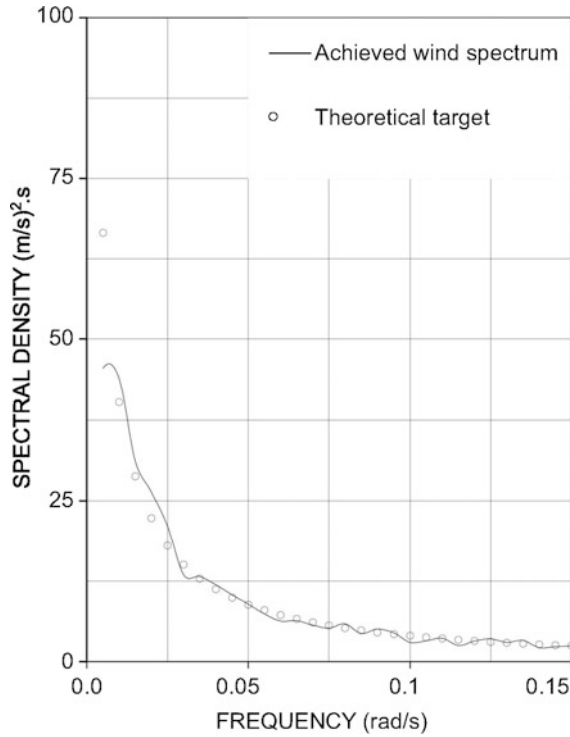
Furthermore, the lower 11.3 m of the tower was of a larger diameter than the
remainder of the tower in order to more closely match the OC3 Hywind tower
center of gravity and fundamental bending mode shape. The total topside mass,
which included the wind turbine, tower and all accompanying instrumentation, was
699.4t. This value was 16.6 % larger than the standard specifications for the NREL
5 MW Reference Wind Turbine and OC3 Hywind tower.

As a fundamental step in the floating wind turbine model testing program, fixed
base testing of the scale model wind turbine was performed in order to characterise
the aerodynamic behaviour of the model NREL 5 MW reference wind turbine in a
Froude-scaled environment. The performance of the turbine was characterised by
two parameters: the power coefficient C_p and thrust coefficient C_T. These
non-dimensional quantities are computed as:

$$C_P = \frac{P}{\frac{1}{2}\rho U^3 A}, \quad C_T = \frac{T}{\frac{1}{2}\rho U^2 A} \tag{107}$$

where P is the rotor power, T is the rotor torque, ρ is the density of the air and A is
swept area of the rotor. To obtain the C_p and C_T test data, the rotor power and

Fig. 43 Image of 1:50-scale model wind turbine used in DeepCwind model test campaign

torque were measured from the model at various rotor speeds which are expressed in a non-dimensional form as the tip-speed ratio *TSR*:

$$TSR = \Omega r / U \tag{108}$$

where Ω is the rotor rotational speed and r is the blade tip radius. The results of the testing, in addition to the theoretical full scale performance as computed from NREL's coupled aero-hydro-servo-elastic wind turbine simulator, FAST (e.g. see Jonkman and Buhl 2005), is given in Fig. 44. As is evident from the figure, the model rotor aerodynamic performance is markedly lower than the theoretical prototype performance, particularly for the performance coefficient. The poor performance stems from designing the turbine based on Froude-scaling techniques, which did not address the change in performance of the turbine at lower Reynolds numbers resulting from the scaling approach.

To compensate for the low turbine performance, alterations were made to the wind environment in order to correctly scale the dominant aerodynamic thrust force as it has a far greater influence on the global motions of the FOWT than does the aerodynamic torque. To achieve the correct aerodynamic thrust force, the operating wind turbine required wind speeds that were approximately 80 % greater than dictated by strict Froude scaling. A graphical depiction of how this process was executed is given in Fig. 45.

Fig. 44 Comparison of ideal prototype rotor aerodynamic performance and realised model rotor aerodynamic performance
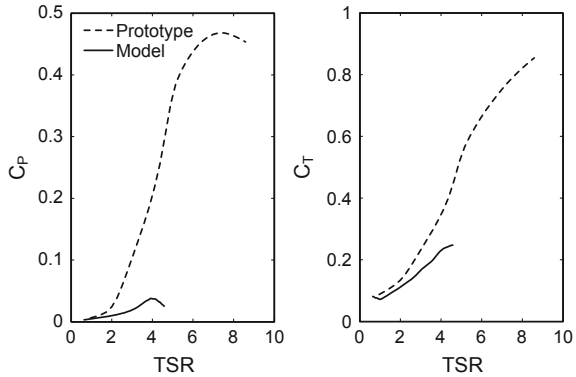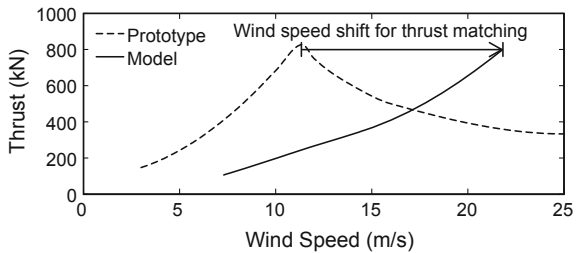

Fig. 45 Illustration of increase in wind speed required to match prototype and model mean thrust for the DeepCwind wind turbine

Corrective Measures Devised Since DeepCwind Test Campaign

Subsequent to the 2011 DeepCwind testing at MARIN, efforts were undertaken to redesign a turbine to better match the performance of the NREL 5 MW reference turbine. Methods were developed and tested which employed low-Reynolds number-specific airfoils, marginally larger chord lengths and slightly diminished angles of attack to mimic the thrust response of the NREL 5 MW in a Froude-scale wind environment.

The culmination of this work resulted in a performance-matched wind turbine produced by MARIN in 2013, the MARIN stock wind turbine. The turbine is shown in Fig. 46 atop the DeepCwind semi-submersible platform which was re-tested in 2013 after the initial tests focused on in this chapter. The creation of this turbine started with the design basis outlined in Martin et al. (2014), but modified and optimised the blade section shapes for both manufacturability and performance using a series of computational fluid dynamics and BEM theory design tools. The turbine used low-Reynolds number airfoil sections and chord lengths that were 125 % of the NREL 5 MW reference turbine, resulting in a turbine that produced the correct blade lift forces at lower lift coefficients than found on the full-scale prototype. The MARIN stock wind turbine also improved the power output as compared to the original scaled turbine, that while still not up to the target 5 MW, was large enough to perform realistic active blade pitch control experiments that focused on regulating power.
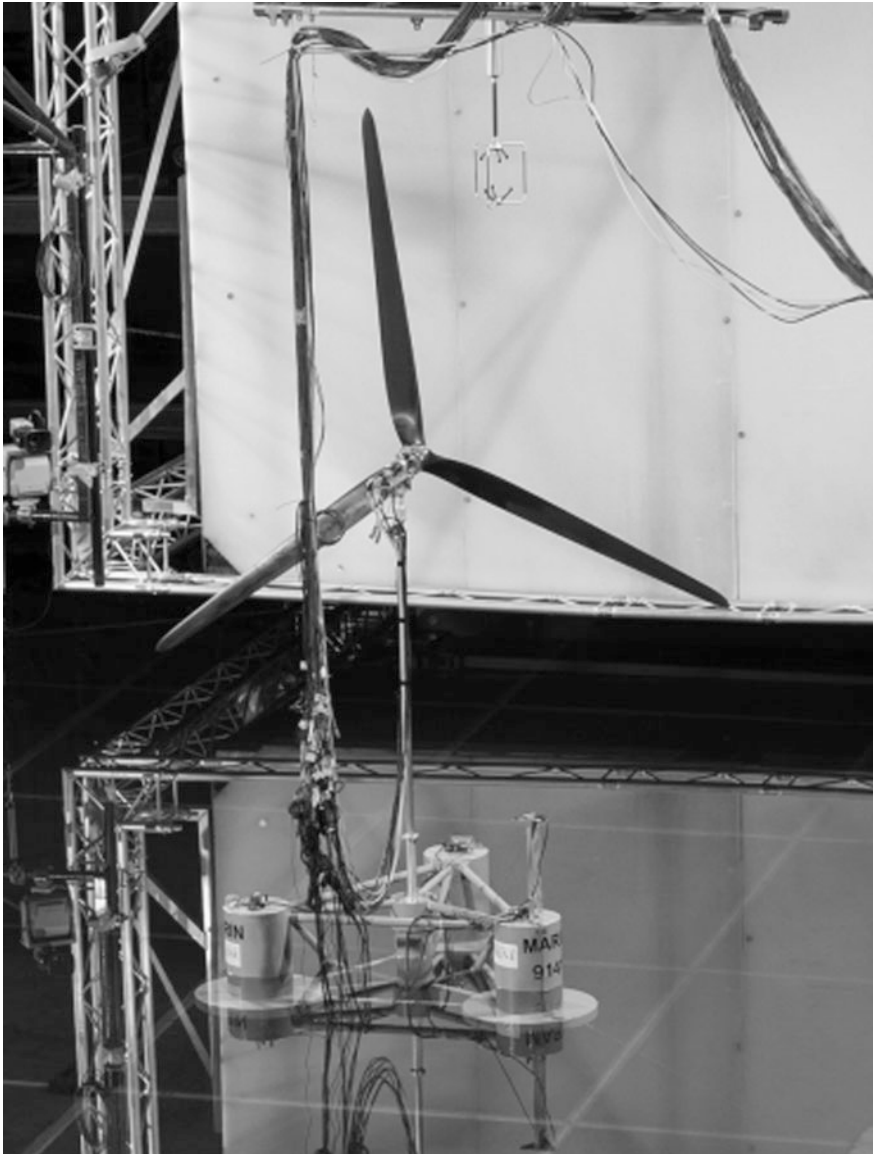
Fig. 46 Image of the MARIN stock wind turbine atop the DeepCwind semi-submersible platform

A comparison of the prototype, DeepCwind and MARIN stock wind turbine power and thrust performances is given in Fig. 47. As seen in the figure, the MARIN stock wind turbine matches the thrust behaviour of the full-scale target much better than the DeepCwind wind turbine model in addition to producing far
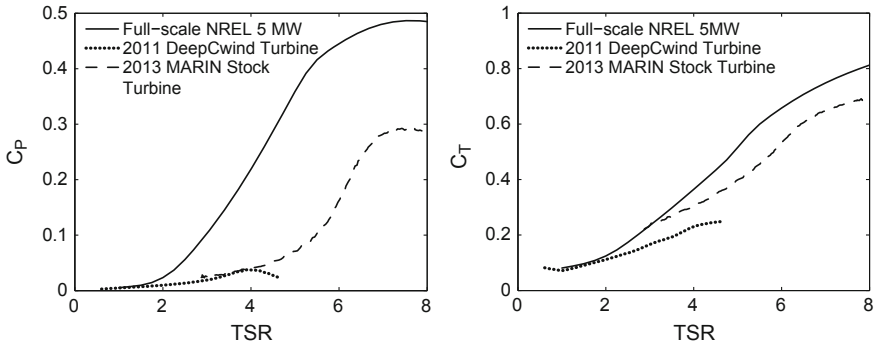
Fig. 47 Comparison of NREL 5 MW target, DeepCwind model and MARIN stock wind turbine performance and thrust coefficients

more power. This improved performance permitted use of near Froude-scaled winds during testing and enabled advanced experiments involving active blade pitch control which was not studied in the 2011 DeepCwind test campaign (Goupee et al. 2014).

Floating Platform and Mooring Systems

While most floating wind turbine concepts under consideration employ a horizontal axis wind turbine, the platform designs employed in current concepts vary widely. Therefore, to make the test results useful to as broad an audience as possible, the previously described wind turbine and tower was tested atop three different floating platforms. The platforms, each modelled after viable offshore oil and gas platform technology, derive stability from differing mechanisms (see Sect. 1 of Chapter "Overview of Floating Offshore Wind Technologies"). The platforms consisted of a TLP (mooring stabilised), a spar buoy (ballast stabilised) and a semi-submersible (buoyancy stabilised). Images of the platforms employed during testing, including the wind turbine, are shown in Fig. 48. Like the blades, each platform was designed to be rigid to eliminate the added complexity of a flexible platform.

Each of the designs was tested in a water depth of 200 m. The first design, the TLP, was restrained by three stiff vertical tendons. The spar buoy was moored by a spread mooring consisting of taut lines attached to the spar buoy via a delta connection similar in nature to the type employed on the actual Statoil Hywind (Jonkman 2010a, b). The last design, the semi-submersible, was restrained by three slack catenary lines with fairlead attachments located at the top of the lower bases. Key features of the three designs are shown in Table 5 including draft, displacement and mooring particulars. The location of the three designs on the stability triangle is shown in Fig. 49.

As can be seen in the table, the TLP was by far the smallest of the designs by mass with the semi-submersible being the largest by mass. The differences in mass are largely attributable to the levels of ballast for the designs, with the TLP having
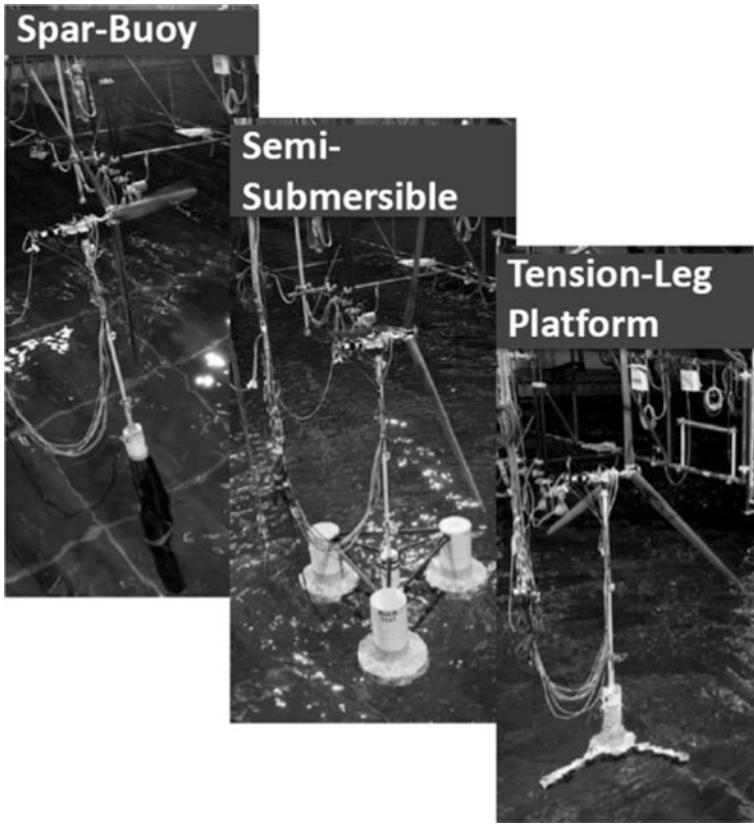
Fig. 48 Images of all three floating wind turbine systems examined in DeepCwind model test campaign

no ballast unlike the other two designs. This aside, it is important to note that these structures were not optimised and intended to be generic. In addition, each system was designed with the purpose of exhibiting the main characteristics that typify the performance of each platform concept. Using generic, open-source platform designs aided in sharing the data for use in numerical model code validation efforts (e.g. see Browning et al. 2012; Stewart et al. 2012; Prowell et al. 2013; Coulling et al. 2013, Robertson et al. 2013).

Examining the table, the measured natural periods of heave, roll and pitch motion for the moored structures indicate that the TLP system was very stiff as opposed to the spar buoy and semi-submersible systems. In all cases, however, the natural periods of motion for these noted rigid body modes did not lie in the range of typical wave energy peak spectral periods, these being from approximately 5–17 s.

Table 5 Select specifications for each of the DeepCwind platforms tested

Platform type	TLP	Spar	Semi
Mass (w)/turbine (t)	1361	7980	14,040
Displacement (t)	2840	8230	14,265
Draft (m)	30	120	20
CG above keel (m)	64.1	43.7	10.1
Roll radius of gyration (m)	52.6	53.5	31.6
Pitch radius of gyration (m)	52.7	53.6	32.3
Number of mooring lines (–)	3	3[a]	3
Mooring spread diameter (m)	60	890	1675
Mooring line wet weight (N/m)	0.0	0.0[a]	1065.3
Mooring line extensional stiffness (MN)	7430.0	121.0[a]	753.6
Mooring line pretension (kN)	4755.3	1901.5[a]	1085.5
Natural surge period (s)	39.3	43.0	107
Natural sway period (s)	39.3	42.8	112
Natural heave period (s)	1.25	28.1	17.5
Natural roll period (s)	3.7	32.0	26.9
Natural pitch period (s)	3.7	31.5	26.8
Natural yaw period (s)	18.2	5.5	82.3

[a]Spar-buoy values are for the main mooring lines; for details on the delta connection lines, see Koo et al. (2014)
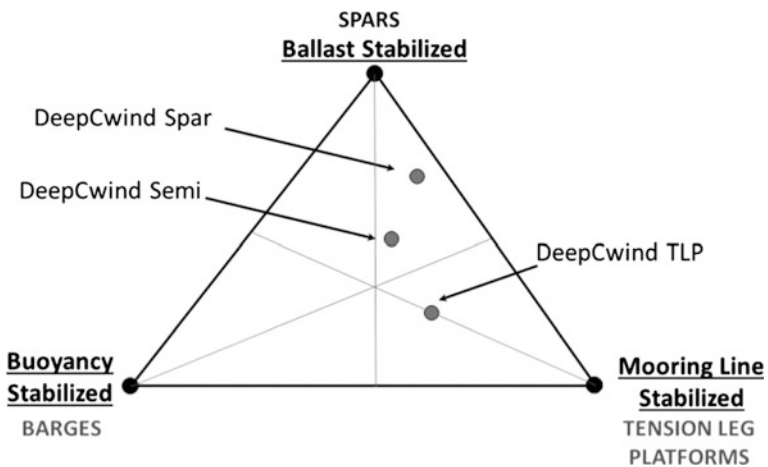

Fig. 49 Location of each of the DeepCwind FOWT systems on the stability triangle

Instrumentation

In order to measure loads and motions of the FOWTs, a total of about 40–50 channels were used in the model tests depending on the floater. The 6-DOF motions of the floating wind turbine were measured by an optical tracking system. Three accelerometers were located at the base, middle and top of the turbine tower to measure accelerations. The natural frequencies of the wind turbine tower were derived from these accelerometers. The nacelle was connected to the tower by means of a six component load cell that measured the 6-DOF forces and moments between the tower and nacelle. The global connection loads between the wind turbine and the platform were measured by another six-component load cell between the tower base and platform top. The turbine performance was measured by the torque sensor between the motor and the blades. The mooring top tensions were measured by ring-type transducers at the fairlead location. A-shaped strain gauges were installed at each tendon porch to measure tendon top tensions. Data was collected at 14.14 Hz full-scale (100 Hz model scale) for most tests with the exception of hammer tests which were recorded at 141.4 Hz full-scale (1000 Hz model scale). An image depicting the entire suite of measurements as made on the semi-submersible system is shown in Fig. 50.

Experimental Observations

In this section, select observations from the model test campaign will be discussed. The results presented are intended to highlight important behaviours and trends in FOWT responses, as well as occasionally provide insight into methods for improving model testing of floating wind turbines in the future.
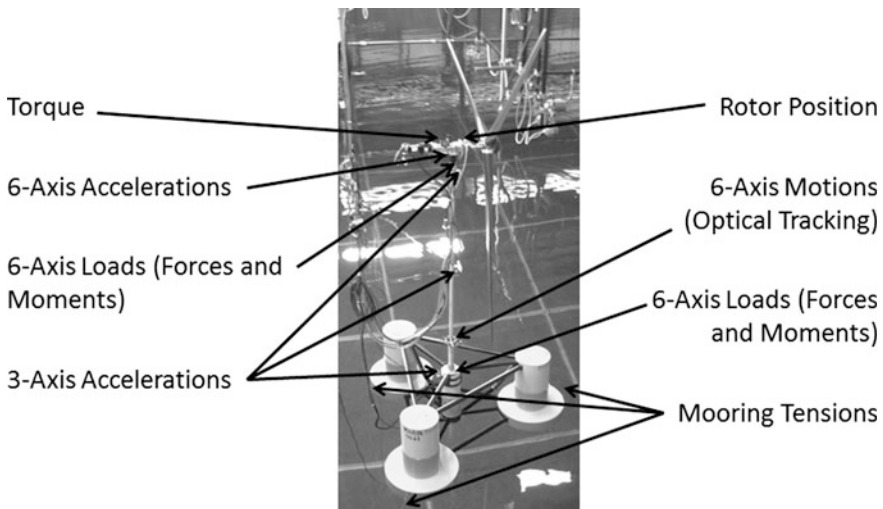

Fig. 50 Locations of sensors for testing of the semi-submersible FOWT during the DeepCwind model test campaign

Influence of Platform Compliance on Tower Bending Frequencies

For the DeepCwind program, all three platforms were tested with the same exact wind turbine and tower. Despite the fact that the turbine mass, as well as the tower mass and elastic properties were identical for all three systems, the fundamental bending frequencies of the tower in the fore-aft and side-side directions varied from platform to platform. The tower bending frequencies obtained from hammer testing of the three systems is shown in Table 6. This phenomenon can be attributed to the platform compliance, with the platforms stiffer in pitch and roll exhibiting a lower bending frequency than the compliant foundations. This is not unexpected as stiffer foundations are more representative of a fixed boundary condition for the base of the tower, while the softer foundations are more akin to a free condition at the tower base (e.g. see Rao 2004).

Another consideration for these systems is the coupling between the tower bending frequency and the pitching motion of the turbine. For most systems, this means that 1-DOF may excite the other, but for the TLP these 2-DOFs are more tightly coupled. The pitching frequency of the TLP will be shifted based on the flexibility of the tower, and efforts to model the system without accurately representing this flexibility will result in incorrect estimates of system behaviour.

Platform Hydrodynamic Response

As a part of the test campaign, several tests were run in the absence of wind loads to characterise the unique hydrodynamic responses of the three floating platforms. Results are presented here for the platform hydrodynamic damping, RAOs and motion response in larger irregular seas.

The first result provided is displayed in Fig. 51, which illustrates the differences in hydrodynamic damping for the three FOWT systems. The results, which are based on surge motions of the various systems as measured at the centre of gravity from free-decay tests, show that the spar-buoy exhibited the least amount of surge damping and the TLP the most. The semi-submersible lay more or less between each of these systems. As the platform had several blunt arms and a small mass, it is unsurprising that the TLP exhibited the highest damping ratio of the three systems. The semi-submersible also possessed numerous opportunities to create drag when travelling in a horizontal direction; however, it was far larger than the TLP and therefore displayed a smaller damping ratio. For the systems with the largest damping, these being the TLP and the semi-submersible, the damping response was strongly dependent on initial cycle amplitude indicating strong contributions from viscous damping. In numerical model validation studies, these behaviours have

Platform type	TLP	Spar	Semi	Turbine alone
Tower fore-aft (Hz)	0.28	0.43	0.35	0.29
Tower side-side (Hz)	0.29	0.44	0.38	0.29

Table 6 Fundamental tower bending frequencies of the three DeepCwind FOWT systems and the wind turbine clamped alone

Fig. 51 Surge damping as a function of initial cycle amplitude for the three FOWT systems
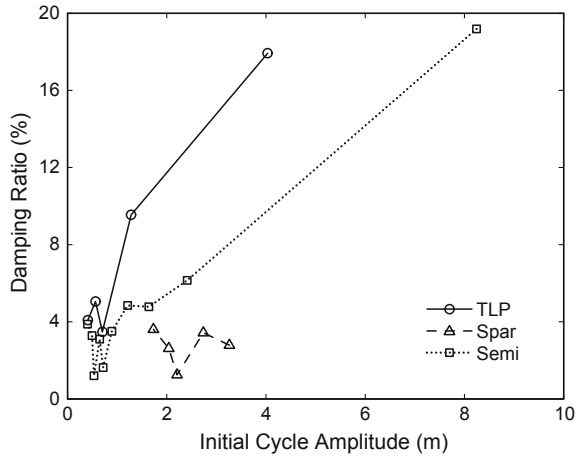
been captured fairly well by damping models which incorporate both linear and quadratic damping coefficients.

Additional insight into the hydrodynamic performance of the three floating wind turbine systems can be gleaned from the RAOs shown in Fig. 52. The RAOs for the surge, pitch, and heave motion of the systems were calculated from a white noise wave test with significant wave height (H_s) of 7.1 m. The RAOs show that the surge response as measured at the centre of gravity for a given wave was largest for the TLP and smallest for the spar buoy. The pitch response was small for the TLP (as would be expected due to the taut moorings) and the pitch response for the spar buoy grew steadily as the wave period was increased. The semi-submersible response rose more sharply than the other systems with increasing period up to a point at which the pitch RAO levelled off until the resonant pitch period was reached. In heave, the semi-submersible exhibited by far the most motion due to the presence of the heave resonant frequency lying within the wave excitation band at 17 s. However, this is a fairly long wave period that will not typically be encountered during normal operation. Still, this large motion shows the importance of desiging the system eigenfrequencies to lie outside the range of wave excitation.

The last comparison of the hydrodynamic behaviour of the systems is given in Fig. 53. The figure displays the surge frequency domain response of the three systems when subjected to a H_s of 10.5 m in the absence of wind forces. As can be seen in the figure, the response in the wave energy frequency range (0.05–0.1 Hz) is largest for the TLP and smallest for the spar for this particular degree of freedom. However, second-order hydrodynamic loads created by the interaction of different wave components creates larger excitation for the semi-submersible below the wave frequency range at the semi-submersible's surge natural frequency. This result indicates the need to properly model second-order wave components when simulating the behaviour of an offshore wind system, especially for semi-submersible type systems (Gueydon and Weller 2013). A pitch response peak at natural period

Fig. 52 Response amplitude operator magnitudes of all three floating wind turbines in surge, pitch and heave as determined from a 7.1 m significant wave height white noise wave
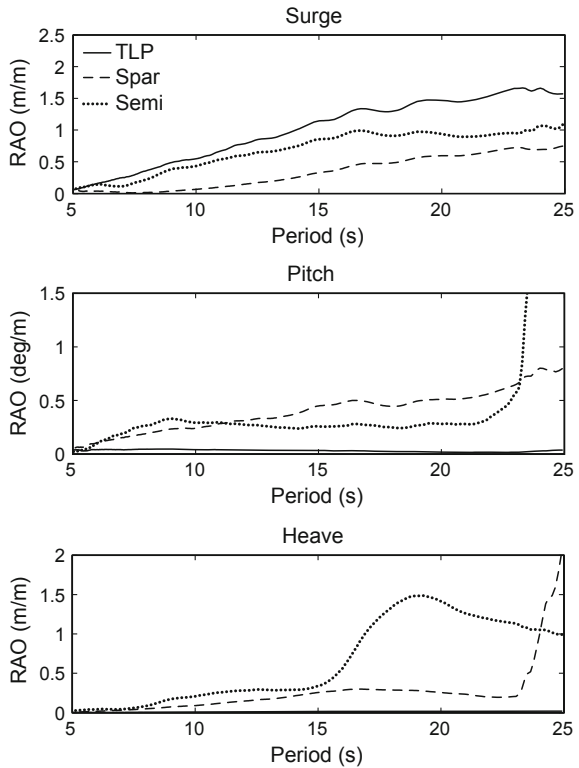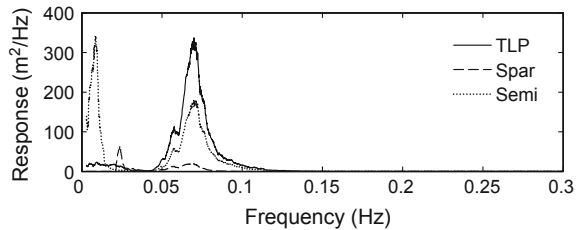
Fig. 53 Surge response in a 100-year, 10.5 m significant wave height irregular sea for all three DeepCwind FOWTs

was also observed for the semi in waves only. Further analysis reinforced by simulations have demonstrated that the difference frequency second-order wave loads were at the origin of this resonance peak (Gueydon 2015).

Influence of Aerodynamic Loads on Global Motions and Structural Loads
A major objective of the DeepCwind model test program was to understand the interplay of wind and wave loads on the global performance of floating wind turbine structures. Observations from the model test program regarding the influence of aerodynamic loads from an operating wind turbine on motion and structural load response are now discussed.

The first result of interest is given in Fig. 54. The figure shows two free-decay tests for the semi-submersible floating wind turbine. One of the tests had the blades feathered to reduce drag and no wind applied; the other involved an operating wind turbine in a moderate operating environment. As is clear from the figure, the presence of the operating wind turbine for this scenario increased the platform pitch damping significantly, raising the damping ratio by several percent. In general, for all three floating wind turbine systems, the presence of an operating turbine in a wind field often increased damping and diminished motions, particularly for low-frequency resonant platform motions.

The spar buoy pitch response in wind-only, wave-only and wind/wave conditions is shown in Fig. 55. Aerodynamic forces damped the wave-induced second-order pitch frequency motion ($\sim$0.03 Hz). However, the low frequency response was nearly identical between the wind-only and wind/wave cases. This shows that while second-order wave excitation can have significant influence on system behaviour, wind excitation is generally significantly larger, and tends to mask this influence.

Figure 56 shows the effect of wind-only, wave-only and wind/waves for the semi-submersible floater tower base bending moment. The presence of wind significantly damped the low-frequency resonant platform pitch-associated response as

Fig. 54 Comparison of free-decay response for the semi-submersible with and without an operating wind turbine
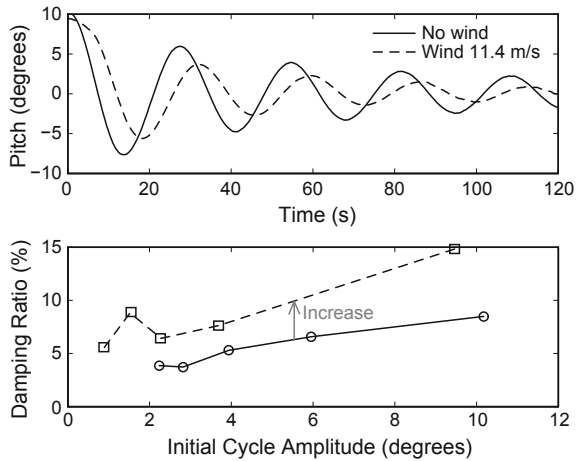

Fig. 55 Spar-buoy pitch response for wind only, wave only and with wind/waves. Wind turbine operates at 12.7RPM, wave case is JONSWAP H_s = 10.5 m, T_p = 14.3 s
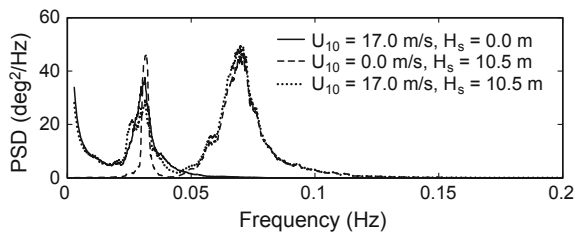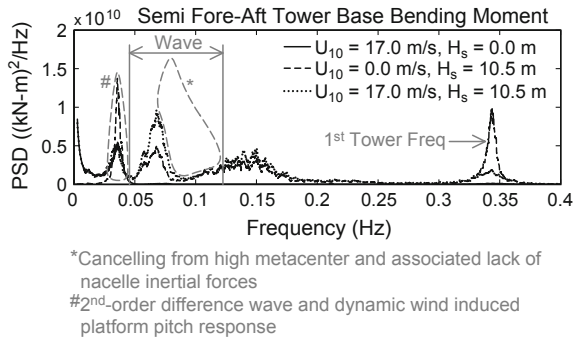
Fig. 56 Semi-submersible tower bending moment response with wind only, wave only and with wind/waves. Wind turbine operates at 12.7 RPM, wave case is JONSWAP $H_s = 10.5$ m, $T_p = 14.3$ s

Semi Fore-Aft Tower Base Bending Moment

— $U_{10} = 17.0$ m/s, $H_s = 0.0$ m
--- $U_{10} = 0.0$ m/s, $H_s = 10.5$ m
······ $U_{10} = 17.0$ m/s, $H_s = 10.5$ m

1st Tower Freq →

*Cancelling from high metacenter and associated lack of nacelle inertial forces
#2nd-order difference wave and dynamic wind induced platform pitch response

well as the tower excitation at 0.34 Hz. This suggests that the second-order low frequency pitch motions are reduced by aerodynamic damping when wind loading is applied. In all cases, there was evidence of load cancelling effects in the wave frequency range due to the high meta-centre and the reduced motion of the nacelle at these frequencies. It was observed that the semi-submersible appeared as though the system was pivoting about a point near the nacelle such that nacelle motions were minimal for moderate to large wave periods. Estimated second-order response regions and the wave load cancelling effect are depicted on the graph for visual reference. The increase in pitch response with wind in the wave frequencies observed is likely due to turbine thrust response effects.

The findings covered in the previous paragraphs indicate the coupling effect that the wind and wave excitation has on the system response, and shows the need to consider both excitations simultaneously when testing a floating wind system. In addition, the response of the turbine and platform to these excitations could excite responses in other portions of the structure, which would then alter the loading effect, indicating also the need for a complete model of an offshore wind system when doing testing.

Mooring System Response

Each of the three DeepCwind FOWT models possessed very different mooring systems. The TLP used stiff tension legs, the spar buoy employed a taut spread mooring system with a bridle configuration at the fairlead to provide yaw stiffness, and the semi-submersible utilised a slack catenary chain system. As such, each exhibited very different mooring tension behaviours.

The fairlead mooring tension response spectra for an environment consisting of a dynamic wind speed with a mean of 20.7 m/s at hub height and an operational sea state with a significant wave height of 2.0 m is shown for all three systems in Fig. 57. This scenario is representative of the day-to-day aerodynamic and hydrodynamic loads a FOWT would see while in operation. From the figure, it is clear that the energy in the response of the TLP tendons was an order of magnitude greater than the response for the other two systems. This was not entirely unexpected as the TLP system gains its stability from highly loaded, stiff mooring tendons. For the spar buoy, the mooring load response was tied closely to the surge

Fig. 57 Fairlead mooring
tension response spectra for
all three systems in a
combined wind and wave
environment
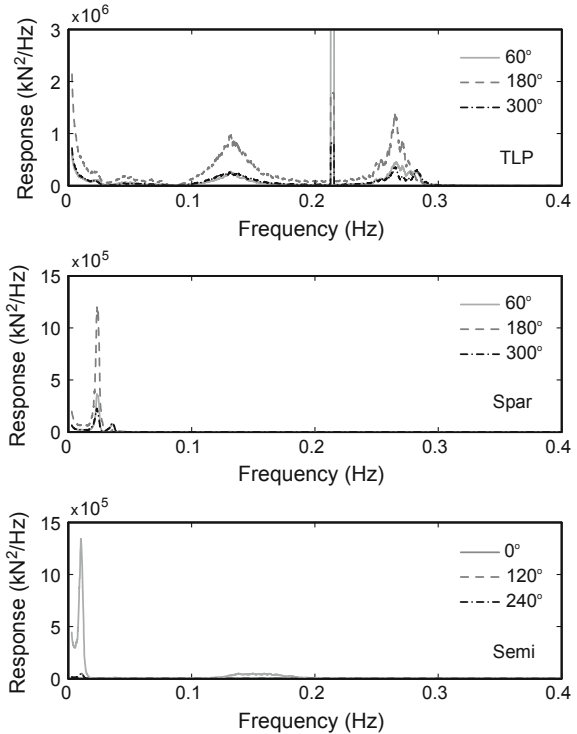
natural period, as was the peak response of the semi-submersible. The TLP, on the
other hand, exhibited significant response at frequencies associated with the wind
energy, wave energy, and platform pitch/tower bending natural frequency of
0.28 Hz. Surprisingly, all three TLP tendons also displayed a sharp response at the
once per revolution rotor excitation frequency of 12.7RPM (0.21 Hz). This was
likely a result of the vertically stiff and lightweight nature of the floating TLP wind
turbine system tested. This indicates that the lightweight and vertically stiff TLP
was over sensitive to rotor loads and may have been under designed.

In extreme events, two of the systems, the TLP and semi-submersible, experi-
enced slack line events which would be avoided at all costs in an actual deploy-
ment. The slack line events for the TLP were exacerbated greatly by the presence of
wind loads. The wind loading provided an overturning moment that significantly
reduced the downwind mean tendon tension and in turn minimised the resistance to
slack tendon events in the presence of wave loads. An occurrence of a slack line
event for the downwind TLP tendon is shown in Fig. 58. For the semi-submersible,
the upwind mooring line experienced the slack line events. It is surmised that these
events occurred when the platform motion was rapid enough that the wet weight of
the line could not overcome the viscous drag force on the line to maintain a
non-zero tension near the fairlead of the line. An example of a slack line event for
the semi-submersible is given in Fig. 59.

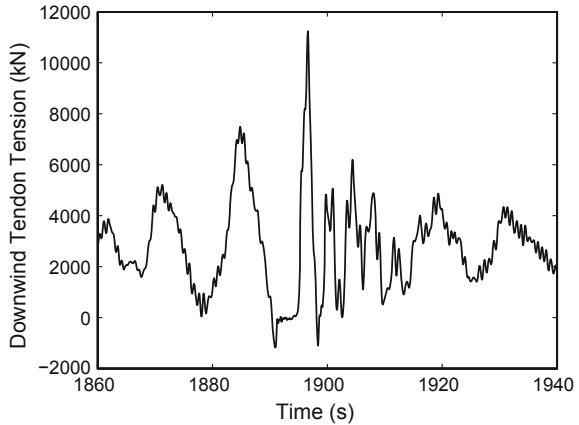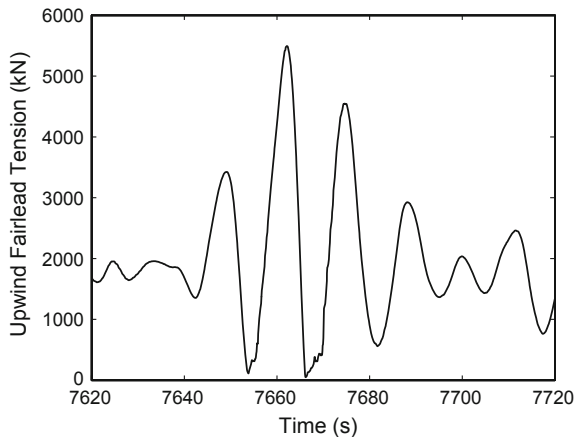**Fig. 58** Slack downwind tendon for the TLP, steady wind of 21.8 m/s, H_s of 10.5 m


Fig. 59 Slack upwind fairlead for the semi-sub., steady wind of 21.8 m/s, H_s of 10.5 m

Turbine Yaw Error

As part of the DeepCwind test program, tests were performed with the turbine yawed 20° relative to the incoming wind to simulate turbine yaw error effects on the floater response. Figure 60 shows the spar buoy yaw, pitch and roll frequency domain response with and without yaw error. The environment consisted of a dynamic wind with a mean wind speed of 20.7 m/s and an irregular wave environment with a significant wave height of 10.5 m. As seen in the figure, there was a modest increase in the yaw response of the turbine due to the yaw error in the wave frequency range. The yaw motion associated with the once per revolution frequency of the turbine was damped slightly. Unsurprisingly, the yaw error had little effect on pitch, but roll response increased due to the side forces on the yawed turbine. A final observation to be made with the figure concerns the relative magnitudes of the yaw and pitch responses, with the yaw response being smaller even in the state with turbine yaw error. This indicates that the taut mooring system with bridle

Fig. 60 Effect of turbine yaw error on spar-buoy yaw, pitch and roll
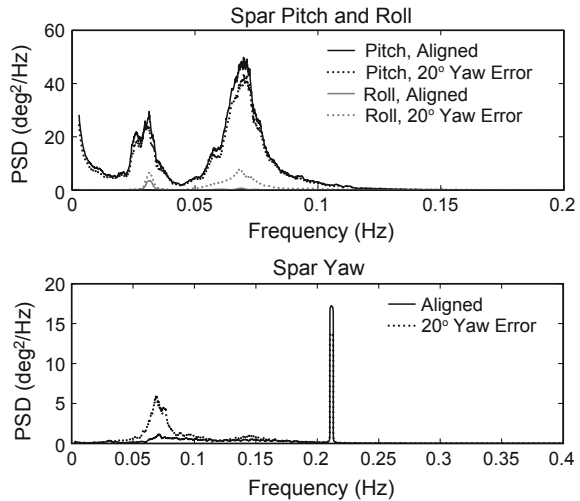
connections at the fairleads performed well at controlling the yaw motion of the spar-buoy floating wind turbine.
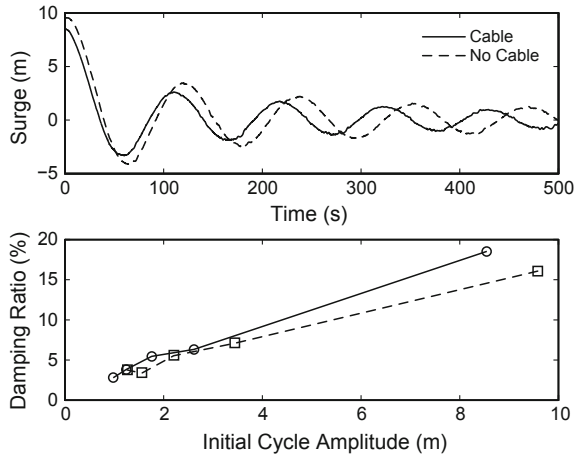
Testing Issues

As the DeepCwind tests are the first FOWT tests to be open to the public, they provide an opportunity for others to learn from the issues encountered during the testing campaign. The following sections summarises some of the issues encountered.

Instrumentation

During the test campaign, there was a concern that the larger number of instrumentation cables attached the floating wind turbines, which can be seen in Fig. 61, were acting as an additional, unwanted mooring line. If the influence of this cable was significant, then deviations from the target global restoring forces provided by the calibrated mooring systems could alter the system performance. In order to understand the influence of these instrumentations cables, free-decay tests for the semi-submersible system in surge were performed with and without the instrumentation cables attached. A comparison of the data from these tests is shown in Fig. 61. As seen in the figure, the instrumentation cable bundle added additional surge stiffness, which shortened the surge natural period, as well as provided additional surge damping. Ideally, instrumentation cables would be managed to minimise these effects in future testing. That stated, the results of Fig. 61 were used to compute the effective stiffness and damping of the cables and these influences were included in model calibration studies employing the data (e.g. see Coulling et al. 2013).

This issue highlights the importance of having instrumentation that is light-weight and does not alter the dynamic behaviour of the offshore wind system. At 1:50 scale, the systems are so small that the weight of the sensors and the cabling

Fig. 61 Surge-decay response for the DeepCwind semi-submersible with and without instrumentation cables attached

becomes significant. Therefore, it is suggested that, if possible, wireless sensors or smaller cabling should be used for small-scale testing.

In addition, two load cells were placed at the connection points between the platform and the tower, and the tower and the turbine. The load cells enabled the measurement of tower loads/moments at the top and bottom, but also potentially induced compliance at the connection points, which could decrease the stiffness of the tower. If these types of sensors are used, it is suggested that periodic inspection be performed to understand the compliance that they induce into the system.

Finally, the 6-DOF response motion of the platform was measured via an optical sensor pointed at the base of the tower. While this system worked well in general, it was not sensitive enough to accurately capture the very small pitching and rolling motions of the TLP.

Wind Quality

The wind in the model basin was generated by fans, which require special attention due to the recirculation of the wind field in the basin and the variation of the wind speed with the distance from the fans. While the flow from the bank of fans was fairly consistent with minimal swirl and an average turbulence of less than 5 %, there were some drawbacks. The bank of fans needed to be placed high enough as to not interact with the water. This height decreased the wind speed on the lower portion of the rotor; thus, the nozzle was tilted downward by 2.16°. This downward angle improved the wind speeds at the bottom of the rotor, but introduced a vertical component to the wind velocity. Even with this modification, wind speeds at the lower end of the rotor decreased by 20 % and the turbulence intensity increased to 15 %.

In order to obtain an appropriate representation of the wind using modelling tools, a shear law was needed to represent the change in wind speed with height, as well as a slight decrease in the average wind speed. No accommodations were made in the simulations for the vertical wind speed components or turbulence variations.

This helped to match the wind excitation; however, a full representation of the wind field is not possible due to not having a full spatial and temporal characterisation of the velocity. These inconsistencies in the wind induced unwanted excitation in the system, such as the 3P, 6P, and 9P frequencies. In modelling the system, the aerodynamics model also needed calibration due to test limitations. The altered performance of the wind turbine at model scale required large alterations to the airfoil data from what is appropriate at full scale. An attempt was made to create this model within XFOIL (Drela 1989), but due to its questionable ability to model the separated flow experienced by this turbine, tuning of the lift and drag curves was needed using the experimental data.

Conclusions of the DeepCwind Model Test Programme

The two main purposes for the DeepCwind testing campaign were to better understand the behaviour of floating offshore wind systems and to obtain experimental data to be used for validating FOWT system modelling tools. The tests were essential in meeting these goals, and were groundbreaking in regard to producing data that was widely disseminated for use by FOWT researchers.

Upon conclusion of the tests, several important observations were noted. Many pertained to areas of improvement for future tests. These areas of improvement included fully understanding the need for performance-matched wind turbines for Froude-scale floating wind turbine model tests, as well as providing insight on what the objectives should be in designing such a turbine. Additional areas of experimental improvement were identified including smaller, more flexible instrumentation cables to reduce unwanted restoring and damping forces on the platform as well as diminished wind turbulence at the lower edge of the rotor plane. Each of these improvements were made in subsequent model tests performed at MARIN (e.g. see Huijs et al. 2014; Goupee et al. 2014).

Despite observing several areas of potential enhancement for the DeepCwind model tests, the data still provided a great deal of insight into the coupled dynamics of FOWT systems. Simple hammer tests revealed the strong influence of platform compliance on the tower bending frequencies. For the softer platforms, the tower bending frequencies rose and remained distinct from the eigen-frequencies of the platform's motions whereas they merged with the roll and pitch eigen-frequencies for the TLP.

Wave-only testing revealed that the hydrodynamic response of each of the platforms was markedly different. The TLP possessed the largest hydrodynamic damping in surge as well as the largest response amplitude operators in surge. The spar buoy exhibited the least damping of the three systems, but exhibited generally good performance as measured at the system centre of gravity. The semi-submersible exhibited by far the most slow drift response of any of the systems tested. Low frequency second-order wave loading had a visible effect on the roll and pitch responses of the softer platforms. When wind loads were applied via an operating wind turbine, damping of motions, particularly platform pitch at low frequencies, were fairly strong. For two of the systems, the TLP and the semi-submersible, large sea states resulted in undesirable slack line events

indicating that the station keeping systems would need improvement for an actual full-scale deployment. Nonetheless, these highly nonlinear mooring events provide unique data that is well suited for testing even the most capable of computer-aided-engineering tools. Last but not least, numerous interactions between the aerodynamic loading, the hydrodynamic responses, the tower flexibility and the mooring loads show the need for detailed testing in combined wind and waves conditions for a good assessment of the behaviour of a FOWT system.

References

References (1)

Anderson JD Jr (2007) Fundamentals of aerodynamics, 4th edn. McGraw-Hill, New York

Bekiropoulos D, Rieß RM, Lutz T et al (2012) Simulation of unsteady aerodynamic effects on floating offshore wind turbines. In: Proceedings of the German wind energy conference (DEWEK), Bremen, Germany, 7–8 Nov 2012

de Vaal JB, Hansen MOL, Moan T (2012) Effect of wind turbine surge motion on rotor thrust and induced velocity. Wind Energy 17(1):105–121

IEC 61400-12 (2005) Wind turbines—Part 12-1: power performance measurements of electricity producing wind turbines. International Electrotechnical Commission (IEC), Geneva, Switzerland

Leishman JG (2006) Principles of helicopter aerodynamics, 2nd edn. Cambridge University Press, New York

Matha D, Fischer S-A, Hauptmann S et al (2013) Variations in ultimate load predictions for floating offshore wind turbine extreme pitching motions applying different aerodynamic methodologies. In: Proceedings of the 23rd international offshore and polar engineering (ISOPE 2013), Anchorage, Alaska, USA, 30 June–4 July 2013

Moriarty PJ, Hansen AC (2005) AeroDyn theory manual. National Renewable Energy Laboratory (NREL), Golden, CO, USA

Quallen S, Xing T, Carrica P et al (2013) CFD simulation of a floating offshore wind turbine system using a quasi-static crowfoot mooring-line model. In: Proceedings of the 23rd international offshore and polar engineering (ISOPE 2013), Anchorage, Alaska, USA, 30 June–4 July 2013

Sant T (2007) Improving BEM-based aerodynamic models in wind turbine design codes. Dissertation, Delft University Wind Energy Research Institute, Delft, The Netherlands

Sebastian T (2012) The aerodynamics and near wake of an offshore floating horizontal axis wind turbine. Ph.D. thesis, University of Massachusetts Amherst

References (2)

Aubault A, Cermelli C, Roddier D (2009) WindFloat: a floating foundation for offshore wind turbine—Part III: structural analysis. In: Proceedings of the 28th international conference of offshore mechanics and arctic engineers (OMAE), Honolulu, HI, USA, 31 May–5 June 2009

Bredmose H, Mariegaard J, Paulsen BT et al (2013) The wave loads project. DTU Wind Energy, no. 0045

Bunnik T, Veldman A, Wellens P (2008) Prediction of extreme wave loads in focused wave groups. In: Proceedings of the 18th International offshore and polar conference, Vancouver, BC, Canada, 6–11 July 2008

Cruz J (2009) Numerical and experimental modelling of offshore wave energy converters. Ph.D. thesis, Instituto Superior Técnico

Day AH, Babarit A, Fontaine A et al (2015) Hydrodynamic modelling of marine renewable energy devices: a state of the art review. Ocean Eng 108(2015):46–69

Faltinsen OM (1990) Sea loads on ships and offshore structures. Cambridge University Press, Cambridge

Havelock T (1942) The damping of the heaving and pitching motion of a ship. Phil Mag 33 (7):666–673

Hess J (1990) Panel methods in computational fluid dynamics. Annu Rev Fluid Mech 22:255–274

Hess J, Smith A (1964) Calculation of nonlifting potential flow about arbitrary three-dimensional bodies. J Ship Res 8:22–44

Jonkman J (2009) Definition of the floating system for phase IV of OC3, National Wind Technology Center (NWTC), National Renewable Energy Laboratory (NREL), 12 Feb 2009

Lamb H (1932) Hydrodynamics, 6th edn. Cambridge University Press, Cambridge

Le Méhauté B (1976) An introduction to hydrodynamics and water waves. Springer, New York

Lee C-H, Maniar HD, Newman JN, Zhu X (1996) Computations of wave loads using a B-spline panel method. In: Proceedings of the 21st symposium on naval hydrodynamics, Trondheim, Norway, pp 75–92

Linton CM (1991) Radiation and diffraction of water waves by a submerged sphere in finite depth. Ocean Eng 18(1/2):61–74

Lopez-Pavon C, Souto-Iglesias A (2015) Hydrodynamic coefficients and pressure loads on heave plates for semi-submersible floating offshore wind turbines: a comparative analysis using large scale models. Renew Energy 81:864–881

Maniar H (1995) A three-dimensional higher order panel method based on B-splines. Ph.D. thesis, Massachusetts Institute of Technology

Mei CC (1989) The applied dynamics of ocean surface waves. Advanced series on ocean engineering, vol 1. World Scientific, Singapore

Mei CC, Stiassnie M, Yue DKP (2005) Theory and applications of ocean surface waves, Part 1: linear aspects, Part 2: nonlinear aspects. Advanced series on ocean engineering, vol 23. World Scientific, Singapore

Morison JR, O'Brien MP, Johnson JW, Schaaf SA (1950) The force exerted by surface waves on piles. Petrol Trans 189:149–154

Newman JN (1977) Marine hydrodynamics. The MIT Press, Cambridge

Newman JN (1992) Panel methods in marine hydrodynamics. In: Proceedings of the 11th Australasian fluid mechanics conference, Hobart, Australia, Keynote Paper K-2

Newman JN, Lee CH (1992) Sensitivity of wave loads to the discretization of bodies. In: Proceedings of the 6th behaviour of offshore structures (BOSS) international conference, London, UK, vol 1, pp 50–63

Robertson A, Jonkman J, Vorpahl F et al (2014) Offshore Code Comparison Collaboration Continuation within IEA Wind Task 30: Phase II results regarding a floating semisubmersible wind system. In: Proceedings of the 33rd international conference on ocean, offshore and Artic engineering, San Francisco, CA, USA, 8–13 June 2013

Sarpkaya T, Isaacson M (1981) Mechanics of wave forces on offshore structures. Van Nostrand Reinhold Company, New York

Sethuraman L, Venugopal V (2013) Hydrodynamic response of a stepped spar floating wind turbine: Numerical modelling and tank testing. Renew Energy 52:160–174

Sumer BM, Fredsøe J (1997) Hydrodynamics around cylindrical structures. Advanced series on ocean engineering, vol 12. World Scientific, Singapore

UpWind (2011) Deliverable D4.3.6: final report for WP4.3: design methods and standards

Wehausen JV, Laitone EV (1960) Surface waves. Volume IX of Encyclopaedia of physics. Springer, New York, pp 446–778

References (3)

API RP 2SK (2005) Design and analysis of stationkeeping systems for floating structures, 3rd edn. American Petroleum Institute (API), Washington D.C.

API RP 2SM (2014) Design, manufacture, installation, and maintenance of synthetic fiber ropes for offshore mooring, 2nd edn. American Petroleum Institute (API), Washington D.C.

Bae Y, Kim M, Im S, Chang I (2011) Aero-elastic-control-floater-mooring coupled dynamic analysis of floating offshore wind turbines. In: Proceedings of the 21st international offshore and polar engineering conference (ISOPE), Maui, Hawaii, USA, 19–24 June 2011

Balzola R (1999) Mooring line damping in very large water depths. Ph.D. thesis, Massachusetts Institute of Technology

Bauduin C, Naciri M (2000) A contribution on quasi-static mooring line damping. J Offshore Mech Arct Eng 122(2):125–133

Buckham B, Driscoll FR, Nahon M (2004) Development of a finite element cable model for use in low-tension dynamics simulation. J Appl Mech 71(4):476–485

Cermelli C, Bhat S (2002) Fiber mooring for ultra-deepwater applications. In: Proceedings of the 12th international offshore and polar engineering conference (ISOPE), Kitakyushu, Japan, 25–31 May 2001

Chai Y, Varyani K, Barltrop N (2002) Semi-analytical quasi-static formulation for three-dimensional partially grounded mooring system problems. Ocean Eng 29(6):627–649

Chandrasekaran S, Jain A (2002) Dynamic behaviour of square and triangular offshore tension leg platforms under regular wave loads. Ocean Eng 29(3):279–313

Choo Y, Casarella M (1973) A survey of analytical methods for dynamic simulation of cable-body systems. J Hydronaut 7(4):137–144

Chung J, Hulbert G (1993) A time integration algorithm for structural dynamics with improved numerical dissipation: the generalized-α method. J Appl Mech 60(2):371–375

De Zoysa A (1978) Steady-state analysis of undersea cables. Ocean Eng 5(3):209–223

Friswell M (1995) Steady-state analysis of underwater cables. J Waterw Port Coast Ocean Eng 121(2):98–104

Garrett D (1982) Dynamic analysis of slender rods. J Energy Res Technol 104(4):302–306

Gatti-Bono C, Perkins N (2004) Numerical simulations of cable/seabed interaction. J Offshore Polar Eng 14:118–124

Gobat JI (2000) The dynamics of geometrically compliant mooring systems. Ph.D. thesis, Massachusetts Institute of Technology (MIT) and Woods Hole Oceanographic Institution

Gobat JI, Grosenbaugh M (2001) Application of the generaliszed-α method to the time integration of the cable dynamics equations. Comput Methods Appl Mech Eng 190(37):4817–4829

Huang S (1994) Dynamic analysis of three-dimensional marine cables. Ocean Eng 21(6):587–605

Hughes TJ (1977) Unconditionally stable algorithms for nonlinear heat conduction. Comput Methods Appl Mech Eng 10(2):135–139

Inman DJ, Singh RC (1994) Engineering vibration. Prentice Hall Englewood Cliffs, NJ

Irvine M (1992) Cable structures, vol 5. Dover Publications, New York

ISO 19901-7 (2013) Petroleum and natural gas industries–specific requirements for offshore structures–part 7: station keeping systems for floating offshore structures and mobile offshore units, 2nd edn. International Standards Organization (ISO), Geneva

Jain R (1980) A simple method of calculating the equivalent stiffnesses in mooring cables. Appl Ocean Res 2(3):139–142

Jonkman JM (2007) Dynamics modeling and loads analysis of an offshore floating wind turbine. Ph.D. thesis, University of Colorado

Kamman JW, Huston RL (1999) Modeling of variable length towed and tethered cable systems. J Guid Control Dyn 22(4):6020–6608

Ketchmam J, Lou Y (1975). Application of the finite element method to towed cable dynamics. In: Proceedings of the IEEE OCEANS 75 conference, pp 98–107, San Diego, CA, USA, 22–25 Sept 1975

Leonard JW, Nath JH (1981) Comparison of finite element and lumped parameter methods for oceanic cables. Eng Struct 3(3):153–167

Liu Y, Bergdahl L (1997) Influence of current and seabed friction on mooring cable response: comparison between time-domain and frequency-domain analysis. Eng Struct 19(11):945–953

Liu Y, Shu CW, Tadmor E, Zhang M (2008) L2 stability analysis of the central discontinuous galerkin method and a comparison between the central and regular discontinuous galerkin methods. ESAIM: Math Model Numer Anal 42(4):593–607

Low Y (2009) Frequency domain analysis of a tension leg platform with statistical linearization of the tendon restoring forces. Mar Struct 22(3):480–503

Malaeb D (1983) Dynamic analysis of tension-leg platforms. Ph.D. thesis, Texas A&M University

Masciola MD, Nahon M, Driscoll FR (2011) Static analysis of the lumped mass cable model using a shooting algorithm. J Waterw Port Coast Ocean Eng 138(2):164–171

Masciola M, Jonkman J, Robertson A (2013) Implementation of a multisegmented, quasi-static cable model. In: Proceedings of the 23rd international offshore and polar engineering (ISOPE 2013), Anchorage, Alaska, USA, 30 June–4 July 2013

Mehrabi AB, Tabatabai H (1998) Unified finite difference formulation for free vibration of cables. J Struct Eng 124(11):1313–1322

Mekha B, Johnson C, Roesset J (1996) Implications of tendon modeling on nonlinear response of TLP. J Struct Eng 122(2):142–149

Merchant H, Kelf M (1973) Nonlinear analysis of submerged ocean buoy systems. In: Proceedings of the IEEE OCEANS 73 conference, Seattle, WA, USA, 25–28 Sept 1973, pp 390–395

Morgan J (1983) Dynamic analysis of tension-leg platforms. ASME energy sources technology conference and exhibition, Houston, TX, USA

Nicoll RS (2006) Dynamic simulation of marine risers with vortex induced vibration. Master's thesis, University of Victoria

Nordgren R (1987) Analysis of high-frequency vibration of tension leg platforms. J Offshore Mech Arct Eng 109(2):119–125

Oran C (1983) Overall dynamic characteristics of tension leg platform. In: Proceedings of the 15th annual offshore technology conference, Houston, TX, USA, 2–5 May 1983, pp 2–5

Peyrot A, Goulois A (1979) Analysis of cable structures. Comput Struct 10(5):805–813

Powell G, Simons J (1981) Improved iteration strategy for nonlinear structures. Int J Numer Meth Eng 17(10):1455–1467

Ran Z (2000) Coupled dynamic analysis of floating structures in waves and currents. Ph.D. thesis, Texas A&M University

Rupe R, Thresher R (1975) The anchor-last deployment problem for inextensible mooring lines. J Manuf Sci Eng 97(3):1046–1052

Schram JW, Reyle SP (1968) A three-dimensional dynamic analysis of a towed system. J Hydronaut 2(4):213–220

Shugar T (1991) Automated dynamic relaxation solution method for compliant structures. In: Proceedings of the annual meeting of the American Society of Mechanical Engineers, New York, NY, vol 4, pp 1–12

Skop R (1988) Mooring systems: a state-of-the-art review. J Offshore Mech Arctic Eng 110 (4):365–372

Strang G (1988) Linear algebra and its applications, 3rd edn. Harcourt Brace Jovanovich, Fort Worth

Sun Y, Leonard J, Chiou R (1994) Simulation of unsteady oceanic cable deployment by direct integration with suppression. Ocean Eng 21(3):243–256

Van den Boom H (1985) Dynamic behaviour of mooring lines. In: Proceedings of the 4th behaviour of offshore structures (BOSS) international conference, Delft, The Netherlands, 1–5 July 1985

Veselic K (1995) Finite catenary and the method of Lagrange. SIAM Rev 37(2):224–229

Walton T, Polachek H (1960) Calculation of transient motion of submerged cables. Math Comput 14(69):27–46

Webster R (1980) On the static analysis of structures with strong geometric nonlinearity. Comput Struct 11(1):137–145

Williams P, Trivailo P (2007) Dynamics of circularly towed aerial cable systems, Part I: optimal configurations and their stability. J Guid Control Dyn 30(3):753–765

Wilson JF (2003) Dynamics of offshore structures. Wiley, Hoboken

Wu S (1995) Adaptive dynamic relaxation technique for static analysis of catenary mooring. Mar Struct 8(5):585–599

Zienkiewicz OC, Taylor RL (2000) The finite element method. Solid mechanics, 5th edn, vol 2. Butterworth-Heinemann, Oxford

Zueck R, Powell G (1995) Stable numerical solver for cable structures. In: Proceedings of the international symposium on cable dynamics, Liege, Belgium, 19–21 Oct 1995

References (4)

Bachynski EE (2014) Design and dynamic analysis of tension leg platform wind turbines. Dissertation, Norwegian University of Science and Technology

Bachynski EE, Moan T (2014) Ringing loads on tension leg platform wind turbines. Ocean Eng 84:237–248

Cook RD, Malkus DS, Plesha ME, Witt RJ (2002) Concepts and applications of finite element analysis, 4th edn. Wiley, Hoboken

DNV-RP-C203 (2010) Fatigue design of offshore steel structures. Det Norske Veritas, Høvik

DNV-OS-J103 (2013) Design of floating wind turbine structures. Det Norske Veritas, Høvik

Dr.techn. OLAVOLSEN (2012) EU Seventh framework programme: high power, high reliability offshore wind technology (HiPRwind) project—WP1: Platform concept

Hibbeler RC (2011) Mechanics of materials, 8th edn. Pearson Prentice Hall, Boston

Hoff JR (2001) Estimation of linear and quadratic roll damping from free-decay tests. Norwegian University of Science and Technology, Trondheim

Krenk S (2009) Non-linear modelling and analysis of solids and structures. Cambridge University Press, Cambridge

Kvittem MI (2014) Modelling and response analysis for fatigue design of a semi-submersible wind turbine. Dissertation, Norwegian University of Science and Technology, Trondheim, Norway

Taghipour R, Perez T, Moan T (2008) Hybrid frequency-time domain models for dynamic response analysis of marine structures. Ocean Eng 35:685–705

References (5)

Aksnes V, Berthelsen P, Da Fonseca N, Reinholdtsen S (2015) On the need for calibration of numerical models of large floating units against experimental data. In: Proceedings of the 25th international offshore and polar engineering conference (ISOPE) Kona, Hawaii, USA, 21–26 June 2015

Bae YH (2014) Development of a dynamic mooring module FEAM for FAST v8. Texas A&M University (TAMU), TX, USA

Bellew S, Yde A, Verelst D (2014) Application of the aero-hydro-elastic model, HAWC2-WAMIT, to offshore data from floating power plants hybrid wind-and-wave-energy test platform, P37. In: Proceedings of the 5th international conference on ocean energy (ICOE), Halifax, Canada, 4–6 Nov 2014

Bossanyi EA (2003) GH Bladed theory manual, Issue no. 11. Garrad Hassan and Partners Ltd., Bristol

Buils Urbano R, Nichols J, Livingstone M et al (2013) Advancing numerical modelling of floating offshore wind turbines to enable efficient structural design. In: Proceedings of the European Wind Energy Association (EWEA) Offshore, Frankfurt, Germany, 19–21 Nov 2013

Bulk M (2012) Evaluation of a lifting line free vortex wake method for wind turbine simulations. Thesis, University of Stuttgart

Cordle A (2010) State-of-the-art in design tools for floating offshore wind turbines. Project UpWind, deliverable report D4.3.5 (WP 4: Offshore Foundations and Support Structures)

Cordle A, Jonkman J (2011) State of the art in floating wind turbine design tools. In: Proceedings of the 21st international offshore and polar engineering conference (ISOPE), Maui, Hawaii, USA, 19–24 June 2011

Goupee AJ, Koo BJ, Lamrakos KF et al (2012) Offshore wind energy: model tests for three floating wind turbine concepts. In: Proceedings of the offshore technical conference, Houston, TX, USA, 30 April–2 May 2012

Hall M (2015) MoorDyn user's guide v.1.0.1. Department of Mechanical Engineering, University of Maine, Orono, ME, USA

Jonkman J (2010) Definition of the floating system for phase IV of OC3. Technical report NREL/TP-500-47535, National Renewable Energy Laboratory (NREL), Golden, CO, USA, May 2010

Jonkman J (2013) The new modularization framework for the FAST wind turbine CAE tool. In: Proceedings of the 51st AIAA aerospace sciences meeting, Dallas, TX, USA, 7–10 Jan 2013

Jonkman B, Jonkman J (2015) FAST v8.12.00a-bjj - Guide to changes in FAST v8. National Renewable Energy Laboratory (NREL), Golden, CO, Oct 2015

Jonkman J, Musial W (2010) Offshore code comparison collaboration (OC3) for IEA Task 23 offshore wind technology and deployment. Technical report NREL/TP-5000-48191, National Renewable Energy Laboratory (NREL), Golden, CO, USA, December 2010

Jonkman J, Butterfield S, Passon P el al (2007) Offshore code comparison collaboration within IEA Wind Annex XXIII: Phase II results regarding monopile foundation modeling. In: Proceedings of the IEA European offshore wind conference, Berlin, Germany, 4–6 Dec 2007

Jonkman J, Butterfield S, Musial W, Scott G (2009) Definition of a 5-MW reference wind turbine for offshore system development. Technical report NREL/TP-500-38060, National Renewable Energy Laboratory (NREL), Golden, CO, USA, Feb 2009

Jonkman J, Larsen T, Hansen A et al (2010) Offshore code comparison collaboration within IEA Wind Task 23: Phase IV results regarding floating wind turbine modelling. In: Proceedings of the European wind energy conference (EWEC), Warsaw, Poland, 20–23 April 2010

Jonkman J, Hayman G, Jonkman B, Damiani R (2015a) AeroDyn v15 user's guide and theory manual—draft version 6-Oct-2015. National Renewable Energy Laboratory (NREL), Golden, CO, USA

Jonkman J, Robertson A, Hayman G (2015b) HydroDyn user's guide and theory manual—draft version. National Renewable Energy Laboratory (NREL), Golden, CO, USA

Larsen TJ, Hansen AM (2015) How 2 HAWC2, the user's manual. Technical report Risø-R-1597 (ver. 4–6), Risø National Laboratory, Technical University of Denmark, Denmark

Lindenburg C, Schepers JG (2000) Phatas-IV aeroelastic modelling release "dec-1999" and "nov-200". Technical report ECN-CX-00-027, Energy Research Centre of the Netherlands (ECN), The Netherlands

Matha D, Beyer F (2013) Offshore wind turbine hydrodynamics modelling in SIMPACK. SIMPACK News, Ed. July 2013

Matha D, Fischer T, Kuhn M, Jonkman J (2009) Model development and loads analysis of an offshore wind turbine on a tension leg platform. In: Proceedings of the European offshore wind conference (EOWC), Stockholm, Sweden, 14–16 Sept 2009

Matha D, Schlipf M, Cordle A et al (2011) Challenges in simulation of aerodynamics, hydrodynamics and mooring-line dynamics of floating offshore wind turbines. In: Proceedings of the 21st international offshore and polar engineering conference (ISOPE), Maui, Hawaii, USA, 19–24 June 2011

Nichols J, Camp T, Jonkman J et al (2008) Offshore code comparison collaboration within IEA wind annex XXIII: Phase III results regarding tripod support structure modelling. In: Proceedings of the 47th AIAA aerospace sciences meeting. Orlando, FL, USA, 5–8 Jan 2008

Ormberg H, Bachynski EE (2012) Global analysis of floating wind turbines: code development, model sensitivity and benchmark study. In: Proceedings of the 22nd international offshore and polar engineering conference, Rhodes, Greece, vol 1, pp 366–373

Passon P, Kühn M, Butterfield S et al (2007) OC3-Benchmark exercise of aero-elastic offshore wind turbine codes, J Phys Conf Ser (Online) 75:12

Popko W, Vorpahl F, Zuga A et al (2012) Offshore code comparison collaboration continuation (OC4), Phase I—results of coupled simulations of an offshore wind turbine with jacket support structure. In: Proceedings of the 22nd international ocean and polar engineers conference (ISOPE), Rhodes, Greece, 17–23 June 2012

Robertson A, Jonkman J, Vorpahl F et al (2014) Offshore code comparison collaboration continuation within IEA Wind Task 30: Phase II results regarding a floating semisubmersible wind system. In: Proceedings of the 33rd international conference on ocean, offshore and Artic engineering, San Francisco, CA, USA, 8–13 June 2014

Skaare B, Hanson TD, Nielsen FG et al (2007) Dynamics of floating wind turbines utilising integrated hydro- and aerodynamic analysis. In: Proceedings of the European wind energy conference (EWEC) 2007, Milan, Italy, 7–10 May 2007

Vorpahl F, Popko W, Kaufer D (2011) Description of a basic model of the "UpWind reference jacket" for code comparison in the OC4 project under IEA Wind Annex XXX. May 2011. Fraunhofer Institute for Wind Energy and Energy System Technology (IWES), Bremerhaven, Germany

References (6)

Browning JR, Jonkman JM, Robertson AN, Goupee AJ (2012) Calibration and validation of the FAST dynamic simulation tool for a spar-type floating offshore wind turbine. In: Proceedings of the science of making torque from wind conference, Oldenburg, Germany, 9–11 Oct 2012

Chakrabarti SK (1994) Offshore structure modeling. World Scientific Publishing Co. Pte. Ltd., Singapore

Coulling AJ, Goupee AJ, Robertson AN et al (2013) Validation of a FAST semi-submersible floating wind turbine model with deepcwind test data. J Renew Sustain Energy 5:023116

de Ridder E-J, Otto W, Zondervan G et al (2014) Development of a scaled-down floating wind turbine for offshore basin testing. In: Proceedings of the 33rd international conference on ocean, offshore and arctic engineering, San Francisco, CA, USA, 8–13 June 2014

Drela M (1989) XFOIL: An analysis and design system for low Reynolds number airfoils. In: Mueller T (ed) Low Reynolds number aerodynamics. Lectures notes in engineering, vol 54. Springer, Heidelberg, pp 1–12

Goupee AJ, Fowler MJ, Kimball RW et al (2014) Additional wind/wave basin testing of the deepcwind semi-submersible with a performance-matched wind turbine. In: Proceedings of the 33rd international conference on ocean, offshore and arctic engineering, San Francisco, CA, USA, 8–13 June 2014

Gueydon S (2015) Verification of the second-order wave loads on the OC4-semisubmersible. Work presented at the 12th deep sea offshore wind R&D conference EERA DeepWind'2015, Trondheim, Norway, 4–6 Feb 2015

Gueydon S, Fernandes G (2013) Scaling methodologies for floating wind turbines. In: Proceedings of European Wind Energy Association offshore conference, Frankfurt, Germany, 19–21 Nov 2013

Gueydon S, Weller S (2013) Study of a floating foundation for wind turbines. J Offshore Mech Arct Eng 135(3):031903

Huijs F, de Ridder E-J, Savenije F (2014) Comparison of model tests and coupled simulations for a semi-submersible floating wind turbine. In: Proceedings of the 33rd international conference on ocean, offshore and arctic engineering, San Francisco, CA, USA, 8–13 June 2014

Jonkman JM (2010) Definition of the floating system for phase IV of OC3. NREL technical report NREL/TP-500-47535, National Renewable Energy Laboratory (NREL), Golden, CO, USA, May 2010

Jonkman JM, Buhl Jr ML (2005) FAST user's guide. NREL technical report NREL/EL-500-38230, National Renewable Energy Laboratory (NREL), Golden, CO, USA, Aug 2005

Jonkman JM, Butterfield S, Musial W, Scott G (2009) Definition of a 5-MW reference wind turbine for offshore system development. NREL technical report NREL/TP-500-38060, National Renewable Energy Laboratory (NREL), Golden, CO, USA, Feb 2009

Kimball RW, Goupee AJ, Fowler MJ et al (2014) Wind/wave basin verification of a performance-matched scale-model wind turbine on a floating offshore wind turbine platform. In: Proceedings of the 33rd international conference on ocean, offshore and arctic engineering, San Francisco, CA, USA, 8–13 June 2014

Koo BJ, Goupee AJ, Kimball RW, Lambrakos KF (2014) Model tests for a floating wind turbine on three different floaters. J Offshore Mech Arct Eng 136(2):021904

Martin HR (2011) Development of a scale model wind turbine for testing of offshore floating wind turbine systems. M.Sc. thesis, University of Maine

Martin HR, Kimball RW, Viselli AM, Goupee AJ (2014) Methodology for wind/wave basin testing of floating offshore wind turbines. J Offshore Mech Arct Eng 136(2):020905-1

Nielsen FG, Hanson TD, Skaare B (2006) Integrated dynamic analysis of floating offshore wind turbines. In: Proceeding of the 25th international conference on offshore mechanics and arctic engineering, Hamburg, Germany, 4–9 June 2006

Prowell I, Robertson AN, Jonkman JM et al (2013) Numerical prediction of experimentally observed scale-model behaviour of an offshore wind turbine supported by a tension-leg platform. In: Proceedings of the offshore technology conference 2013, Houston, TX, USA, 6–9 May 2013

Rao SS (2004) Mechanical vibrations, 4th edn. Pearson Prentice Hall, Upper Saddle River

Ren N, Li Y, Ou J (2012) The effect of additional mooring chains on the motion performance of a floating wind turbine with a tension leg platform. Energies 5(4):1135–1149

Robertson AN, Jonkman JM, Masciola MD et al (2013) Summary of conclusions and recommendations drawn from the DeepCwind scaled floating offshore wind system test campaign. In: Proceedings of the ocean, offshore and arctic engineering conference, Nantes, 9–14 June 2013

Roddier D, Cermelli C, Aubault A, Weinstin A (2010) WindFloat: a floating foundation for offshore wind turbines. J Renew Sustain Energy 2:033104

Stewart GM, Lackner MA, Robertson AN et al (2012) Calibration and validation of a fast floating wind turbine model of the DeepCwind scaled tension-leg platform. In: Proceedings of the 22nd international Ocean and polar engineering conference, Rhodes, Greece, 17–22 June 2012

Weller S, Gueydon S (2012) Analysis of the DeepCwind model tests and a first attempt to simulate a semi-submersible floating wind turbine. Report no. 24602-MSG-1, MARIN, Wageningen, The Netherlands

Windsea AS (2010) Next generation floating wind farm. Scand Oil-Gas Mag 7(8):250–253

Key Design Considerations

James Nichols, Knut O. Ronold and Anne Lene Hopstad

Floating offshore wind turbines are exposed to varied combinations of environmental loads. The theories behind how the different environmental forces cause loading on the wind turbine have been covered in Chapter "Modelling of Floating Offshore Wind Technologies"; Sect. 1 addresses the combinations of environmental situations which need to be investigated when designing a floating wind system as well as how they are transferred into design fatigue and extreme loads. The design of FOWT must achieve a system with an acceptable level of structural reliability, based on the environmental conditions they are exposed to.

For the various stakeholders in the wind turbine industry, such as owners, designers and insurance companies, it may be of interest to obtain independent proof or evidence that the units that together form a floating wind farm meet certain standards with respect to safety and structural integrity. Adherence to a certification scheme, based on a set of structural design standards, is a formalised way of obtaining such evidence. Sect. 2 presents an overview of the design standards for FOWT structures and outlines the certification process.

J. Nichols (✉)
Lloyd's Register EMEA, 71 Fenchurch Street, London EC3M 4BS, UK
e-mail: james.nichols@lr.org

K.O. Ronold · A.L. Hopstad
DNV GL, Veritasveien 1, N-1322, Høvik, Norway
e-mail: knut.ronold@dnvgl.com

A.L. Hopstad
e-mail: anne.lene.hopstad@dnvgl.com

1   Design Loads

James Nichols

Loads on a FOWT are a function of several environmental processes occurring simultaneously and interacting with one another. In principal all environmental effects should be considered in combination according to the return period of an environmental state. However, the lack of studies comprising detailed measurements of combined wind, wave, current, tidal and other environmental variables means that each is traditionally taken as an individual effect before being combined according to standard rules.

At the time of writing, a number of standards, guidelines, technical specifications and guidance notes for the design of floating offshore wind turbines have been prepared by the IEC and recognised classification societies. These give guidance as to the methods for combining environmental effects in order to produce a system with an acceptably high level of structural reliability. This section will follow the guidelines' approach while giving an overview of the possible developments which may follow in the years to come.

1.1   Environmental Loads

Wind Loading

Chapter "Modelling of Floating Offshore Wind Technologies", Sect. 1 examined the aerodynamic loading on the wind turbine. In principle, the wind conditions for a FOWT do not substantially differ from those experienced by a fixed offshore wind turbine (see Chapter "The Offshore Environment", Sect. 1). Nevertheless, there are some important subtleties caused by the difference in frequency of the platform motion. The first of these is the required time period for design related simulations; the length of the simulation is also governed by wave loading, but the time period of the natural periods of surge and sway may exceed 100 s and a 10-min simulation may no longer be sufficient to give a representative description of fatigue or extreme loads, especially for the mooring system. The length of simulation has been studied in detail by, for example, Stewart et al. (2013). A full discussion of the effects will be left to Sect. 1.3.

It should also be noted that the wind loading is a combination of aerodynamic loading on the rotor as well as drag on the tower and nacelle. This can have a significant importance on the stability of the control algorithm. As noted in, for example, Jonkman (2007), a traditional floating wind turbine control algorithm can become unstable on a floating wind turbine because of the combination of the long period of the platform surge and pitch motions, with the negative slope of the thrust with respect to wind speed. However, including drag on the tower and nacelle as well
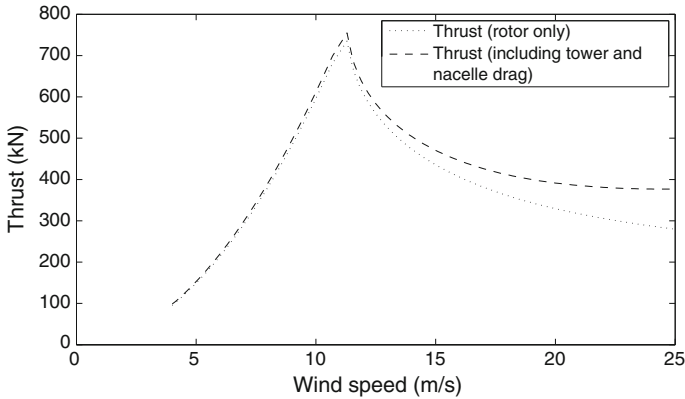
Fig. 1 Example rotor thrust and total thrust as a function of wind speed for a FOWT

as rotor thrust moderates this effect, increasingly so at high wind speeds (Fig. 1). A key issue with the modelling of combined wind forces is how they interact with each other; the models used to predict changes in flow around the wind turbine tower and the blade element momentum theory, which is used to predict the overall wind inflow across the rotor, are both formulated independently and a simple summation of the effects may not be accurate. Additionally, the drag forces on the tower and nacelle will be influenced by the induction of the rotor. Different assumptions made when combining these forces could lead to significant differences or may be masked by assumptions made in specifying the drag coefficients of the different structures.

Wave Loading

Wave loading will be of prime importance for the analysis of FOWTs, far more so even than for bottom-fixed offshore wind turbines because of the larger water plane area of many of the concepts. However, because of the high importance of dynamic wind loading relative to structures in the offshore oil and gas industry, time-domain methods must be used for analysis and there is a resulting challenge to cover all of the relevant sea states and corresponding wind conditions in the time-frame of the development of a project. For a general offshore project, the starting point would be to obtain the $H_s - T_p$ scatter diagram showing the probability of significant wave height and wave period for each wave direction. From this, a contour of extreme sea state conditions can be drawn, see Fig. 2. This would then be combined with a frequency-domain analysis of the floating structure motion and loading in order to find the extreme loading conditions for every directional sector.

For the FOWT, the problem is compounded by the necessity of performing the analysis for a number of different wind speeds. Additionally, with the use of frequency domain methods not being widely accepted, the result is a large number of time-domain simulations. Response amplitude operators (RAOs) are used to characterise the linear response of floating platforms. For the floating offshore wind turbine, the concept of *effective RAOs* has been introduced, see Jonkman and Musial

Fig. 2 Extreme wave
contour based on the Upwind
Design Basis (2010)
deepwater site
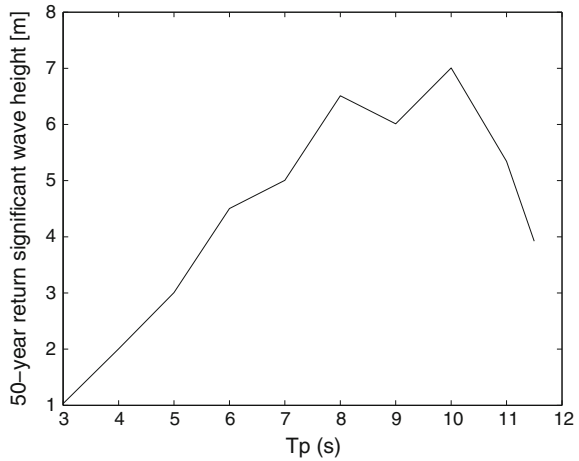
(2010), which show the response of the platform including the aerodynamic
damping which reduces the response during operation. The approach has the benefit
of showing the sea-states which should drive the loading. However, it also has
significant drawbacks. Firstly, the wind loading is highly nonlinear so the driving
sea-states at one amplitude are not guaranteed to be the same when the amplitude
increases. Additionally, it takes no account of the variation in loading due to wind
speed variations.

The importance of second-order wave loading is also an issue which requires
attention. Standards and guidelines such as GL-IV-2 (2012) prescribe that
second-order wave loads must be included in calculations. However, it is not clear
to what extent second-order wave loads are important, at least for the operational
load cases (see also Chapter "Modelling of Floating Offshore Wind Technologies",
Sect. 2). In these scenarios the sea-states are not generally as extreme as those in
storm conditions when the turbine is shut down so that the effect on ultimate loads
may be fairly small, as described in for example Duarte and Sarmento (2014) which
looks at a spar platform. The balance may be different for larger water-plane area
platforms such as the semi-submersible considered by Bayati et al. (2014).

More highly nonlinear effects need to be considered for platforms with bracing or
other structures which might experience impact from waves. These forces are known
as slapping, if a steep wave impacts on a structure, or slamming, when the rising sea
surface immerses part of the platform. While near-shore wind farms may be concerned
about these effects from breaking waves, floating offshore wind turbines with braced
platforms may encounter these conditions due to the motion of the platform relative to
the sea surface. There are a number of empirical methods which are employed
involving slap and slam coefficients to calculate effective pressure over the exposed
area. This loading is localised and is impulsive, which can cause higher-frequency
structural vibrations than would be predicted by linear or second-order wave models.
Two models widely used are those by Wienke (2001) and DNV-OS-J101 (2011).

One issue with floating structures is that for extreme sea states, the loading predicted by linearised models may be under-conservative. For fixed offshore structures, this difference was noted for the case of extreme sea state calculations and resulted in methods being developed for including stream function waves into stochastic sea states and included in international standards such as IEC 61400-3 (2009). The question for floating structures is whether the nonlinear effects from the instantaneous wetted area and stretching of the wave kinematics are more important than the diffraction effects.

For a cylinder (see also Chapter "Modelling of Floating Offshore Wind Technologies", Sect. 2), the diameter at which diffraction becomes significant is given by the approximate relationship:

$$d \approx 0.2\lambda \tag{1}$$

Taking this as a hard cut-off, most extreme states (assuming that an extreme sea state would have a H_s larger than 6 m and using the relationship from the IEC 61400-3 (2009) standard for the time period of the extreme wave):

$$11.1\sqrt{H_s/g} \leq T \leq 14.3\sqrt{H_s/g} \tag{2}$$

This time period, 8.7 s, would mean that structures with a characteristic diameter of less than 23 m would not be subject to significant wave diffraction effects (Fig. 3).

Current Loading

Currents arise from astronomically driven tidal flows, wind generated near-surface flows, density currents, storm surges and wave driven flows near to shore (see Chapter "The Offshore Environment", Sect. 3.1 for further information on currents). Depending on the site, these effects may or may not be correlated and may come from different directions. Additionally, they will have different profiles with depth with wind generated currents assumed to decay linearly with depth over a range of

Fig. 3 Time period at which diffraction becomes important
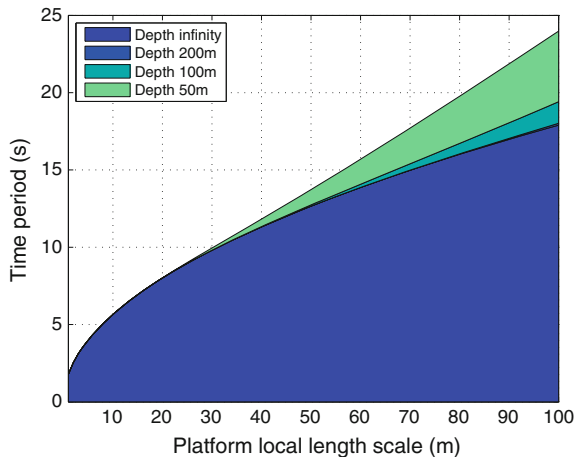
20–50 m (according to the standard used), astronomical tides varying with a 1/7th power law and currents due to breaking waves assumed to be constant with depth.

Current loading will cause the platform position to vary from the position in still water. Mooring system responses can be highly nonlinear and this may influence the surge, sway and yaw natural periods of the floating platform. However, except for barge-type platforms, with a large water plane area, the displacement is likely to be small compared to that from the wind loading.

It should be noted that while a wave-dominated sea state may be stationary over three hours, the current velocity may have changed by 100 % over that time. Nevertheless, for extreme load cases, the current would be taken as the maximum possible over a tidal cycle for the given return period. However, for fatigue design cases, the current is assumed to be zero in some design periods. This is because the fatigue damaged is dominated by the range of the cyclic loading rather than the mean and while the current may increase the mean load, a current may also increase the hydrodynamic damping of the platform, reducing cycle ranges.

This assumes that current flows do not result in additional sources of loading such as vortex induced vibrations. These are expected to be most significant for spar buoy floating platforms where there is the possibility of highly collimated flow along the length of the spar. It requires large depths so that the variation in current speed does not cause the Strouhal frequency to vary too significantly along the length of the spar:

$$f_{Strouhal} = \frac{St.V}{D} \tag{3}$$

where St is the Strouhal number which is a function of the cross-sectional shape and the Reynolds number; V is the relative flow velocity; and D is the relative length scale, for example the diameter of the cylinder.

1.1.1   Tidal Loading

The influence of tide is most pronounced for structures with taut moorings because of the influence on pre-tension. However, the influence of tide can have an effect on catenary moorings as well. For example, the OC3 Hywind spar (500 m line for a spar in 320 m water depth) there would be a 2 % increase in the tension for an increase in water depth of 1 m.

It might be expected that floating offshore wind farms would be predominantly sited in areas where the tidal range is not a significant factor but for example the Pelastar tension leg platform was destined for a site in the Bristol Channel where the average tidal range is 3.5 m (Hurley and Nordstrom 2014).

Seismic Loading and Tsunamis
For catenary moored structures, seismic loading is generally considered unimportant. However, it is important that the anchoring system is designed to withstand the

geotechnical conditions which may occur during seismic activity such as the dynamic soil behaviour and liquefaction (ISO 19901-4 2003).

For taut-moored systems, the seismic motion of the seabed may directly induce loading on the floating platform and this needs to be assessed in design. Several design simulation packages for wind turbines include the ability to model seismic loading. However, it needs to be assessed that they are capable to model the differential loading due to the passage of the seismic wave.

Sea Ice Loading

Sea ice can cause loading either from collisions or from slow passage around an offshore structure (see Chapter "The Offshore Environment", Sect. 3.3). Loading from collisions is highest in arctic areas and depends on the probability of collision, iceberg size distribution, relative speed, ice pressure, contact pressure and water-line shape of the floating structure as described in detail in ISO 19906 (2010).

The slow passage of an ice sheet past an offshore structure has been studied more closely in offshore wind turbine literature since the passage of sea ice may be applicable for some sites in the Baltic. Jussila et al. (2013) describes the application of a method for ice loading adapted from the offshore industry to simulate the loading from continual build-up of ice and subsequent crushing along with the phenomenon of lock-in where the frequency of ice failure adapts to the natural frequency of the offshore structure. ISO 19906 (2010) states that observations of this phenomenon are limited to frequencies of 0.4–10 Hz which is likely to be higher than the surge and sway frequencies of floating offshore wind turbines. SAMCOT (2013) states that, while lock-in has not yet been observed for floating offshore structures, this may be due to lack of experience. Additionally, arctic offshore floating structures have been deployed with icebreaker assistance, something which may not be economically feasible for an offshore wind farm. SAMCOT (2013) also states that the mechanism which results in lock-in for floating structures would be ice-breaking due to bending, rather than crushing, which has a lower natural frequency allowing it to potentially couple to floating offshore structure modes.

Farm Effects

To date floating offshore wind turbines have only been deployed as isolated installations far from the nearest neighbouring turbine. However, the Hywind Scotland pilot park, as described by Meulepas (2014) and presented Chapter "State-of-the-Art", Sect. 2.4, will feature the first farm of five turbines as a steppingstone on the way to large commercial projects.

One of the stated aims of the project is to demonstrate the operation of multiple units. This is important because of the impact wake effects have on the energy yield of large wind farms. Before embarking on constructing large floating farms, governments and investors want to know that the energy predictions given for floating farms are as reliable as those for fixed installations. Larsen et al. (2008) presents a model of wake effects which has been gaining acceptance as the best way to effectively model the dynamic loading effects of wind turbines operating in each

other's wakes. However, to apply it to floating wind turbines, it would be necessary to incorporate the dynamic translation and yaw of the floating platform (and therefore the wake). This may result in wind loading at the platform periods of motion and therefore introduces the possibility of collective phenomena for floating platforms which are not seen for fixed turbines.

The Hywind Scotland pilot park is of particular interest from the perspective of system dynamics because, along with the interaction between turbines from wake dynamics, the turbines will be coupled through the tension in the intra-farm electrical cables which are not anchored to the seabed. Although this effect is likely to be small, the damping for the platform modes is also likely to be low and small effects may be important for platform control design.

The third area which could result in turbine dynamic interactions is the effect on the incident waves of other platforms. It is known from the wave energy industry that these array effects can be significant. However, the design philosophy of a floating wind platform is such as to minimise the response of the platform due to waves. Nevertheless, for some concepts such as the barge a large waterplane area is presented and the effects may be such that the effects could be felt at neighbouring turbines.

1.2 Ultimate and Fatigue Loads

Designers are concerned with the probability of failure. It's a quantity which is easy to define but much harder to calculate. If the whole of a system were deterministic, it could be designed such that it would definitely last for a certain lifetime. Unfortunately for wind turbines, the environmental conditions are stochastic; the failure properties of materials are only determined to within a range of uncertainty and the numerical models used to simulate them also introduce their own uncertainties. These individual random (and also sometimes systematic) errors are often hidden behind the processes encompassed in design standards where quantification of uncertainties is replaced by defined safety factors. The partial safety factor method is widely used in the wind industry whereas the allowable stress method is more commonplace in the marine and offshore industries.

A starting point for use of reliability analysis in the design of wind turbines is given for example in Veldkamp (2006) and it is now being incorporated into the latest generation of standards.

Limit States

The offshore industry has been accustomed to using limit states to define the boundaries of acceptable loading and motion on a system. For example, the ISO 19904-1 (2006) standard defines the use of ultimate, fatigue, serviceability and accidental limit states. Conversely, the wind industry has traditionally partitioned design situations into only fatigue and ultimate design load cases. With increasing crossover due to the growth of the offshore wind industry, these ideas have become more mixed in the establishment of offshore and floating offshore design standards.

This difference in approach is due to the special way in which the environmental loading is dependent on the operation of the turbine. This means that ultimate structural loads may be caused not during extreme environmental conditions with low return periods but during moderate environmental conditions combined with either unlikely short term environmental conditions (gusts), or failure conditions of the turbine control or safety systems. Therefore, for a wind turbine, serviceability and accidental limit states are assessed as different interpretations of the ultimate design load cases rather than by separate groups of load cases. For example, the serviceability limit state would address the torque that a pitch actuator drive requires in order to pitch a blade during extreme events; the ultimate limit state would consist of the structural loading created by the event.

Serviceability is one area where uncertainty is not well catered for and there is no recognised format for safety factors. For instance, according to standards, the turbine could be designed such that the maximum torque available from the pitch actuator could be just over the maximum value from simulations. However, the loading that could result from the pitch actuator torque being exceeded (and the pitch angle changing uncontrollably) could be highly nonlinear.

1.3 Design Load Cases

In an ideal world, the professional wind turbine designer would simulate the wind turbine with the exact flow conditions it will experience over the next twenty years. The simulation would model the turbulent inflow across neighbouring physical constraints, and also the wakes from neighbouring wind farms which might spring up over the coming decades. Unfortunately, so far, no designer has had the computing resources available to perform this mammoth task. The current design methods have evolved from days of relatively small computing power compared to today where the events which might be expected over the course of a 20-year or more lifecycle were distilled down to a few-dozen events ranging from 1 to 10-min in length. These design load cases had to capture two main scenarios: the rare, once in 50 years' occurrences which would drive extreme loading on the turbine; and the day-to-day loading experienced by the turbine in order to estimate its fatigue life without too much over conservatism.

So what is a load case? Broadly defined for an offshore wind turbine, it is a combination of environmental conditions coupled with the control state of the wind turbine. Load cases will have a return period or probability of occurrence associated with them. The environmental conditions can consist of wind, wave, current, earthquake, sea ice conditions. Each will have several parameters associated with it, for example the wind may be turbulent, steady, or model a specific transient gust, while the waves will be characterised by significant wave height, peak spectral period, direction and the form of the spectrum.

For an onshore turbine to a set of class conditions defined by the IEC 61400-1 (2005) standard, there are a minimum of around 2500 simulations which need to be

run consisting of various combinations of wind speed, yaw error, starting azimuth angle, turbulence intensity and fault condition or wind transient condition. With today's software, this amounts to just under 10 days of CPU time assuming the simulations can be run in real-time, which is possible in many currently available software packages. For an offshore wind turbine, these load cases may be combined with multiple sea states of varying significant wave height, spectral peak period and direction leading to a much larger number of simulations, and with the extra computing cost of calculating the wave loading on a complex support structure, the simulations may be several times slower.

Fatigue Load Cases

Fatigue load cases cover events which might be expected to occur over the lifetime of the structure. Most wind turbine design standards require that simulations are performed over the operational range of the wind turbine with hours binned for every 2 m/s wind speed range. This results in 10–15 operational wind speed bins. Additional bins are required to accommodate wind speed ranges below cut-in and above cut-out wind speed. For offshore wind turbines, the operational wind speed range also needs to be accounted for with the turbine in a standby condition to account for the availability. For onshore wind turbines, this is neglected since the operational state generally results in conservative loading. However, for offshore wind turbines this is not necessarily the case. Finally, transient simulations are included to account for the load cycles caused by the turbine starting up and shutting down since this typically results in a large change in thrust and torque.

For each of the wind speed bins, an equivalent turbulence intensity is defined representing the 90th percentile value of turbulence. Various studies have been done to assess to what degree this assumption is conservative such as Veldkamp (2006) with the conclusion that it is conservative but not to a large extent.

The wind conditions have to be combined with probability according to the wave scatter diagram, Table 1 shows an example scatter diagram used in a European research project. This is part of the typical design procedure (see for example Sect. 10.3 of ISO 19901-4 (2003)) for offshore structures when frequency-domain analysis is used. However, when time-domain analysis is used, the number of simulations required becomes impractical and efforts are made to reduce this by lumping different sea states into coarser bins, see for example the RECOFF Project (2006). While for fixed offshore structures, it is acceptable to assume that the load is proportional to the height of the wave, for a large floating structure where diffraction may be important this may no longer be true.

Instead of using the following equations for damage equivalent sea states as follows:

$$H_{s,eq} = \sqrt[m]{\sum_{i=1}^{n} P(H_{s,i}) \cdot H_{s,i}^{m}} \tag{5.4}$$

Table 1 Example scatter diagram, Upwind Design Basis (2010) deepwater site

H_s (m)	T_p (s)									
	3	4	5	6	7	8	9	10	11	>11.5
7.00										0.00003
6.50								0.00002	0.00009	0.00005
6.00								0.00019	0.00014	0.00005
5.50							0.00008	0.00061	0.00033	0.00005
5.00							0.00084	0.00138	0.00031	0.00006
4.50						0.00011	0.00342	0.00132	0.00014	0.00002
4.00					0.00003	0.0024	0.00663	0.00087	0.00019	0.00002
3.50					0.00058	0.01269	0.00709	0.00078	0.00008	0.00002
3.00				0.00002	0.01058	0.02576	0.00478	0.00045	0.00003	0.00006
2.50				0.00098	0.05074	0.02189	0.00263	0.0005	0.00011	0.00002
2.00			0.00006	0.03047	0.07924	0.01285	0.00255	0.00028	0.00002	0
1.50			0.00649	0.11598	0.06449	0.01419	0.00252	0.00014	0.00002	0.00003
1.00		0.00313	0.08888	0.12814	0.04869	0.00978	0.00143	0.00011	0.00003	0.00003
0.50	0.00008	0.0474	0.10613	0.05166	0.01355	0.00241	0.00082	0.00017	0.00003	
<0.25		0.00224	0.0056	0.0012	0.00006					

$$\frac{1}{T_{p,eq}} = \sum_{i=1}^{n} \frac{P(T_{p,i})}{T_{p,i}} \tag{5.5}$$

The equations would need to be modified to account for the loading changing as a function of frequency as well as wave height. One way of doing this would be to replace the assumption of linear variation of force with wave height by the result from the response amplitude operator (RAO). While for offshore structures, these RAOs have been generated using the linearised hydrodynamic models of the platform, for wind there may be the necessity to generate them using time-domain simulations to account for the effects of wind turbine operation (see Fig. 4). For this, the sea state spectrum needs to be used to account for each sea state containing a range of frequencies, and finally, the frequency used should be chosen to attain the correctly averaged response.

Extreme Load Cases

The method for extreme load cases should follow that for fixed offshore structures with the exception that the results are likely to be much more dependent on the wave frequency. Over the last fifteen years or so, the wind turbine industry has progressed from using short, transient simulations to using a larger number of longer simulations with stochastic wind and wave conditions. For the current set of load cases defined in the IEC 61400-3 (2009) standard, either the effect of wind or waves dominates such that normal conditions are chosen for wind and extreme for wave; or vice versa.

The control system is often critical for determining the extreme loads and the load cases involving failures are important to get correct. The challenge for floating wind is to perform simulations in a way that reliable values for short term events can be found without the length of simulations being excessive. For example, the peak yawing moment generated by a blade pitch failure may be very sensitive to

Fig. 4 Platform surge response amplitude operator for the DeepCWind platform
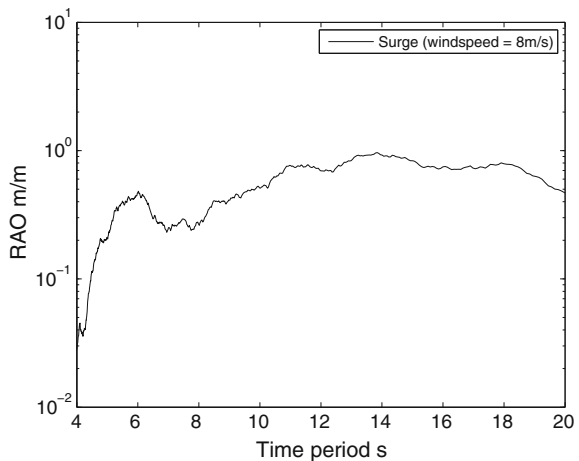
rotor azimuth angle but it will also depend on the platform pitch angle which might vary over the course of over 100 s.

The current generation of standards uses averaging over a number of realisations of stochastic environmental conditions (designated by seed numbers referring to the numerical input used to generate the time series) for all load cases with turbulent wind, with the exception of the extreme load extrapolation load case where normal conditions are used but the response is extrapolated to a 50-year return. This analysis normally consists of a minimum of 15 seeds per wind speed bin but, in order to get a reliable estimate, often many more seeds need to be used in order to capture the tail of the distribution.

The next years of development are likely to see further optimisation of the methods used with greater experience enabling the probability of failure scenarios to be estimated and more testing of materials and structural geometries specific to wind turbines allowing safety factors to be tailored to the specific design. A thorough reliability based design will clarify some of the conservative factors which can be introduced when uncertainties over many input variables are accounted for by single values.

1.3.1   Conservatism and Tolerances

Design calculations are often boiled down to a single set of parameters which are intended to be a marginally conservative representation of the installation over its lifetime. However, each parameter represents a distribution, both of variations during an installation's lifetime, as well as tolerances in the manufacturing and installation processes. Factors that need to be considered include masses of all components, growth of marine organisms on the exterior (resulting in a change in hydrodynamic coefficients as well as dimensions), corrosion, any additional items/personnel transferred to the platform for maintenance, accreted snow and ice for turbines in cold climates, tension and position of mooring lines and leakage. These need to be considered in addition to the tolerances associated with modelling the wind turbine behaviour such as set angle of the blades and aerodynamic parameters.

The complication is that the way changes to these parameters affects loading may not be straightforward. For example, marine growth may increase loading by causing a marginal increase in water plane area but this effect may be increased by the additional viscous drag loading from waves, or the damping from this additional surface roughness may result in lower overall response. Careful thought needs to go into the choice of model parameters, and where an analytical argument for the resulting effect is not conclusive; justification may need to be made with simulations of model tests.

1.3.2   Simulation Length

Simulation length is an important issue for floating wind turbines because of the significant interaction between aerodynamic loading and wave loading and the long time period of platform motion. Traditionally, wind turbines have been simulated with 10-min simulations (Burton et al. 2011) in order to capture the turbulent fluctuations while maintaining statistical stationarity of the spectrum due to the spectral gap in the van der Hoven wind spectrum between 10-min and 1 h. Conversely, conventional wisdom in the offshore industry tells us that 3–6 h simulations are necessary to capture the extremes of wave loading.

Therefore, several standards and guidelines have required that simulations lengths for floating wind turbines be extended beyond the ten minutes usually required for fixed bottom wind turbines. For example, the GL-IV-2 (2012) Guideline asserts that simulation length should be doubled to twenty minutes while the DNV-OS-J103 (2013) standard asserts that 3–6 h' simulations may be necessary to capture some of the extreme and fatigue loading due to second order wave forces and long period platform motions, while acknowledging that this conflicts with the assumption of the wind spectrum being stationary over the length of the simulation which is no longer true for timescales longer than 1 h.

The study by Stewart et al. (2013) showed that the method showed that, using the same amount of turbulent wind information, the increases in fatigue and extreme loads varied by a relatively small amount (of the order of 2 % for fatigue loads and negligible influence on extreme loading). However, the results were specific to a spar buoy with minimal second order response which was not considered in the study. A procedure for compromising between the requirements for simulation length between the wind and wave modelling has been prepared in the development of the upcoming technical specification IEC 61400-3-2 which consists of using periodic wind time histories of length 10-min, combined with 3–6 h wave kinematic time histories.

1.3.3   Faster Design Tools and Pre-Selection of Load Cases

With the large amount of time required to perform the number of design load cases, there has been increasing effort in the field of developing tools to provide alternative calculation methods which can be used to progress designs during selection of different concepts and optimisation of a chosen platform design. These normally come in two different flavours: (i) frequency-domain tools and (ii) reduced order methods.

While a full set of simulations for certification may take several weeks running on a handful of processors, these faster tools would be expected to run in a few days or less on a single machine. Their utility depends on the relative importance of the physics which they remove from the problem relative to a full-order time-domain code and the result may differ depending on the platform type. If they are to be used in order to pre-selection of load cases for certification, it is essential that they are

conservative relative to higher fidelity methods. If they are to be useful for optimisation of designs, it also needs to be shown that the relative difference in loading between different models does not vary so much that an optimal solution arrived at using the lower fidelity method does not turn out to be far away from the true optimum.

Reduced-order models, as described by Matha et al. (2014), remove higher-frequency modes of motion such as structural degrees-of-freedom in order to run time-domain simulations many times faster than would be possible for a typical wind turbine model used for final design. Whether this is a reasonable approximation depends on the frequency of the degrees-of-freedom which are omitted and the relative magnitude of the deflections due to rigid body platform motion and those due to structural deflections of the tower and blades. As well as the inertial loading due to structural vibrations, the deflections of the blades will also contribute to the change in overturning moment, reducing stability.

Frequency-domain methods restrict the calculation to linear or weakly nonlinear analysis. Lupton (2014) shows how frequency-domain and time-domain analysis compare across structural dynamics, aerodynamics, hydrodynamics and control system dynamics. Frequency-domain approaches are widely used in the offshore industry while they have been widely rejected in the wind industry; currently, they are not permitted in the wind industry for producing design loads for certification, however, that would not prevent them being used as a tool in the design process and may be used as a basis to identify driving sea states for some load cases at the discretion of the certification body. There are of course many linear assumptions that are used in widely used simulation methods such as linear deflections for towers and blades, linear hydrodynamic excitation forces and linear assumptions in dynamic wake models and it is important to understand which are the nonlinear elements which are crucial for an accurate estimation of loading and in what range of conditions for which linear approximations are valid.

1.3.4 Simulation of Platform Control

Modern wind turbines have much more complex control systems than were used originally onshore where industrial PID loops were used to give basic control of generator speed and torque. Many modern turbines use signals from accelerometers mounted in the nacelle to provide active damping to tower-top motion and this will be even more important for floating turbines than for fixed structures. Floating turbines may use six degree of freedom monitoring devices and use individual blade pitch control as well as collective blade pitch behaviour to control platform surge, sway, pitch, roll and yaw motion. With the frequency of these modes being very low compared to onshore wind turbine natural frequencies, the control will be more sensitive to low frequency changes in wind speed and second-order wave drift forces.

Additionally, modern wind turbines in large farms may be optimised to perform in different conditions such as temperature (and hence air density) variations,

reduced power output required by the grid and reducing wake effects on down-stream turbines. While traditionally, the yaw control of wind turbines is not required to be simulated in design cases, the frequency of this motion and the dynamics of the platform yaw motion may mean that it becomes important to include the effect.

A few floating wind concepts introduce physical control mechanisms onto the platforms themselves. Principal Power, for instance includes a dynamic ballast system which pumps water between different columns of the semi-submersible in order to maintain the inclination of the platform as vertical as possible when the turbine is yawed in different directions. The Ideol platform includes a dynamic mooring system which alters the platform position in order to reduce overall farm wake losses. It has been asserted that these platform behaviours take place over a timescale which is much longer than the dynamic platform motion so only the mean values of these need to be considered but this is something which should be considered for each new platform design. It also includes new variables for which the conservative value needs to be chosen for the design simulations.

Gust Cases

Wind turbines were much smaller when the original definition of the Extreme Operating Gust (EOG) was introduced additionally, the response of wind turbines was based either on the stalling behaviour of the blades or the pitch response, both of which were over the period of a few seconds. Therefore, the extreme operating gust with frequency components of 10.5, 21 and 4.2 s (Fig. 5) covered the range of response periods relatively well (although with larger fixed turbines produced very high loading for towers with a frequency of around 0.24 Hz).

For many floating platforms the surge, sway, pitch and roll periods greatly exceed the time period of the EOG. However, there can be large changes in wind speed over these timescales of 15–150 s. What is more, the largest change expected over these timescales will exceed that for the original rise time of the gust of 2.8 s,

Fig. 5 Extreme operating gust with harmonic decomposition
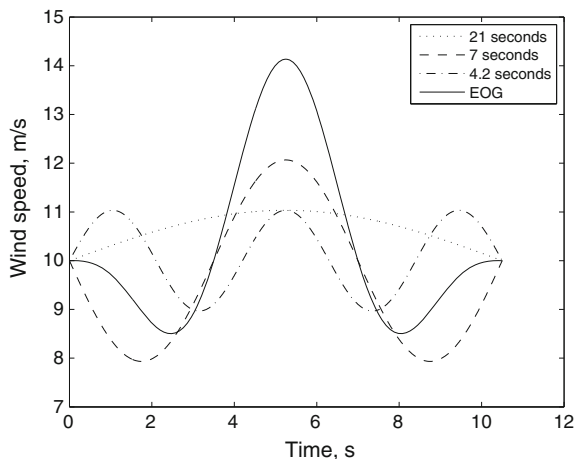
as has been seen experimentally at offshore wind farms, for example at Vindeby by Mann (2001). As yet no significant studies into the response of floating turbines to the EOG of differing period and amplitude has been carried out although the DNV-OS-J101 (2011) standard requires taking into account different gust periods; the new IEC technical specification for floating offshore wind turbines may go further. Of course, it is possible that other gusts such as extreme direction changes and wind shear could become design driving for some platform designs if simulated for different wind periods.

Mooring Line Failures

As mentioned in Sect. 1.1, the development of offshore wind has led to a combination of the traditional wind turbine design philosophy with that from the offshore oil and gas industry. In particular, there has been an increased emphasis on the accidental limit state (ALS). One of the cases which must be considered is the loss of a single mooring line. Whereas for offshore structures, loss of position could result in a disaster with massive environmental impact, motion of an offshore wind turbine by a few hundred metres will only have an impact on the remaining mooring lines and the electrical cable. Depending on the cost of repair and recovery, a system with minimal redundancy may be optimal. By way of example, Statoil's Hywind project uses three lines to restrain the spar buoy; loss of a line would result in significant drift and would damage or detach the electrical cable (see Chapter "State-of-the-Art", Sect. 2 for further information on the Hywind device). However, the drift would not be so significant as to impact neighbouring turbines which would be located more than 1 km away (for the current generation of off-shore wind turbines spaced by eight to ten diameters).

Damaged Stability

Alongside loss of a mooring line, the other ALS which should be accounted for is damaged stability, otherwise referred to as a leakage case or loss of hull integrity. This can be a contentious issue with opinions on whether damaged stability should be a mandatory requirement giving rise to polarised views. The author will not give an opinion as to whether any particular approach is correct; only present the arguments which have been made. It is likely that the best solution will only be arrived at through experience and in the meantime it will be at the discretion of national regulatory bodies as to whether non-redundant hulls are permitted.

Starting from the position of the offshore oil and gas industry, it is natural to design floating platforms to survive with multiple compartments such that a single puncture to the external hull will not result in loss of the platform. Requirements in standards for design of offshore structures state that, for the analysis of damaged stability, compartments that would be exposed to flooding by a penetration of 1–2 m over a height of several metres close to sea level, as would be expected to occur due to collision with a boat, need to be considered to be flooded in this case. Additionally, the case where a compartment adjacent to an attachment for a mooring line or electrical cable is flooded must be considered so that there may be many different scenarios for one platform.

Conversely, from the fixed-bottom offshore wind industry, there is a history of non-redundant structures being used, namely monopiles. A steel spar buoy is relatively similar to a monopile in size and construction and for this reason designers may consider that the design requirements should be similar; you cannot imagine a monopile surviving very long with a several-metre wide puncture. Offshore wind turbines are produced to be one of many units; loss of a single floating platform therefore does not have the same economic impact as the loss of the whole installation.

There is also a difference in safety level required by the two classes of structure: offshore platforms generally contain either personnel, large quantities of hydro-carbons or both whereas floating offshore wind turbines are termed unmanned. The unmanned term can cause controversy on its own since maintenance an inspection crews may often visit floating wind installations and it is postulated that for future, far-offshore farms crews may be permanently stationed offshore. The difference comes from the environmental loads which the platform might be subjected to while there are personnel on-board. Maintenance and inspection visits are typically restricted to wind speeds of 15 m/s or less and significant wave heights of the order of 2 m. However, although these environmental conditions are lower, they might not mean the probability of damage is reduced by the same factor. Collisions are most likely to occur when there are other boats in the neighbourhood; and corrosion or fatigue related failures of sub-surface connections might occur in relatively benign situations.

If the risk to personnel can be minimised such that the probability of sinking less than other risks such as structural failure then national bodies may be able to approve structures without damaged stability; however, they will also take into account environmental concerns due to the sunken turbine, costs for retrieving the structure; and the potentially hidden navigational hazard it poses while submerged. This, along with the likelihood of collisions varying with the proximity to shipping lanes means that the issue could become a local rather than a global one.

Simulation of Instabilities

The floating wind industry has been relatively successful in using the knowledge and models from the wind and offshore industries in order to predict possible instabilities before they have occurred. Examples include the instability which would be caused by an onshore wind turbine controller being used on a floating turbine installation, see for example Larsen and Hanson (2007); the possible effect of a failed blade pitch system on the platform yaw motion, see Jonkman (2007).

Care should be taken to avoid complacency which can result in repeating mistakes which have already been made in the onshore wind industry. Examples are the coincidence of structural modes with multiples of the blade passing frequency (considering the structural frequencies when they have been transformed into the stationary frame); and stall induced vibrations caused by aerodynamic damping turning negative when a blade aerofoil is in stall, see for example Hansen (2007). Additional cases for floating platforms include ringing and springing excitations

caused by higher-order wave forces, vortex induced vibrations from spar platforms, mooring lines and electric cables; and the Mathieu instability.

1.4 Discussion

While the wind industry is used to asking the offshore industry not to neglect the effect of wind loading on the fixed support structures which have been installed to-date, the situation in floating offshore wind may be different. With concepts that have a large water-plane area, it is quite possible that the driving loads will be driven by cases which are dominated by the wave loads in extreme seas and the inertial loading from the motion of the platform and turbine.

The prototypes which have been launched to-date have been heavily conservative in order to reduce risk at a crucial phase for the industry. In order to meet targets of comparable costs to fixed offshore wind, it will be necessary to substantially reduce the weight of the floating platform relative to the size of the turbine and this is likely to make wind loading comparatively more important. Even before these changes happen it is likely that the driving cases for the yaw loading on the platform will come from wind turbine operational cases since, for many platform types, the wave loads do not introduce yaw loading. Large yaw loading typically results from the wind changing direction, failure of a single blade pitch system, or high wind shear in the horizontal direction.

With such a variety of novel structures to analyse, there are bound to be surprises when a full dynamic analysis of platform and turbine is performed for the first time. The challenge is to predict these effects before each design progresses too far and use that knowledge to develop more cost-effective floating wind systems.

2 Certification

Knut O. Ronold, **Anne Lene Hopstad**
Certification is in this context defined as an action by a certification body in which written assurance that adequate confidence can be associated with the asset in question. Certification is the final statement that all requirements of the relevant standard or normative document have been satisfied or conformed to. A certificate to this effect can then be issued.

The process leading to the issue of a certificate usually consists of a number of certification phases, each of which consists of one or more verification activities. A conformity statement is usually issued at the successful completion of the verification activities for each certification phase. The conformity statement is sometimes referred to as a statement of compliance.

For the units that together constitute an offshore wind farm, the term project certification is commonly used to describe the certification process that leads to the

issue of a certificate for the wind farm. This is in line with the wording used in IEC 61400-22 (2010). For a floating wind turbine unit consisting of wind turbine, tower, floating support structure and station-keeping system, the following certification phases are usually covered in a project certification:

- Verification of design basis
- Verification of design
- Manufacturing survey
- Installation survey
- Commissioning survey
- In-service surveys

Verification consists of evaluating and checking information to establish that an object in question meets a technical requirement or standard. Multiple verification activities are performed and successfully completed to support the decision to issue a conformity statement.

Stakeholders may opt for a full certification covering all certification phases or they may opt for a tailored package consisting of the verification activities of only a selected subset of certification phases.

The certification can be preceded by an early-phase, less formal conceptual design verification to assess the feasibility of a design for further development. Such conceptual design verifications may be particularly useful for assessment of novel floater concepts which are still in an early phase of development.

2.1 Design Standards for Floating Offshore Wind Turbines

Most major classification societies are among the certification bodies that offer services for certification of floating wind turbine units and also of substations for floating wind farms consisting of such units. Certification schemes for wind farms and wind turbine units are usually based on the IEC certification scheme as outlined in IEC 61400-22 (2010). The major classification societies have their own structural design standards, with technical requirements to be met before these societies will be confident that the structural safety is adequate, and before they will issue conformity statements and ultimately a certificate.

At the time of writing, the following standards for design of floating wind turbine structures are published and available:

- ABS Guideline #195, *Guide for building and classing floating offshore wind turbine installations*, published 2013. This document also contains service specifications for a certification service.
- DNV-OS-J103, *Design of floating wind turbine structures*, published 2013. This document is to be used with DNV-OS-J101 (2014), *Design of offshore wind turbine structures*. The service specifications for a certification service based on these standards are kept in a separate document denoted DNVGL-SE-0073.

- Class NK, *Guidelines for offshore floating wind turbine structures*, first edition, published 2012. This document also contains service specifications for a certification service.
- GL-IV-2 (2012), *Guideline for the certification of offshore wind turbines*, published in 2012. This document is common for bottom-fixed and floating wind turbines and also contains service specifications for a certification service.

IEC currently does not have a standard for floating wind turbines and their floating support structures; however, work is well under way on a technical specification to cover these structures, eventually to be used together with the existing standard IEC 61400-3 (2009) for design of offshore wind turbines.

2.2 Design Basis Verification

The design basis is a document which specifies the owner's requirements and conditions to be taken into account for design of the floating wind turbine units and substations in a floating wind farm. This document specifies all governing design standards. The document often recapitulates important parts of the governing design standards such as safety factor requirements and it may even specify crucial input for design such as characteristic loads and characteristic strengths. The design basis typically also includes any requirements that come in addition to the requirements specified in the governing design standard.

The design basis usually includes documentation on the following:

- Soil conditions
- Metocean conditions including weather windows
- Codes, standards and requirements
- Design criteria
- Transport, installation and commissioning requirements
- Operation and maintenance requirements
- Wind turbine type

Once the design basis has been verified by the certification body and a conformity statement has been issued, the design phase which is based on the approved design basis can commence. As a minimum, the verification of the design of floating wind turbine units covers verification of the following issues based on documentation reviews and independent analysis for compliance with the approved design basis and relevant standards:

- Loads and response
- Wind turbine type (by checking for valid type certificate)
- Design and stability of primary support structure, including tower and floater
- Design of station-keeping system, including moorings and anchors
- Design of secondary structures

- Load-out, transportation, installation and commissioning plan
- Operation and maintenance plan

Verification of other design elements such as design of control system, cables and mechanical equipment may come in addition. For a floating substation unit, the list of design issues subject to verification will be much the same as for the floating wind turbine units. However, verification of the topside arrangement and electrical design may come in addition, whereas checking for a valid wind turbine type certificate is of course not relevant.

Special floater-specific issues encountered in design of floating wind turbine units are addressed in more detail in the following subsection.

2.3 *Floater-Specific Design Issues*

Many design issues are the same for floating wind turbine units as for bottom-fixed offshore wind turbine structures. Material selection, structural design principles and corrosion protection, to name a few, are issues which are independent of whether the unit is bottom-fixed or floating. However, some issues are floater-specific and not relevant for bottom-fixed units. Such floater-specific issues need special consideration when a floating wind farm is subject to certification. The most important floater-specific issues include:

- Floating stability
- Station keeping
- Floater motion control system

These issues as well as other issues are addressed separately in the following sub-sections.

Floating Stability

Floating stability is an important issue for a floating wind turbine unit. Floating stability implies a stable equilibrium and reflects a total integrity against downflooding and capsizing. Satisfactory floating stability of floating wind turbine units is necessary in order to support the safety level required for the involved structures. Static floating stability needs to be demonstrated in the early stages of design. This is merely a matter of determining where the centre of gravity (CoG) of the floating unit should be located in order to ensure that the unit is stable.

Current standards for floating wind turbine units address the issue of floating stability and set forth requirements for this stability to be fulfilled in various service modes for the unit:

- Operation, i.e. a normal working condition with the wind turbine operating,

- Temporary conditions, i.e. transient conditions such as tow-out, installation and changing of draught,
- Survival conditions, i.e. conditions during extreme storms.

All standards require intact stability. Regarding requirements for damaged stability, there are some differences between the standards and they require damaged stability to various degrees. Class NK is probably the strictest in this respect by requiring double hull. GL-IV-2 requires damaged stability by requiring *Code for the construction and equipment of mobile offshore drilling units* (2009) satisfied *in principle*. ABS #195 also requires damaged stability. DNV-OS-J103 (2013) deviates from this and requires damaged stability only for manned units. For unmanned units DNV-OS-J103, with a view to the balance between large costs and limited gains, does not require damaged stability, but includes damaged stability to be assessed as an option which may be opted a voluntary basis only.

For assessment of whether damaged stability is necessary for an unmanned floating wind turbine unit, one can carry out an economic risk evaluation, e.g. by means of a cost-benefit analysis, since the consequences of a failure of the unit are purely economic. The critical event of interest is flooding which eventually will lead to instability and subsequent sinking of the unit. The probability of flooding must therefore be evaluated and so must the monetary equivalent of the consequences, which usually consist of total loss of one floating wind turbine unit and temporary damage to part of the cable system. This must then be balanced against the cost of constructing the unit with damaged stability, e.g. in terms of a compartmentalisation of the hull. Based on the results of this investigation it can be assessed whether the probability of flooding is large enough to conclude that damaged stability is profitable and should be opted for.

A somewhat simpler approach would be to just evaluate the probability of flooding and then check whether this probability exceeds the target failure probability specified for structural design in the relevant standard, in which case damaged stability should be opted for. This approach is less optimal in that it does not take into account the cost of implementing damaged stability, e.g. in terms of a compartmentalisation of the hull.

For assessment of whether damaged stability is necessary it does not suffice to only consider the probability of flooding. In this assessment one should also take into account the potential loss of reputation associated with the flooding and the total loss of a floating wind turbine unit and the harm that this loss of reputation may cause to the industry.

Flooding can be envisaged to take place either following a ship collision which leads to penetration of the hull, or it can take place through doors and other openings. For spar type floaters the probability of perforating the hull by a ship collision appears to be very small, the spar will just give way, such that a ship collision as a potential cause for leakage and flooding will in practice be irrelevant. Doors and other openings can be located high enough that they will not serve as leakage points. In case failure of mooring line brackets would cause perforation and flooding, this can be avoided by designing such brackets to be stronger than the

weakest link of the mooring line. Minor leakages owing to cracks can be handled by surveillance of the ballast water level in conjunction with a bilge pump.

Station Keeping

Station keeping in the context of floating wind turbines implies catenary or taut systems of chain, wire or fibre ropes, or tendon systems for restrained systems like TLPs. The station keeping system is vital for keeping the wind turbine in position such that it can generate electricity and such that the transfer of electricity to a receiver can be maintained.

Redundancy is a key issue for station keeping systems and governs the safety requirements for such systems. For station keeping systems without redundancy, ABS #195 and DNV-OS-J103 both have requirements for use of higher partial safety factors in the design of station keeping systems without redundancy than in the design of station keeping systems with redundancy. GL-IV-2 requires station keeping systems to have redundancy and requires redundancy checks to be carried out. Class NK has requirements for mooring analysis for the case that one mooring line is broken, in practice this implies requirements for redundancy checks.

The requirements for redundancy or for higher safety factors in the case without redundancy reflect the risk for collision with adjacent wind turbine structures, should the floater happen to disengage from its station keeping system and float about within the wind farm that it constitutes a part of, for example in the event of a mooring line failure.

In some cases, it is obvious whether a station keeping system is redundant or not. For example, it is obvious that if failure of a tether in a TLP causes capsizing then the station keeping system of the TLP is a system without redundancy. In other cases, it is not so obvious whether a station keeping system is redundant or not.

For example, failure of a slack mooring line in a three-line system for a spar, causing a large drift-off, does not necessarily imply a system without redundancy. In such cases, it may be necessary to carry out a qualification of the redundancy of the station keeping system, for example by documenting that the system is capable of withstanding loads in the damaged condition after the accidental loss of one mooring line. For this purpose, characteristic environmental loads defined as one-year loads can be assumed in conjunction with load factors for the accidental limit state. The turbine is not necessarily operating and cables are maybe not intact. Survival is the issue and survival for one-year loads represents accepted offshore practice.

Floater Motion Control System

Floater motion control for the purpose of limiting the excitation and associated responses of the floating wind turbine unit is of utmost importance. This can be achieved in different ways, and one of the options is to capitalise on the capabilities of the control system of the wind turbine.

A floater motion control system is used to minimise excitation in the pitch mode of motion of the floater unit and thereby stabilise the unit and minimise the structural responses. The experience from the Hywind spar prototype off the coast

of western Norway shows how important this is for the fatigue loads, see Skaare et al. (2007). For a TLP which is restrained from pitch motions, the floater motion control system is used to minimise excitation in the surge mode of motion.

The floater motion control system can be based on and integrated with the control system for the wind turbine, in which case the motions can be controlled by appropriate adjustment of the rotor blades. The floater motion control system can also be accomplished by other means such as pumping ballast water back and forth.

ABS #195, GL-IV-2 and Class NK do not address the issue of a floater motion control system and have thus no requirements for such a system. DNV-OS-J103, however, requires such a system to be implemented.

A floater motion control system based on the wind turbine control system may give rise to special load cases which then need to be identified and accounted for in the design of the floating unit, even if such load cases are not particularly mentioned in the governing design standards. This applies in particular in the case that the wind turbine control system is subject to modifications when it is being integrated with the floater motion control system.

Load and Response Analysis

For verification of site-specific loads for design of floating wind turbine units and their station-keeping systems, it may be necessary to perform an independent load and response analysis. Critical load cases and load combinations have to be considered for this purpose.

It is common to base such analyses on the design load cases specified in IEC 61400-3 (2009) for bottom-fixed units; however, these load cases may not necessarily be sufficient and may have to be supplemented by a number of additional load cases which may be relevant only for a floating unit. This can for example be load cases associated with gust events, which are critical with respect to low-frequency responses of the floating unit, and survival load cases of interest for robustness checks of the station-keeping system. It can also be special load cases reflecting the behaviour of the control system which is used to keep the turbine in place by minimising excitation.

It may be necessary to carry out the independent load and response analysis as a coupled analysis of the floating wind turbine unit and its station keeping system. This is an analysis in which the structural dynamic responses from the aerodynamic and hydrodynamic loads are coupled.

2.4 Post-design Verification Phases

The certification process is not completed when the verification tasks of the design phase have been completed with the issue of a conformity statement. After completion of the design phase there are other phases to follow that require follow-up by the certification body before a certificate can be issued. The manufacturing is followed-up by manufacturing surveys and subsequently both installation and

commissioning are also followed-up by surveys. Testing involved with these three phases may be followed-up by witnessing.

Manufacturing surveys are carried out in order to verify compliance between the approved design and the manufactured product. The surveys are typically carried out at the manufacturer's production premises and in the wind turbine assembly shop. The surveys involve evaluation of the production and the quality system, execution of product-related quality audits, surveys of quality assurance activities, and periodical surveys.

Installation surveys are carried out in order to verify compliance with load-out manuals and installation manuals. These surveys cover the following three temporary phases in a wind farm project: Load-out, transport and installation. The installation surveys can be complemented by optional marine warranty surveys in order to reduce the risks involved with these temporary phases.

Commissioning surveys are carried out during commissioning of the wind turbines and their floating support structures. The purpose is to verify that the wind turbines that are erected on the actual site are commissioned according to the requirements of the manufacturer and in compliance with relevant documentation provided in the design phase.

2.5 *Issuance and Maintenance of Certificate*

Following the successful completion of the manufacturing, installation and commissioning phases, a certificate for the wind farm can be issued. Such a certificate has a limited period of validity. The certificate can be maintained and have its period of validity extended by periodic validation based on successful in-service surveys in the in-service phase. This requires that the wind turbine and its floating support structure and station-keeping system are surveyed regularly during their entire operational life. For this purpose, the certification body will have to conduct periodical in-service surveys in order to verify that the required standard is observed and maintained and in order, thereafter, to validate the project certificate.

2.6 *Discussion*

Requirements for design of floating offshore wind turbines set forth by IEC are under development and are expected to come into force within a not too distant future. It is expected that when this happens, currently existing standards published by various certification bodies are expected to be updated to become aligned with IEC's requirements. Likewise, the verification and certification services offered by these certification bodies are expected to be subject to adjustment to become aligned with the IEC scheme.

In the future, with large floating wind farms being developed and commissioned, mass production of floating wind turbine units can be foreseen to take place, and type certification of such units can then be expected to emerge as a relevant supplement to the site-specific project certification described above. This will be just as natural as wind turbines are subject to type certification today.

Such type certification of floating wind turbine units will necessarily refer to designs to a specific class of metocean conditions and to a specific class of wind turbines. Subsequently, qualification of such mass-produced type-certified units for application in a floating wind farm on a particular location can then be carried out on a case-by-case basis. The type certification for the floating unit and the qualification of the unit for a particular wind farm can then serve as part of the basis for project certification of the wind farm. The station-keeping system will still have to be designed individually for the specific wind farm on the specific site and is therefore not suited for such type certification.

References

References (1)

Bayati I, Jonkman J, Robertson A, Platt A (2014) The effects of second-order hydrodynamics on a semisubmersible floating offshore wind turbine. J Phys Conf Ser 524 (The Science of Making Torque from Wind)

Burton T, Jenkins N, Sharpe D, Bossanyi E (2011) Wind energy handbook, 2nd edn. Wiley, Chichester

DNV-OS-J101 (2011) Design of offshore wind turbine structures. Det Norske Veritas (DNV), Høvik, Norway

DNV-OS-J103 (2013) Design of floating wind turbine structures. Det Norske Veritas (DNV), Høvik, Norway

Duarte T, Sarmento AJNA (2014) Effects of second-order hydrodynamic forces on floating offshore wind turbines. In: Proceedings of the AIAA SciTech 2014 National Harbor, Maryland, 13–17 Jan 2014

GL-IV-2 (2012) Guideline for the certification of offshore wind turbines, edition 2012. Germanischer Lloyd, Hamburg, Germany

Hansen MH (2007) Aeroelastic instability problems for wind turbines. Wind Energy 10(6):551–577

Hurley W, Nordstrom C (2014) Pelastar cost of energy: a cost study of the pelastar floating foundation system in UK waters. Available via DIALOG. http://www.eti.co.uk/wp-content/uploads/2014/03/PelaStar-LCOE-Paper-21-Jan-2014.pdf. Accessed 30th Apr 2015

IEC 61400-1 (2005) Wind turbines—part 1: design requirements. International Electrotechnical Commission (IEC), Geneva, Switzerland

IEC 61400-3 (2009) Wind turbines - part 3: design requirements for offshore wind turbines. International Electrotechnical Commission (IEC), Geneva, Switzerland

ISO 19901-4 (2003) Petroleum and natural gas industries—specific requirements for offshore structures—part 3: geotechnical and foundation design considerations. International Organization for Standardization (ISO), Geneva, Switzerland

ISO 19904-1 (2006) Petroleum and natural gas industries - floating offshore structures and mobile offshore units. International Organization for Standardization (ISO), Geneva, Switzerland

ISO 19906 (2010) Petroleum and natural gas industries—Arctic offshore structures. International Organization for Standardization (ISO), Geneva, Switzerland

Jonkman J (2007) Dynamics modeling and loads analysis of an offshore floating wind turbine. NREL/TP-500-41958, National Renewable Energy Laboratory (NREL), Golden, CO, USA, Nov 2007

Jonkman J, Musial W (2010) IEA Wind Task 23 Subtask 2: The offshore code comparison collaboration (OC3) final report. National Renewable Energy Laboratory (NREL), Golden, CO, USA. Available via DIALOG. https://www.ieawind.org/task_23/23_FinalReports/Subtask2_Final_Report.pdf. Accessed 30th Apr 2015

Jussila V, Popko P, Heinonen J (2013) Interfacing of ice load simulation tools for cylindrical and conical structure with one wind simulation tool for offshore wind turbines. In: Proceedings of the 22nd international conference on port and ocean engineering under arctic conditions, Espoo, Finland, 9–13 June 2013

Larsen TJ, Hanson TD (2007) A method to avoid negative damped low frequent tower vibrations for a floating, pitch controlled wind turbine. J Phys Conf Series (Online) 75:11

Larsen GC, Madsen HA, Thomsen K, Larsen TJ (2008) Wake meandering—a pragmatic approach. Wind Energy 11:377–395

Lupton RC (2014) Characterising dynamic non-linearity in floating wind turbines. J Phys Conf Ser 555:012064

Mann J (2001) Extreme gusts over the coastal waters of Denmark. In: Proceedings of the european wind energy conference (EWEC), Copenhagen, Denmark, 2–7 July 2001

Matha D, Sandner F, Schlipf D (2014) Efficient critical design load case identification for floating offshore wind turbines with a reduced nonlinear model. J Phys Conf Ser 555:012069

Meulepas K (2014) Hywind Scotland—developing the UK's first floating wind park. In: Proceedings of the all energy 2014, Aberdeen, UK, 21–22 May 2014

RECOFF Project (2006) Lumping of fatigue load cases. Available via DIALOG. http://www.risoe.dk/vea/recoff/Documents/Sec_3/RECOFFdoc016.pdf. Accessed 30th April 2015

SAMCOT (2013) Sustainable and arctic marine and coastal technology. NTNU, Trondheim. Norway. Available via DIALOG. http://www.ntnu.no/trykk/publikasjoner/SAMCoT_2013/files/assets/seo/page20.html. Accessed 30th April 2015

Stewart G, Lackner M, Haid L et al (2013) Assessing fatigue and ultimate load uncertainty in floating offshore wind turbines due to varying simulation length. In: Proceedings of the 11th international conference on structural safety and reliability, New York, 16–20 June 2013

Upwind Design Basis (2010) WP4: offshore foundations and support structures. Available via DIALOG. http://repository.tudelft.nl/assets/uuid:a176334d-6391–4821-8c5f-9c91b6b32a27/276271.pdf. Accessed 30th April 2015

Veldkamp HF (2006) Chances in wind energy a probabilistic approach to wind turbine fatigue design. Dissertation, Delft Technical University

Wienke J (2001) Druckschlagbelastung auf schlanke zylindrische Bauwerke durch brechende Wellen—theoretische und großmaßstäbliche Laboruntersuchungen. Dissertation, Technische Universität Carolo-Wilhelmina zu Braunschweig

References (2)

American Bureau of Shipping (2013) Guide for building and classing floating offshore wind turbine installations. ABS Guideline #195, Houston

DNV-OS-J101 (2014) Design of offshore wind turbine structures. Det Norske Veritas, Høvik, Norway

DNV-OS-J103 (2013) Design of floating wind turbine structures. Det Norske Veritas, Høvik, Norway

DNV GL (2014) Project certification of wind farms according to IEC 61400-22. DNVGL-SE-0073, Høvik, Norway

GL-IV-2 (2012) Guideline for the certification of offshore wind turbines, edition 2012. Germanischer Lloyd, Hamburg, Germany

IEC 61400-3 (2009) Wind turbines—part 3: design requirements for offshore wind turbines. International Electrotechnical Commission, Geneva, Switzerland

IEC 61400-22 (2010) Wind turbines—part 22: conformity testing and certification. International Electrotechnical Commission, Geneva, Switzerland

Nippon Kaiji Kyokai (2012) Guidelines for offshore floating wind turbine structures, 1st edn. Class NK, Tokyo

Skaare B, Hanson TD, Nielsen FG (2007) Importance of control strategies on fatigue life of floating wind turbines. In: Proceedings of the 26th international conference on offshore mechanics and ocean engineering (OMAE), San Diego, 10–15 June 2007

State-of-the-Art

Dominique Roddier, Christian Cermelli, Joshua Weinstein, Eirik Byklum, Mairéad Atcheson, Tomoaki Utsunomiya, Jørgen Jorde and Eystein Borgen

In this chapter, a review of some of the prototype FOWT devices that have been deployed to-date is presented. The technologies overviewed throughout the chapter are: Principle Power's semisubmersible WindFloat device; the Hywind spar under development by Statoil; the Goto Island project in Japan and the SWAY system.

Information presented for each technology includes: a brief description of the device; the concept development pathway; information on the prototype testing campaigns, including key achievements, milestone and measured data; and finally the commercialisation route planned for the technology. When applicable, relevant data is presented from initial operations, in an effort to document the experience and lessons learnt from these developments.

D. Roddier · C. Cermelli · J. Weinstein
Principle Power, Inc., Berkeley, CA, USA
e-mail: droddier@principlepowerinc.com

E. Byklum
Statoil ASA, Fornebu, Norway
e-mail: EBYK@statoil.com

M. Atcheson (✉)
Cruz Atcheson Consulting Engineers Lda, Lisbon, Portugal
e-mail: Mairead.atcheson@cruzatcheson.com

T. Utsunomiya
Department of Ocean Energy Resources, Kyushu University, Fukuoka-ken, Japan
e-mail: utsunomiya@nams.kyushu-u.ac.jp

J. Jorde · E. Borgen
Sway AS, Bergen, Norway
e-mail: jjo@inocean.no

E. Borgen
e-mail: Eystein.Borgen@sway.no

1   WindFloat

Dominique Roddier, Christian Cermelli and Joshua Weinstein

1.1   Device Description

The WindFloatis a three-legged semi-submersible offshore platform fitted with water-entrapment (or heave) plates at the base of the columns and a large wind turbine mounted asymmetrically on one of the columns. The holistic approach to this optimised design presents innovative and economically attractive solutions to the offshore wind industry with respect to turbine installation methodology and offshore operations. The structure's inherent stability permits most turbine assembly and commissioning activities to be performed at the quayside, in a sheltered environment. The methodology eliminates the need for specialised heavy-lifting offshore equipment and specialised operations such as a floating-to-floating lifting operations.

The WindFloat's innovative water-entrapment plates increase the hydrodynamic added-mass of the platform and add significant viscous damping, resulting in reduced platform motion in waves. An added benefit of the water entrapment plates is the reduced structural weight of the hull, when compared to larger structures with similar motion performance, ultimately resulting in a reduction of the overall levelised cost of energy (LCOE). Similar benefits have been observed in the oil and gas industry, where truss spars have replaced classic spars. A truss spar has a shorter cylindrical section, but adds vertically staggered heave plates under the structure.

The hull is also fitted with a closed-loop and actively controlled hull-trim system, which moves water between ballast tanks in each column to compensate for changes in average wind velocity and direction. This system enables the mean position of the tower to remain vertical, which improves the turbine's efficiency and allows for structural optimisations.

WindFloat Key Features
The design philosophy of the WindFloat structure, as shown in Figs. 1 and 2, focuses on the reduction of the structural weight and the optimisation of the power to weight ratio of the overall system. However, the lightest structure may not necessarily be the most cost effective solution, as the simplicity of other operations such as fabrication difficulty and installation may have more significant economic benefits. The primary design driver of the WindFloat emphasises the overall cost reduction by simplifying the primary structure, while still ensuring ease of fabrication. In particular, the WindFloat key features include.
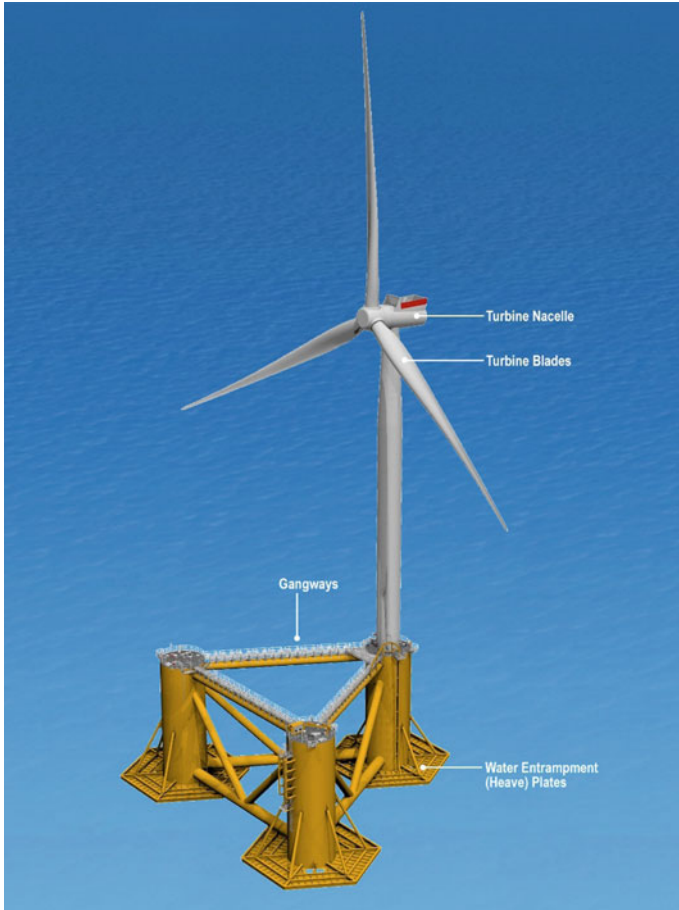
Fig. 1 WindFloat key features

Shallow Draft

When compared to other floating concepts, such as a spar type platform, the WindFloat's transit and operational drafts are minimal. This permits transit from typical commercial offshore yards. Once out of the harbour, the hull is ballasted to its operational draft through a fully reversible ballasting operation.

Turbine Agnostic

The WindFloat is designed as a turbine agnostic system. Turbine loads, both static and dynamic, are design variables which come from the choice of the turbine and its manufacturer. Principle Power has been at the forefront of developing fully-coupled dynamic simulation tools and was one of the first groups to develop a hydro-aero-servo-elastic code (Cermelli et al. 2010). It is important to note that the WindFloat (turbine and hull) is modelled as an integrated system throughout the structural design and analysis.

Fig. 2 WF1 prototype operating at rated wind speed in Aguçadoura (Portugal)

Quayside Final Assembly and Commissioning

Final assembly, erection and commissioning of the wind turbine is completed onshore at the quayside, where the wave environment is not a constraint. This methodology provides significant cost savings opportunities, due to lower labour costs onshore, reduced time needed to complete the installation process, and usage of existing shore-side infrastructure such as shipyards or harbours.

There are no requirements for offshore upending of the hull, a floating-to-floating lifting operation to install the turbine, or complex mooring connection operations whilst offshore. This methodology significantly reduces the offshore contracting risks which is an issue constraining the industry today.

Large Correctives

All installation operations (ballast, mooring and cable hookup, etc.) are fully reversible, allowing for the hull and turbine to be towed back to the shore-side for major repairs to the turbine. This provides an opportunity to reduce OPEX while improving overall production and capacity factors, as the wait on both vessels and weather is suppressed and repair operations can be planned and optimised.

Inherently Stable in Transit

Eliminating transportation challenges for offshore wind turbines provides cost-savings opportunities. The WindFloat's stability in transit is a result of the same design parameters that make it fully stable offshore. The WindFloat is capable of supporting a fully-assembled and commissioned wind turbine in a wet tow configuration. The entire system can be towed at any draft to the project site without the requirement for transport barges or other ancillary marine equipment.

Conventional Mooring

Conventional mooring components are inexpensive, available globally and simple to install. The mooring configuration employed by the WindFloat includes drag embedment anchors, offshore grade chains and cables. The drag embedment anchors permit installation in various soil conditions including mud, clay and sand with simplified consent requirements (when compared to bottom-fixed structures). Drag embedment anchors offer the most economical installed solution and have proven experience in the oil and gas industry, including for permanently moored structures.

Further, the incremental cost increase associated with a WindFloat mooring in a wide range of water depth (e.g. >40 m) is negligible. This permits greater flexibility to developers and utilities.

Installation of the mooring requires only the use of surface vessels. A single anchor handling and tug supply vessel (AHTSV) can accomplish the mooring pre-lay in a very short time and relatively large (H_s = 2–4 m) waves. It is important to consider the moorings as an integral part of the system and recognise the significant engineering effort inherent to the WindFloat mooring design. Failure of a mooring component would be analogous to structural failure of a fixed structure, albeit with less severe consequences. The WindFloat mooring design is based on safety factors provided in the API RP 2SK (2005) recommended practice. A coupled hydrodynamic model is developed using Orcaflex/OrcaFast (FASTlink) software. Time-domain simulations of the platform and mooring dynamics are obtained based on the specified input environment (wind, waves and current). Coupling between the aerodynamics of the turbine and hydrodynamic forces are also taken into account fully.

These tools and knowhow enabled Principle Power to design, fabricate and install their first prototype within three years of a feasibility study with the Portuguese utility, Energias de Portugal (EDP).

1.2   Concept Development

The apparition of the semi-submersible platform fitted with heave plates dates back to 2004, when it was investigated as a means to provide a low cost floating hull with excellent motion characteristics applicable to various offshore industries (Cermelli et al. 2004). Following a few years of development, the hull was fitted with three wind turbines and a feasibility study was conducted (Zambrano et al. 2006). The result from the feasibility study was conclusive, and the concept was optimised with a single larger turbine (more power) and a lighter hull (lower CAPEX). The WindFloat, in its original form, was presented in 2009 (Roddier et al. 2009; Cermelli et al. 2009; Aubault et al. 2009). These publications summarise the first WindFloat feasibility study and include discussions on design requirements, numerical modelling, hydrodynamics and preliminary structural work. The study was later refined and synthesised in Roddier et al. (2010), with initial coupled hull-turbine modelling described in Cermelli et al. (2010).

Model Tests
Two model test campaigns were conducted at the UC Berkeley ship-model testing facility (a 60 m long towing tank outfitted with wave and wind generation) to validate numerical analysis tools. Scale models of the platform were fabricated out of acrylic, as shown in Fig. 3.
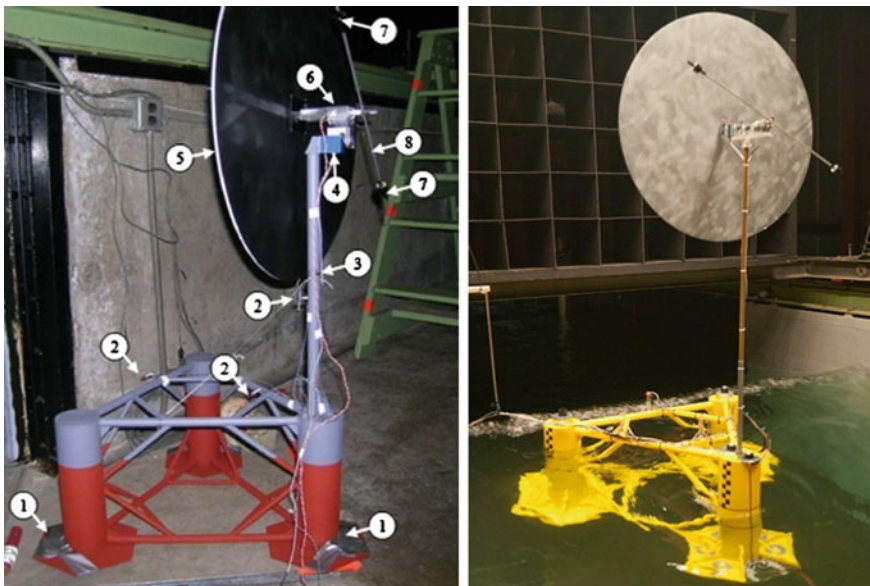
Fig. 3 WindFloat model tests—(*left*) model used in the 1st set of scale tests, (*right*) model used in the 2nd set of scale tests

Lead weights were placed inside the columns and on the water-entrapment plates to adjust the center of gravity to its target position (1). The platform motion was measured using a digital video camera using light emitting diodes (LEDs) placed on the model (2). The system provides 3 degree-of-freedom (DOF) measurements of the motion in the plane of the camera. The tower (3) was made of a thin (not-to-scale) 2.5 mm outer diameter (OD) acrylic pipe (Fig. 3—left) or copper tube (Fig. 3—right). The second scale model used in follow-on model tests (Fig. 3 —right), employed a tower with correctly scaled stiffness.

The turbine model device was connected to the top of the tower and onto a load cell (4) (see Fig. 3), which measured the axial force perpendicular to the tower. A large disk (5), made of foam board, was placed on the model to induce wind loads at the tower base corresponding to the design wind forces. No attempts were made to match the atmospheric turbulence. The wind maker (visible in Fig. 3), produced some level of unsteady flow and the wind fluctuations were absorbed by the large disk. In the end, the wind force was measured and the turbulence level compared to variations in the aerodynamic forces generated by a prototype wind turbine. The disk diameter was a third of the total area covered by the rotor. The drag coefficient on the disk was estimated to be 1.2. An electrical motor (6) was placed at the top of the tower to model the gyroscopic effect. This well-known mechanical force arises when a rotor spinning around a certain axis undergoes a rotation around a different axis. For instance, platform pitch and yaw would lead to gyroscopic forces applied on the tower. These forces are a significant design issue for wind turbine blades and the drive shaft/bearings, but may also have a contribution to the global response of the floater. The motor was adjusted to spin at the Froude-scaled turbine speed, and the inertia of the blades was approximately modelled with two weights (7) positioned on an aluminum rod (8).

The effect of the active hull-trim system was modelled by shifting lead ballast manually on the model to compensate for the mean wind overturning moment.

The second model test was performed in a similar manner, and was part of a front end engineering and design (FEED) study for the WindFloat 1 (WF1) Prototype Project.

Even though recent advances (Robertson et al. 2013; de Ridder et al. 2014) focus on modelling a spinning turbine in tank tests, adhering to basic engineering principles and Froude scaling ensures sound results from model testing, and provides sufficient information to be used during engineering design (see also Sect. 6 of Chapter "Modelling of Floating Offshore Wind Technologies").

WindFloat WF1 Prototype Model

The WF1 unit was commissioned and instrumented with a comprehensive array of sensors, both on the hull, as well as the turbine. The hull instrumentation included accelerometers, inclinometers, gyrometers, multiple pressure sensors and strain gauges, wave radars and multiple GPS in order to obtain 6-DOF measurements during the operational phase of the project. Figure 4 presents a diagram of instrumentation installed on the WF1 hull.
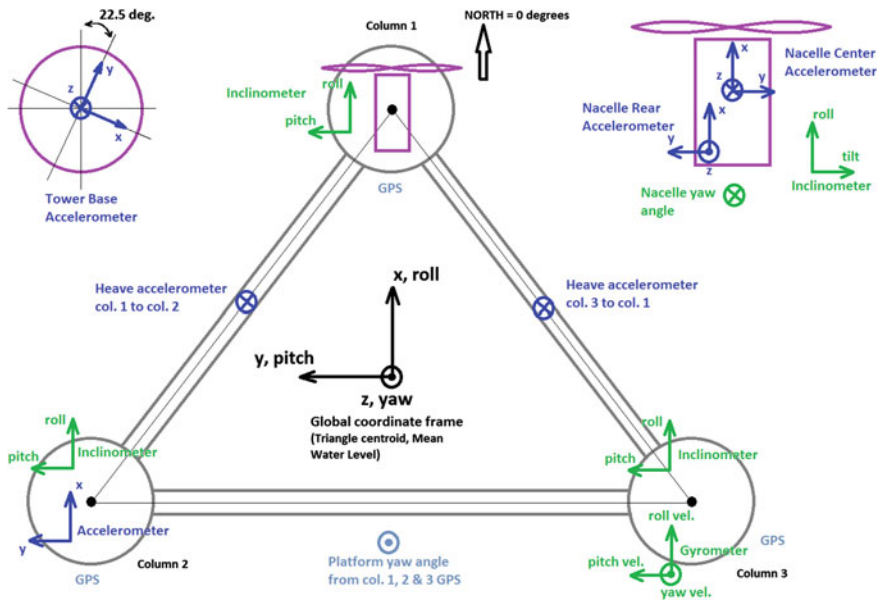
Fig. 4 Sketch of the initial instrumentation of the platform

In addition to the hull instrumentation, the wind turbine generator (WTG) included its own instrumentation package and supervisory control and data acquisition (SCADA) system capable of contributing real-time power production and wind information to the measurement campaign. Some additional instruments were outfitted to the WTG outside of the *standard* Vestas V-80 instrumentation package. These included inclinometers added on the nacelle to control the turbine and strain gauges added in the tower and blades to assess the system performance.

The WF1 data is still undergoing analysis at the time of release of this book and will be used to update and validate current and future versions of the tools used by the engineering team. This dataset is invaluable to the design team as it assists in the forthcoming challenges of making the WindFloat a commercially viable offshore wind technology.

1.3 Prototype Testing

The WF1 (Fig. 5) was installed 5 km offshore of Aguçadoura, Portugal, on October 22nd, 2011. The floating hull supports an off-the-shelf offshore Vestas V-80 turbine, fitted with a Class-I tower. The project and key learnings are described in detail in Cermelli et al. (2012). By July 2015, the WF1 had produced in excess of 15 GWh of renewable wind energy delivered to the Portuguese grid (Fig. 6).
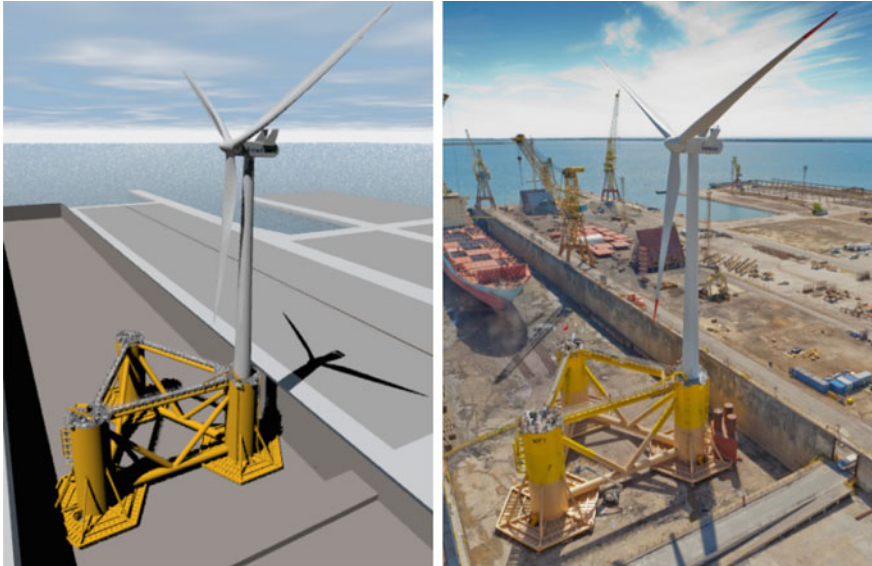
Fig. 5 WF 1: from CAD drawing to fabricated hull
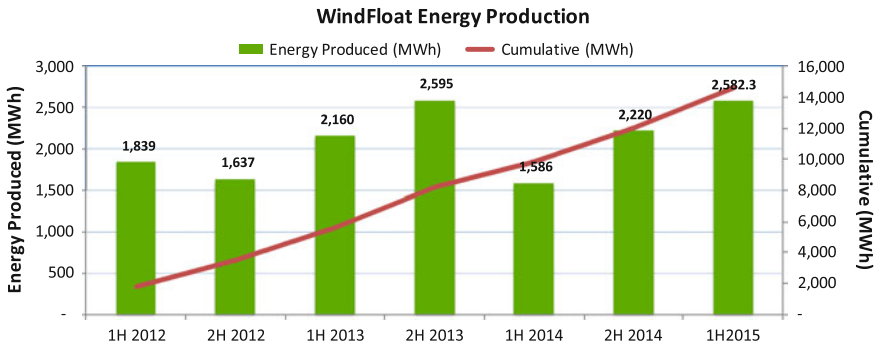
Fig. 6 WindFloat 1 electricity production

The WF1 represented a project of many *firsts* both for the Portuguese energy industry as well as the global offshore wind industry as a whole. The major achievements are listed below:

- First offshore full-scale wind turbine to be installed using a semi-submersible floating foundation worldwide;
- First offshore wind turbine to be installed without the use of any heavy-lift jack-up vessels or floating cranes;
- First offshore wind turbine to be installed at the quayside and towed fully commissioned to site;

- First offshore wind turbine to be installed in open Atlantic waters;
- First offshore structure to be built to oil and gas standards in Portugal.

Post-installation, the WF1 underwent a series of commissioning tests including a phased ramp-up to full power production. During this trial period, several parameters including motions, loads and vibrations were analysed in real-time while the team gained confidence in the WF1's operational performance and the defined performance envelope. The unit was fully commissioned and operating autonomously by March 2012.

Power production analysis has shown that the WTG installed on WF1 has not been affected by the *floating* nature of the system. Throughout a wide range of wind and wave conditions, power production has consistently been on par to that exhibited by the reference system on a fixed foundation. The data has been compared against a certified power curve from Vestas (Fig. 7).

Operation of the platform has provided the project team with invaluable hands-on experience with regards to the performance of all WF1 systems and a keen understanding on the required system specifications for future builds. In addition, such areas as access and implementation of health, safety and environment (HS&E) procedures will inform future WindFloat design efforts.

Over the past four years of operation, the initial objectives of the project have been met. These objectives were driven by the need to demonstrate the following:

- Fabricate, commission at the quayside and install fully-assembled WindFloat;
- Produce power in all weather conditions up to the one-year storm;
- Survive large winter storms;
- Withstand wave- and wind-induced fatigue;
- Perform O&M activities on the platform;
- Operate the active ballast system, other systems and equipment;
- Predict the important responses of the system with numerical tools.

Fig. 7 WindFloat 1 power curve
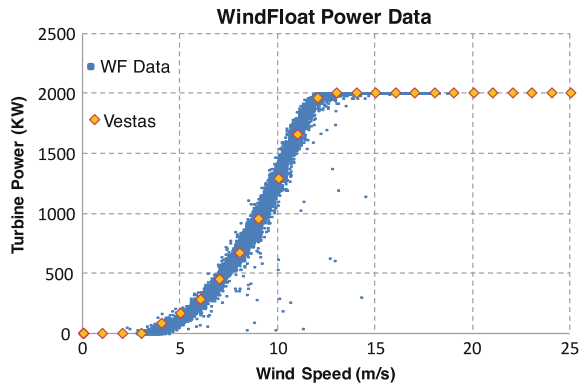
Figure 8 shows a snapshot of a wave run-up event on column three during a large winter storm on Christmas Day, 2013. The WindFloat turbine resumed operations shortly after the picture was taken. Throughout the four winters of operation to date, WF1 has not sustained any structural damages. The turbine has operated in sea states greater than $H_s = 6$ m ($H_{max} = 12$ m), and the structure survived storms of $H_s > 10$ m ($H_{max} = 20$ m).

The platform measurements have been compared to numerical simulation outputs for various observed conditions. The collected full-scale data set is very valuable as it has allowed direct calibration and validation of numerical models, such as hydrodynamic and structural damping coefficients. This ensures that all relevant physics are properly captured in the numerical simulations during engineering design.

The WF1 test and validation campaign, inspections, and adherence to HS&E practices will continue throughout the operational phase of the project. Operation of this system in the harsh North Atlantic offshore environment is challenging. Wave loads, humidity, corrosion, marine growth, and access are examples of obstacles that are challenging the project team daily.

Health and safety has been a primary focus throughout the operational phase of the WF1 project. Through diligence and adherence to HS&E best practices, the project has been able to maintain a zero lost time incident record due to injuries. A summary of the HS&E statistics for the project to date is included in Table 1.

Fig. 8 WindFloat, steady in storms

Table 1 WF1 HS&E project statistics

Summary 2011–2014	
Training actions	14
Persons involved	15
Time spent (h)	204
Safety briefings	33
Toolbox talks	105
Audits	3
Lost time incidents (LTI)	0
On-duty accidents/minor cuts and bruises	2
Emergency drills	2
Recycled waste:	
· Principle power (kg)	643
· Contractors (kg)	24
· Vestas (kg)	27

1.4   Commercialisation Pathway

The WindFloat technology roadmap is summarised in Fig. 9. In addition to the technical objectives discussed earlier, the demonstrator project (WF1) was deployed in an effort to:

- Prove the technology, inclusive of the method of fabrication and deployment,
- Convince the interested parties that the power produced was not being penalised by the floating foundation. The demo unit was not chartered to target LCOE cost
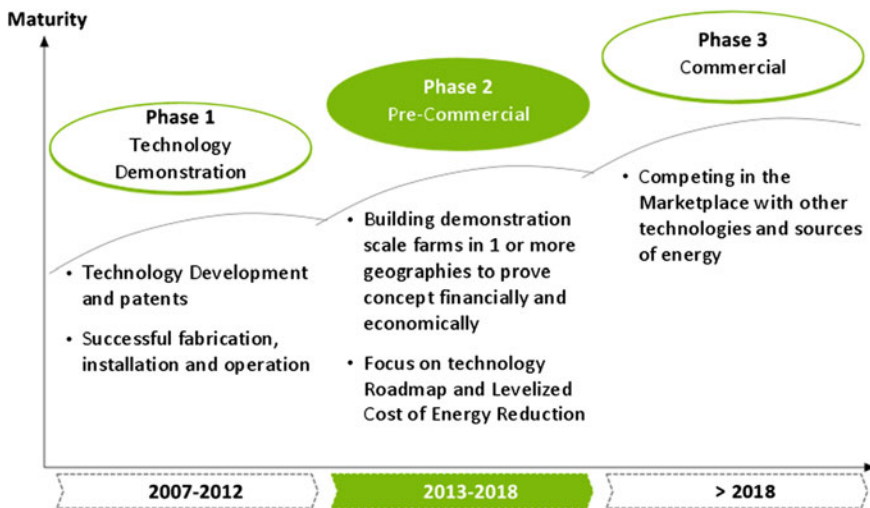
Fig. 9 Technology development roadmap

reduction, but the minimisation of both CAPEX and OPEX is still addressed inherently in the WindFloat design philosophy.

Follow-on, pre-commercial projects are intended to build upon the experience of the WF1 prototype. Lessons learned workshops were performed after the prototype deployment and learnings were captured to be explicitly applied to follow-on projects. In addition to the incorporation of lessons learned, focus on LCOE reduction is an area of particular scrutiny in new design decisions.

Currently, Principle Power is working on the FEED engineering phase of two pre-commercial farms of ~ 25 MW capacity with 6–8 MW turbines (nearly a four-fold increase in turbine power from the WF1). These pre-commercial projects are as follows:

- The WindFloat Atlantic Project, a 25 MW farm in the north of Portugal, was recently the awardee of European Commission NER300 funding, EDP Renováveis (EDPR) is the project developer.
- The WindFloat Pacific Project, awardee of the Department of Energy (DOE) Offshore Wind Advanced Technology Demonstration Projects funding, is located in Oregon and, when constructed, will be the first offshore wind farm in the US west coast.

These two pre-commercial projects represent a significant step towards commercial viability of an offshore floating wind farm. Additionally, for a project to be commercially financed, fabricated and commissioned by a project developer, without any government subsidies, the topic areas discussed below have been identified as being both necessary and achievable.

Structural Optimisation
Work is being performed to minimise steel weight in the hull structure. Even a 100-ton reduction in steel weight, per unit, would be significant to the overall project economics.

Larger Turbines
Potential for economies of scale are quite substantial with larger turbines. The primary sizing for the hull is driven both by the offshore environment and by the thrust force exerted by the turbine. For a given environment, only the latter part of the loading increases. The ratio of hull weight to turbine power is significantly advantageous to the larger hulls and turbines.

Down-Time Minimisation
A direct learning from the WF1 prototype was gained in relation to access. Boarding the platform is a critical operation that can only be done in times of low sea states. Increasing access windows, reducing equipment failures through improving reliability and planned maintenance, minimising time on-board and simplifying operation and maintenance (O&M) tasks are key topics of current R&D activities.

Fabrication in Series

Serial fabrication and learning curve advantages can impact LCOE and are expected to play a role in Principle Power's near-term pre-commercial projects. Various fabrication alternatives are being studied to measure their respective impact on cost savings.

As an example, we consider here an industrialised build of fifty WindFloat units per year. The primary pre-requisites that need to be considered when selecting suitable locations for an industrialised build are:

- Sufficient shoreside area to build multiple WindFloat units concurrently,
- Access to quayside water depth of approximately 10 m deep (dependent on sail-away draft), together with a means of loading out the WindFloat units.

For efficiency and cost saving opportunities, building multiple units should not be done in series, a single WindFloat at the time. Instead, the fabrication schedule must make use of parallel processes and maximise the use of pre-fabricated modules. Ultimately, the goal is to limit assembly outside the workshops to completed modules (already outfitted, coated and prepped for assembly).

In order to achieve an optimised, fully industrialised build, which takes advantage of as many process efficiencies as possible, it has been determined that a purpose built yard, or modification to an existing yard fit for purpose, could be required to minimise overall fabrication costs (which is not possible in pre-commercial projects where flexibility in fabrication methodology is more favourable). The requirements for a fully integrated industrialised facility have been looked at in detail. A few highlights of these requirements are summarised in Table 2.

A graphical depiction of an *ideal* facility is provided in Fig. 10. A rendered version of this facility is depicted in Fig. 11.

WindFloat LCOE Targets

LCOE is defined herein as the net present value of electricity amortised over the lifetime of the generating asset. The inputs for LCOE analysis include (among others) the CAPEX of a project, the OPEX, the net annual energy generation and a discount rate. The aforementioned technology development focus areas (e.g. structural optimisation, larger turbines, downtime minimisation etc.) play a crucial role in the determination the project CAPEX, OPEX and revenue of a given project. In the specific case of WindFloat projects, due to the maturity level of the technology and of the industry, there exist a significant potential for greatly reduced

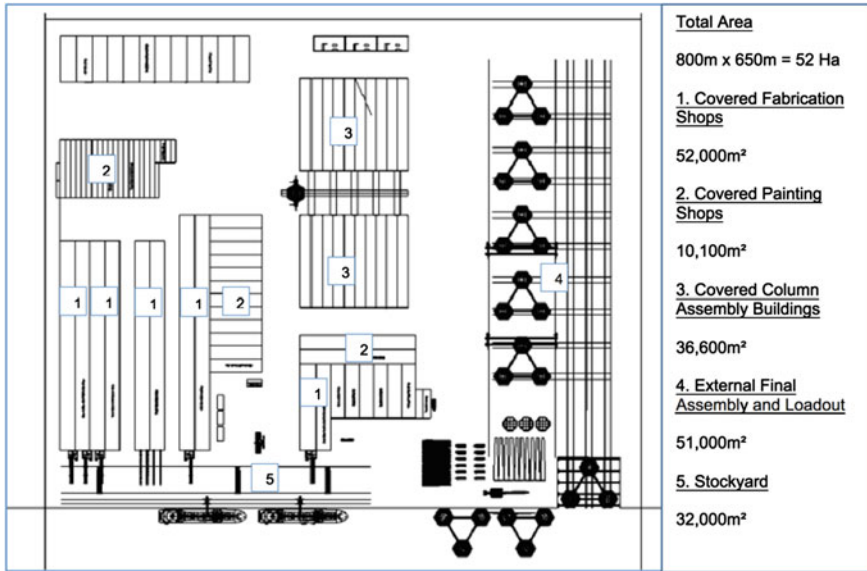| Table 2 Requirements of a fit-for-purpose yard	Area description	Required space (m^2)
	Covered fabrication shops	52,000
	Covered painting shop	10,100
	Covered column assembly building	36,600
	External final assembly and load-out	51,000
	Stockyard	32,000

Fig. 10 Top-view of fully integrated industrialised WindFloat build facility

Fig. 11 Rendered view of a fully integrated industrialised WindFloat build facility

LCOE and ultimately greater profitability for the customer. As part of the technology development effort, detailed LCOE analyses are performed both by Principle Power and third parties to ensure design decisions are informed and LCOE prediction monitored accordingly. Future successful commercial offshore wind projects will have to offer project owners LCOE cost levels below €100/kWh. Current forward-looking models for the WindFloat are on par with this prediction.

2   Hywind

Eirik Byklum and Mairéad Atcheson

Over the last decade Statoil ASA has developed the Hywind floating offshore wind concept. The Hywind concept combines known offshore technologies in a completely new application and opens up the possibility for capturing wind energy in deep-water environments.

2.1   Device Description

Based on Statoil's background in and experience with design, installation and operation of floating offshore oil and gas platforms, Hywind has been designed as a slender cylindrical structure, under the classification of a spar-type platform. The substructure is the lower part of the unit, indicated in yellow in Fig. 12. The wind turbine generator (WTG) is the remaining part in white, consisting of tower, nacelle and rotor. The nacelle and rotor is supplied by a WTG supplier, while the tower is usually separately manufactured by a specialist tower fabricator.

The Hywind structure is ballast-stabilised and anchored to the seabed. The mooring system consists of three mooring lines attached to anchors suited to the seabed conditions on site. In the unlikely event of a mooring line failure, the two remaining lines have adequate reserve strength to prevent the structure from breaking free and drifting off. The electrical cables can be designed to have expansion loops on the seabed to prevent damage in this event.

The substructure design is a ring stiffened tapered cylinder with a larger diameter for the majority of the submerged part, which tapers to a smaller diameter at the waterline to minimise wave actions. The substructure is divided into two compartments; an upper water tight deck close to top of the substructure and a water tight deck between the bottom plate and upper deck. The bottom deck is a traditional plate stiffened structure with stiffeners and girders. The flat bottom plate and water tight decks are stiffened with t-shape girders. The mooring connection points are located close to the top of the lower cylindrical section. The overall size of the structure is a result of several analyses and optimisations with respect to wind turbine generated loads, environmental loads at the specific site, mooring line loads, and requirements related to stability and WTG motion and accelerations.

A full-scale prototype Hywind device (Hywind Demo) was designed and installed in 2009, and has since then completed a comprehensive demonstration programme. By the end of 2015, the unit is still in operation and delivering power to the grid. The demonstration unit was the world's first full-scale grid-connected

Fig. 12 Hywind deep spar concept (courtesy of Statoil)

floating wind turbine and for this reason a conservative design approach was chosen. The Hywind design has since been further developed. By up-scaling to a larger WTG size, and optimising the substructure design, the cost efficiency has been improved for the commercial-size Hywind unit planned for the Hywind Scotland Pilot Park. A description of Hywind Demo and the subsequent modifications made for the Hywind Scotland Pilot Park are presented in the following sub-sections.

Hywind Demo

Hywind Demo consists of a standard Siemens 2.3 MW offshore WTG unit mounted on a ballasted vertical steel cylinder anchored to the seabed. The deep spar platform

prototype was designed for extreme North Sea conditions and was deployed in a water depth of approximately 200 m off the Norwegian coast in 2009 (see Fig. 18). The device rotor diameter is 82.4 m and the rotor nacelle assemble unit weighs 138 t. The Hywind Demo substructure is essentially an 8.3 m diameter tapered cylinder, ballasted with gravel and water, which extends 100 m below the water surface. The substructure has a smaller diameter of 6 m at the waterline to minimise wave action on the structure. The substructure of the Hywind Demo was produced in steel, but a concrete substructure is also considered for future projects.

The Hywind Demo device attaches to the seabed using a three-point spread mooring system, using drag embedded anchors. At approximately half the draft of the hull, the mooring lines are split using a crow-foot configuration to form a y-shaped arrangement of lines that connect to either side of the support structure. The crow-foot configuration acts to increases the yaw stiffness of the overall mooring system (Nielsen et al. 2006a, b). The mooring lines are designed using chain and wire, as well as clump weights to achieve the required mooring line force displacement characteristics (Skaare et al. 2015). A buoyant cable support system is used to support the power cable from underneath the spar.

Hywind Scotland Pilot Project

The full-scale measurements and experience gained from the Hywind Demo project provided the basis for further developments of the Hywind concept to form the basis for a pilot park. The Hywind units for the pilot park will be equipped with a higher rated wind turbine of 6 MW, with a rotor diameter of 154 m, operating at a hub height of approximately 100 m. The device substructure is modified from the original prototype to a shorter, but larger diameter hull. The reduced draft will extend to approximately 78 m below the water surface, with the submerged structural diameter increasing to approximately 14 m, with a diameter of approximately 10 m at the waterline. An example of the Hywind unit due to be deployed in the Hywind Scotland pilot park is illustrated in Fig. 13.

Summary of Hywind Unit Specifications

Table 3 presents the specification for both versions of the device. Figure 14 illustrates the original Hywind Demo and the modified Hywind design for the Hywind Scotland pilot project side-by-side.

2.2 Concept Development

The Hywind technology was first conceptualised in 2001, a scale model was used to test the concept in 2005 and the world's first floating full-scale wind turbine Hywind Demo was installed in 2009. Figure 15 illustrates the initial stages of development of the Hywind concept. Since 2010, the conceptual design for Hywind has been developed further to form the basis for a pilot park considering Hywind solutions up to 6 MW turbines (see Sect. 2.4).

Fig. 13 Hywind substructure with WTG unit (courtesy of Statoil)
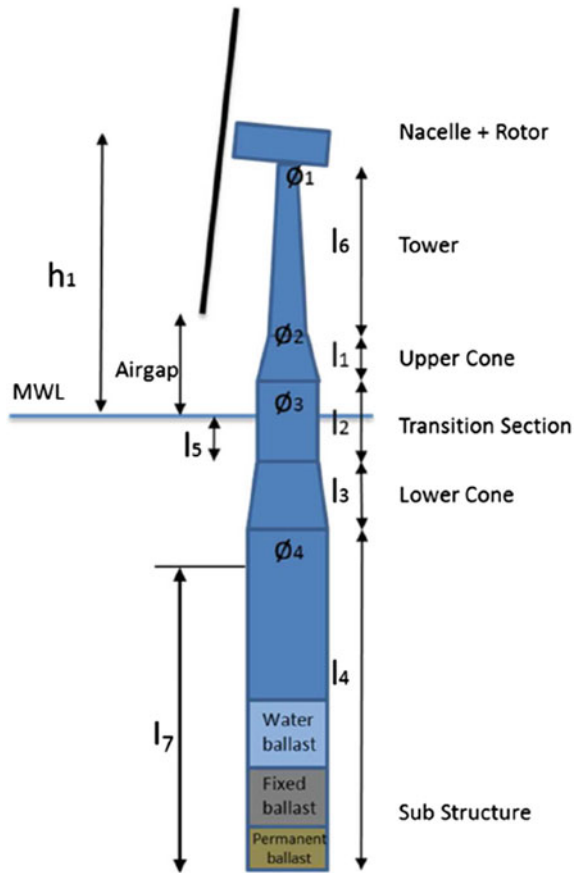
A fundamental factor in the development of the Hywind concept has been the capacity to predict the dynamic behaviour of the system. The dynamic behaviour of a floating offshore wind turbine is a function of several processes (i.e. waves, wind, mooring tension, as well as control functions of the wind turbine) occurring simultaneously and interacting with one another. Throughout the Hywind concept development process, numerical models have been used to simulate the device under different environmental and operating conditions. Results from the numerical models have been compared with experimental data from Hywind model experimental campaigns to validate the results (Nielsen et al. 2006a, b; Hanson et al. 2011). The initial development stages of the Hywind concept, including model scale experiments and numerical model developments, are described in the following sub-sections.

Model Scale Experiments

In 2005, experimental model scale tests were carried out at the Ocean Basin Laboratory run by MARINTEK in Trondheim. The ocean basin simulates wind and

Table 3 Hywind specification approximate figures

Description	Hywind Demo (demonstration unit)	Hywind 6 MW (Hywind Scotland pilot project)
Turbine nameplate capacity	2.3 MW	6 MW
Annual production per unit	7.6–10.1 GWh (actual)	25–30 GWh (predicted)
Hub height	65 m	Approx. 100 m above MSL
Rotor diameter	82 m	154 m
Operational draft	100 m	Approx. 78 m
Top head mass (rotor and nacelle)	138 t	Approx. 420 t
Displacement	5300 m^3	Approx. 12,000 m^3
Water depth at site	200 m	95–120 m
Air gap (MSL to blade tip)	24 m	22 m
Substructure diameter at waterline	6 m	Approx. 10 m
Substructure diameter submerged	8.3 m	Approx. 14.5 m
Mooring lines—radius from centre	Approx. 800 m	Approx. 700 m

Fig. 14 Hywind 6 MW design (*left*) and Hywind Demo (*right*) (courtesy of Statoil)
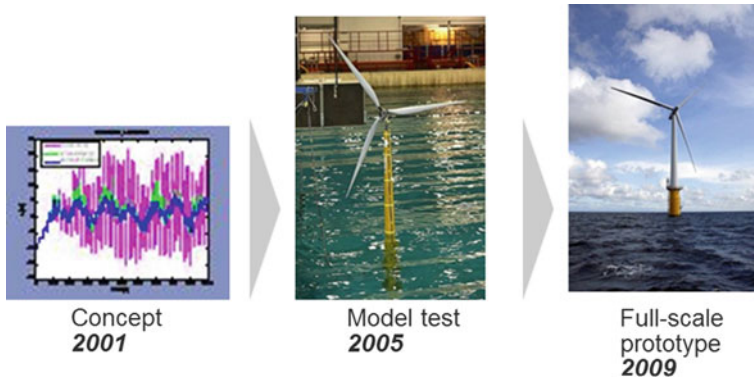
Fig. 15 Initial development stages of the Hywind concept (courtesy of Statoil)

wave conditions at sea. The tests were conducted at 1:47 model scale of a 5 MW Hywind concept. The Hywind model was equipped with a variety of sensors to measure the platform motions and loading on the device. Parameters measured during the tests included: tower motions in 6-DOF; axial acceleration at nacelle level; shear force between the nacelle and tower; rotational speed of the rotor and blade pitch angle. Two DC motors were used to control the rotational speed of the model rotor and the blade pitch angle, based on estimates of the relative velocity between the incoming wind and the turbine.

One of the key design challenges during the development of the Hywind concept has been to avoid resonant pitch motions of the tower during the operation of the wind turbine above rated speed, which required the investigation into control strategies for Hywind (Skaare et al. 2007a). The model tests showed that when the wind velocities were above the rated wind speed, the implementation of a conventional blade pitch control algorithm introduced negative damping of the tower motion. This results in the excitation of the natural frequency of the tower in pitch, which could potentially cause unacceptable tower motions (Nielsen et al. 2006a). A control algorithm for the active damping of resonant wind induced tower motions was implemented to mitigate large tower motions.

The model tests investigated the dynamics of the Hywind concept under a range of environmental and operational conditions, for example: the 100-year wave condition, wind velocities above rated wind speed and with the application of different control algorithms. Model test results also provided data for the verification and validation of numerical simulation results of the Hywind concept under the same test conditions.

Numerical Model Developments

The first numerical analyses for the dynamics of the Hywind concept, including comparisons with model tests, are presented in the publications of Nielsen et al. (2006a, b). These initial analyses were carried out using the HywindSim and

SIMO/RIFLEX computer programs. HywindSim is an in-house MATLAB/Simulink code developed specifically for the dynamic analyses and control of the Hywind concept. SIMO/RIFLEX is a code developed by MARINTEK, which simulates the dynamic response of marine structures and combines the SIMO and RIFLEX computer programs. A comparison between model scale tests and simulation results from both computer programs, under prescribed environmental conditions, confirmed the simulation results and showed that the wave-induced platform motions were similar between simulations and model tests.

Subsequent numerical analyses of the Hywind concept extended the capacity of the numerical code to include an aerodynamic modelling component, using the HAWC2/SIMO/RIFLEX (H2SR) code. The code developments incorporated two existing, independent, computer programs (SIMO/RIFLEX and HAWC2) as the basis for a new tool. The HAWC2 computer program is an aero-elastic code developed by the Risø National Laboratory used to simulate the response of fixed foundation wind turbines. The H2SR code allowed the dynamic response of floating wind turbines exposed to wind, waves and current loads to be simulated. Skaare et al. (2007b) provides details on the integration of the H2SR code and compares simulation results with the model tests carried out at MARINTEK in 2005. The results show good agreement, validating the accuracy of the coupled H2SR code and its capacity to simulate the dynamics of the Hywind model.

An example comparing experimental and simulation results, which also highlight the influence of the control algorithm on the tower motions, originally presented in Skaare et al. (2007b) are presented in Figs. 16 and 17. The square root of the power spectra of the nacelle motion in surge from simulations (H2SR program) and the model scale experiments are shown with and without active damping applied. Results are presented for identical model set-up and environment conditions (i.e. same significant wave height H_s, peak wave period T_p, mean wind velocity U_m and turbulence intensity T_i) and the turbine is operating at above the rated wind speed.

Fig. 16 Square root of the power spectrum of the nacelle surge motion. H_s = 5 m, T_p = 12 s, U_m = 16.44 m/s, T_i = 6.7 % and conventional control (Skaare et al. 2007b)
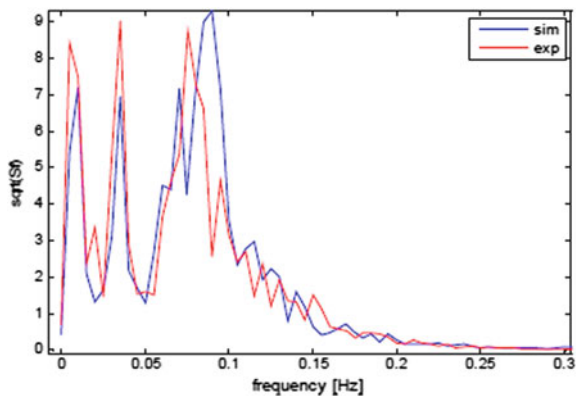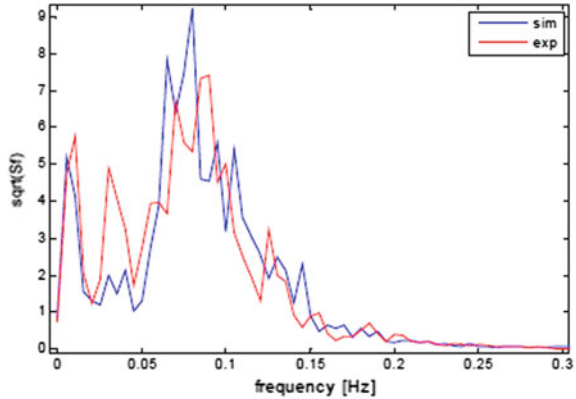
Fig. 17 Square root of the power spectrum of the nacelle surge motion. H_s = 5 m, T_p = 12 s, U_m = 16.44 m/s, T_i = 6.7 % and conventional control with active damping (Skaare et al. 2007b)

A good agreement between the simulation and experimental results was obtained, as illustrated in Figs. 16 and 17. Three peaks are clearly identifiable from the power spectra, these correspond with the following device motions: low frequency response in surge, the medium frequency is the tower pitch response and the higher frequency peak is attributed to the wave response. Figure 17 shows a significant decrease in the peak value recorded at the natural pitch frequency when the active damping term is introduced, highlighting the influence of the control strategy on the tower motions.

Most recently, the SIMO and RIFLEX programs have been included as part of the SIMA analysis tool, and the software has been extended to model offshore wind turbines (for further information on the SIMA tool see Ormberg et al. (2011) and Luxcey et al. (2011)). The dynamic analysis of the Hywind concept using the SIMA analysis tool, including comparisons of the simulation results with corresponding full-scale measurements by Hywind Demo, are presented in Skaare et al. (2015).

2.3 Prototype Testing

The Hywind Demo is currently the most advanced spar concept and was the first floating offshore wind turbine to have reached full-scale prototype testing. The Hywind Demo unit was installed near Karmøy, north of Stavanger and 10 km off the Norwegian coast at 200 m water depth. Figure 18 illustrates the installed Hywind Demo unit. The prototype was deployed in September 2009 and the test programme was initially planned for two years, but the device is still generating electricity and feeding it to the Norwegian grid by the end of 2015. Hywind Demo was equipped with a 2.3 MW standard offshore wind turbine model (SWT-2.3-82) from Siemens Wind Power. Table 4 presents some characteristic data for the SWT-2.3-82 wind turbine.

Table 4 Characteristic data for the SWT-2.3-83 wind turbine (based on information from Siemens Wind Power 2009)

Variable	Characteristic data
Rotor diameter	82.4 m
Rotor speed	6–18 RPM
Gearbox type	3-stage planetary-helical
Cut-in wind speed	3–5 m/s
Rated wind speed	13 m/s
Cut-out wind speed	25 m/s

The manufacturing and installation of the Hywind Demo unit was supported by the following major component contractors: Technip (offshore structure and installation), Siemens (wind turbine) and Nexans (offshore cabling). The spar structure was produced by Technip in Finland and towed to Stavanger, Norway, where it was up-ended by filling the cylindrical structure with water to raise it from a horizontal to a vertical position. This procedure, and the installation and commissioning of the nacelle and rotor assembly, were completed close to the shore in a relatively sheltered deep water fjord, where the depth was sufficient for the structure to be upended. Once assembled, the whole unit was towed to the installation site by

tug boats, where anchors had been pre-installed. Figures 19, 20 and 21 illustrate the sequence of the towing, upending and assembly of the Hywind Demo unit.

During the initial months of operation, the turbine underwent a range of tests and was only operated during online monitoring from the Hywind Operations Room. Following this initial start-up phase, the Hywind Demo unit was switched to automatic operating mode for all wind speeds in January 2010.

Prototype Measurements

The Hywind Demo unit is equipped with more than two hundred sensors continuously logging measurements on aspects such as structural motions and loads, mooring line tension, metocean data and typical conventional wind turbine measurements (i.e. rotational speed, blade pitch angle and generator power).

The motions of the unit are recorded in 6-DOF by a motion reference unit (MRU) fixed to the prototype substructure. Strain gauges were located at four different levels along the tower and substructure. The strain gauge measurements are used to monitor the structural bending moments and axial forces on the structure. The tension in the mooring lines is measured with sensors in the six anchor pins placed in fairleads in the hull, one for each mooring delta line.

Fig. 19 Towing and upending of Hywind Demo (courtesy of Statoil)

Fig. 20 Assembly of Hywind Demo (courtesy of Statoil)

Fig. 21 Hywind Demo installation (courtesy of Statoil)

The wave climate is measured by a wave rider buoy located in close proximity (less than 100 m away) to the floater. The buoy measures the time history of the wave elevation and direction, as well as providing statistical values for other parameters, including current velocity and direction at different water depths.

A measurement of the distance between the Hywind Demo platform deck and the sea surface was estimated from two downward-looking wave radars. The undisturbed wave field at the Hywind Demo location was estimated based on a combination of the different wave field and motion measurements (for further details see Skaare et al. 2015). Wind speed and direction measurements were made on top of the nacelle behind the rotor.

Full-Scale Results

Results from the Hywind Demo project, including a comparison of full-scale measurements with the simulated responses from computer codes, have been presented in Hanson et al. (2011) and Skaare et al. (2015). Some examples of the results recorded by the Hywind Demo prototype are presented within this section.

The natural motion response periods of the device were identified using power spectra plots derived from measurements taken on the Hywind Demo and are presented in Table 5. Eigenmodes derived from simulations using the SIMA software program are also included in Table 5 for comparative purposes.

As previous Hywind studies have highlighted (see Sect. 2.2), a floating wind turbine operating above the rated wind speed experiences a negative damping contribution from the rotor thrust force in the platform pitch mode (Skaare et al. 2007a, 2011). If a conventional control system is used, the floater may become unstable. An active damping floater motion control system was incorporated within the Hywind Demo unit to minimise the platform pitch motion of the device. Figure 22 shows two measured responses of the tower pitch motion on Hywind Demo, one with, and one without the active damping floater motion control system activated. The two tests were run in quick succession of one another, so both tests were completed under similar environmental conditions. In the tests when the motion control was deactivated, the turbine was shut down after approximately 250 s due to large tower pitch angles (Skaare et al. 2015).

The results presented in Fig. 22 confirm that the tower pitch motions are considerably lower and more stable when the floater motion controller is activated. The simultaneous measurements of wind speed and device pitch motion time series data, taken from the Hywind Demo data acquisition software, is shown in Fig. 23. In this example, the wind speed gradually increases to a level above the rated wind speed of 13 m/s. During this period of strong wind speeds, the turbine is operating above

Table 5 Comparison between eigenmodes from simulations and Hywind Demo measurements (data from Skaare et al. 2015)

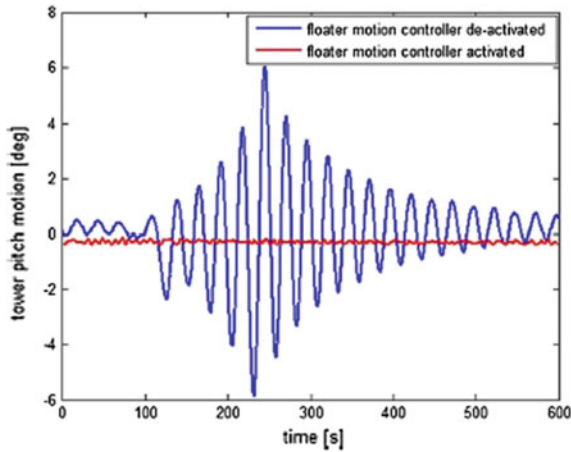| Mode of motion	Numerical analysis (s)	Hywind Demo measurements (s)
Surge	126.3	125.0
Heave	27.8	27.4
Pitch	24.2	23.9
Yaw (with clump weights)	23.4	23.8
Yaw (without clump weights)	7.5	6.2

Fig. 22 Measured tower pitch angle on Hywind Demo with the floater motion controller deactivated (*blue*) and activated (*red*). Mean value removed (Skaare et al. 2011, 2015)
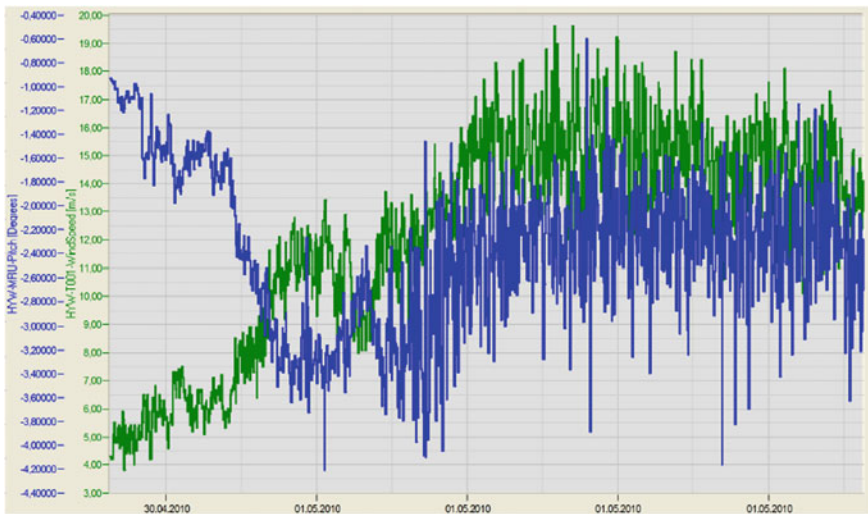

Fig. 23 Hywind Demo operation and monitoring software—wind speed and pitch behaviour of the prototype over a 30-h period, (wind speed (m/s)—*green line*; pitch motion (degrees) of the platform—*blue line*), (Keseric 2014)

the rated wind speed. When the turbine is operating above the rated wind speed, the active floater motion control system is activated to stabilise pitch motions. The stabilising influence of the active floater motion controller on the pitch behaviour can be observed in Fig. 23 during this period.

Power Production

Hywind Demo is the first floating offshore wind technology that has been verified through operational testing under harsh conditions for more than five years, and having produced approximately 41 GWh of electricity (per end October 2014). It performed beyond expectations, having a record year in 2011 with a capacity factor of over 50.1 % and produced 10.1 GWh. A screenshot of the Hywind Demo operating and monitoring software interface, including the Hywind Demo performance curve, with power generated as a function of wind speed is shown in Fig. 24.

Figure 25 shows an example of the power production trend measured by Hywind Demo in heavy seas over a 24-h period, wind speed and wave height measurements are also presented. The average wind speed for the results presented is 16 m/s, with a maximum wind speed of 28 m/s recorded. The wave height increases over the 24-h period, with an average significant wave height of 4.7 m and maximum value of 7.1 m. The results show that the Hywind Demo is capable of continued power production during heavy seas, with the device operating at 96.7 % of the rated power over the 24-h period presented. The Hywind Demo turbine has experienced several storms with maximal wave height of up to 19 m and wind speeds of 44 m/s without any consequence to the structure. Hywind operations have an excellent HS&E record without any major incidents during almost 6 year of operations.

There have been no observable negative effects on the WTG as a consequence of being installed on a floating substructure. The amount of unscheduled maintenance for the demonstration unit was the same as any other turbine of this model from the same manufacturer. The Hywind Demo project has proved that Statoil's floating
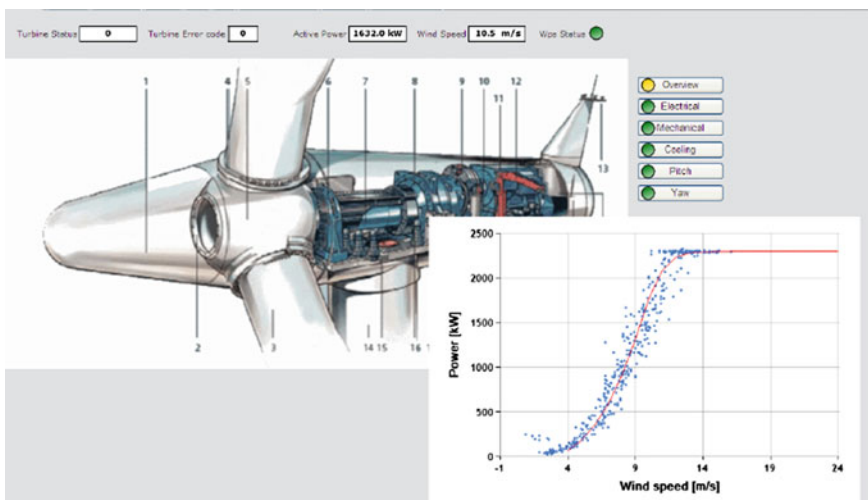
Fig. 24 Hywind Demo operation and monitoring interface and characteristic power curve for Hywind Demo (Keseric 2014)
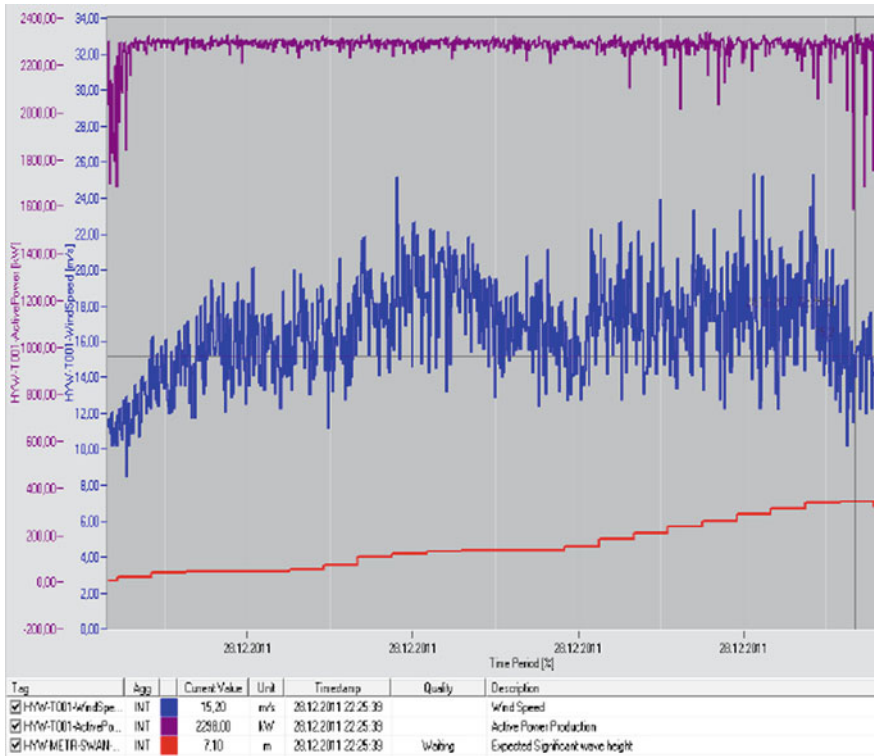
Fig. 25 Power production trend of the Hywind Demo in heavy seas, wind speed and wave height measurements (wind speed (m/s)—*blue line*; active power production (kW)—*purple line*; expected significant wave height (m)—*red line*), (Keseric 2014)

wind concept is a suitable platform for conventional multi-MW turbines, and confirms Statoil's ambitions and objectives on bringing floating wind towards commercialisation.

2.4 Commercialisation Pathway

The feasibility of floating wind turbines has so far been demonstrated through analysis, model testing and prototype testing. Statoil now intends to scale up this technology to larger applications as shown in Fig. 26. The next step in the commercialisation plan of the Hywind concept is the installation of a pilot park to demonstrate improvements and cost reductions achieved by the modified Hywind device. The information in the following section is based on internal documents provided by Statoil (Byklum 2015).
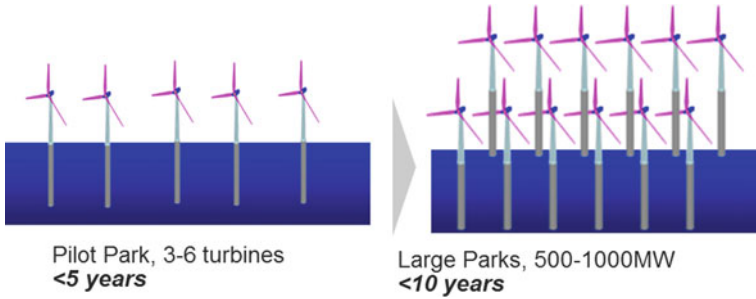
Fig. 26 Commercial development of Hywind (courtesy of Statoil)
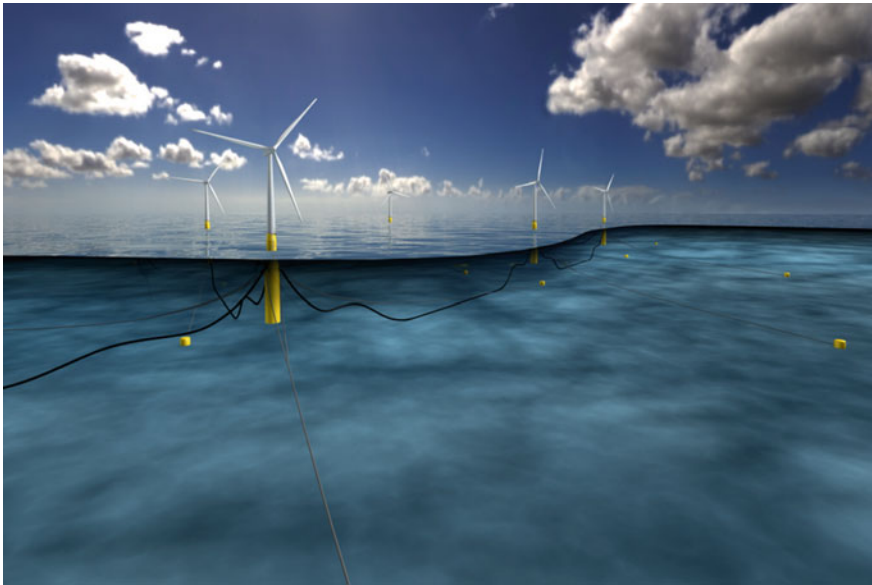
Fig. 27 Hywind Scotland pilot part overview (courtesy of Statoil)

The Hywind Scotland pilot park project is currently underway with plans to complete the final commissioning of the park by 2017. The pilot project will consist of five, 6 MW Hywind units, installed in water depths of 95–120 m (see Fig. 27). The park will be located near Buchan Deep, approximately 25–30 km off the coast of Peterhead in Aberdeenshire (UK).

Technology Development in Hywind Scotland Pilot Park

The Hywind Scotland pilot park project is intended to demonstrate the necessary reductions in both cost and risk from the prototype Hywind Demo to progress the technology toward medium and large scale wind park deployment. The pilot park will support the development of large scale parks through:

- *Technical innovation and validation*:

    - Utilise the Hywind Demo construction experience and operational performance data to develop and demonstrate a more optimised and cost efficient design, with a larger turbine and an optimised substructure. The Project design is being developed by use of a sophisticated coupled dynamic model, scalable to larger turbine units.
    - Furthermore, the project will study the effects of wake and turbulence on the floater motions for floating turbines in a park with multiple units, and demonstrate the concept and the motion controller for use in a park configuration. A critical part of the concept is the Statoil-developed pitch regulator, which has already been tested on Hywind Demo and will be adapted to the new design. Thus, the Hywind Scotland pilot park project will monitor the continued success of this advanced pitch regulator in a new environment.
    - The pilot park will also, to the extent possible/practical, be used to test out and demonstrate new technology which can be used to reduce costs for future large parks.

- *Risk reduction for large park development*: The Hywind Scotland pilot park project will advance the general base of knowledge for offshore floating wind, thereby reducing the risk for future large scale wind park development.
- *Cost reduction and market acceptance*:

    - Obtain validation of construction, installation and operating costs based on a multiple-turbine park. Demonstrating scalability of costs is viewed as a key step to building credibility in the market for the commercialisation of floating wind parks. The objective is to demonstrate the path for Statoil and other developers to achieve cost reduction and full-scale commercial viability.
    - The pilot project will demonstrate scale efficiency, and contribute to maturing the supply chain, in particular when it comes to substructure manufacturing and marine operations.

Due to the up-scaling of the substructure and turbine capacity, floater motion control and mooring system for the large Hywind units require particular attention. One new challenge related to turbines with larger rotor diameters is the effect of the increased wind loads on the yaw and roll motion of the floater, and the design of the mooring system to obtain the correct stiffness. Detailed analytical studies will be carried out to study these effects, but it will also be critical to demonstrate the performance of the concept in full-scale. It is also a continuous on-going effort to improve and optimise the floater motion controller for Hywind. Work is still on-going on Hywind Demo to test out the controller in different sea states to cover as many conditions as possible and analytical work is on-going to improve the controller to be able to control the motions also in yaw and roll, in addition to the pitch motion.

Motion response of a floating wind turbine in a park configuration with multiple units needs further investigation, both analytical and through full-scale demonstration. Wake effects on bottom-fixed structures have been studied extensively previously, but the focus has so far been on the wake loss when it comes to production. For floating WTG units, the critical aspect is rather the effect of the wake on the wind loads acting on the floating turbines in the wake, and how the non-uniform wind loads in the wake affect the floater motions. There is currently a lack of analytical tools to analyse this effect, but there is work on-going to develop tools which can be used. Nevertheless, since this is a new research topic, it will be essential to carry out full-scale measurements in the pilot park to verify the findings. For this reason, the park layout and turbine spacing for the pilot park will be chosen so that it is representative of the wake effects that will be present in a large park.

In the pilot project, a number of studies will be carried out to gain an improved understanding of these challenges and potential solutions. This includes for example advanced fully-coupled dynamic analyses to assess the effect of asymmetric load effects on floating WTGs with large rotors, assessment of asymmetric wake loading on floating units in a park configuration, further development and optimisation of the floater motion control system, and optimisation of the mooring system.

Technology Development from Hywind Scotland Pilot Park to Large Scale Parks

In order to develop the Hywind technology into a commercial, large scale competitive offshore wind solution, further development is needed. The main focus is to reduce the cost of energy to a level which makes floating offshore wind the most attractive and preferred alternative for renewable power production. This can be achieved by improving the concept itself, industrialising and scaling the technological solution as well as reducing the risk. The Hywind concept is mainly based on existing technologies used either in the oil and gas industry or the wind industry, adapted to floating and marine application. Due to this fact Hywind will benefit from the general development in these related industries making the components more cost efficient, safer and suitable for the marine environment. Examples of this development are larger wind turbines, improved reliability, more advanced and efficient marine vessels as well as more cost efficient electrical infrastructure.

However, in some areas the Hywind technology has more specific needs and potential for cost improvements. These areas are installation methods for shallow water areas, repair of major components at site, mass production of substructures as well as alternative anchoring solutions.

Improved installation methods for shallow water sites are a technology needed for areas where deep water is not available close to shore. Several alternative solutions are identified, however more work is needed to validate, qualify and commercialise these technologies without increasing the cost of installation. The solutions considered require investments in new type of vessels and will therefore

not be realised before a commercial scale project is under development. It will therefore be of vital importance to time this development and investments in order to meet the project needs. In June 2014, the Hywind Installation Challenge was launched as an open innovation challenge on Statoil's Innovate website. The campaign was open until 15 November 2014, and during this period a large number of proposals for new installation methods were received from the industry. Going forward, Statoil will work together with the companies with the most promising solutions to develop the ideas further.

Exchange of major components is a general issue for offshore wind as the expensive vessels with long mobilisation time are needed. There are also relatively strict weather limitations related to some of the lifting operations and as new sites tend to be more exposed to wind and waves, these operations are becoming increasingly expensive and unpredictable. Due to the fact that Hywind is a floating structure in deep waters, all lifting operations will be between two floating bodies, a more challenging task than between a bottom fixed turbine and a jack-up vessel. The limitations related to such operations are currently being studied and new solutions are looked into in order to improve the maintainability. Hywind also has the alternative to tow the whole unit to shore. This holds a potential reduction in both downtime and cost as the operations can be done in sheltered waters, but is currently considered to be a more expensive operation than the standard procedure for bottom fixed turbines, especially where deep water quays are not available. The tow-to-shore procedure is currently being studied in order to increase the understanding of the related costs and downtime.

A mass production supply chain of the spar substructure is not established in the industry today. Huge improvements are foreseen as more efficient production techniques, simpler design and logistical solutions are implemented. Efforts are being made to develop such solutions, however this has to be done together with local industry as well as be timed correctly with market development of floating offshore wind, as this might require investments from the supplier industry.

New anchoring solutions for alternative sites are under development in order to have a fit-for-purpose and cost efficient solution for installation of Hywind anchors. Several alternatives are developed or under development, however these need to be qualified and adapted to Hywind application. A wider selection of anchors and anchor line solutions will make the Hywind technology even better suited for different seabed solutions as well as reduce the seabed footprint of the anchor solution.

All these areas are worked with through internal improvement programs in Statoil, as well as in cooperation with the supplier industry. This will be a continuous effort going forwards balancing time to market, cost improvement potential and use of resources.

3 Goto Island Project

Tomoaki Utsunomiya

3.1 Device Description

In the Goto Island Project, funded by the Ministry of the Environment, Japan, a pre-stressed concrete (PC)-steel hybrid spar has been developed. The hybrid spar consists of PC rings at the bottom part and steel cylindrical shells at the upper part. Figure 28 shows the general view of the prototype model and Fig. 29 shows the dimensions of the same model. There is an expectation that using concrete for the bottom part will be beneficial for reducing the CAPEX.

Fig. 28 General view of the prototype model
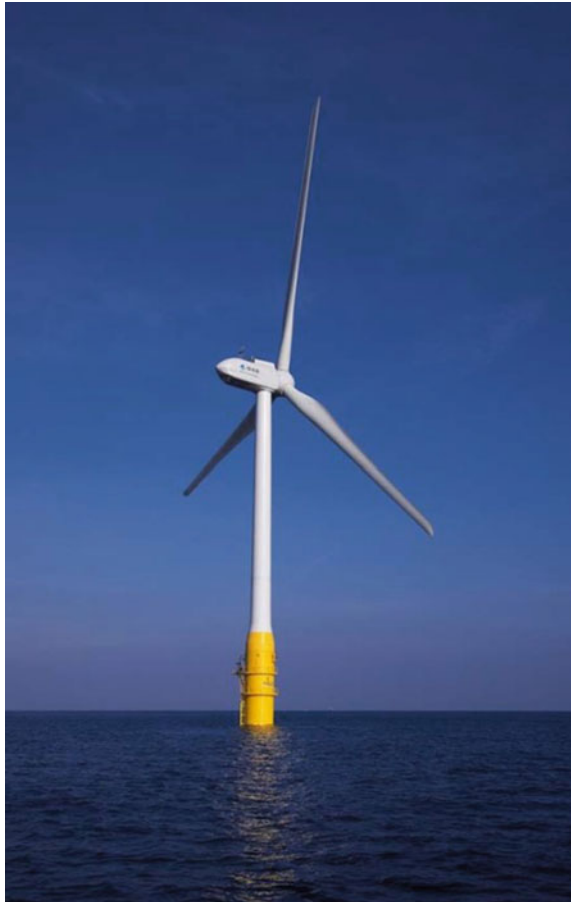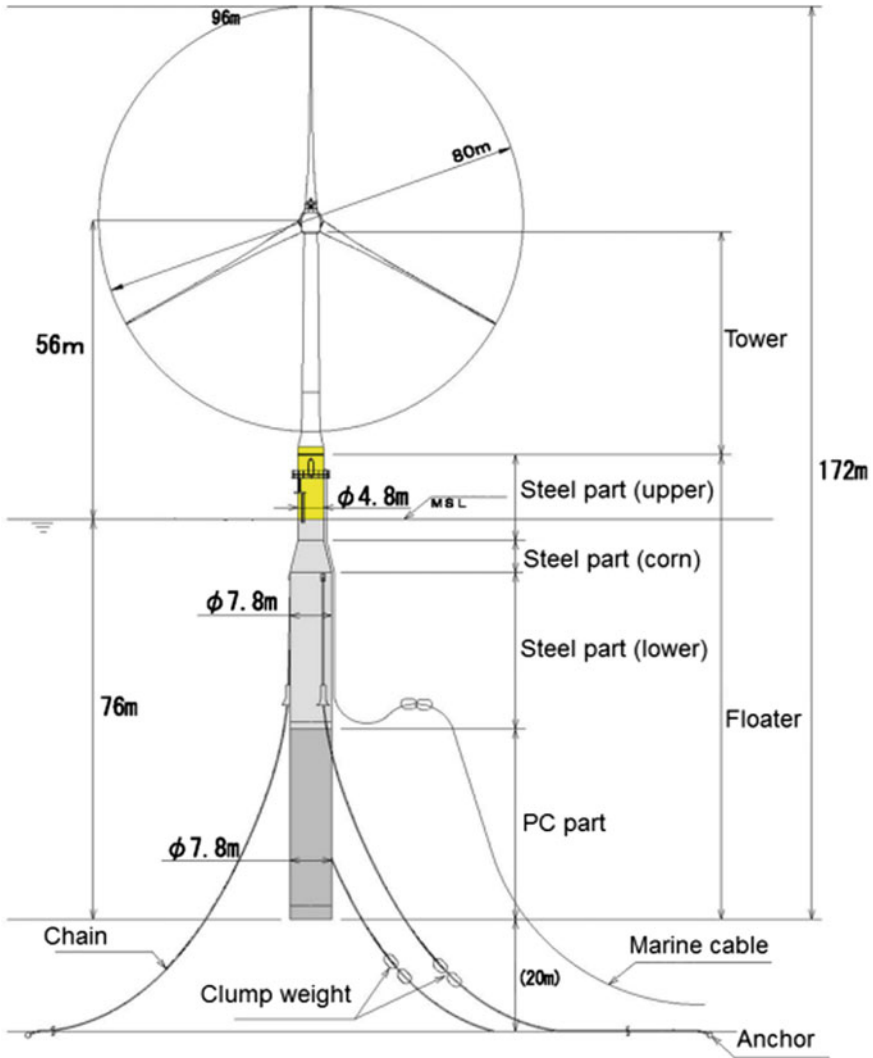
Fig. 29 Dimensions of the prototype model

The prototype model supports a downwind turbine, HTW 2.0-80 (Hitachi Ltd.), the rated output of which is 2 MW and the rotor diameter 80 m. The tower is made of steel, similar to a tower for a land-based wind turbine.

The spar floater is a simple cylindrical structure with varying diameters. The outer diameter of the upper part is 4.8 m, whereas the outer diameter of the lower part is 7.8 m. The main reason for the variable diameter is to control the natural

heave period. The natural heave period should be long enough, that is, well apart from the wave energy dominant range (typically 4–14 s). The bottom of the spar floater is filled with ballasting solids and sea water, as the center of gravity is designed to be lower than the center of buoyancy.

The spar floater is moored by three catenary mooring chains (R3S studless chains). The nominal diameter of the chains is 132 mm. Among the three mooring lines, two of them are equipped with clump weights in order to increase the weight of the lines. Only the weather-side mooring lines are equipped with the clump weights.

The mooring lines are anchored to the sea-bed by drag-type anchors. The pre-installed mooring lines were test-tensioned with the maximum design loads. The design and installation of the prototype model are presented in more detail in Utsunomiya et al. (2015a, b).

3.2 Concept Development

The spar concept presented herein was first examined experimentally by using 1:100 scale models of the 2 MW prototype model as shown in Fig. 30 and in Table 6. In the experiment, a simple cylindrical shaped floater with constant diameter (Fig. 30a) and a stepped cylindrical shaped floater with variable diameter (Fig. 30b) were used. The experimental results for wave responses were compared with numerical simulations using Morison's equation as the wave force formula. The results showed that the stepped cylindrical shaped floater may be applicable as
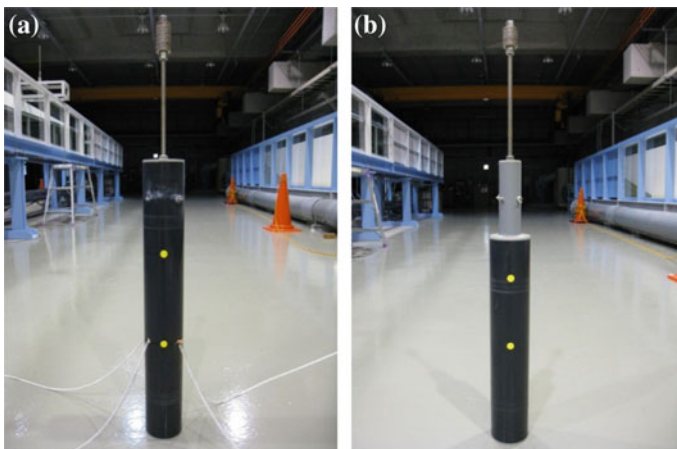

Fig. 30 1:100 scale models of the 2 MW prototype model **a** simple cylindrical shaped floater (*left*), **b** stepped cylindrical shaped floater (*right*)

Table 6 Dimensions of the 1:100 scale models (in prototype model scale) and the significant values of the responses in irregular waves at $H_{1/3}$ = 12 m, $T_{1/3}$ = 13.4 s

Description	Simple cylindrical shaped floater	Stepped cylindrical shaped floater
Draft	60 m	60 m
Outer diameter	8.9 m	8.9 m (lower part), 4.8 m (upper part)
Center of gravity	KG = 24.8 m	KG = 24.8 m
Fairlead location	4 m below water line	4 m below water line
Natural period in surge	174 s	168 s
Natural period in heave	16 s	27 s
Natural period in pitch	28 s	54 s
Surge response	5.68 m	6.62 m
Heave response	6.14 m	1.50 m
Pitch response	11.76°	4.22°

Fig. 31 1:22.5 scale model of the 2 MW prototype model in the deep sea wave basin at National Maritime Research Institute (Japan)

a floating foundation of a wind turbine, although the simple cylindrical shaped floater would be pessimistic. More details can be seen in Utsunomiya et al. (2009a).

In the next development stage, a stepped spar with 1:22.5 scale of the 2 MW prototype model was examined in the deep-sea wave basin at National Maritime Research Institute in Japan, as shown in Fig. 31 (Utsunomiya et al. 2009b). The dimensions of the 1:22.5 scale model are shown in Fig. 32. Here, the wind loadings at the hub height were simulated by a steady horizontal force using a constant weight. Both regular and irregular waves with/without the steady horizontal force were examined in the wave tank experiment. The experimental results were then compared with the simulations using Morison's equation. Table 7 summarises the

Fig. 32 Dimensions of the 1:22.5 scale model of the 2 MW prototype model (in mm)
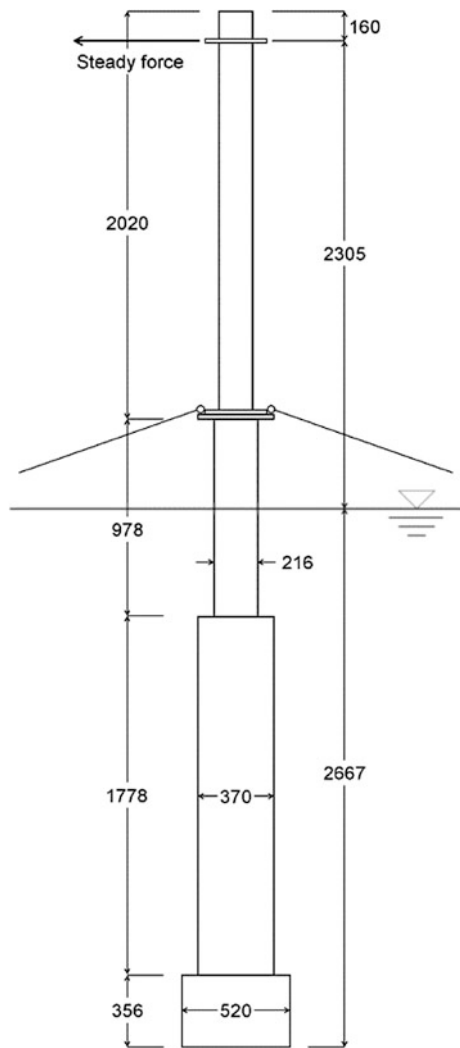
experimental results and the comparisons with the simulations. Good agreement was observed between the experiment and the numerical simulations. More importantly, no surprising phenomenon was observed in the wave tank experiment. From this experiment, confidence was gained that the spar concept for floating wind turbine would be feasible.

Subsequently, at-sea experiment of a hybrid spar using 1:10 scale model was made in Sasebo port, Nagasaki prefecture (Utsunomiya et al. 2013a). The purpose of this experiment was to demonstrate the feasibility of the hybrid-spar concept. The demonstrative experiment included:

Table 7 Summary of the 1:22.5 scale model experiments and simulations (in prototype model scale). The responses are the significant values for the irregular waves at $H_{1/3}$ = 2.25 m, $T_{1/3}$ = 11.86 s

Description	Experiment	Simulation	Exp./Sim.
Natural period in surge	111.5 s	113.5 s	0.98
Natural period in heave	27.5 s	27.5 s	1.00
Natural period in pitch	25.0 s	25.6 s	0.98
Natural period in yaw	23.3 s	24.3 s	0.96
Surge response	1.117 m	1.190 m	0.94
Heave response	0.571 m	0.573 m	1.00
Pitch response	1.590°	1.554°	1.02

1. construction of the hybrid-spar foundation using PC and steel, the same as the prototype;
2. dry-towing and installation to the at-sea site at 30 m distance from the quay of the Sasebo shipbuilding yard;
3. generating electric power using a 1 kW horizontal axis wind turbine; and
4. removal from the site.

During the at-sea experiment, wind speed, wind direction, tidal height, wave height, motion of the spar, tension in mooring chains, and strains in the tower and

Fig. 33 General view of the at-sea experiment

the spar foundation have been measured. Figure 33 shows the general view of the at-sea experiment, and Fig. 34 shows the schematic representation of the 1:10 scale model of the 2 MW prototype model. In Fig. 35, the power spectrums of the roll
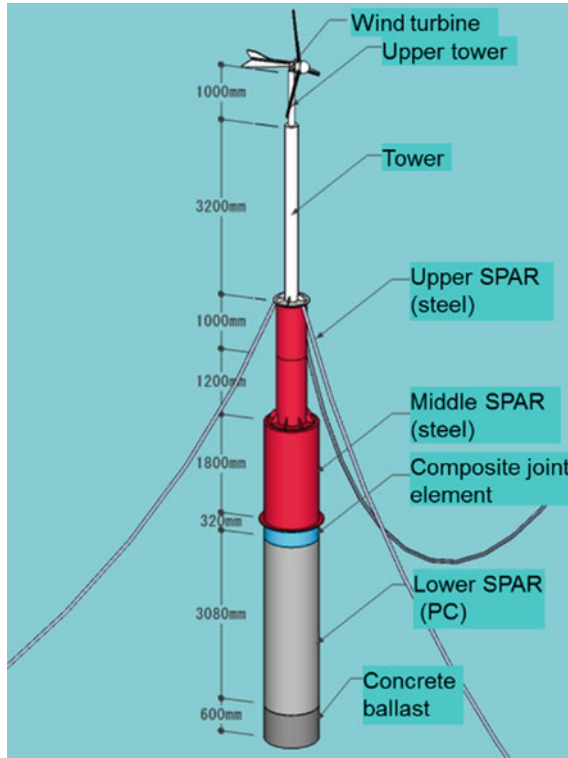

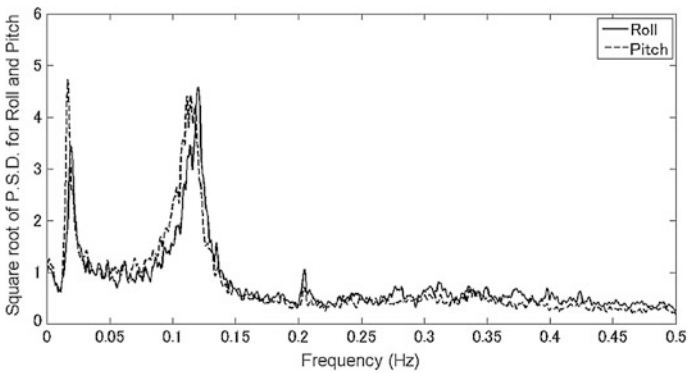**Fig. 34** Schematic representation of the 1:10 scale model of the 2 MW prototype model

Fig. 35 Power spectrum of roll and pitch responses of the 1:10 scale model

and pitch responses are shown. Each spectrum has two clear peaks, corresponding to surge and roll natural frequencies for roll motion, and sway and pitch natural frequencies for pitch motion, respectively. Through this at-sea experiment, the feasibility of the hybrid-spar concept has been confirmed.

3.3   Prototype Testing

Demonstration Project Outline

From the fiscal year of 2010, the demonstration project on floating offshore wind turbine was kicked-off by the Ministry of the Environment, Japan (Utsunomiya et al. 2015a). The ultimate objective of the demonstration project is to reduce the greenhouse gas emission through commercialisation of FOWTs in the Japanese exclusive economic zone (EEZ). Towards the commercialisation of FOWTs, the demonstration of the technical feasibility in a real sea environment is critical, as well as gaining social acceptance. Thus, the demonstration project was initiated as a national project in Japan.

Figure 36 shows the master schedule of the demonstration project. The project will spread over 6 years. In the project, two demonstration models have been installed. The first one is called the *half-scale model*, since the model is almost half in the length dimensions of the 2 MW *full-scale model*. The second one is called the *full-scale model*. The reason why two models have been installed is because a
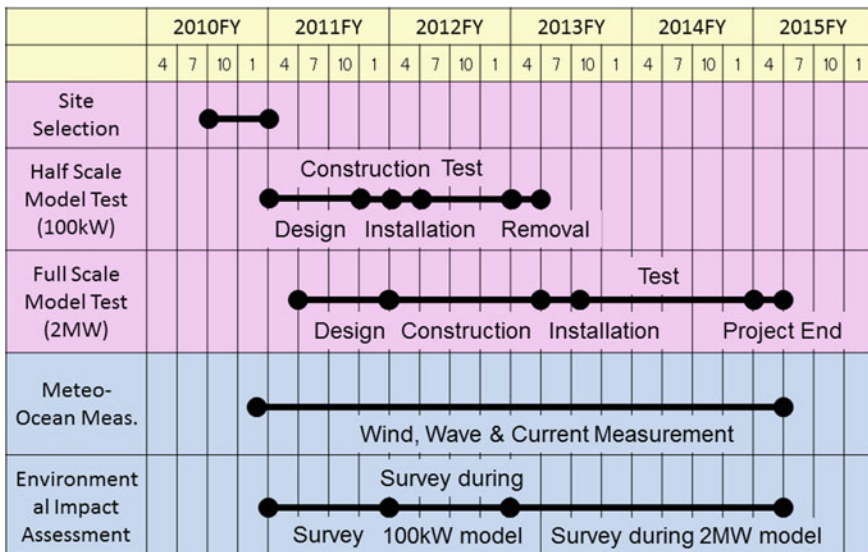
Fig. 36 Master schedule of the demonstration project on FOWT
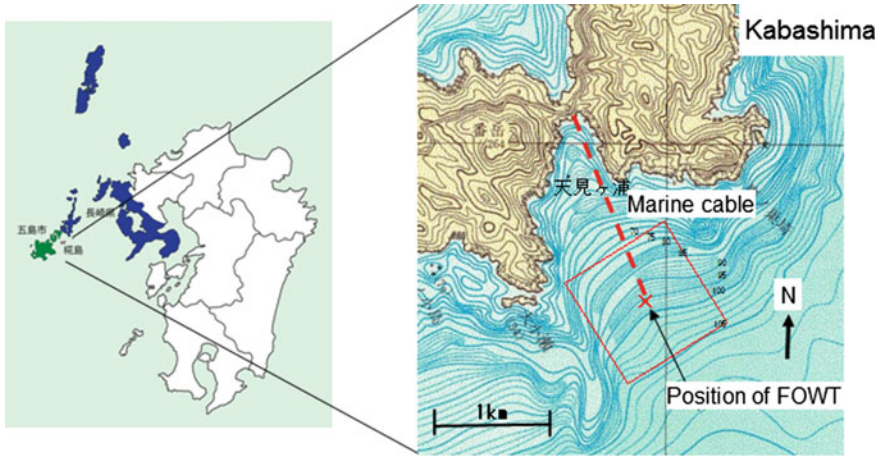
Fig. 37 Demonstration site of the project, Kabashima, Goto city, Nagasaki prefecture

step-by-step approach is preferred in order to reduce possible technical risks. Another reason is because the social acceptance would be gained by such a step-by-step approach.

Figure 37 shows the site of the demonstration project. The site is about 1 km offshore of Kabashima Island, Goto city, Nagasaki prefecture. The mean water depth is 97.2 m at mean sea level (MSL). A marine cable has been installed for the grid-connection. The distance to the shore from the FOWT along the marine cable is about 1.8 km.

Half-Scale Model

Figure 38 shows the outline of the half-scale model, and Fig. 39 shows the dimensions. The lower part of the spar is made of pre-stressed concrete (PC) whereas the upper part is made of steel. The spar was moored by three catenary anchor chains whose nominal diameter was 56 mm (G3 stud chains). The mooring chains were anchored to seabed by concrete sinkers (200 ton-force(tf) in air) at two ends and by a Danforth-type anchor (10 tf in air) at one end.

The wind turbine for the half-scale model is SUBARU 22/100, the rated output is 100 kW and the diameter is 22 m. The original wind turbine of SUBARU 22/100 was an upwind-type, but for this particular project, the wind turbine was modified to a down-wind type. Also, the maximum power was limited to 40 kW in order to increase the possibility of occurrence of wind speed above rated wind speed, where pitch control of the blades is made.

The structural design of the floating wind turbine was made by relying on the time-domain numerical simulations. Some details of the numerical simulations and the experiments used for validation are presented in Utsunomiya et al. (2014a) and in Kokubun et al. (2012). The half-scale model was installed offshore in June 2012 as the first grid-connected floating wind turbine in Japan. Figure 40 shows the general view of the half-scale model with an access ship.
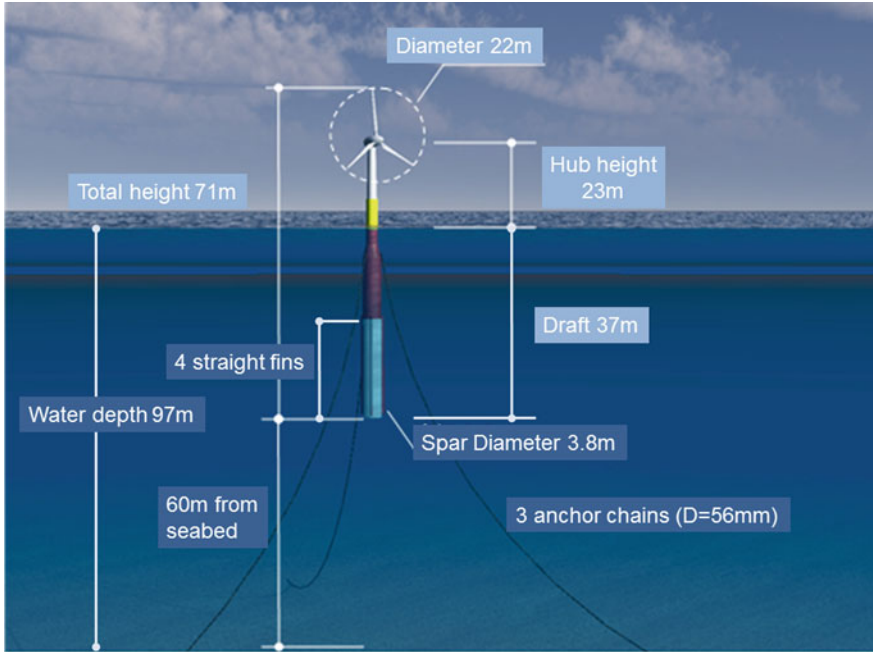
Fig. 38 Outline of the half-scale model

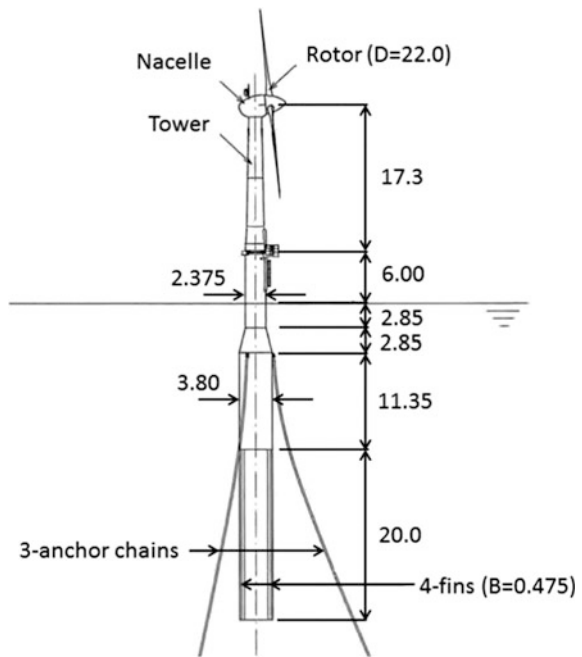**Fig. 39** Dimensions of the
half-scale model (in m)

Fig. 40 General view of the half-scale model

During the demonstrative experiment of the half-scale model, the FOWT was attacked by two separate sever typhoons. Among them, Sanba (international designation: 1216) was a record-breaking typhoon event, with a maximum wind speed of 36.8 m/s, as the 10-min average wind speed, measured at the top of the nacelle by the cup-type anemometer. At the same time, the maximum wave height of $H_{1/3} = 9.5$ m and the wave period of $T_{1/3} = 13$ s was recorded by a wave buoy close to the site (for 1-h reference period). The maximum wave height of 9.5 m exceeded the design wave height of 8.4 m corresponding to a 50-year return period event. However, the half-scale model survived for the severe typhoon with no

Fig. 41 Pitch responses for the half-scale model. *Solid line* simulation for turbulence intensities (T.I.) at IEC category A; + T.I. above IEC category A; *circle* T.I. between IEC category A and C; *triangle* T.I. below IEC category C. *Top* mean values. *Bottom* standard deviations
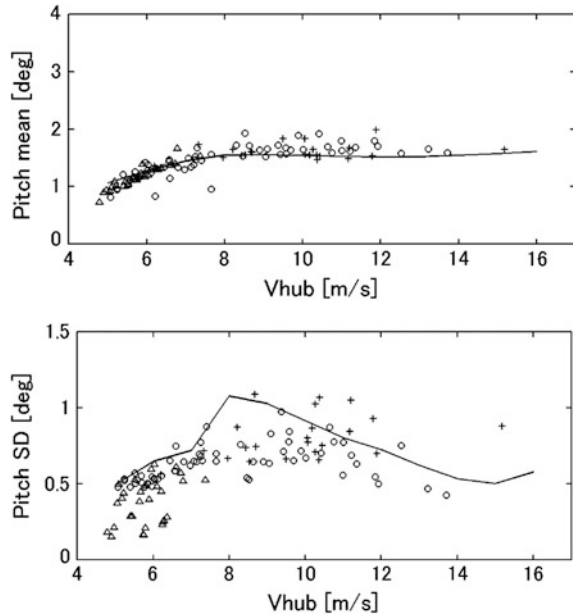
damage. The behavior during the typhoon event is reported in more detail in Utsunomiya et al. (2013b) and in Ishida et al. (2013).

Figure 41 shows an example of the platform responses during power production. The dynamic behavior during the power production can be predicted well by the numerical simulations. It is noted that the standard deviations of the pitch response are affected by the turbulence intensities of the wind, although the mean values of the pitch response are insensitive to the turbulence intensities (Utsunomiya et al. 2014b).

Full-Scale Model

After removal of the half-scale model from the site, the full-scale model was installed at the same site. Figure 28 shows the general view of the full-scale model in completion and Fig. 29 shows the main dimensions.

The structural design was made by following the ClassNK guideline (ClassNK 2012). The design load cases were set-up as given by the ClassNK guideline, and then, the time-domain simulations were made for all design load cases. The sectional design loads were then determined as the maximum value at the corresponding section among all design load cases. The load calculations were made by the validated program for the half-scale model test. More detailed design procedures are presented in Utsunomiya et al. (2015b).

Figure 42 shows the photographs of the different construction phases and procedures. The precast pre-stressed concrete (PC) segments were fabricated in a factory of Hume pipe at Kitakyushu city, Fukuoka prefecture. The precast segments were fabricated as a 1/4 part of the circular section (outer diameter: 7.8 m) with the
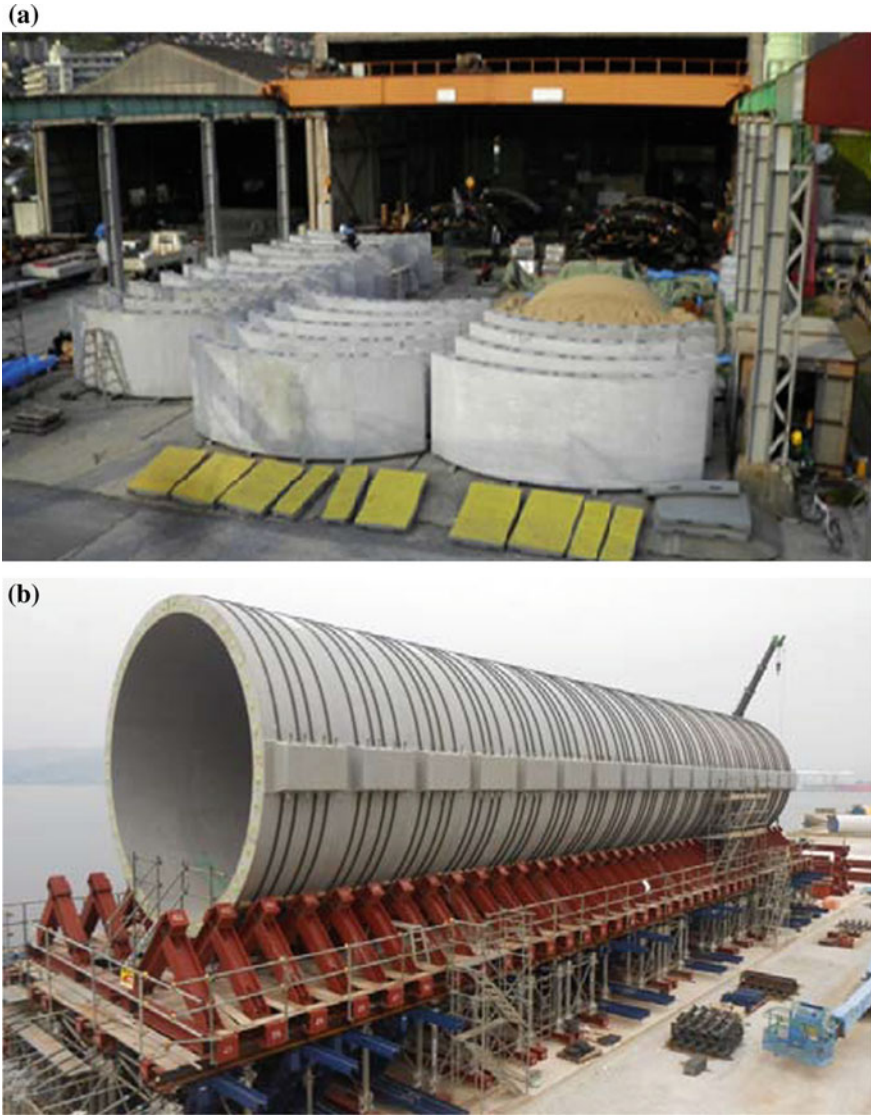
Fig. 42 Construction and installation procedures. **a** Fabrication of the concrete segments. **b** Construction of the PC part of the spar structure. **c** Joining the PC part and the steel part, and completion of the hybrid spar. **d** Dry-towing of the hybrid spar. **e** Upending of the hybrid spar. **f** Assembly of the rotor. **g** Towing to the demonstration site

height of 2 m because of the restrictions for land transportation (a). After the accelerated curing with vapor, the demolding and the air curing, the completed PC segments were transported to the construction quay at Matsuura city, Nagasaki prefecture by using conventional truck transportation. At the same time, the steel

Fig. 42 (continued)

part of the spar structure was fabricated at a shipyard in Sakai city, Osaka prefecture. The completed steel part was then transported to the same construction quay at Matsuura city by using a conventional barge.
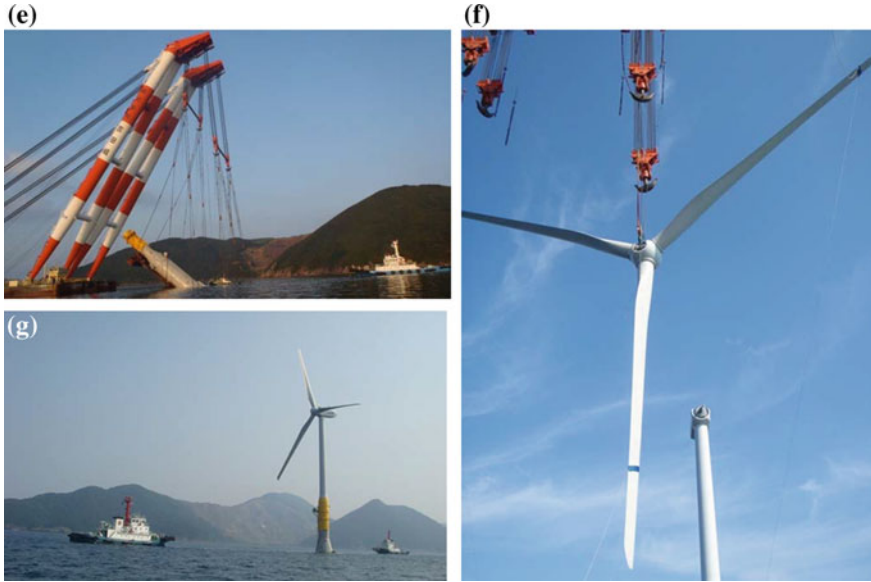
Fig. 42 (continued)

At the construction quay in Matsuura city, four segments were firstly joined together to form a ring-shaped part with the outer diameter of 7.8 m and the height of 2 m in the horizontal position. The completed ring-shaped parts were then assembled together to form a circular cylinder by using post-tensioning steel bars for the bottom half of the spar structure (b). After the completion of the PC part of the spar structure, the upper steel part was joined to the lower PC part by using a floating crane (c). The completed hybrid structure was dry-towed to the north area of the Kabashima Island, where the wave conditions are gentler than those at the demonstration site (d). Then, the hybrid-spar structure was upended with the help of a floating crane (e). After completion of the upending, the sea water was filled to stabilise the spar at the design draft. Then, the solid ballasting material was filled, where part of the sea water was replaced by the solid ballast. The tower sections (divided in two pieces), the nacelle, and the rotor were then assembled by using a floating crane (f). Having a weather window of more than three days, the temporary moorings at the north construction area were unhooked. Then, the floating wind turbine structure was towed to the demonstration site by using two tug-boats (g). As soon as it arrived at the demonstration site, the pre-laid anchor chains were hooked-up to the spar structure.

Final hook-up of the mooring chains was completed on October 18, 2013. After connection of the marine cable for the grid-connection, it began to operate from October 28, 2013 as the first multi-megawatt floating wind turbine in Japan (Fig. 28).

As of April 2015, the prototype model has been operating with no major accidental matters. During the operation, the prototype model was also attacked by several typhoons of moderated strength, but it behaved as it was so designed. This prototype testing has proven the feasibility of the hybrid-spar as a cost-effective solution for a floating wind turbine.

3.4 Commercialisation Pathway

With the success of the prototype testing mentioned above, the next step will be to form a moderate level wind farm using the same proven technology. Also, it is desirable to increase the rating of the turbine. Very recently, Hitachi Ltd. has completed the development of 5 MW downwind turbine (HTW 5.0-126; see Saeki et al. 2014). This turbine could be used for next-generation floating wind turbine using the hybrid-spar technology.

4 Sway

Jørgen Jorde and Eystein Borgen

4.1 Device Description

The Sway concept was originally developed for the electrification of offshore oil and gas platforms in the North Sea for depths of 100–400 m. From 2001, Sway AS has developed the SWAY® floating Wind power system. The Sway system can enable large scale power production for export to the onshore grids around the world in countries where water depths of greater than 50–60 m are available offshore. Outside the southern part of the North Sea (which is very shallow) most coastal waters world-wide have suitable water depths. This also allows floating wind parks to be placed outside a visible distance from shore, thus reducing potential visual impacts. The general configuration of the Sway system is shown in Fig. 43.

The Sway system consists of a horizontal axis wind turbine mounted in a downwind (or upwind) configuration on a floating tower, anchored directly or via a tension/torsion leg to the seabed. The floating tower gains its stability from ballasting the slender tower in addition to fixing it to the seabed through a tension leg (long or short). The concept is based on the entire floating tower turning (yawing) with the wind, enabling the use of tension cables (wire stays) for structural re-enforcement. The yaw mechanism is placed at the bottom of the tower, which
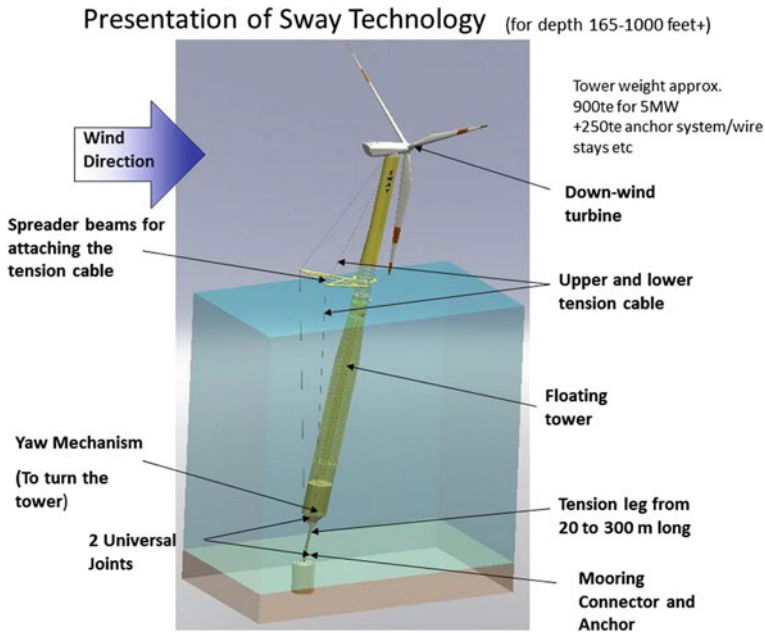
Presentation of Sway Technology (for depth 165-1000 feet+)

Wind
Direction

Tower weight approx.
900te for 5MW
+250te anchor system/wire
stays etc

Down-wind
turbine

Spreader beams for
attaching the
tension cable

Upper and lower
tension cable

Floating
tower

Yaw Mechanism

(To turn the
tower)

2 Universal
Joints

Tension leg from
20 to 300 m long

Mooring
Connector and
Anchor

Fig. 43 Sway technology

allows the nacelle with the generator to be fixed to the top of the tower, leaving the entire tower to weather vane. This feature also allows for an aerodynamic shape of the tower in front of the downwind rotor, minimising rotor turbulence. Another benefit of the yaw mechanism is that the wire stays remain in the direction always facing the wind, significantly reducing the bending moments and fatigue damage of the tower structure. This patented feature is important for the deployment of turbines larger than 5 MW on the floating mono tower and allows turbines up to 10 MW to be installed on the floating tower. The power cable will be pulled in through a service pipe in the centre of the tower ensuring the cable is well protected inside the tower and kept away from the splash zone. An electrical swivel is placed in air at the cable hang-off point at the top of the service pipe inside the tower.

The turbine hub height above sea level, for a 5–7 MW WTG, will be approximately 80–100 m, while the remaining 60–80 m of the tower will be below sea level. The total weight of the steel in the tower and anchor system is approximately 1000–1500 tonnes. The system can be optimised depending on the water depth and environmental conditions at each installation site and size of wind turbine.

The original Sway system for 100 m+ water depth has been designed to resist the fatigue load for 20 years' service life and the 100-year storm condition in the North Sea and the Norwegian Sea, having one of the roughest environmental climates in the world. Dynamic analyses have verified an acceptable level of motion

at the rotor under its working conditions in the downwind configuration on the Sway tower. The maximum pitch for normal operation will be about 8° and for extreme conditions (100-year storm) it will pitch a maximum of 15°.

A preliminary concept design was carried out for the Energy Technologies Institute (ETI) using 60 m water depth as a *worst case* minimum water level. The system was also tested for extreme tide differences of ±5 m (10 m range). The extreme loads and fatigue loads were only slightly larger than the original design for 100 m+ depth which indicate that it is fully possible to make the Sway tower work in as little as 60 m water depth. The fatigue loads without the wire stays were checked but found unacceptable (up to 4 times higher stresses in the tower) and therefore a mono tower connected directly to the seabed without the wire stays would not be economically feasible.

The evolution of the Sway system started in 2001 and has resulted in an engineered verification of the original idea, and with several important improvements to optimise the system. Sway has developed a simulation tool, SwaySim, based on the non-linear code Usfos capable of dynamic simulation of the interaction of wind, waves, tide and currents with the entire wind turbine based on finite element time domain analysis. The software was validated to simulate the simultaneous co-functionality of rotor, tower, turbine, control system, waves and wind, which allows, for example pitch control together with varying wind to be simulated. This was used to identify critical design points and optimise the design for low weight and sufficient strength.

The Sway system uses a downwind rotor. The rotor tilt angle can therefore be tailored to an optimum tilt angle for maximum alignment with the wind, without the risk of the blades clashing with the tower. Meaning that the tower is tilting in "the right" direction when the rotor is placed downwind. Therefore, the fixed rotor tilt angle is reduced (instead of increased) when the wind pushes the tower back. As a result, the Sway tower can be designed with a smaller structure for a given wind turbine, due to the non-critical tower dynamic tilt angle for the Sway design, which results in considerably less tower costs per MW. Typical tower dynamic tilt angle for the Sway design are 5–8°. The rotor has a fixed tilt of 5°, hence typically only 0°–3° of an effective tilt angle between the rotor and the wind during operation is achieved, which is less than for an onshore turbine. For an upwind rotor, the resultant tilt would be 5 + 8 = 13° which is not favourable.

The Sway floating wind turbine system is designed for use with a standard offshore turbine in a downwind configuration, with a control system adapted for the floating support structure. A feasibility study was performed by Multibrid (Areva Wind) together with Aerodyn, Garrad Hassan and Sway. The study describes the modifications to be made on the Multibrid M5000 turbine and proves that the Multibrid M5000 turbine performs well in a downwind configuration, with a modified control system and a nacelle without yaw mechanism. The modifications to the turbine itself, except for the modification of the control system, are regarded as small.

Up to 2013, there have been few downwind WTG on the market, this is however changing now, and several large 2–3 bladed downwind WTGs are currently available.

A floating mono tower is exposed to extreme fatigue loading. Therefore, the Sway solution is to place the yaw bearing at the bottom of the tower, allowing the installation of a wire stay system from the bottom of the floating tower to the top on the up-wind side of the tower (no clashing with the rotor since the nacelle itself is fixed in one position on the tower). This system reduces the bending stresses in the tower by typically 30–50 %, which allows the installation of a double sized turbine on top of the same tower compared to an un-stayed tower. Hence the economy is considerably improved.

The subsea yaw system is a simple passive swivel without motoring (Fig. 44). The swivel bearing consist of maintenance free aluminium-bronze sliding pads against a high grade stainless steel, which have been qualified through more than 20-year service life on loading buoys in the offshore industry. The design wear life of the sliding pads in the Sway system is 60 years. However, this component is still designed to be changed out offshore to lower the O&M risk. The active yawing is done entirely by individual pitching of the turbine rotor. In no wind conditions, the turbine can be yawed by driving the rotor (using the generator in motor mode) and then use the individual blade pitch to create the necessary yaw moment. To eliminate the risk of not being able to unwind the cable in this manner the power cable is terminated at a slip ring arrangement at the hang-off inside the tower.

Finally, the Sway tower for 60–100 m water depth connects directly to a single anchor with a very moderate extreme anchor force (approx. 1000 t including load factors) compared to other tension platform systems with multiple anchor cables. Since the anchor system constitutes a considerable part of the total costs this system further reduces the total CAPEX per installed turbine.
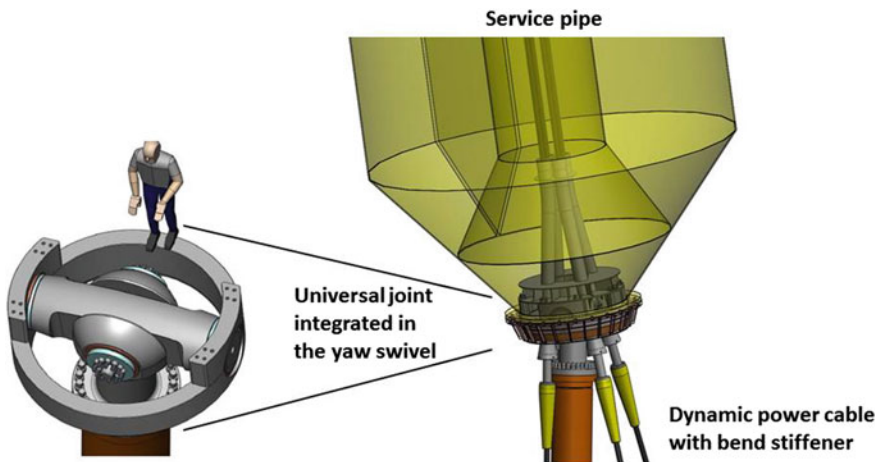

Fig. 44 Yaw system at the lower part of the tower

4.2 Concept Development

During the last years, Sway has successfully accomplished several technology milestones, which position the technology in one of the most developed stages compared to other existing designs. Figure 45 illustrates the technological evolution over last nine years, including a planned full-scale prototype.

In 2007, a 1:45 scale model tower was carefully tested by MARIN in their wave tank in the Netherlands. The results corresponded very closely to the simulations of the scaled down model. The tested and simulated static tilt of the tower varies from 2° at zero wind, up to 8° at rated wind speed. Above rated wind speed (12.5 m/s) the blade pitching to control the output power to 5 MW also reduces the rotor thrust forces. The wave-induced tower tilt variation is typically only ±0.5° at 8°.

In March 2011, Sway commissioned a 1:6.5 scale prototype off the coast of Norway near Kollsnes (northwest of Bergen) which was tested until the end of 2011. The objective of the model testing was to verify design assumptions and performance in a real environment, according to Technology Readiness Level 7. The testing was focused on the motions of the wind turbine/floating tower dynamics with the individual pitching control (IPC). The tower model had a total length of 29 m (16 m draught). It was installed at a water depth of 25 m. The initial testing was performed with an open loop control system demonstrating system stability, followed by a closed loop system, optimising control system variables for system motions versus power production maximisation. The testing was conducted in varying wind and sea conditions replicating appropriate full scale conditions. The
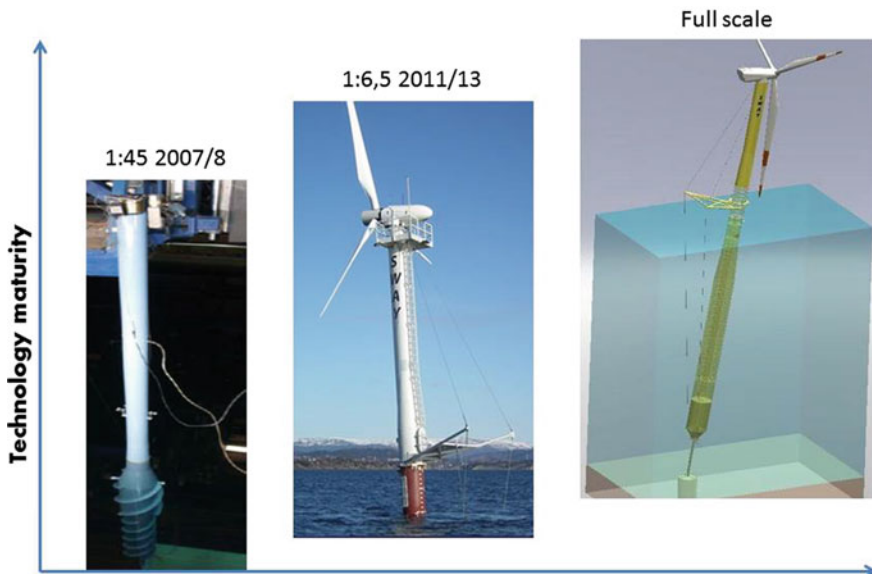

Fig. 45 Sway technology milestone

rotating tower was equipped with an aerodynamic fairing to reduce the turbulence level behind the tower for the down-wind rotor. The tests showed that this works well and no signature can be seen on the blade root bending moments when the blades passes the tower.

4.3 Prototype Testing

During the development of the Sway concept it was discovered that existing numerical design tools did not capture the design features of the Sway system, and a development program was initiated to develop a numerical tool, SwaySim based on the existing Usfos program suite (Fig. 46). Key features of the simulation program were validated through comparisons with available results, as well as through a small scale model test in moderate as well as extreme waves at MARIN in 2007 and 2008.

The validated SwaySim software was then used for further development and design of the Sway concept. In 2010, it was decided to validate the Sway concept through a large scale prototype, and funds were secured both from the owners as well as from public research funding. A scale of 1:6.5 of a 5 MW project would give a reasonably large tower, with a 7 kW turbine on top. The design of the scaled prototype was completed within a three-month period, with fabrication of the floating tower initiated immediately. The downwind configuration was the prime design focus at the time, and this concept required a downwind turbine with individual pitch control. Such a turbine was not commercially available, but a
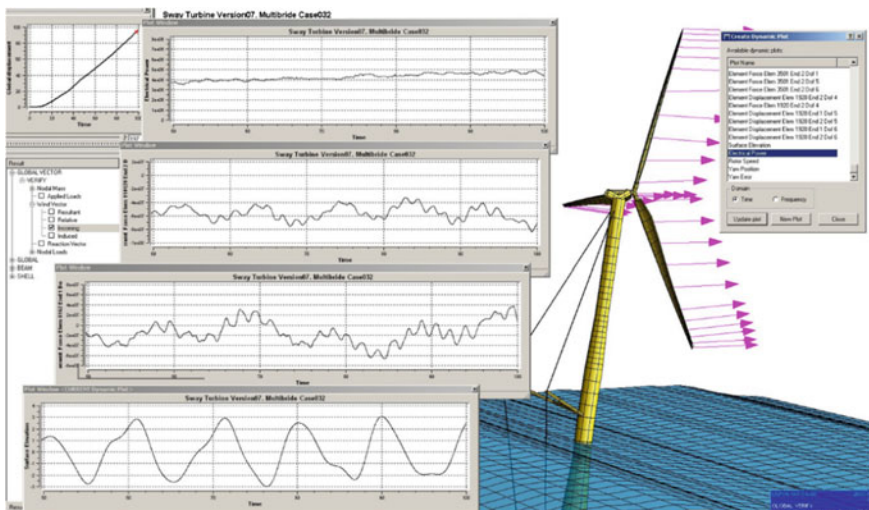

Fig. 46 SwaySim software

collaborative effort lead by Sway, with Step in Austria, Prototech in Norway, Garrad Hassan in UK and with blades from Denmark, resulted in a downwind scale turbine, with individual pitch control being designed and delivered within a four-month period.

The Sway scaled prototype was initially deployed in the spring of 2011, with testing in the fall. The installation was carried out outside Bergen, Norway, at Kollsnes, in protected waters which were intended to reflect scaled environmental conditions as shown in Figs. 47 and 48.

During a storm in December 2011, the wave heights exceeded 40 m in full scale, and were well outside the design conditions of the prototype. The water level in the J-tube inside the tower rose higher than the top of the J-tube for the scaled prototype. This flooded the tower and caused the device to sink. This incident was not linked to the concept as such and can easily be avoided in the full scale prototype (the root cause for this event is possible to avoid by having the J-tube termination at a higher level inside the tower, or alternatively have a water tight deck just below the top of the J-tube). The tower was recovered without any physical damage although the electronic equipment had to be replaced. The prototype was redeployed in the spring of 2012 with further testing carried out to the fall of 2013.

Fig. 47 Sway scaled prototype installed at Kollsnes, Norway

Fig. 48 Installed Sway scaled prototype

Through the prototype testing, the main concept features for the Sway device were demonstrated. These include the tower motions and stability with the producing downwind turbine on top, yaw bearing functionality and the yaw control through individual pitch control. The testing has also been used as a basis for several papers (Koh et al. 2013, 2015).

4.4 Commercialisation Pathway

Sway is a pioneer in the development of floating wind technologies, and is currently monitoring technology development projects and demonstrator projects that are carried out worldwide, in both benign and moderate sea conditions. These

demonstrator projects will form a very good benchmarking basis for different concepts, and Sway welcomes results and commercial projects, which will open up the market for technically and economically advantageous concepts.

Further development and commercialising of the Sway concept will preferably involve industrial partners with key interests in the floating wind industry. On the other hand, this industry is only slowly evolving, with key projects mainly ongoing in Japan as well as UK and USA. Different stakeholders (government, academia, utility companies as well as industry) are currently spending significant time and resources in gaining knowledge and experience on design, installation and operation of floating wind.

Partnering for full scale projects in either stand-alone configuration (in conjunction with e.g. oil and gas applications or Baltic surface water circulation projects) will be likely routes for Sway in the future. Potential partners may either be industrial or financial, and will likely bring market presence to the table for initial projects.

Depending on market perception either an upwind/downwind catenary moored version of the Sway patents or a tension moored downwind version will be pursued. Further development will probably be focused on detail engineering and optimisation of the concept, as well as site specific engineering related to local conditions and regulations. Of particular interest for further investigations will be launching and tow-out methodologies from specific fabrication and assembly sites of interest. Sway has developed methodologies for different quayside water depths and for assembly both horizontally quayside and vertically at sea. The Sway tower can be towed both in a vertical position as well as in a slanted posture, depending on water depths available. More detailed studies of launching, tow-out and installations are likely to be requested for different demo sites, and may form part of the work ahead.

As a closing remark, Sway is looking forward to the upcoming commercialisation phase for floating wind power, which will have room for several design concepts, and where the Sway concept hopes to take a leading position.

References

References (1)

API RP 2SK (2005) Design and analysis of station keeping systems for floating structures. American Petroleum Institute (API), Washington DC, USA

Aubault A, Cermelli C, Roddier D (2009) WindFloat: a floating foundation for offshore wind turbine—Part III: structural analysis. In: Proceedings of the 28th international conference of offshore mechanics and Arctic engineers (OMAE), Honolulu, HI, USA, 31 May–5 June 2009

Cermelli C, Roddier D, Busso C (2004) MINIFLOAT: a novel concept of minimal floating platform for marginal field development. In: Proceedings of the 14th international offshore and polar engineering (ISOPE) conference, Toulon, France, 23–28 May 2004

Cermelli C, Roddier D, Aubault A (2009) WindFloat: a floating foundation for offshore wind turbine—Part II: hydrodynamics analysis. In: Proceedings of the 28th international conference of offshore mechanics and Arctic engineers (OMAE), Honolulu, HI, USA, 31 May–5 June 2009

Cermelli C, Aubault A, Roddier D, McCoy T (2010) Qualification of a semi-submersible floating foundation for multi-megawatt wind turbines. In: Proceedings of the offshore technology conference (OTC), Houston, Texas, USA, 3–6 May 2010

Cermelli C, Roddier D, Weinstein A (2012) Implementation of a 2 MW floating wind turbine prototype offshore Portugal. In: Proceedings of the offshore technology conference, Houston, Texas, 30 Apr–3 May 2012

de Ridder E-J, Otto W, Zondervan G et al (2014) Development of a scaled-down floating wind turbine for offshore basin testing. In: Proceedings of the 33rd international conference on ocean, offshore and Arctic engineering (OMAE), San Francisco, 8–13 June 2014

Robertson A, Jonkman J, Goupee A et al (2013) Summary of conclusions and recommendations drawn from the DeepCwind scaled floating offshore wind system test campaign. In: Proceedings of the 32nd international conference on ocean, offshore and Arctic engineering (OMAE), Nantes, France, 9–14 June 2013

Roddier D, Cermelli C, Weinstein A (2009) WindFloat: a floating foundation for offshore wind turbine—Part I: design basis and qualification process. In: Proceedings of the 28th international conference of offshore mechanics and Arctic engineers (OMAE), Honolulu, HI, USA, 31 May-5 June 2009

Roddier D, Cermelli C, Aubault A, Weinstein A (2010) WindFloat: a floating foundation for offshore wind turbines. J Renew Sustain Energ 2(3):033104

Zambrano T, MacCready T, Kiceniuk T et al (2006) Dynamic modeling of deepwater offshore wind turbine structures in Gulf of Mexico storm conditions. In: Proceedings of the 25th international conference on offshore mechanics and Arctic engineering (OMAE), Hamburg, Germany, 12–17 June 2006

References (2)

Byklum E (2015) Internal communication. Statoil ASA, 14 Jan 2015

Hanson TD, Skaare B, Yttervik R et al (2011) Comparison of measured and simulated responses at the first full scale floating wind turbine Hywind. In: Proceedings of the European Wind Energy Association (EWEA), Brussels, Belgium, 14–17 Mar 2011

Keseric N (2014) Norway's solution: Hywind—world's first full-scale floating turbine. Statoil presentation, May 2014

Luxcey N, Ormberg H, Passano E (2011) Global analysis of a floating wind turbine using an aero-hydro-elastic numerical model. Part 2: benchmark study. In: Proceedings of the international conference on ocean, offshore and Arctic engineering (OMAE) 2011, Rotterdam, Netherlands, 19–24 June 2011

Nielsen FG, Hanson TD, Skaare B (2006a) Integrated dynamic analysis of floating offshore wind turbines. In: Proceedings of the international conference on ocean, offshore and Arctic engineering (OMAE), Hamburg, Germany, 4–9 June 2006

Nielsen FG, Hanson TD, Skaare B (2006b) Integrated dynamic analysis of floating offshore wind turbines. In: Proceedings of the European wind energy conference (EWEC), Athens, Greece, 27 Feb–2 Mar 2006

Ormberg H, Passano E, Luxcey N (2011) Global analysis of a floating wind turbine using an aero-hydro-elastic numerical model. Part 1: code development and case study. In: Proceedings of the international conference on ocean, offshore and Arctic engineering (OMAE), Rotterdam, Netherlands, 19–24 June 2011

Siemens Wind Power (2009) Built on experience. Siemens Wind Turbine SWT-2.3-82 VS, Technical Brochure

Skaare B, Hanson TD, Nielsen FG (2007a) Importance of control strategies on fatigue life of floating wind turbines. In: Proceedings of the 26th international conference on offshore mechanics and ocean engineering (OMAE), San Diego, California, 10–15 June 2007

Skaare B, Hanson TD, Nielsen FG et al (2007b) Dynamics of floating wind turbines utilising integrated hydro and aerodynamic analysis. In: Proceedings of the European wind energy conference (EWEC), Milano, Italy, 7–10 May 2007

Skaare B, Hanson TD, Yttervik R, Nielsen FG (2011) Dynamic response and control of the Hywind demo floating wind turbine. In: Proceedings of the European Wind Energy Association (EWEA), Brussels, Belgium, 14–17 Mar 2011

Skaare B, Nielsen FG, Hanson TD et al (2015) Analysis of measurements and simulations from the Hywind Demo floating wind turbine. Wind Energ 18:1105–1122

References (3)

ClassNK (2012) Guidelines for floating offshore wind turbine structures, 1st edn. June 2012

Ishida S, Kokubun K, Nimura T et al (2013) At-sea experiment of a hybrid spar type offshore wind turbine. In: Proceedings of ASME 2013 32nd international conference on ocean, offshore and Arctic engineering, Nantes, France, 9–14 June 2013

Kokubun K, Ishida S, Nimura T et al (2012) Model experiment of a spar type offshore wind turbine in storm condition. In: Proceedings of the ASME 2012 31st international conference on ocean, offshore and Arctic engineering, Rio de Janeiro, Brazil, 1–6 July 2012

Saeki M, Tobinaga I, Sugino J, Shiraishi T (2014) Development of 5-MW offshore wind turbine and 2-MW floating offshore wind turbine technology. Hitachi Rev 63(7):414–421

Utsunomiya T, Nishida E, Sato I (2009a) Wave response experiment on spar-type floating bodies for offshore wind turbine. In: Proceedings of the 19th international offshore and polar engineering conference, Osaka, Japan, 21–26 June 2009

Utsunomiya T, Sato T, Matsukuma H, Yago K (2009b) Experimental validation for motion of a spar-type floating offshore wind turbine using 1/22.5 scale model. In: Proceedings of 28th international conference on ocean, offshore and Arctic engineering, Honolulu, Hawaii, USA, 31 May–5 June 2009

Utsunomiya T, Matsukuma H, Minoura S et al (2013a) At sea experiment of a hybrid spar for floating offshore wind turbine using 1/10-scale model. J Offshore Mech Arctic Eng 135 (3):034503-1–034503-8

Utsunomiya T, Sato I, Yoshida S et al (2013b) Dynamic response analysis of a floating offshore wind turbine during severe typhoon event. In: ASME 2013 32nd international conference on ocean, offshore and Arctic engineering, Nantes, France, 9–14 June 2013

Utsunomiya T, Yoshida S, Ookubo H et al (2014a) Dynamic analysis of a floating offshore wind turbine under extreme environmental conditions. J Offshore Mech Arctic Eng 136 (2):020904-1–020904-11

Utsunomiya T, Yoshida S, Kiyoki S et al (2014b) Dynamic response of a spar-type floating wind turbine at power generation. In: Proceedings of ASME 2014 33rd international conference on ocean, offshore and arctic engineering, San Francisco, California, USA, 8–13 June 2014

Utsunomiya T, Sato I, Shiraishi T et al (2015a) Floating offshore wind turbine, Nagasaki, Japan. In: Wang BT, Wang CM (eds) Large floating structures. Springer, Berlin, pp 129–155

Utsunomiya T, Sato I, Kobayashi O et al (2015b) Design and installation of a hybrid-spar floating wind turbine platform. In: Proceedings of ASME 2015 34th international conference on ocean, offshore and Arctic engineering, St. Joh's, Newfoundland, Canada, 31 May–5 June 2015

References (4)

Koh JH, Robertson A, Jonkman J et al (2013) Building and calibration of a FAST model of the SWAY prototype floating wind turbine. In: Proceedings of the international conference on renewable energy research and applications (ICRERA), Madrid, Spain, 20–23 Oct 2013

Koh JH, Robertson A, Jonkman J et al (2015) Validation of SWAY wind turbine response in FAST, a focus on the influence of tower wind loads. In: Proceedings of the international offshore and polar engineering conference (ISOPE 2015), Kona, Hawaii, 21–26 June 2015

Looking Forward

Johan Sandberg

Floating wind technology has a number of key advantages compared to the more conventional offshore, bottom-fixed wind. Floating solutions allow the offshore wind industry to move towards high-yield sites, often found in deeper waters. Also from the fabrication side significant scale benefits can be anticipated. In a wind farm, bottom-fixed structures frequently require special designs for the individual foundations whereas all floating structures within a wind farm can be identical, being less restricted by water depth and local site constraints.

In 2011, DNV GL started working on an offshore standard for floating wind turbine structures via a joint industry project together with eight industry partners. In June 2013, the offshore standard *Design of Floating Wind Turbine Structures (DNV-OS-J103)* was released. The release of a design standard has brought confidence into the market and accelerated developments. In parallel, a large amount of work related to establishing floating offshore wind forecasts and assessing the prospects for floating wind technology has been conducted. These forecasts have enabled an analysis of the cost reduction potential from applying learning effects to different scenarios.

This chapter presents an overview of the global market potential for floating offshore wind farms and commercial applications where floating offshore wind technologies may be applied.

J. Sandberg (✉)
DNV GL, Veritasveien 1, N-1322, Høvik, Norway
e-mail: Johan.Sandberg@dnvgl.com

1 Global Markets

While the vast majority of installed capacity for offshore wind is currently located in northern Europe in relatively shallow water depths (<30 m), the offshore wind markets in Asia and the US are gaining momentum. By the end of 2014, scaled-turbines or prototypes had been installed in China, Japan, and the American state of Maine. Both the deployments in Japan and the state of Maine focused on floating turbine technologies, while fixed offshore turbines were installed in China. The following sub-sections briefly summarise the market activities for floating offshore wind technologies in Europe, Asia and the USA.

1.1 Europe

The floating wind turbine industry has to a large extent started in Europe, with a few early movers like Hydro, Sway and Blue H. When Statoil and Hydro merged in 2008, the new company StatoilHydro installed the world's first full scale floating wind turbine Hywind outside Karmoy on the Norwegian west coast. Only two years later, Principle Power installed its first full-scale floater on the northern Portuguese coast. At present, there are at least ten concepts under development in Europe.

Europe accounts for more than 90 % of the installed offshore wind capacity globally and the first small arrays consisting of floating wind technology are planned to be deployed in European waters by 2017–2018. Furthermore, a number of demonstration projects are in the pipeline, with developments planned in the UK, Portugal, Spain, Germany, France, Sweden, and in the Mediterranean.

One of the leading markets for floating wind in Europe today is Scotland, who have declared a strong ambition in the offshore renewables industry. Energy minister Fergus Ewing has stated that Scotland should be leading in the floating wind industry and has delivered on the promise by introducing a subsidy scheme to attract investment and development to Scotland. As a result, one of the most mature projects in the world is planned for installation in Scotland, Statoil's Hywind Scotland pilot project, with five units and 30 MW installed capacity (see Sect. 2.4 of Chap. "State-of-the-Art").

France and Portugal also have relatively mature pilot projects in the pipeline as well. In 2014 in France, DCNS announced the plan for a 50 MW floating wind farm at the Atlantic coast in northern France. Portugal has had a long commitment to offshore renewables and plans are underway to deploy a 25 MW WindFloat pilot project in the coming years (see Sect. 1.4 of Chap. "State-of-the-Art" for further information).

Scandinavia, with its vast potential of onshore wind resources, also has plans for floating wind. Norway installed the first full-scale turbine and have had an ambitions innovation program going for almost a decade, including the Sway concept, Olav Olsen, and the academic programs Nowitech and Norcowe.

Sweden has had a few technical concepts on floating wind like Hexicon, Seatwirl and FLOW. So far none of them has materialised into more than a small prototype of Seatwirl's concept in the water outside Halmstad on the Swedish west coast. However, Hexicon has managed to attract investors for their projects and are actively driving floating wind to make Sweden a player in the industry on both political and industrial levels. Hexicon have also announced plans for a demonstration project off Dounreay in Scotland. A combination of this initiative with a technology that works could make Sweden a very interesting market and create opportunities for the whole industry.

1.2 Asia

The main country in Asia that has made significant progress in floating wind is Japan. The Fukushima disaster has accelerated significantly the developments and Japan is now probably one of the global leaders in floating wind developments.

While other markets are focusing on pilot installations, Japan can also be considered the most interesting market for large scale floating wind technology and Japan's Wind Power Association (JWPA) projection is 18 GW cumulative capacity by 2050, which is inspiring for the wider industry. Japan is likely to be the place where floating wind first will be fully commercialised, hopefully triggering further developments in Europe, the US, and the rest of the world. The cost of floating offshore wind could be significantly reduced if Japan decides to pursue large scale build-out of the floating wind energy technology.

The country has a rich history in ship building and a large number of highly skilled and well equipped shipyards. It is also a country with world leading knowledge in steel and material sciences. Combined with the incredible experience in mass production and lean manufacturing, Japan has all the ingredients for rolling out offshore wind on a wide scale.

However, Japan is also a country where political risk has to be taken into consideration and managed. Although the current feed-in tariff for offshore wind is a generous 36 yen/kWh, few developers dare to take the risk on planning major projects at this stage. It has not been established exactly how long the feed in tariff will be valid for, and there is a widespread fear of the rules of the game changing depending on the political agenda.

Another major factor to consider in the Japanese market is the influential and powerful fishing industry. Seafood and fish are a cornerstone in Japanese culture and history and it is not an easy task to integrate a whole new industry in the seas where fishermen have roamed almost freely for centuries. At first this can be seen as a major obstacle, but if the stakeholder management process is implemented right from the start, the fishing industry could likely be flexible enough to let offshore wind into the waters.

There are also ambitious targets in play at the Fukushima floating offshore wind farm. The Fukushima project is a brave endeavour initiated by the government to

kick start the floating wind development in Japan. The project will primarily use Japanese technology and suppliers. However, with the government's backing the project faces lower political risk than commercially driven projects and as such could show good progress in relatively little time. The hull of the semi-submersible structure carrying the 7 MW SeaAngel has already been built and is (at the time of writing) awaiting completion.

Other Asian markets of special interest are China and South Korea. India could be an interesting future market for offshore wind, but they are likely to explore the shallower waters first, before moving into the deeper seas. More detailed studies on India's deep sea potential is also required in order to appreciate the full potential for floating wind energy in the country.

1.3   United States

The United States has a very large potential for floating offshore wind and recent developments on a political level have shown indications that the US would like to take advantage of this resource. A good sign is that the very first offshore wind installation in US waters is a floating wind turbine, the VolturnUS 1:8 prototype off the coast in Maine. The prototype has performed well, and next step is planned to comprise of two full scale turbines of 6 MW each. In addition, the American based firm Principle Power are planning a pilot park outside Oregon, WindFloat Pacific. The state of California has also indicated interest in offshore wind power driven by their ambitious renewable energy targets.

The US has a significant amount of deep waters and good wind resources. A recent offshore wind target of 22 GW by 2030, and 86 GW for 2050 also indicates good ambitions on the political level. The fact that the Department of Energy (DOE) does not distinguish between bottom fixed and floating could also be a good indication that they consider the two to have equal potential and that a large portion of the targets could be floating. In addition, DOE has supported several floating technologies through dedicated development support. Estimations indicate that the American coast line alone holds resources of up to 1700 GW of offshore wind, a large part of which is in deep waters (US DOE 2015).

2   Commercial Applications

2.1   Offshore Oil and Gas

Norway has an almost 100 % renewable energy system based on hydro power, but has a great potential for using floating wind turbines in their oil and gas industry. There is a strong political pressure to reduce the emissions from the oil and gas industry and new platforms are now often electrified with cables from land. While
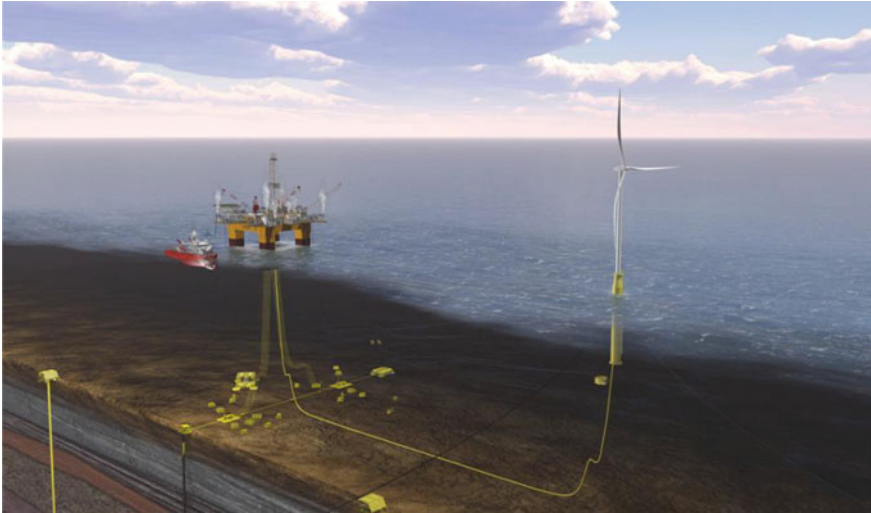
Fig. 1 Direct connection between wind turbine and oil platform (courtesy of DNV GL)

this reduces emissions, it does not exactly drive technology development or reduce costs. In that context, the idea of connecting floating wind turbines to an oil platform is a highly relevant option. In many cases this could be a profitable solution also without subsidies and even if there are only a handful of cases where it will actually happen that could still provide valuable learning.

In 2014, DNV GL launched the idea of wind powered water injection and initiated a Joint Industry Project called WIN WIN. At the time of writing this project has four oil and gas operators on board as well as a number of technology suppliers.

The concept could be applied in several different ways but two applications dominate the discussion:

1. Connecting the turbine directly to the oil platform where it could run the water injection system either with or without back up power from gas or diesel turbines (Fig. 1).
2. An autonomous system where the water injection system is placed together with the turbine, either inside the foundation structure or on the seabed right next to the injection well head (Fig. 2).

2.2 Water Pumping

In some parts of the world there is a need for water circulation in order to increase the level of oxygen on the bottom, often as a result of excessive algae growth from over-fertilisation from agriculture. This is particularly relevant for the Baltic Sea
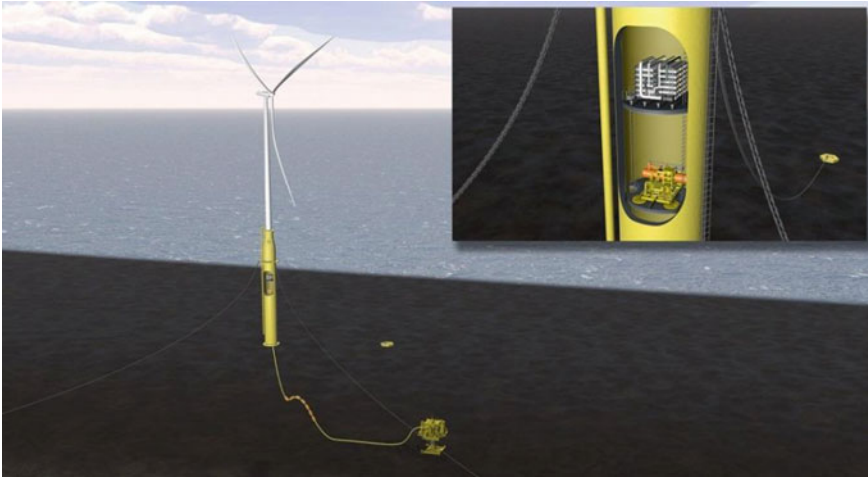
Fig. 2 Autonomous system with injection system integrated in structure (courtesy of DNV GL)

where over fertilisation and dead sea beds have been a huge problem for many years. It has always been a difficult challenge to create circulation of oxygen rich surface water down to the seabed. This poses a potential for a commercially driven market for floating wind turbines. The technology resembles the oil and gas application, but with the significant difference that the water is pumped into water and not into an oil reservoir.

At this stage there has not been any significant development in this field, most likely because the technology has been considered too immature or too expensive. With the recent developments and qualification of floating wind power this issue could soon be re-visited by the countries surrounding the Baltics and potential solutions discussed.

3   Discussion

While fixed offshore wind power is more mature than floating wind power, its main limitation is the maximum water depth of approximately 40–50 m. Although there are many areas within this range, the vast majority of the world's oceans are significantly deeper. There are also substantial interests from other industries like fishing and aquaculture in the same range of water depths but when going into deeper areas of a few hundred meters or more there are less conflicts with such stakeholders. It could also be combined with new forms of energy storage and carriers like hydrogen to create a more flexible and accessible energy market.

For renewable energy technologies in general, long-term and stable frameworks are required to incentivise projects. This will in turn trigger developments and the

cost reduction initiatives that enables further industry growth. The levelised cost of energy (LCOE) is and established benchmark when comparing the competitiveness of different energy sources. However, the LCOE does not capture all relevant elements in relation to (e.g.) market frameworks under which the different technologies compete, the time and location of the production. While technology developments are key to reducing LCOE, volume is also very important. Here the floating wind industry will benefit from growth in fixed offshore wind as turbines are similar and infrastructure can be shared.

In order to attract the necessary investment required to progress FOWT technologies, a combined industry effort is required to address technical, political and economic barriers faced, including:

- The commercialisation of an idea from concept to product will always require commitment, stamina and determination for quite some time. Like with any new technology floating wind power started with a sketch on a paper, but is now in a phase where it will require hundreds of millions of euros to mature into a commercial technology. In such a phase, it is important to gain support to survive the so called *valley of death*, where so many great ideas have succumbed to the costs of development. As such, most development projects will require government funding support, so the political risk is substantial in many markets.
- The technical challenges with floating wind technologies are substantial, but with the current level of development there are now tools that can predict behaviour and highlight critical issues at an early stage of development. The experiences gained through developments in recent years have also built up a relatively wide range of knowledge and expertise in the industry, with both developers and the supply chain. But the technical risks are always closely linked to economic side of things and the link between the two is essential. The challenge with technical risk is often to communicate it and to put it in relation to other risks.
- The economic risks of a floating wind project are of course based on a technical concept that should have been proven through a qualification process. Hence the risk picture will be rather similar to other offshore wind projects, with regards to risk exposure to currency, commodity prices, and the offtake price etc. However, for floating wind the risks could be perceived to be larger due to less track record of the technology, but hopefully solid demonstration of technology should eliminate any additional risk premium from investors.

Floating wind technologies offer the potential for the offshore wind sector to bring previously inaccessible regions within reach and allowing for site selection on the basis of optimum wind speed as opposed to depth of water. The demonstration projects have been successful and assisted in demonstrating the feasibility of the technology. The most advanced concepts have now entered the next phase, focusing on optimising the technology, reducing costs and the first array's consisting of floating wind turbines are expected to be deployed in 2017–2018.

The development of the floating offshore wind industry will be critical to the task of producing clean, reliable and affordable energy to the world's population. It opens up the almost unlimited resources of wind power over the deep oceans and could play a vital role in solving the world's critical energy challenge. The energy industry needs leadership and vision and floating wind provides one of the most exciting opportunities available.

References

DNV-OS-J103 (2013) Design of floating wind turbine structures. Det Norske Veritas (DNV), Høvik, Norway
US Department of Energy (DOE) (2015) Wind vision: A new era for wind power in the United States. DOE/GO-102015-4557, April 2015

Author Index